

---

DOCTORAL THESIS

**ICE DOMES -  
DEVELOPMENT OF CONSTRUCTION METHODS**

submitted in satisfaction of the requirements of the degree of  
Doctor of Science in Civil Engineering  
of the Vienna University of Technology, Faculty of Civil Engineering

---

DISSERTATION

**EISKUPPELN -  
ENTWICKLUNG VON HERSTELLUNGSVERFAHREN**

ausgeführt zum Zwecke der Erlangung des akademischen Grades eines  
Doktors der technischen Wissenschaften  
eingereicht an der Technischen Universität Wien Fakultät für Bauingenieurwesen

---

von

Dipl.-Ing. Sonja Dallinger  
Matrikelnummer 0125296  
Knöllgasse 33/43, 1100 Wien, Österreich

Referent: o.Univ.Prof. Dipl.-Ing. Dr.-Ing. Johann Kollegger, M.Eng.  
Institut für Tragkonstruktionen - Betonbau, Technische Universität Wien  
Karlsplatz 13/212, 1040 Wien, Österreich

Koreferent: Tsutomu Kokawa, Professor of Tokai University, Dr. Eng.  
Tokai University, School of Art and Technology (Ashikawa Campus)  
Department of Architecture and Environment Design, KOKAWA Lab.  
224 Chuwa, Kamui-cho, Asahikawa, Hokkaido 070-8601 Japan

Wien, im Juni 2011

.....

# Acknowledgement

I want to express my heartfelt thanks to my supervisor Prof. Johann Kollegger for his guidance, the valuable advice during my years at the institute and for giving me the chance to work on such an interesting and unique topic.

Fascinating and exciting but also labor-intensive and time consuming field experiments on ice domes were a major part of my thesis. These would not have been possible without the untiring efforts of all my colleagues at the Institute for Structural Engineering. Many days and nights were spent in one of the coldest regions of Austria with the aim to create a unique ice structure. I am deeply grateful for the help and support of everyone who took part in this project, on site in Obergurgl or providing support from Vienna. To express my thanks to the many supporters, the photo-collage on the next page shows pictures of everyone who took part in the project “Ice Shell”. I hope that some of you look back at the time in Obergurgl with a smile on their face like I do. I want to express my special thanks to Herbert Pardatscher, Philip Egger, Susanne Gmainer, Anton Schweighofer, Edith Schotkowsky, Andreas Kainz and Prof. Johann Kollegger who provided energetic, reliable and dedicated support for me and my rather time-consuming project over several years.

I would also like to express my gratitude to the Platzer family, owners of the Hotel Alpina in Obergurgl, who provided the construction site as well as the infrastructure and therefore made this project possible in the first place. I really appreciated the wonderful time I was allowed to spend in Obergurgl thanks to the Platzer family and all the employees of the Hotel Alpina. Moreover, I want to thank the Santer family, owners of the Hotel Enzian, who also provided a site and resources for the building of an ice dome.

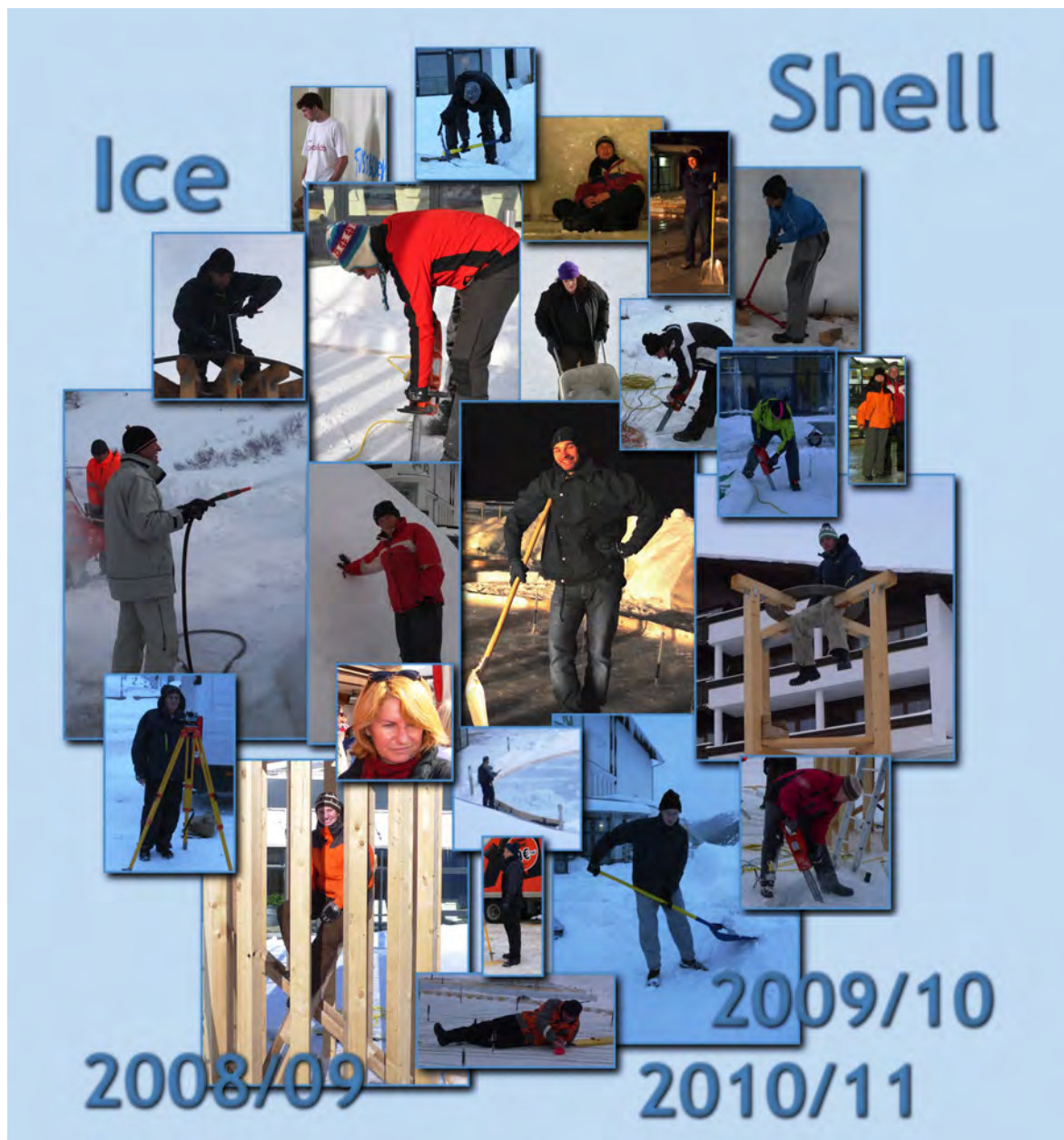
Moreover, I would like to thank all project partners who took part in the FFG-project “Herstellungsverfahren für Schalen aus ebenen Betonfertigteilen”. Special thanks to the Austrian Research Promotion Agency (*FFG*), the Verband der Österreichischen Beton- und Fertigteilwerke, the Franz Oberndorfer GmbH & Co, the Vereinigung der Österreichischen Zementindustrie and the Austria Wirtschaftsservice.

It is an honor for me to thank Prof. Kokawa for taking on the task of being second advisor of this doctoral thesis and for the inspiring, interesting and helpful discussions during his visit in Vienna.

I was in the fortunate position to be a member of the Institute for Structural Engineering while writing my thesis. For this I want to thank Prof. Kollegger who always made a great effort to make my employment at the institute possible and Prof. Litzka who

authorized my first job as a research assistant at Vienna University of Technology. At this point I also want to sincerely thank the Austrian Academy of Science for granting me a three-year DOC-fFORTE fellowship, so that I could exclusively focus my energy on my thesis.

I would also like to thank all my colleagues of the Institute for Structural Engineering for the positive work environment and the good collaboration. Last but not least, I want to thank my boyfriend, Josef Zellner, my family and friends for their continuous support during the years. Without them I would have never been able to complete my studies.





# Abstract

This thesis deals with the development of new construction methods for ice domes. Domes are esthetic, logical and functional load carrying systems, fascinating because of their shape, thinness and structure. Additionally, for the load transfer of a uniformly distributed load, the dome structure is the perfect choice because mainly normal forces occur in the cross-section. When building ice domes, use can be made of the superior load carrying system of dome structures. Since ice has low mechanical properties compared to other construction materials, it has to be deployed when low stresses occur. Thus, the combination of dome structures and the construction material ice is definitely advantageous. The construction of ice domes, however, remains a challenging task.

Part I of this thesis consists of an introduction which provides an overview of the state-of-the-art of ice domes and gives an insight into the research topic. Two new construction methods for ice domes are presented in this thesis. The basic concept is similar for both construction methods: In the initial position the intended shell structure consists of a plane plate which is subsequently transformed into a shell.

The first method to be presented is called *Pneumatic Formwork Method* - described in part II. Using this construction method, the shell consists of individual plane elements, molded according to the final shape of the shell. Complying with this construction method, the elements are placed on a planar working surface and are assembled by means of tendons. In order to transform the flat plate into a shell a pneumatic formwork is used. While air is inflating the pneumatic formwork, the plane plate is transformed into a shell.

First, the basic principle of this method is explained in detail and numerical und analytical simulations help to understand the stresses occurring during the construction as well as in the finished dome structure. An essential part of this construction method is the pneumatic formwork. The materials used and the considerations regarding the shape of the formwork as well as the loading are presented in chapter 5. The first approach for testing this newly developed technique was to carry out preliminary experiments. Two wooden models helped to gain a deeper understanding of the transformation process. Then, a thin concrete shell with a diameter of  $8,4\text{ m}$  consisting of 96 individual precast concrete elements was erected. With the insights gained from the preliminary tests, the Pneumatic Formwork Method was tested on two ice shells. In their initial position both ice shells consisted of 96 plane ice elements assembled in such a way that circular plates with diameters of  $6\text{ m}$  and  $13\text{ m}$  were created.

Part III of this thesis presents a second construction method. Using this alternative technique, a flat plate is divided into segments which are distorted uniaxially and subsequently lifted into their final position. This method is called *Segment Lift Method*. In order to distort the ice segments, these elements have to be lifted and kept in an elevated position so that the curvature produced, both by elastic deformation and creep deformation, can develop. For this purpose two different lifting methods are presented in this thesis - the *Segment Lift Method with Pneumatic Formwork* and the *Segment Lift Method without Pneumatic Formwork*. One way to lift the segments is by means of a pneumatic formwork which has to be placed underneath the ice elements before producing the ice plate. Another option is to lift them with a lifting device.

In chapter 8, the basic principle of this method is explained and different shapes are taken into consideration. As the lifting of the ice segments and the creeping behavior of the ice are crucial factors within this technique, preliminary tests on ice beams were carried out to simulate parts of the subsequently built ice shells. In the winters of 2009/10 and 2010/11 large scale field tests on ice domes were carried out. First, the Segment Lift Method with Pneumatic Formwork was used and in the following winter season, the ice segments were lifted by means of a lifting device. Chapter 10 contains a detailed description of all construction stages of these two experiments as well as numerical and analytical simulations of the force and stress distributions during the different stages of the construction and in the finished structure. The successfully completed ice dome in the winter of 2010/11 was then monitored until the shell collapsed in spring 2011.

In part IV, advantages, disadvantages, achievements and limitations of the newly developed methods are discussed.

# Contents

<b>I</b>	<b>Introduction</b>	<b>12</b>
<b>1</b>	<b>Motivation for this work</b>	<b>13</b>
<b>2</b>	<b>State-of-the-art</b>	<b>14</b>
2.1	Shell structures . . . . .	14
2.1.1	Historical outline . . . . .	14
2.1.2	Properties . . . . .	15
2.1.3	Structural behavior . . . . .	16
2.1.3.1	Load transfer . . . . .	16
2.1.3.2	Stresses in a flat slab and a hemispherical dome . . . .	17
2.1.3.3	Definition of the stresses and the sectional forces . . .	19
2.1.4	Construction methods . . . . .	20
2.2	Ice . . . . .	21
2.2.1	Ice as construction material . . . . .	21
2.2.2	Mechanical properties of ice . . . . .	25
<b>3</b>	<b>New construction methods</b>	<b>28</b>
3.1	Basic principle . . . . .	28
3.2	Field experiments - ice domes . . . . .	29
<b>II</b>	<b>Pneumatic Formwork Method</b>	<b>31</b>
<b>4</b>	<b>Basic principle</b>	<b>32</b>
4.1	General description of the method . . . . .	32
4.2	Experiments . . . . .	34
4.3	Numerical and analytical simulations . . . . .	35

<i>CONTENTS</i>	8
4.3.1 Polyhedron versus dome . . . . .	35
4.3.2 Stresses occurring during the construction process . . . . .	37
4.3.3 Considerations regarding the shape . . . . .	38
4.3.4 Stresses in the finished structure . . . . .	39
<b>5 Pneumatic formwork</b>	<b>42</b>
5.1 Material of the pneumatic formwork . . . . .	42
5.1.1 The PVC-membrane . . . . .	42
5.1.2 Material tests . . . . .	43
5.1.2.1 Experiments on the seams . . . . .	43
5.1.2.2 Determination of the tensile strength . . . . .	46
5.1.2.3 Determination of the Young's modulus and the Poisson's ratio . . . . .	47
5.1.3 Air blower . . . . .	50
5.2 Shape of the pneumatic formwork . . . . .	51
5.3 Producing the pneumatic formwork . . . . .	51
5.4 Tensile forces in the membrane . . . . .	52
5.5 Possible solution for larger shell structures . . . . .	54
<b>6 Preliminary Experiments</b>	<b>55</b>
6.1 Timber models . . . . .	55
6.1.1 Description of the models . . . . .	55
6.1.2 Knowledge gained from the timber models . . . . .	56
6.2 Concrete shell . . . . .	60
6.2.1 Preface . . . . .	60
6.2.2 Description of the essential elements . . . . .	61
6.2.2.1 Concrete Elements . . . . .	61
6.2.2.2 Pneumatic Formwork . . . . .	63
6.2.2.3 Tendons . . . . .	63
6.2.3 Test setup . . . . .	66
6.2.4 The experiment . . . . .	70
6.2.5 Experience gained from this experiment . . . . .	72

<i>CONTENTS</i>	9
<b>7 Ice shells</b>	<b>76</b>
7.1 Preface . . . . .	76
7.2 Description of the essential elements . . . . .	76
7.2.1 Ice elements . . . . .	76
7.2.2 Pneumatic formwork . . . . .	80
7.2.3 Tendons . . . . .	81
7.3 Test setup . . . . .	81
7.4 The experiments . . . . .	82
7.4.1 Small ice shell . . . . .	82
7.4.2 Large ice shell . . . . .	83
 <b>III Segment Lift Method</b>	 <b>87</b>
<b>8 Basic principle</b>	<b>88</b>
8.1 General description of the method . . . . .	88
8.2 Field experiments . . . . .	89
8.3 Considerations regarding the shape . . . . .	90
8.3.1 Stresses during the construction process depending on the rise .	90
8.3.2 Stresses in the finished structure . . . . .	92
8.3.3 Cloister vault versus dome . . . . .	95
 <b>9 Preliminary experiments</b>	 <b>97</b>
9.1 General . . . . .	97
9.2 Test setup . . . . .	97
9.3 Results . . . . .	101
9.4 Insights gained from the preliminary tests . . . . .	103
 <b>10 Ice shell</b>	 <b>107</b>
10.1 Preface . . . . .	107
10.2 Design of the ice segments . . . . .	107
10.3 Creating the ice segments . . . . .	110
10.3.1 Preparing the formwork . . . . .	110
10.3.2 Producing ice . . . . .	111
10.3.3 Inserting the reinforcement . . . . .	113

<i>CONTENTS</i>	10
10.3.4 Cutting the ice segments . . . . .	115
10.4 Deforming the ice segments . . . . .	116
10.4.1 Deforming the ice segments with a pneumatic formwork . . . . .	117
10.4.1.1 Lifting the ice segments with the pneumatic formwork . . . . .	117
10.4.1.2 Stresses in the ice segment and the membrane . . . . .	118
10.4.1.3 Initial deformation . . . . .	121
10.4.1.4 Creeping behavior of the ice segments . . . . .	122
10.4.2 Deforming the ice segments without a pneumatic formwork . . . . .	126
10.4.2.1 Lifting the ice segments with the lifting devices . . . . .	126
10.4.2.2 Triggering cracks . . . . .	130
10.4.2.3 Placing the ice segments on stacks of wood . . . . .	131
10.4.2.4 Initial deformation . . . . .	132
10.4.2.5 Stresses in the ice segment . . . . .	134
10.4.2.6 Creep behavior of the ice segments . . . . .	137
10.5 Lifting the ice segments . . . . .	142
10.5.1 The mounting tower . . . . .	142
10.5.2 Preparing the ice segments for the lifting process . . . . .	143
10.5.2.1 Compression arch with tension tie . . . . .	143
10.5.2.2 Properties of the chains . . . . .	144
10.5.2.3 Problems with the assembly of the chains in winter 2009/10 . . . . .	146
10.5.3 The lifting process . . . . .	150
10.5.4 Stresses in the segments . . . . .	152
10.6 Creating a shell structure . . . . .	155
10.7 The finished ice shell . . . . .	157
10.7.1 Characteristics of the ice dome . . . . .	157
10.7.2 Numerical simulation . . . . .	158
10.8 Monitoring the ice shell until collapse . . . . .	161
<b>IV Conclusion</b>	<b>166</b>
<b>11 Achievements and limitations</b>	<b>167</b>
11.1 Pneumatic formwork method . . . . .	167
11.2 Segment lift method . . . . .	168

<i>CONTENTS</i>	11
<b>12 Building larger ice domes</b>	<b>171</b>
<b>Bibliography</b>	<b>173</b>
<b>A Pneumatic Formwork Method</b>	<b>187</b>
A.1 Concrete shell . . . . .	188
A.2 Ice shells . . . . .	192
A.3 Pneumatic formwork . . . . .	203
<b>B Segment Lift Method</b>	<b>206</b>
B.1 Creating the ice segments . . . . .	207
B.2 Deforming the ice segments . . . . .	219
B.3 Mounting tower . . . . .	238
B.4 Final Position . . . . .	250

# Part I

## Introduction



# Chapter 1

## Motivation for this work

Domes are esthetic, efficient and impressive examples of fascinating architecture because of their shape, thinness and structure. A particular feature of doubly curved shells, which include the domes, is the effective load transfer. Loading is mostly carried by normal forces in the middle surface of the shell which causes a very uniform and efficient distribution of the stresses in the entire cross section. Thus, large spans can be achieved while the stresses in the structure are kept relatively small.

Ice is a 100 % natural material with a striking appearance. In regions where water is sufficiently available and low temperatures are inherent, producing ice can be done without any external energy supply. Nowadays, as the awareness of sustainability, resource conservation and environmental compatibility increases, environmentally friendly solutions are sought-for.



Figure 1.1: Ice Dome built during this thesis (pictures: Günter R. Wett)

As the ice has low mechanical properties compared to other construction materials, it has to be deployed when low stresses occur. Therefore its field of application in architecture and civil engineering is mainly limited to being a decorative material on a supporting carrying structure. In building a dome structure, ice can be used as construction material which conducts the load transfer, due to the low stresses in this kind of structure. The construction of shells is a challenging task which has not been accomplished all too often with the complex material ice. This thesis, however, rises to the challenge of developing new construction methods for ice domes.

# Chapter 2

## State-of-the-art

### 2.1 Shell structures

#### 2.1.1 Historical outline

Shells are natural, logical and functional load carrying systems. Nature has always been using these structures long before architecture even existed. If a space is surrounded by a minimal area of surface, the shell is the logical optimum. Additionally, for the load transfer of a uniformly distributed load, the shell structure is the perfect choice. These structural and functional advantages are applied by nature in several areas. There are numerous examples of shells in the flora and fauna. Microbes, like diatomeens and radiolarien, or clams are using shell structures.

Moreover, egg shells, nuts and many fruits make use of the double curved surface structure [54]. These shells serve two purposes: On the one hand, they present a protective cover against environmental influences. On the other hand, they are an efficient static load carrying system. Furthermore, mammals and human beings also make use of the shell structures to protect sensitive vital parts, e.g. - the cranial bone, to mention just one example.

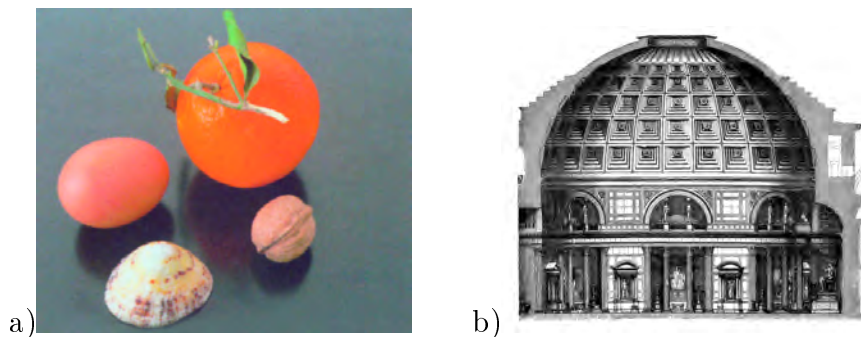


Figure 2.1: a) Examples of shells in nature b) Pantheon in Rome [29]

This functional, stable and esthetic load carrying system has been fascinating mankind for thousands of years [75]. The first documented cupola was built in the Bronze Age.

Also the ancient Greeks and Egyptians used cupolas and arches in their architecture. Especially the ancient Romans were interested in arches and cupolas and numerous magnificent buildings were erected - e.g. the Pantheon in Rome - see Figure 2.1 - which possessed the world's largest cupola for a period of more than 1700 years [29].

Later on, the shell structures experienced a revival documented by the erection of buildings like St. Peter's Basilica in Rome, St. Paul's Cathedral in London and Karlskirche in Vienna - to mention only a few of the best known domed structures. During the 20<sup>th</sup> century, robust and solid materials were developed, thus providing new opportunities for the construction of shells. This enabled the building of thinner shells with wider spans [33]. To the present day shells have not lost their fascination. Many famous architects and civil engineers use shell structures in their works. They try to advance shapes and production methods. Famous names like Heinz Isler Ramm and Schunk [67] and Frei Otto Otto [62] are often mentioned when shell structures are being discussed.

### 2.1.2 Properties

Shell structures belong to the category of surface structures [57] whose thickness  $h$  is small compared to its other dimensions. Surface structures can be divided into three categories: panels, slabs and shells. The definition for the panel states that its plane middle surface remains plane in the course of deformation, whereas the plane middle surface of a slab becomes curved by applying a load. By contrast, a shell has a middle surface which is already curved prior to deformation.

Shells can be classified in thin and thick structures. A shell can be called thin if  $(\frac{h}{L})_{max} \ll 1$  is fulfilled, so that the full three dimensional theory of elasticity is not required. In this condition the variable  $h$  describes the thickness of the shell.  $L$  is a characteristic dimension of the middle surface. The middle surface of a shell can be singly or doubly curved. Examples for singly curved surface structures are barrel vaults and cylinders, whereas a sphere and a hyperbolic paraboloid are doubly curved.

In order to classify doubly curved shells the *Gaussian curvature* is used [57, 30]. The Gaussian curvature  $K$  of a point on a surface is the product of the principal curvature  $\kappa_1$  and  $\kappa_2$ , of a given point – see equation 2.1.

$$K = \kappa_1 \cdot \kappa_2 = \frac{1}{R_1 \cdot R_2} \quad (2.1)$$

The principal curvature  $\kappa$  is defined as the reciprocal of the radius  $R$ . Basically three different situations can be identified: a positive  $K > 0$ , negative  $K < 0$  or zero  $K = 0$  Gaussian curvature. A sphere, for example, has a positive curvature whereas the hyperbolic paraboloid is a typical representative of a surface with negative curvature. Naturally, hybrid forms are also possible. If the Gaussian curvature amounts to zero, the shell structure is only singly curved, e.g. a cylinder. As a dome is a structural element of architecture that resembles the hollow upper half of a sphere, in this thesis only shells with positive Gaussian curvature are considered.

### 2.1.3 Structural behavior

#### 2.1.3.1 Load transfer

Due to their geometry, doubly curved shells are excellent load carrying systems transferring the loadings very efficiently to the foundations [21]. The advantages of a shell over a plane structure are going to be discussed in this chapter.

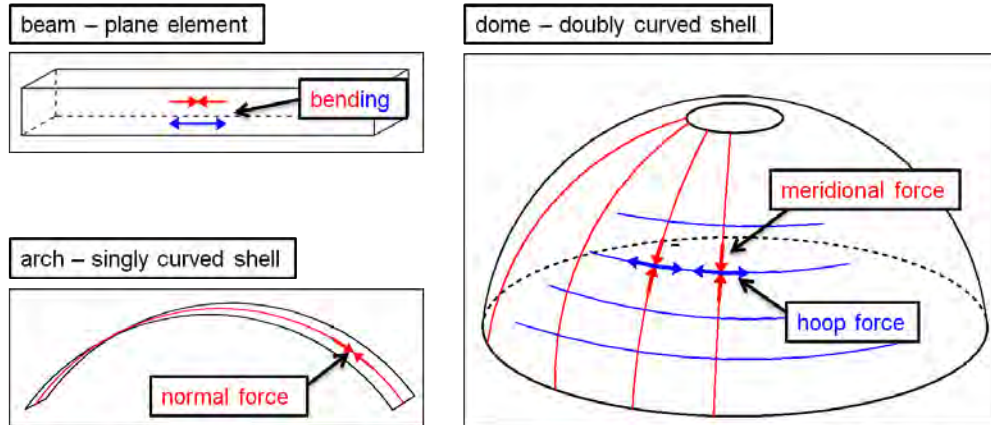


Figure 2.2: Load transfer of a beam, an arch and a dome [21]

A plane structure carries a load which is applied orthogonally to the center plane by bending – see Figure 2.2. Therefore, the distribution of the stresses over the height of the cross section is linear and, consequently, only the edges of the cross section can be used to their full capacity. Singly curved shells, however, have the attribute that uniform loads are mainly carried by normal forces – as long as the footings do not permit horizontal displacement. This is the optimal way to transfer the load to the foundations. As only normal forces appear, the stresses are equally distributed over the whole cross section so that every part of this cross section is uniformly involved in the load transfer.

When a uniformly distributed load is applied onto an arch, practically no bending appears in the structure. But once the load is changed to a partial load, substantial bending develops in the arch. In the case of a dome the uniform load is carried by forces in the plane of the shell that are similar to the forces carrying the uniform load in the arch. However, in the dome additional forces – called hoop forces – are set up at right angle to these arching or meridional forces.

Considering a dome bearing a partial load, the shell is able to carry this load almost entirely by arching forces as long as this load has a smooth variation. This action is quite unlike the action of the arch, and the reason for the difference is the existence of the hoop forces. Thus, whereas the arch is best suited to only one type of loading, the dome is well suited for almost any type of loading within certain restrictions.

Moreover, hoop forces allow a ring-by-ring construction of a dome without centering, an unfeasible task regarding an arch. As a result, though an arch is unstable without its keystone, a dome with an oculus is perfectly stable, as evidenced by the “incomplete” domes around the world.

### 2.1.3.2 Stresses in a flat slab and a hemispherical dome

The following example compares the stresses appearing in a circular plane plate to the ones in a hemispherical dome. The purpose of this sample calculation is to show the superior structural efficiency of a double curved shell structure.

Modeled after the ice dome built in the winter of 2010/11 which is described in chapter 10, the following requirements have to be fulfilled by the two structures discussed below. A space with a circular base area with a diameter of 10 *m* is to be surrounded by an ice structure with a thickness of 200 *mm*. Two different approaches are investigated. First, the stresses in the structure are calculated assuming that a flat circular plate is used to cover this area. An analytical solution to this problem is presented by Girkmann [28] using Kirchhoff's normal hypotheses. He gives a solution for a circular simply supported plate with a uniformly distributed load which is quoted in equation 2.2 and 2.3. The used parameters are according to Figure 2.3a [28].

$$m_r = (3 + \mu) \cdot \frac{p}{16} \cdot (a^2 - r^2) \quad (2.2)$$

$$m_\varphi = \frac{p}{16} \cdot [(3 + \mu) \cdot a^2 - (1 + 3\mu) \cdot r^2] \quad (2.3)$$

$m_r, m_\varphi$	sectional moment per unit of length according to the coordinate system in Figure 2.3a
$\mu$	Poisson's ratio
$r, a$	radius according to Figure 2.3a
$p$	vertical loading e.g. self weight of the shell or plate

Instead of using a flat slab as a roof, a dome structure can also be used. In this example a hemispherical cupola with a radius of 5 *m* is investigated. Pflüger gives an analytic solution for hemispherical domes using membrane theory [65]: The drawing in Figure 2.3b shows the parameter in these equations.

$$N_\vartheta = -p_E \cdot r \cdot \frac{\cos \vartheta_0 - \cos \vartheta}{\sin^2 \vartheta} \quad (2.4)$$

$$N_\varphi = p_E \cdot r \cdot \left( \frac{\cos \vartheta_0 - \cos \vartheta}{\sin^2 \vartheta} - \cos \vartheta \right) \quad (2.5)$$

$N_\vartheta$	normal force per unit of length in meridian direction
$N_\varphi$	normal force per unit of length in hoop direction
$\vartheta$	angle between the axis of the shell and the normal of the shell
$\varphi$	perimetrical angle

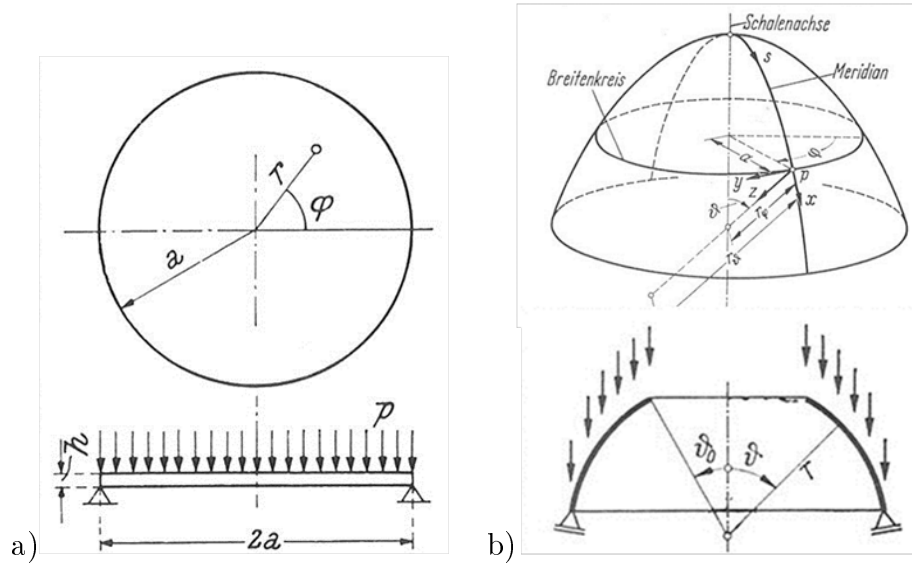


Figure 2.3: a) Definition of the parameters in equation 2.2 and 2.3 by [28] b) Definition of the parameters in equation 2.4 and 2.5 by [65]

$r$  radius

$p_E$  self weight of the shell

$\vartheta_0$  angle between the axis of the shell and the edge of the oculus

Figure 2.4 compares results of these two structures. The horizontal axis of this diagram shows the middle surface of the structure originating in the center of the plate or the apex of the shell. For the circular plate, this axis equals the polar axis of this slab. For the hemispherical shell the stresses following a meridian are depicted. This diagram shows the normal stresses in the middle surface. The stresses labeled  $\sigma_{xx}$  are the stresses acting in the same direction as the horizontal axis of the diagram in Figure 2.4 whereas the stresses  $\sigma_{yy}$  act perpendicularly to  $\sigma_{xx}$ . Positive values represent tension and negative ones compression. In this example, the specific weight of the ice is assumed to be  $9 \text{ kN/m}^3$  – see chapter 2.2.2. Figure 2.4 shows that the maximum stresses in the slab obviously occur in the center of the plate. The maximal tensile stress for this example amounts to  $1,35 \text{ N/mm}^2$  occurring on the underside of the slab. In the hemispherical dome, however, the tensile stress never exceeds  $0,045 \text{ N/mm}^2$  regarding this example, which is only 3 % of the tension in the flat slab. The behavior of the relation of the size of the maximum compressive stress in the two structures is identical: The maximum compressive stress in the slab is 30 times larger than the one in the dome.

This example shows that in a dome structure, the maximum stresses are considerably smaller than in a flat slab. Since ice was to be used as construction material, a structure in which small stresses occur is especially suitable due to the relative low strength of the ice compared to other construction materials.

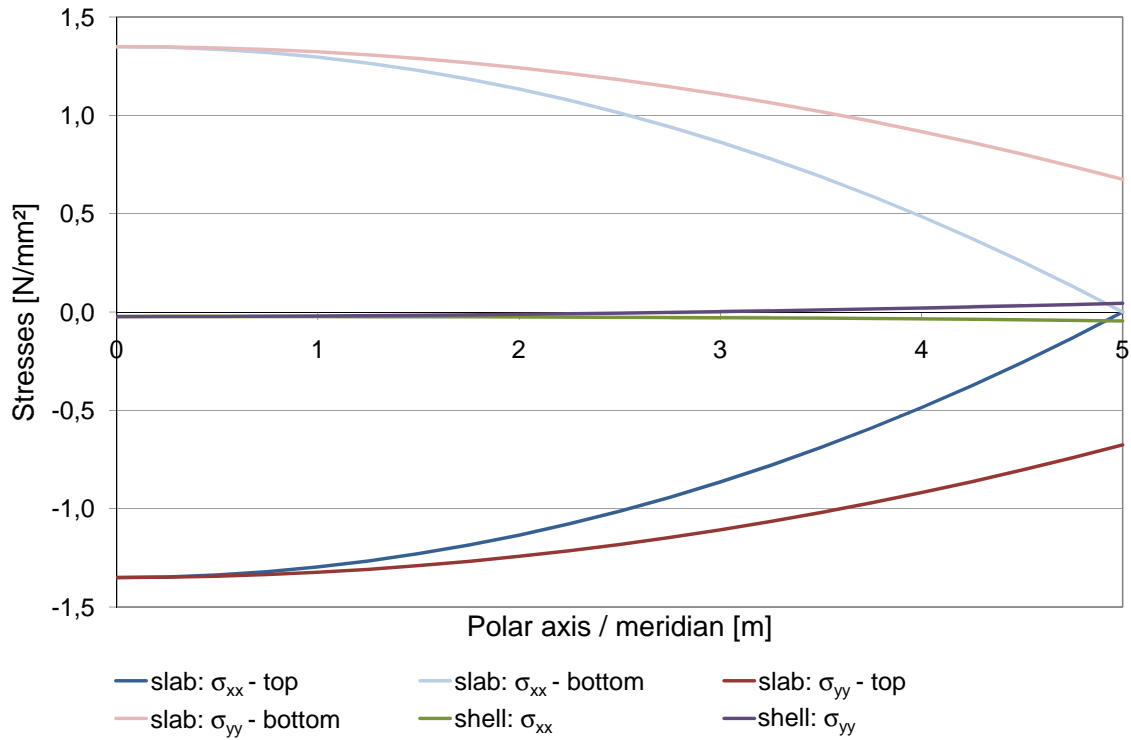


Figure 2.4: Stresses in the slab and the hemispherical dome

### 2.1.3.3 Definition of the stresses and the sectional forces

Figure 2.5 shows the definition of the section forces and moments used throughout this thesis. The index  $x$  always represents the direction of a meridian and the index  $y$  runs in hoop direction. Consequently, the stresses  $\sigma_{xx}$  are the normal stresses in meridional direction and  $\sigma_{yy}$  the normal stresses in hoop direction.

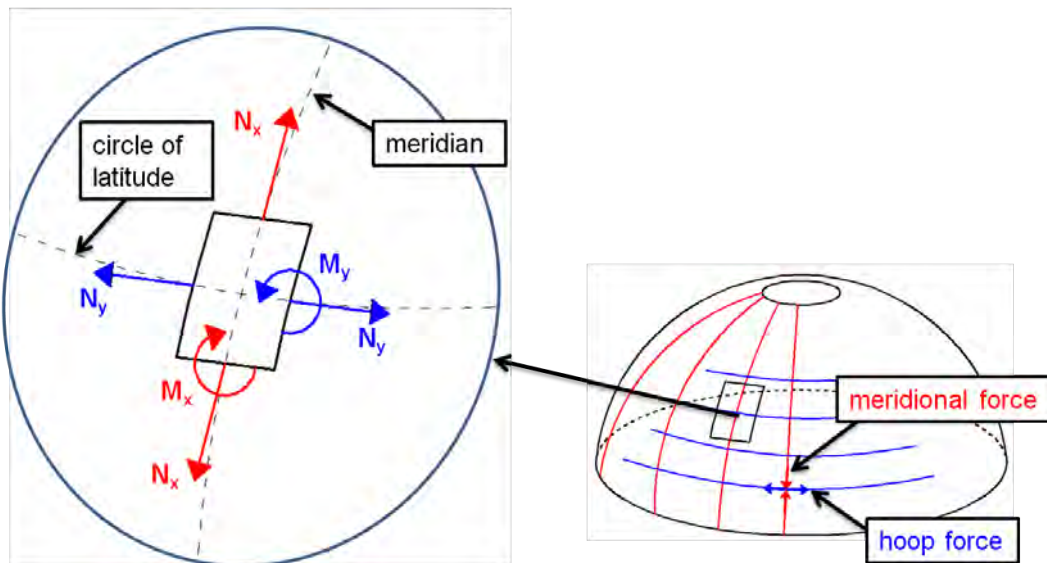


Figure 2.5: Definition of the sectional forces and moments

### 2.1.4 Construction methods

Finding the best concept of constructing a shell structure is highly dependent on the material used and the type of the shell. A geodesic dome, for example, consists of struts which are traditionally made of wood, steel or a lightweight material. For this kind of shell structure, pourable materials such as concrete or ice are not the optimum choice. As this thesis focuses on ice domes, only construction methods which are suitable for this material are going to be discussed in this chapter. Both materials, ice and concrete, are well suited for the building of a monolithic dome.

Traditionally, monolithic domes are produced by means of complex doubly curved timber or steel formwork. This formwork needs to carry the entire weight of the not yet matured material and therefore has to be robustly constructed. The building of this auxiliary construction requires a high level of attention in planning as well as in calculation – almost like a self-contained construction. But the whole formwork has to be removed after finishing the construction work and, in the majority of cases, the material cannot be reused after the shell has been completed. Since additional resources, such as time and material, are needed, the costs of this production method are thus raised significantly.

In order to achieve a more economic production of shell structures many new construction methods have been developed. Isler [67], for example, used a single formwork structure for more than one concreting step.

Another possibility to build concrete shells is the usage of precast elements. The prefabricated parts can easily be produced at the factory and subsequently be transported to the site. The same molds can be used several times to increase the cost effectiveness. An example for the application of precast parts is the extension of the hot springs in Bad Hofgastein in Austria [68], where a 7,45m high cupola was built with 20 precast elements. Because of the fact that these 20 precast parts were very large and unwieldy, the transportation and the assembly were a major challenge.

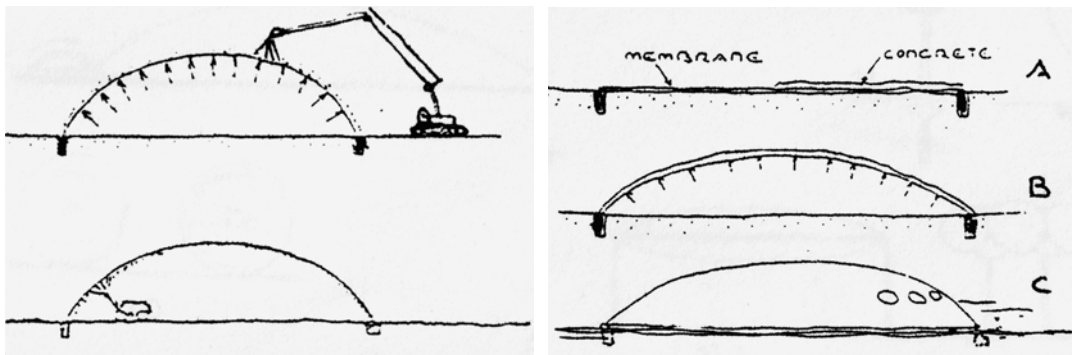


Figure 2.6: Construction methods of shells by Otto [63]

As an alternative to the conventional timber or steel formwork, pneumatic formworks may be used. Otto describes different applications of pneumatic formworks in his works [63, 62]. One possibility to build a thin concrete shell is to spray concrete on top of an inflated membrane. The membrane can be removed as soon as the concrete



is hardened. It is also possible to spray the inner surface of a pneumatic formwork with a non-dripping material. In this method, the pneumatic formwork also serves as a temporary mold (see Figure 2.6). Another procedure consists in inflating a membrane covered with freshly mixed steel reinforced concrete. The concrete matures according to the shape defined by the membrane. The pneumatic formwork is removed after the concrete has completely matured. Using a pneumatic formwork has the advantage that it can be delivered factory-assembled. On site the formwork only has to be inflated and no complex timber or steel formwork is necessary. Achieving the desired shape of the formwork can be problematic because the air-pressure in the pneumatic formwork has to be adjusted according to the progress of concreting. Moreover, working with fresh concrete and pneumatic formworks can be complicated when spraying or lifting the still free-flowing concrete.

Pneumatic formworks also prove to be an efficient method for the erection of ice domes. Kokawa [77] built numerous ice domes with various dimensions by covering an inflated membrane with thin layers of snow-ice sherbet. This construction method is described in detail in chapter 2.2.1.

Another construction method [51] can be applied for shells which are of the pure “hanging type”. On a frame of steel beams a cable net is constructed which consists of the reinforcement of the shell. Then a thin wire mesh is attached at the bottom side of the cable net to serve as lost formwork for the concrete. After the hardening of the concrete a reinforced concrete shell is obtained which is upside down with respect to its final position and therefore is has to be turned.

The Swiss engineer Isler [67, 22] became a pioneer in the field of form-finding by designing new shapes of shells for which no mathematical description existed. In his text *New Shapes for Shells* [32] he describes three different methods for finding nongeometric shapes for shells:

- *The freely shaped hill, for instance melded earth is the form.*
- *The membrane under pressure, where an inflated rubber membrane gives the shape.*
- *The hanging cloth reversed, where a draped fabric defines a surface shape just as a hanging cable defines a funicular line.*

With the material ice, he created numerous new and attractive variations of shell structures by spraying hanging webs, supported fabrics or inflated balloons with water.

## 2.2 Ice

### 2.2.1 Ice as construction material

Ice is a fascinating and natural material. Most people associate ice with images of glaciers, icebergs, frozen waterfalls or lakes, icicles or ice crystals. But there are also

numerous examples where ice is used as a load-bearing construction material. Ice roads or bridges are wide spread in the far north. In countries like Canada, Estonia, Finland, Norway, Sweden, Russia, United States and the Antarctica these human-made structures on the surface of rivers, lakes, bays or seas are part of the transport network during the winter season. To guarantee the safety of this transportation network, many investigations regarding the thickness and the loading of the ice were carried out, e.g. [40]. Moreover, governmental institutions of these countries provide reference values for the necessary thickness in order to be able to drive on the ice, e.g. *Environment Canada* [2]. Another example of a civil engineering structure made of ice is the railway ice bridge which was built over the river Dnieper during World War II [19].

Ice is also used in the field of superstructure work. Inuit used to build igloos with blocks of ice or compacted snow. These blocks were arranged hemispherical in order to form a dome.



Figure 2.7: LumiLinna - Snow Castle in Kemi, Finland

Nowadays, ice is used to build ice hotels or even ice villages mainly for temporary events or winter tourism. One example for an application is the yearly rebuilt ice hotel in Jukkasjärvi, Sweden [4] where catenarian structures are made of artificial snow. Artificial snow machines supply tons of snow with a high pressure to cover the formwork. This artificial snow thaws during the day, the water flows over the curve of the arch and turns into solid ice during the night. Moreover, large ice blocks weighing nearly 2 tons, and harvested from a wild river are also used for creating this ice complex.

A similar concept is used at *The Hôtel de Glace* in Canada [3]. In Finland the Snow Castle “*LumiLinna*” as well as the Snow Village in Lainio are built every year [5, 6]. Pictures of the Snow Castle in Kemi are shown in Figure 2.7. For constructing this snow castle molds are used in which snow is blown with a special snow blower. As soon as the snow has hardened, the molds are removed. Other examples of ice and snow constructions during the winter season are the *Alta Iglu Hotel* in Norway [7], the *Aurora Ice Museum* in Alaska, USA [8] and the *Iglu Dorf* in Switzerland [9]. In order to build the igloos in the *Iglu Dorf* in Switzerland, inflatable balloons are covered with snow thus obtaining the basic shape of the igloo. In the same manner igloos are added to the village until the desired number of igloos is reached. The entire igloo village is built as a tunnel system, so that from the outside the igloo village looks like a huge pile of snow with a few entrances.

Numerous applications of ice shell constructions for winter activities can be found in the north of Japan. In the 1980s, Kokawa developed a construction method for large ice shells. Since then he has built numerous ice domes with this method. In

the early 1980s, many field studies on ice domes with spans of  $10\text{ m}$  [43],  $15\text{ m}$  [45] and even  $20\text{ m}$  [50] were carried out by Kokawa in Asahikawa. These field studies included construction and creep tests. In 1991, the ice dome was even effectively used as storehouse and workshop in the basement-area of the Japan Observatory at the South Pole [42]. In 2001 a field study showed that the application of a  $30\text{ m}$  span ice dome for an architectural facility could be basically possible [46, 47].

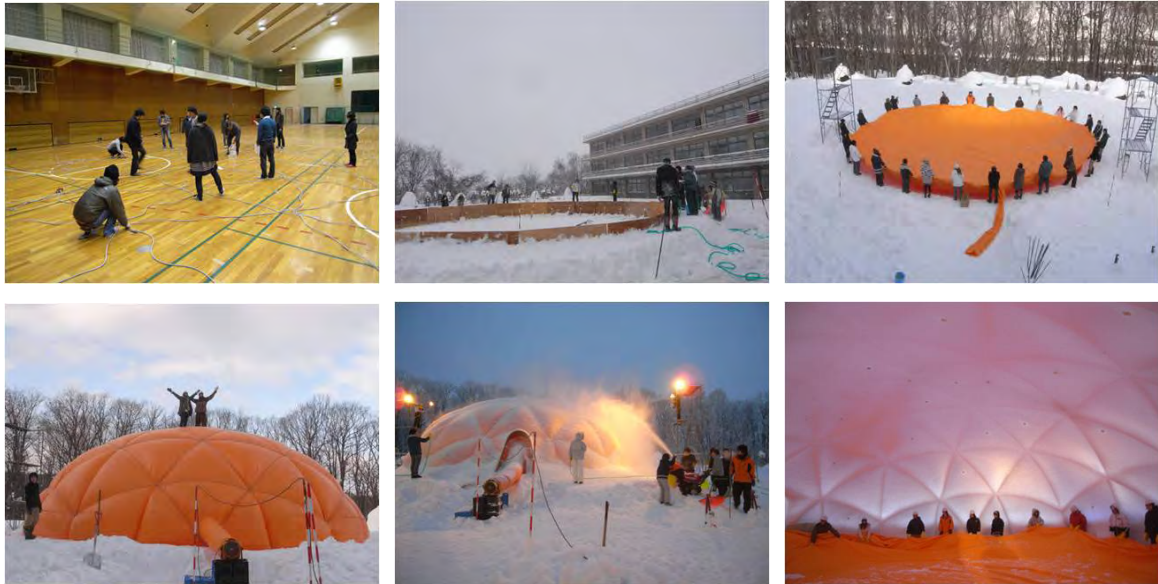


Figure 2.8: Construction sequence of Kokawa's ice dome construction method [77]

Figure 2.8 shows pictures of the construction of a  $15\text{ m}$  ice dome which Kokawa built in the winter of 2010 with his students. He describes the outline of the constructional sequence as follows [77]:

1. *Construct snow-ice foundation ring [...].*
2. *Building up the 3-dimensional formwork by inflating a 2-dimensional membrane bag [...], covered with ropes with a reticular pattern determined by the geodesic division of the non-spherical shape anchored to the snow-ice foundation ring.*
3. *Covering the membrane with thin snow-ice sherbet by blowing snow with a rotary snow blower and spraying tap water with an adjustable nozzle. The thin layer snow-ice sherbet is frozen by cold outside air per one operation of snow blowing.*
4. *Repeat the application of snow and water up to the designed ice thickness. Then remove the bag and ropes for reuse.*

Since 1997 these ice shells have been used as leisure facilities and a variety of temporary shelters such as winter storage of vegetables, a factory house for making Japanese “sake”, an exhibition hall for winter festivals and an indoor space for ice fishing. Ice shells have been built, inter alia, in Tomamu, Asahikawa, Syumarinai and Nakagawa [81, 48, 49].

Research on construction methods for ice shells were also carried out at Vienna University of Technology. In 2004 Kollegger presented a new construction method for dome structures for which he filed a patent under the title *Verfahren zur Herstellung von zweifach gekrümmten Schalen* [35, 34]. This construction method is suitable for both materials concrete and ice.

By applying said method, it is possible to build a doubly curved shell from a plate [54, 66, 41, 24, 53]. The key element consists in building a flat circular plate made of concrete or ice and soft styrofoam components. These soft styrofoam components are placed between concrete or ice segments and therefore enable the plate to be deformed.

A steel tendon is placed along the edge of the plate and a pneumatic formwork is situated under the concrete or ice plate. After the complete hardening of the concrete or the ice, the erecting becomes possible by stressing the tendon and simultaneously inflating the pneumatic formwork. The pneumatic formwork triggers the desired vertical impulse and it outweighs the dead load. During this lifting process the wedges made of styrofoam are compressed and thus it is possible to transform a plane plate into a doubly curved shell.



Figure 2.9: Transforming a concrete plate into a shell

The pictures in Figure 2.9 demonstrate the shaping process of a reinforced concrete shell with a diameter of 13 m built by the Institute for Structural Engineering at Vienna University of Technology, in June 2005.

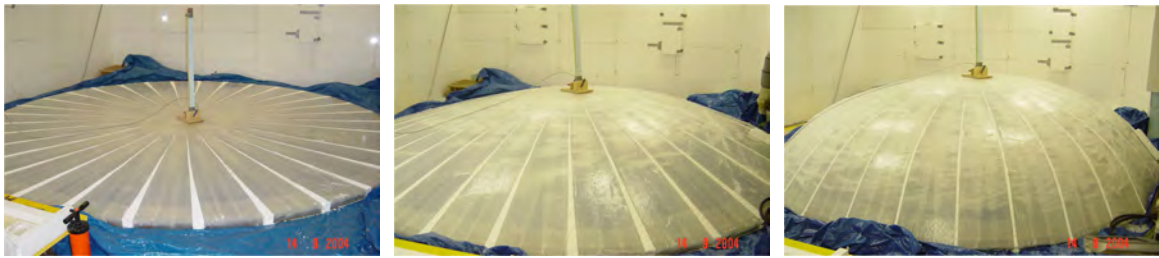


Figure 2.10: Laboratory experiment

The method was also applied for ice domes [36]. The shape of a dome with a span of about 5 m and a height of 0,9 m was chosen for the construction of the first shells and were made in the laboratory of the Institute for Structural Engineering which was isolated and equipped with a cooling unit for this purpose. A 40 mm thick and glass fiber web reinforced flat ice plate with 32 styrofoam segments was produced. Along the edge of the ice plate an unbounded tendon was placed and two stressing anchorages were provided. The tendon was stressed simultaneously at both anchorages up to a force of 50 kN. During the transformation from a flat plate to a shell the diameter was

reduced from  $5,2\text{ m}$  to  $4,8\text{ m}$  whereby the styrofoam segments were compressed from  $57\text{ mm}$  to  $17\text{ mm}$  at the circumference in order to gain the desired rise.

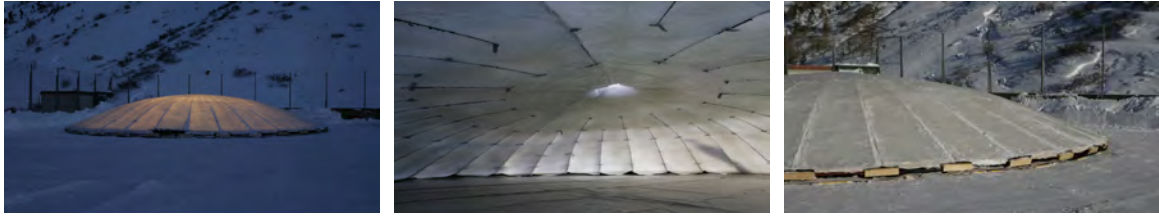


Figure 2.11: Ice dome 2005

This very same construction method was also used to build a large ice dome. In December 2005, a field test was carried out in Obergurgl, Tyrol. An ice dome with a diameter of  $13\text{ m}$  and a thickness of  $160\text{ mm}$ , originating from one flat plate was constructed. With this experiment, the functional capability of this construction method for ice shells could be proven on a large scale.

## 2.2.2 Mechanical properties of ice

Ice is a very complex material since its properties depend on numerous parameters which can change significantly over time. The aim of this thesis, however, is to develop new construction methods for ice domes, therefore the ice is only viewed as a construction material and no research was done to gain new insights in the material and structural behavior.

A great deal of research work on the material behavior of ice has been done all over the world. Naturally, the leading countries in this field of research are the ones with low temperatures and an abundance of ice and snow during the better part of the year, such as Canada, Norway, Sweden, Finland, Alaska and Antarctic.

Studying research literature, it can be observed that the strength of the snow and ice exhibit dependency on a variety of parameters such as strain rate, temperature, density, age, salinity, porosity, confinement pressure and orientation of loading.

Many experiments have been carried out in order to find a correlation between the compressive strength of the ice and the strain rate [64, 73, 25, 31, 69, 72, 20, 74]. Although it is difficult to compare these tests, due to the fact that they were carried out under different conditions, a basic trend could be observed in the behavior of the compressive strength: If the strain rate increases, the uniaxial compressive strength of the ice increases as well.

Studies in Norway [27] showed that the uniaxial compressive strength of polycrystalline ice is also very sensitive to temperature. At a constant strain rate the strength increased about one order of magnitude as the temperature decreased from  $-0,1^{\circ}\text{C}$  to  $-54^{\circ}\text{C}$ . But also in a temperature range between  $-0,1^{\circ}\text{C}$  and  $-3^{\circ}\text{C}$  a significant increase of the compressive strength can be observed. The tensile strength, however, does not seem to be influenced by the temperature that much.

Regarding the density of the ice, it can be summarized that the strength of the ice increases with increasing density [64, 20].

The strength of ice more than one year old stays more constant during changes in temperature than first-year ice [55]. Moreover, it has been investigated that the strength of sea ice is significantly lower than that of freshwater ice [64]. Age and salinity, however, do not play any role when a temporary ice dome is built on an inland site because only ice which is younger than one year and is made entirely of fresh water is used.

Like the strength of the ice the Young's modulus is also not a constant value as it is also highly dependent on influences like strain rate and temperature [16].

Standards on ice and snow construction are very rare all over the world. In Finland, however, the Association of Finnish Civil Engineers *RIL* published the standard *Snow constructions – General rules for design and construction* which also provides data on the strength and the deformation properties of snow ice [20].

Also at Vienna University of Technology test series on the material properties of ice were carried out [71]. Considering the results of these tests and the data existing in literature as well as the information provided by the Association of Finnish Civil Engineers *RIL* [20], the following material properties of ice are assumed for most of the calculations done in the course of this thesis and summarized in Table 2.1.

compressive strength	$\sim 4 - 5 \text{ N/mm}^2$
tensile strength	$\sim 1 \text{ N/mm}^2$
Young's modulus	$\sim 400 \text{ N/mm}^2$
specific weight	$\sim 9 \text{ kN/m}^3$

Table 2.1: Material properties of ice

Another complex material property of ice is its creep behavior [59, 80, 44]. In materials science, creep is the tendency of a solid material to deform permanently under the influence of stresses. Creeping is classified in three stages – see Figure 2.12. In the primary stage, the strain rate is relatively high, but decreases with increasing strain. The most important stage is the secondary stage which has a constant strain rate. The strain rate  $\dot{\epsilon}$  with the unite  $1/\text{sec}$  is defined as following:

$$\dot{\epsilon} = \frac{\Delta\epsilon}{\Delta t} \quad (2.6)$$

In tertiary creep, the strain rate exponentially increases which often leads to a collapse of the structure.

As shown in different experiments, the strain rate and therefore also the creep behavior of the ice, is dependent on the magnitude of the stresses. Many stress-strain-rate diagrams can be found in literature [56]. The stress strain rate is influenced by many parameters including temperature and the density of the ice. Basically it can be observed that the strain rate increases while the stresses or the temperature increase. At a certain strain-rate, however, the failure mode of the ice changes from ductile to brittle [58].

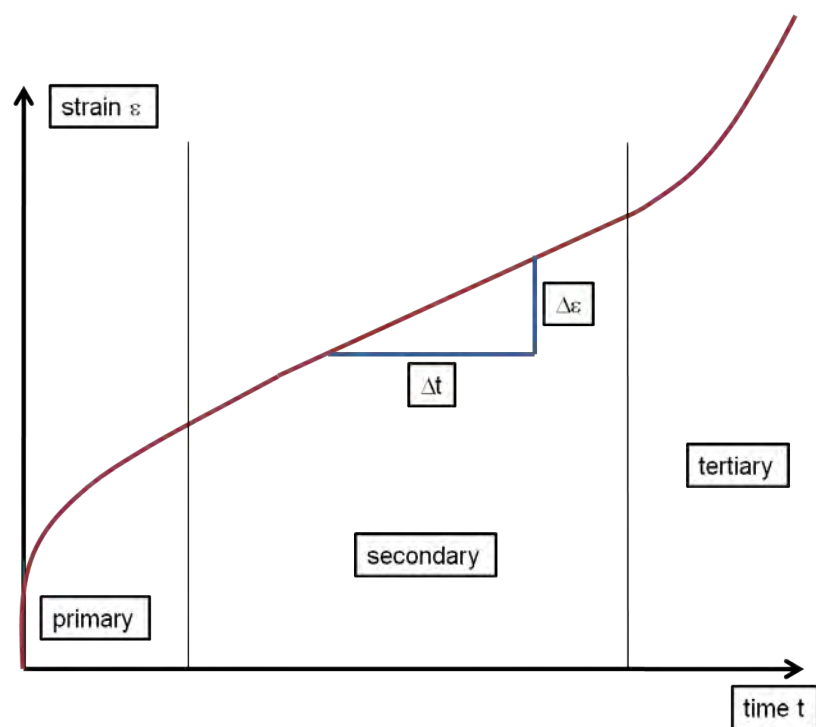


Figure 2.12: Stages of creep

# Chapter 3

## New construction methods

### 3.1 Basic principle

This thesis presents two new construction methods for shell structures using ice as building material. The basic concept is similar for both construction methods: In the initial position the intended shell structure consists of a plane plate which is subsequently transformed into a shell structure.

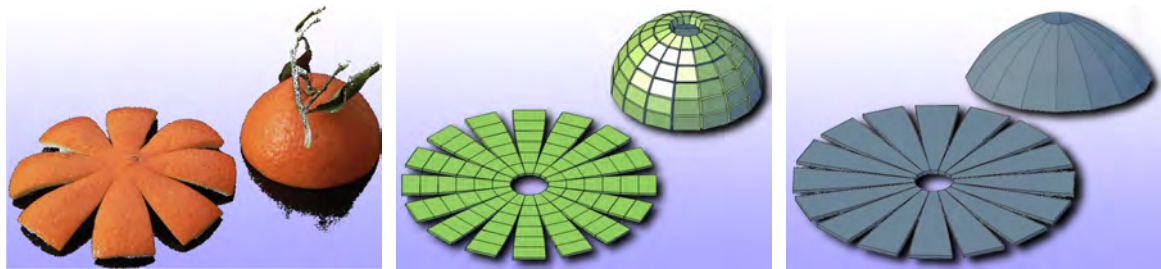


Figure 3.1: Basic principle of the new construction methods

One characteristic of doubly curved shells is that the surface is not developable which means that the surface cannot be flattened into a plane without distortion. If one tries flattening the hemispherical half of an orange peel into a plane surface, wedge-shaped gaps will open - see picture on the left in Figure 3.1. Referring to the example of the orange peel, a shortening of the circumference of 36 % is necessary to transform a circular disc into a hemisphere. These new construction methods make use of this very concept. Therefore the shape of the plane plate, which is going to be transformed into a shell, has to be chosen according to the final shape of the shell.

Two different construction methods will be presented in this thesis. The first method to be presented is called *Pneumatic Formwork Method*. For this construction method the shell consists of individual plane elements – see image in the center of Figure 3.1. The shape of these elements has to be chosen according to the final shape of the shell. The elements are placed on a planar working surface and are assembled by means of tendons. In order to transform the flat plate into a shell a pneumatic formwork is used –



hence the designation. While air is inflating the pneumatic formwork, the plane plate is transformed into a shell. For this construction method an Austrian patent application was filed in 2008 and granted in 2011 [38] and an European patent application was filed in 2009 [37].

In the alternative construction method the flat plate is divided into segments - see picture on the right of Figure 3.1 - which are distorted uniaxially and lifted into their final position. This method is called *Segment Lift Method*. For this construction method also a patent application was filed in 2009 [39]. Both construction methods will be described in details in the parts II and III.

### 3.2 Field experiments - ice domes

The two construction methods were first investigated theoretically and then tested in field experiments. After carrying out preliminary tests for both methods, they were tested in experiments.

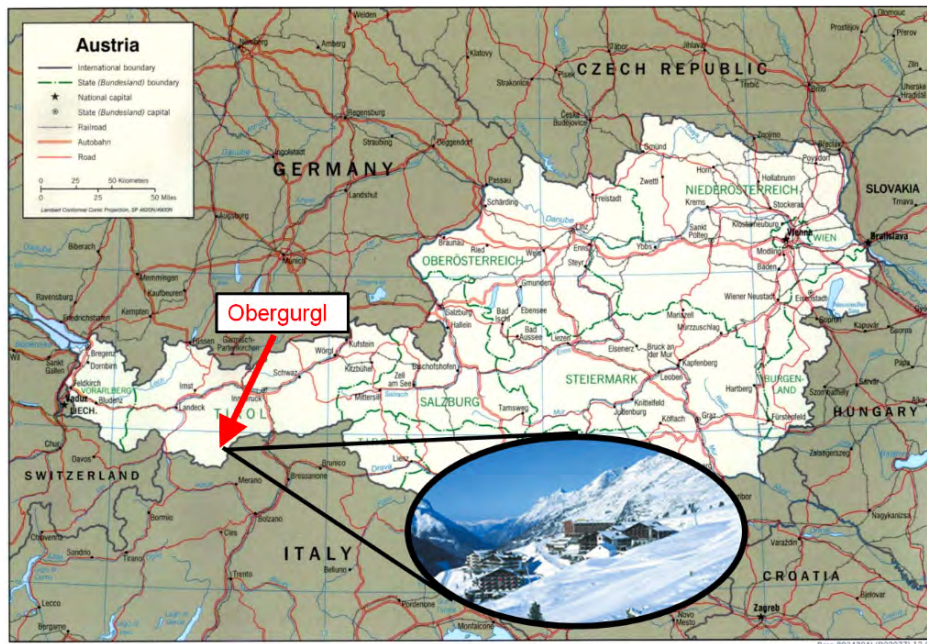


Figure 3.2: Map of Austria - Obergurgl

All four attempts to build an ice shell took place in Obergurgl, a village in the Alps in Tyrol, Austria, situated almost 2000 meters above sea level. Located in the municipality of Sölden, Obergurgl is a well known ski resort in Austria. Obergurgl is especially suitable for building ice shells because it is - referring to air temperature - one of the coldest villages in Austria. The location of Obergurgl can be learned from the map of Austria in Figure 3.2

The *Central Institute for Meteorology and Geodynamics (ZAMG)* [23], Austria's national weather service agency, has a weather station in Obergurgl. Figure 3.3 gives

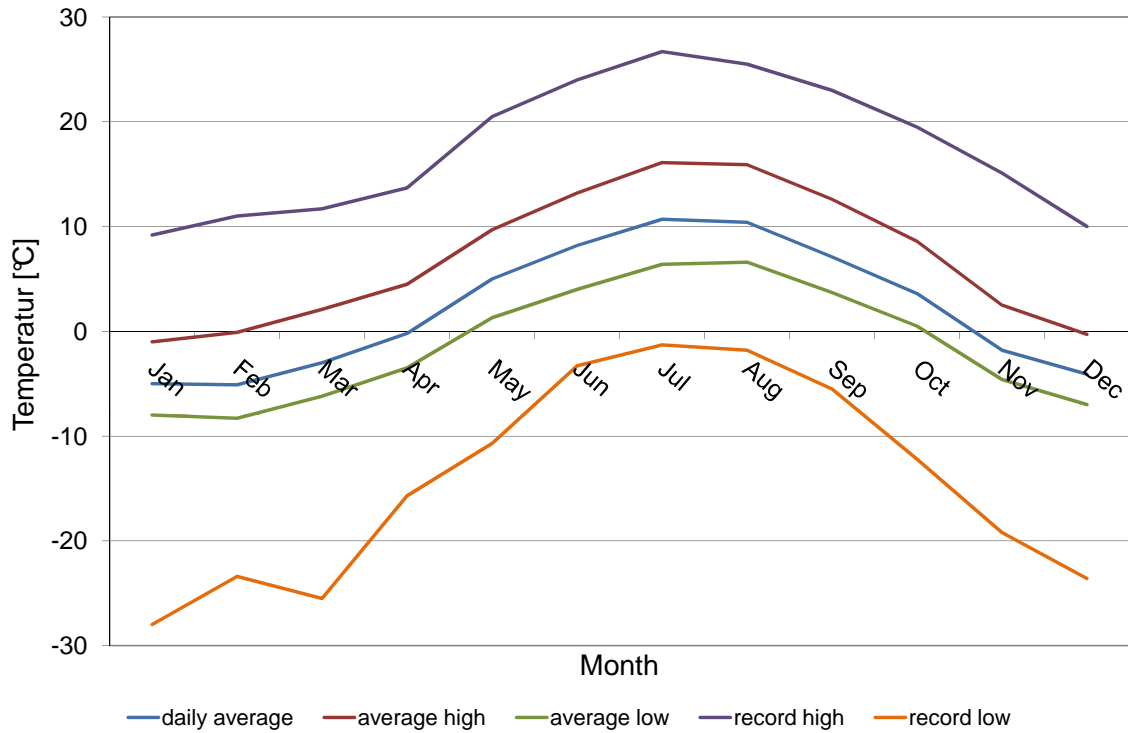


Figure 3.3: Air temperature in Obergurgl

an overview of the air temperatures in Obergurgl during the last 30 years. It can be observed that during the winter months, the average of the lowest temperature per day, is approximately  $-8^{\circ}\text{C}$ , which means that ice can easily be produced in this region. In this area, however, there are also warmer periods during the winter, when the so-called *föhn wind* is blowing in over the Alps coming from the Mediterranean Sea. During these warm periods the temperature can rise above freezing and the ice making process has to be delayed. Normally such föhn wind periods do not last more than a few days.

Finding a suitable location for the building of the experimental ice shells, low temperatures are not the only requirement. Moreover, a level area where water and electricity are available has to be found. Since Austria is a mountainous country and a lot of the available developed area is used for winter tourism, the construction site had to be chosen carefully. Fortunately, a level space where an ice plate with a maximum diameter of  $13\text{ m}$  could be built was provided by the Hotel Alpina to the Institute for Structural Engineering. In three consecutive winter seasons field tests were carried out in front of this hotel. The chapters 7 and 10 contain a detailed description of these field experiments.

## Part II

# Pneumatic Formwork Method

# Chapter 4

## Basic principle

### 4.1 General description of the method

The key element of this method consists of building a doubly curved shell emanating from a plane starting position.

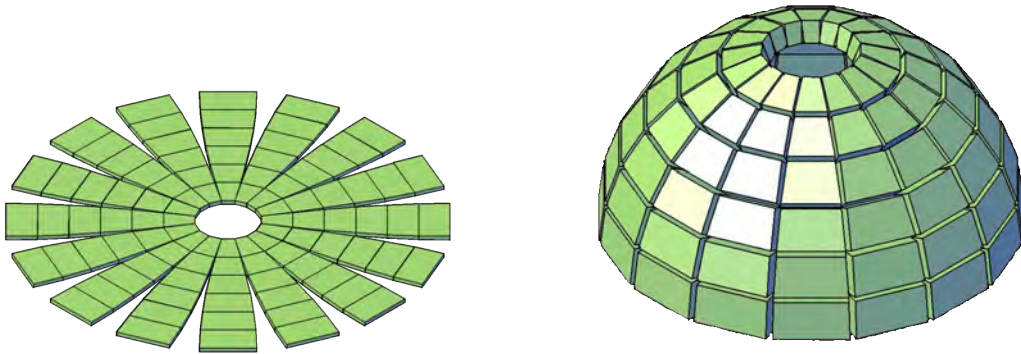


Figure 4.1: Pneumatic formwork method - from the starting position to the finished shell

A shell built by this construction method consists of individual plane elements which are connected in order to form a flat plate and are subsequently transformed into a shell. The shape of the plane elements has to be chosen according to the final shape of the shell. Strictly speaking, this structure is not a shell but a polyhedron because the shell is approximated by flat faces and straight edges.

This construction method is shown by an example of a hemispherical cupola consisting of 96 elements. These elements can either be prefabricated and subsequently transported to the building lot, or produced directly on site depending on the material used and the environmental influences.

The elements are placed on a plane working surface as shown in the plan view in Figure 4.2. In order to build a hemispherical dome the structure is divided into sixteen

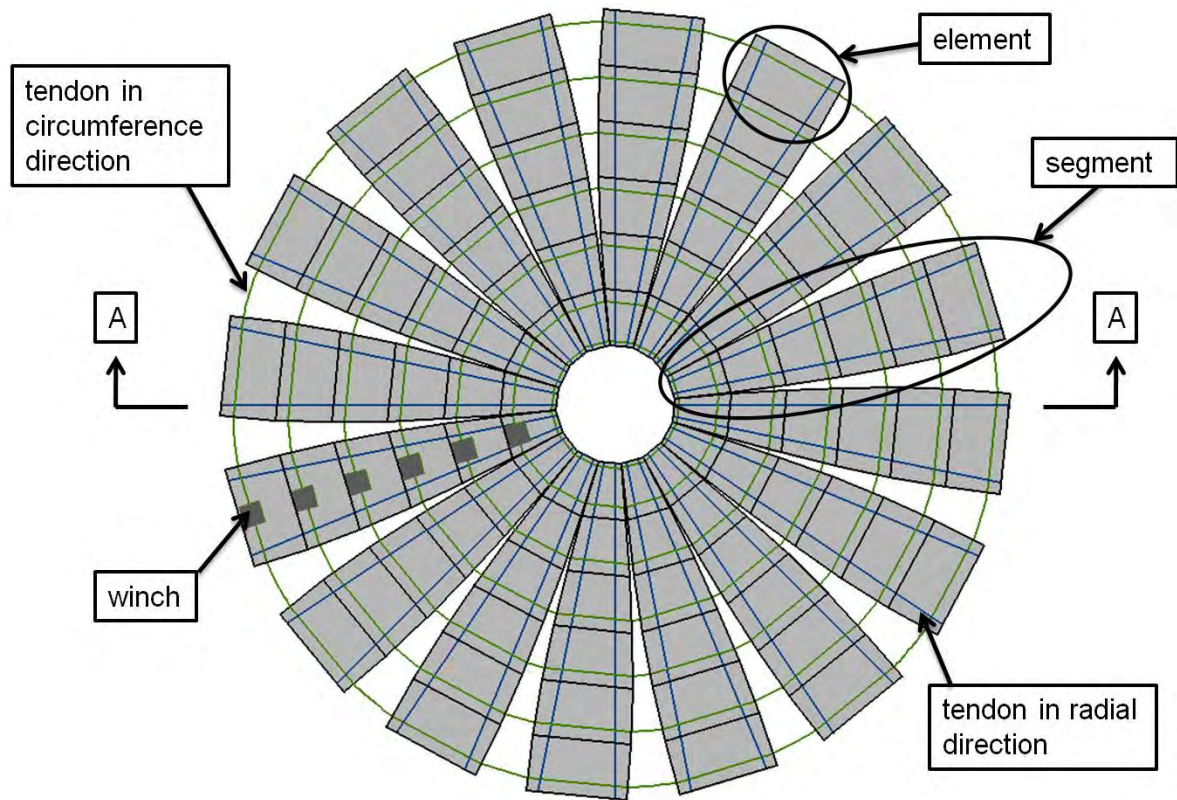


Figure 4.2: Pneumatic formwork method - plan view

segments and each of them is subdivided into six individual elements. Therefore this structure consists of  $16 \times 6 = 96$  elements approximating a hemispherical dome.

The elements placed on the working surface are kept together by tendons and, thus, they have to be equipped with ducts during their production process. These individual elements are connected to form a plate by the tendons and these tendons create a hinged connection. As shown in Figure 4.2, there are tendons in the radial direction holding the elements together as well as tendons in the circumference direction. During the erection process these tendons in circumference direction are instrumental for the assembly of the elements. Winches are needed to tighten these tendons ensuring that the elements are joining properly.

In order to transform the plate into a shell a pneumatic formwork placed under the precast elements, is used. The pneumatic formwork has the same shape as the finished shell structure. While air is inflating the pneumatic formwork the elements lift and as a result the plane plate is transformed into a shell. Simultaneously, the winches tighten the tendons in the circumference direction to ensure the desired final position. After the transformation process the interfaces are filled with grouting material. Moreover, after the erection process and after deflating the pneumatic formwork, the tendons in the circumference direction at the bottom of the dome may be used to carry the horizontal force.

Figure 4.3 shows the sectional view A – A of the plate shown in Figure 4.2 before as well as after the transformation into a shell.

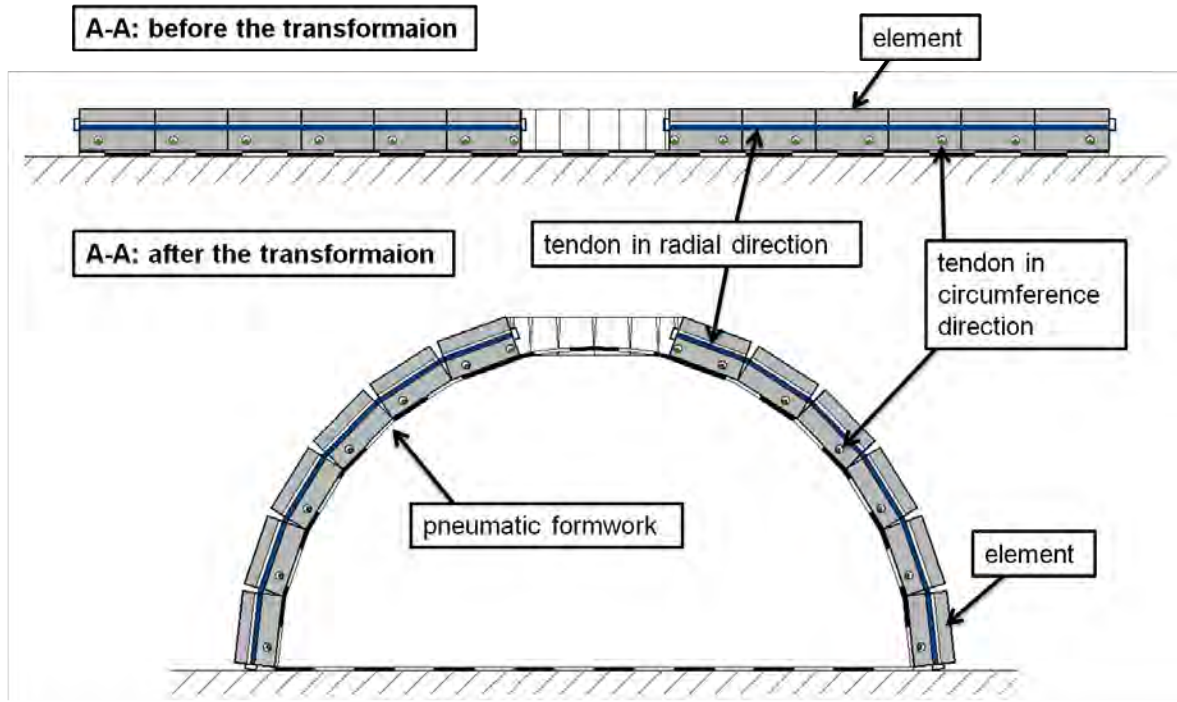


Figure 4.3: Pneumatic formwork method - sectional view

## 4.2 Experiments

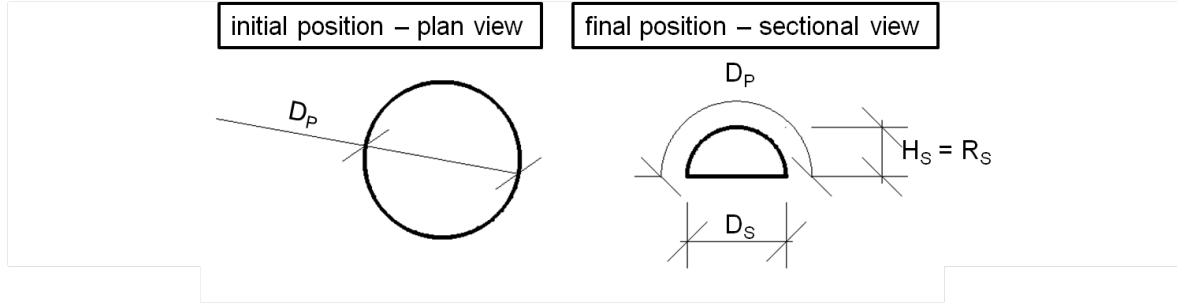
Field experiments were carried out to demonstrate and test this new construction method. Preliminary tests were performed by building wooden models and a concrete shell. Afterwards this method was tested on two ice shells. All experimental structures had a similar geometry. The shells were polyhedrons approximating a hemisphere with 96 elements – sixteen segments with six elements each – as shown in the example in chapter 4.1. Table 4.1 provides an overview of the geometry and the dimensions of

	diameter		height $H_S [m]$	material	thickness $t [mm]$	slenderness $R_S/t [ ]$
	plate	shell				
	$D_P [m]$	$D_S [m]$				
Timber model 1	2	1,3	0,65	wood	20	33
Timber model 2	4	2,6	1,3	wood	20	65
Concrete shell	13	8,3	4,1	concrete	50	82
Small ice shell	6	3,8	1,9	ice	120	16
Large ice shell	13	8,3	4,1	ice	200	21

Table 4.1: Overview of the experiments

the experiments which were carried out using this method. In their initial position the domes were plane plates with a plate diameter  $D_P$ . By inflating the pneumatic formwork, which was situated underneath the elements, the flat plate transformed into a hemispherical dome. The respective diameters of the shells  $D_S$  and their heights  $H_S$  can also be seen in Table 4.1. Because of the fact that all shells were hemispheres the



Figure 4.4: Correlation between  $D_P$  and  $D_S$ 

correlation of the plate diameter to the shell diameter can be described with equation 4.1 (see Figure 4.4).

$$D_S = \frac{2 \cdot D_P}{\pi} \quad (4.1)$$

Table 4.1 provides the thickness of each shell as well as its slenderness. The slenderness is defined as the ratio of the radius  $R_S$  to the thickness  $t$ . The preliminary experiments as well as the ice shells are described in detail in the chapters 6 and 7.

## 4.3 Numerical and analytical simulations

### 4.3.1 Polyhedron versus dome

The geometrical structure of an ice dome built by this construction method resembles a polyhedron. According to the example described in chapter 4.1, the polyhedron consists of 96 elements approximating a hemispherical shell.

In this chapter the sectional forces and moments of a hemispherical shell structure are compared to the ones received by calculating with the actual shape. These numerical simulations are carried out using the properties and geometries of the large ice shell designed for the field experiment – see chapter 7. The 96 individual elements are shaped according to Figure 6.9 and Table 6.2 in chapter 6.2.2 with a thickness of 200 mm.

The 3D finite element analysis program *RFEM 4* created by Dlubal Software [13] was used to study the influence of a facet shaped surface. Three different linear elastic 3D models were created. In the first model, the ice structure is shaped as a polyhedron with its 96 faces. In the second model, a polyline consisting of six straight lines resembling the polyhedron is rotated around a rotational axis. Therefore, a rotationally symmetrical dome develops which still has discontinuities along the meridians. In the third model these discontinuities are ignored and a smooth circular curve is rotated around the rotational axis, in this way a hemispherical shell with an oculus is created. In all three models the mass density of the ice is set to  $9 \text{ kN/m}^3$  and the Young's modulus amounts to  $400 \text{ N/mm}^2$  – compare chapter 2.2.2. Moreover, all three models experience identical boundary conditions. The base of the dome is always fixed with

horizontally moveable supports assuming that no thrust force can be carried by the subsoil.

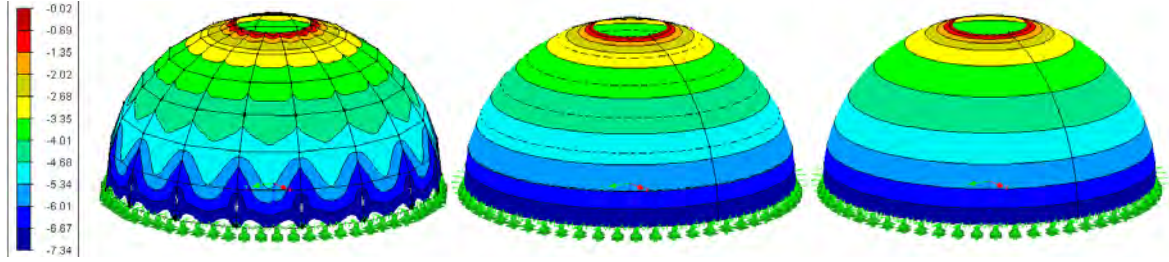


Figure 4.5: Meridian section forces  $N_x$  [ $kN/m$ ]

Figure 4.5 to 4.8 compares the results of these simulations. Figure 4.5 shows the normal forces in meridian direction  $N_x$  in  $kN/m$ . It can be observed that these forces are almost identical, independent of the precise geometry of the shell structure. Only because of the non-rotationally symmetrical geometry of the polyhedron, the loading is also not rotationally symmetrical with higher values on the edges of the segments.

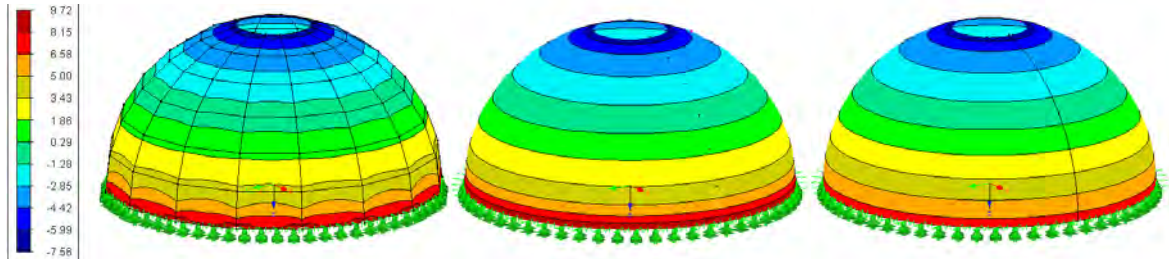


Figure 4.6: Hoop section forces  $N_y$  [ $kN/m$ ]

The forces in the hoop direction  $N_y$  are also not highly influenced by the differences in the geometry – see Figure 4.6. A small increase of the tensile forces can be observed on the base of the shell of the first and second model. The boundary conditions in these two models do not meet the requirements of the membrane theory. According to the membrane theory, only reaction forces tangential to the shell structure are permitted. The horizontal moveable supports are exactly perpendicular to the hemispherical sphere. If this sphere, however, is approximated with six plane elements in meridian direction, the part on the very bottom does not include an angle of  $90^\circ$  with the vertical.

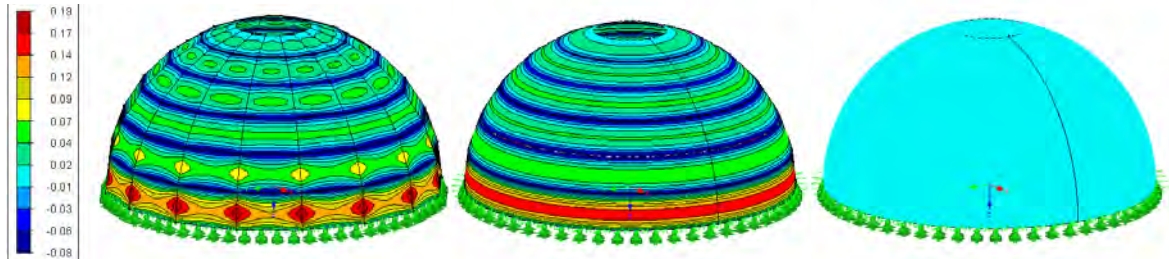


Figure 4.7: Section moments  $M_x$  [ $kNm/m$ ]



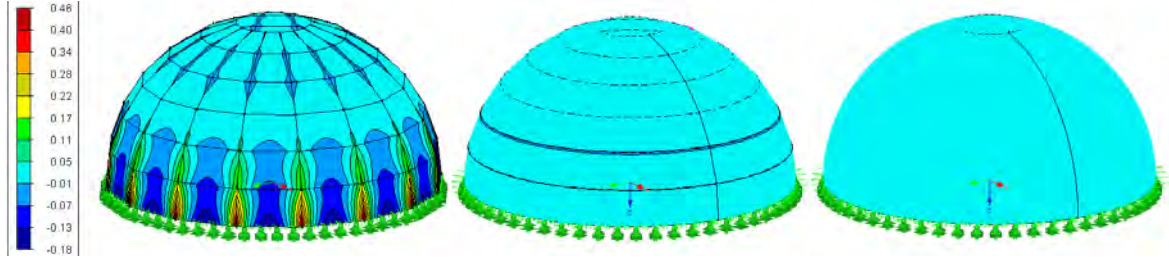
Figure 4.8: Section moments  $M_y$  [ $kNm/m$ ]

Figure 4.7 and 4.8 show the sectional moments  $M_x$  and  $M_y$ . The definition of these moments is given in Figure 2.5. Obviously, the bending moments in a spherical shell supported with boundary conditions according to membrane theory and a uniformly distributed load, disappear almost completely. The larger the discontinuities in the dome structure, the larger the sectional moments occurring on the edges between the elements. The highest bending moments, however, appear on the base of the shell structure.

Regarding these simulations on three different models, it can be derived that no significant simplifications are made by calling this polyhedron a hemispherical shell structure.

### 4.3.2 Stresses occurring during the construction process

During the construction process the elements are supported by the pneumatic formwork practically on the entire surface and held together by the tendons. Therefore, no large loads and stresses occur in the shell structure during the construction process in the material ice. The weight of the ice dome, however, has to be carried by the pneumatic formwork. The air pressure required in the membrane depends on the weight of the elements and on the size of the base area of the pneumatic formwork. As described in equation 4.2, the pressure  $p$  in the formwork is proportional to the dead weight  $G_{shell}$  of the structure and inversely proportional to the base area  $A_{base}$  of the pneumatic formwork.

$$p = \frac{G_{shell}}{A_{base}} \quad (4.2)$$

	air pressure [mbar]
Concrete Shell	24
Small Ice Shell	23
Large Ice Shell	36

Table 4.2: Overview of required air pressure

Table 4.2 gives an overview of the air pressure required during the preliminary test with the concrete shell and the field experiments with the ice shells. In these calculations

it is assumed that the base diameter of the pneumatic formwork always equals the diameter of the shell  $D_s$  of the respective shell – shown in Figure 4.4 . Moreover, the self weight of the pneumatic formwork is neglected. It can be observed that the pressure in the pneumatic formwork is always located in the range of millibar.

During the construction process this equally distributed air pressure in the pneumatic formwork causes a tensile force in the membrane. The size of the tensile force  $F_t$  in the membrane is proportional to the air pressure  $p$  and to the radius  $R$  of the formwork – shown in equation 4.3 and 4.4. Therefore the stresses in the membrane can be influenced by the air pressure and the shape of the formwork.

$$F_t \propto p \quad (4.3)$$

$$F_t \propto R \quad (4.4)$$

The loading of the tendons in radial direction is only influenced by the self weight of the shell structure and therefore these tendons have to be chosen accordingly, e.g. steel ropes. The tendons in the circumference direction are instrumental during the erection process and have to be tightened by means of winches. Therefore the maximum tension experienced by these tendons depends on the force applied by the winches.

### 4.3.3 Considerations regarding the shape

As shown in the preliminary experiments in chapter 6.2, the tensile stresses in the membrane are a crucial factor. These stresses are dependent on the air pressure and the radius of the formwork. In the following considerations the shape of the ice dome is varied with the aim to reduce the forces in the membrane. In the following simulations the arch length, the thickness as well as the specific weight of the shell are given values and are not varied. According to equation 4.3, the tensile forces in the membrane can be reduced by reducing the air pressure in the membrane. The air pressure, however, increases with the self weight of the shell and decreases with the base area of the pneumatic formwork – compare equation 4.2. Due to the fact that the surface load is a constant factor in this consideration, the ratio of the curved area of the spherical cap  $M$  to the surface area of the flat disk  $A$  is calculated while varying the central angle  $\theta$  . The central angle  $\theta$  is depicted in Figure 4.9. When decreasing  $\theta$  and keeping the

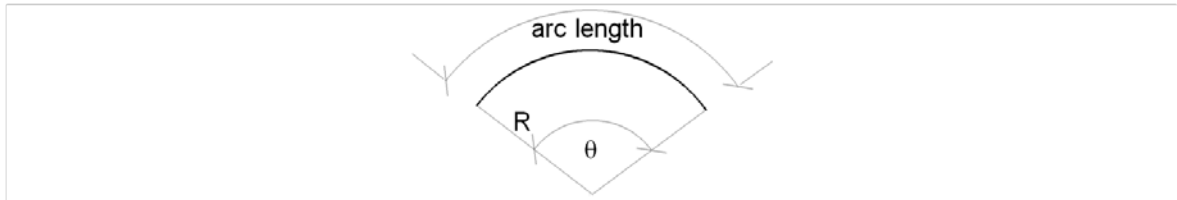


Figure 4.9: Spherical cap with the central angle  $\theta$

arc length constant the radius changes, thus the hemisphere becomes a spherical cap.

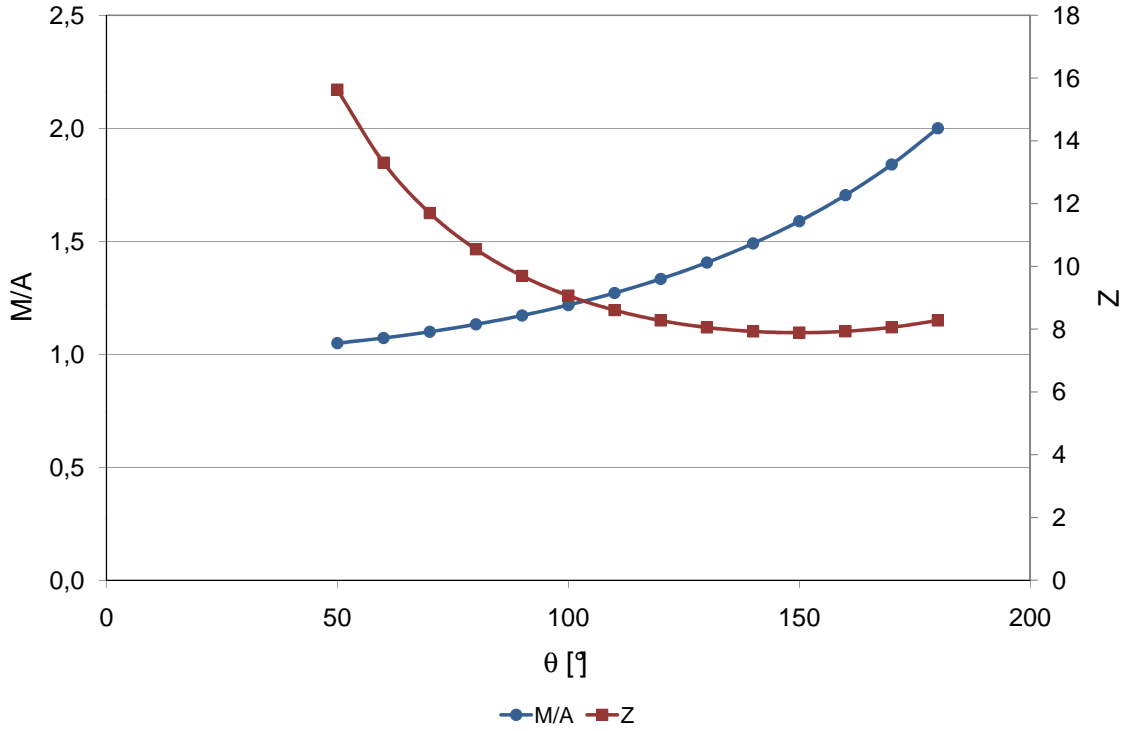


Figure 4.10: Correlation between  $M/A$  and the central angle  $\theta$  and  $Z$  and  $\theta$

The blue curve in Figure 4.10 shows the value of the ratio  $M/A$  which is directly proportional to the air pressure in the membrane considering different central angles  $\theta$ . Considering this curve, it could be assumed that building an ice shell with the shape of a spherical cap with a small central angle decreases the forces in the membrane dramatically. But the forces in the pneumatic formwork do not only depend on the air pressure but also on the radius – see equation 4.4. Therefore the indicator  $Z$  is introduced as defined in equation 4.5.

$$Z = \frac{M \cdot R}{A} \quad (4.5)$$

$Z$  is directly proportional to the tensile force in the membrane, taking the air pressure and the radius into account. The red line in Figure 4.10 refers to the secondary vertical axis and shows the indicator  $Z$  considering different central angles  $\theta$ . This line, however, increases when  $\theta$  is decreasing. Therefore building a spherical cap may decrease the necessary air pressure but has little influence on the tensile forces  $F_t$  in the membrane.

#### 4.3.4 Stresses in the finished structure

As described in chapter 4.1, in the finished shell the interfaces between the elements are filled and thus the entire structure functions as a shell, carrying the load by meridian and hoop forces. In meridian direction, only compressive stresses occur as shown in Figure 4.5 in chapter 4.3.1. These stresses can easily be carried by the ice. In

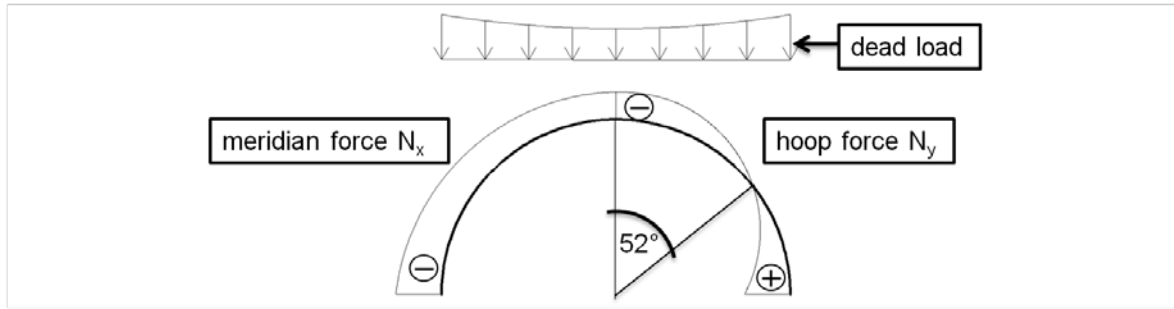


Figure 4.11: Schematic drawing of the force distribution of a hemispherical dome under self weight

circumference direction of a spherical dome, the hoop forces caused by dead load are distributed as shown in Figure 4.11. At the top of the dome, compressive forces occur, whereas below a vertical angle of  $52^\circ$  tensile stresses exist.

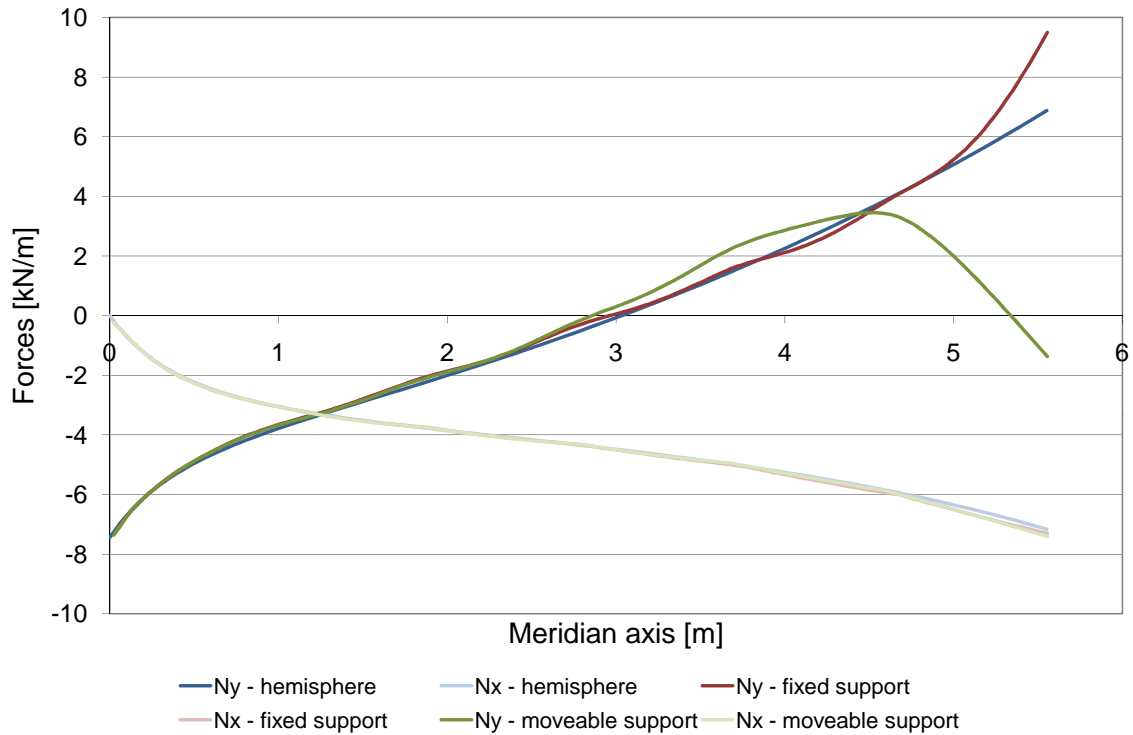


Figure 4.12: Meridian and hoop forces in the finished shell structure

Figure 4.12 shows the size of the meridian and hoop forces regarding a shell structure with the same geometric and material specific properties as the one described in chapter 4.3.1. The horizontal axis in Figure 4.12 represents a meridian axis of a hemispherical ice dome with its point of origin at the edge of the oculus. On the vertical axis, the forces per unit length in  $kN/m$  are depicted – positive values represent tension and negative values compression. The curves displayed in light colors show the meridian forces and the ones in dark colors the hoop forces. Three different situations are taken into account.

The blue curves show the meridian forces  $N_x$  and the hoop forces  $N_y$  calculated analytically with the equations given by Pflüger [65] and shown in equation 2.4 and 2.5.

The forces displayed as red lines refer to the finite element analysis of the second model in chapter 4.3.1. Moreover, in this figure, another boundary condition of the same finished ice shell is also investigated. The green curves show the forces occurring when the shell is fixed to the subsoil in such a manner that neither vertical nor horizontal displacement is permitted. Due to this boundary condition the line supports experience a horizontal reaction force of approximately  $1,0\text{ kN}/m$ .

Due to the fact that the tensile strength of the ice is quite low – see chapter 2.2.2 – the tendons in the circumference direction are used to carry the tensile forces in the hoop direction. By integrating the tensile hoop forces the total tensile force in the circumference direction can be calculated. When the red curve is integrated in the area between  $2,86\text{ m}$  and  $5,58\text{ m}$  it can be seen that the tendons have to carry a total force of  $8,5\text{ kN}$ . Considering the model with the fixed supports, the area under the dark green curve only amounts to  $5,2\text{ kN}$ . However, using these boundary conditions, part of the horizontal thrust is carried by the supports. When converting the horizontal reaction force into a force in the circumference direction, a tensile force of  $3,2\text{ kN}$  is gained. When adding this force carried by the supports to the  $5,2\text{ kN}$  it can be shown that the total horizontal thrust is independent from the boundary conditions. This tensile force has to be carried by the tendons in the circumference direction. As three tendons are situated in this area, each of them only has to carry a maximum force of  $2,8\text{ kN}$ .

# Chapter 5

## Pneumatic formwork

### 5.1 Material of the pneumatic formwork

#### 5.1.1 The PVC-membrane

The material used for the pneumatic formwork was a polyvinyl chloride membrane. Its material properties are summed up in Table 5.1. The PVC membrane used is fabricated by the Austrian company *Sattler AG* and sold under the label *641 Polyplan Complan®* [18].

base	PES
yarn	1100 <i>dtex</i>
weave	L 1 : 1
total weight [ $g/m^2$ ]	670
tensile strength [ $N/5cm$ ]	3000
tear resistance [ $N$ ]	220/200
adhesion [ $N/5cm$ ]	110
cold resistance	$-30^{\circ}C$
heat resistance	$+70^{\circ}C$
colour fastness	<i>min.7</i>
flame retardness	$< 100mm/min$

Table 5.1: Data sheet of 641 Polyplan Complan® [17]

This type of material was chosen based on preliminary experiments with different materials and seams for pneumatic formwork. The results of these tests carried out at our institute, the Institute for Structural Engineering at Vienna University of Technology are summarized in a Master's Thesis [70]. In this thesis four different types of membranes were tested; three of them were made of polyethylene and one of polyvinyl chloride. Moreover, different types of seams were tested, e.g. adhesive tape and PVC glue. These preliminary experiments show that a PVC-membrane is the most suitable of the materials mentioned. The seams were made by means of appropriate PVC glue produced by the same company as the PVC membrane.

### 5.1.2 Material tests

In order to gain a better understanding of the material used for the pneumatic formwork, three series of tests were carried out.

The PVC membrane used – described in chapter 5.1.1 – is composed of a woven fabric. This kind of textile consists of two distinct sets of yarns. The threads which run lengthwise are called the warp and the threads which run across from side to side are called the weft. Because of this particular manufacturing method it can be assumed that this material is isotropic, therefore the membrane was tested in the direction of the warp as well as the weft. Most of the PVC-membranes used to create a pneumatic formwork were printed with single-color stripes. This print always runs parallel to the warp yarn.

The next chapters describe these three sets of uniaxial tensile tests. The load was always applied displacement controlled. In the Tables 5.2, 5.3 and 5.4 the geometry of the specimens is summarized. The length always refers to the dimension of the specimen in the direction of the applied load whereas the width is the size perpendicular to the direction of the force. In all experiments the same PVC-membrane with a thickness of  $0,41\text{ mm}$  as described in chapter 5.1.1 was used.

#### 5.1.2.1 Experiments on the seams

In the first series of experiments different types of seams were tested. In a total of fourteen experiments different possibilities to glue, sew and weld were investigated.

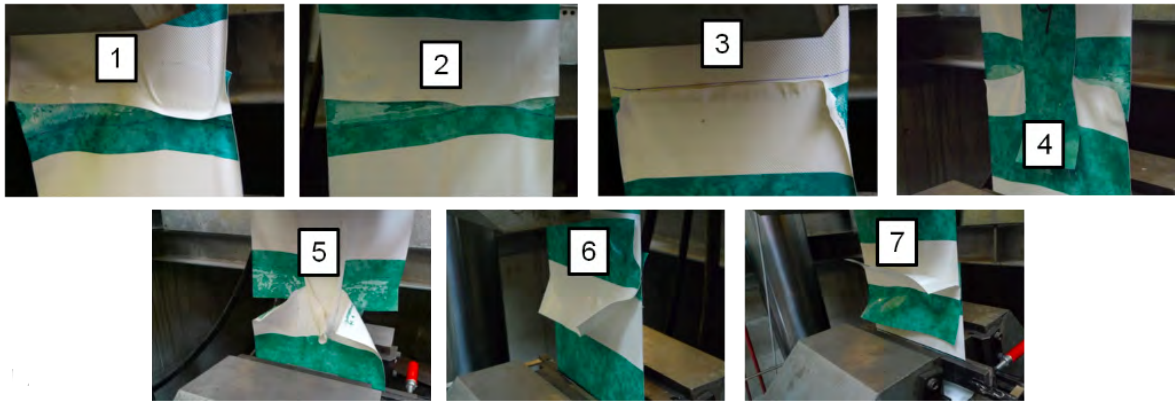


Figure 5.1: Glued seams - specimen 1 to 7

In principle, a seam can either be made by overlapping or by folding in the two membranes. To make an overlapping glued seam the border area of two membranes is coated with glue and the two foils are put on top of each other. At a folded in seam both glue-coated surfaces are on the inner side of the membranes. Both boundary areas of the foils are flexed  $90^\circ$  and glued together on the facing surface.

All seams were arranged parallel to the warp, therefore the force was applied perpendicular to the warp and to the printed stripes. This configuration was chosen because

spec. No.	width [mm]	length [mm]	type of seam	max load [kN/m]
1	250	310	glued - 60 mm overlapping	14,8
2	250	325	glued - 60 mm overlapping	13,6
3	250	293	glued - 100 mm overlapping	16,8
4	250	315	glued - 60 mm overlapping, vertical strip	14,0
5	250	318	glued - 60 mm overlapping, vertical strip	9,6
6	250	315	glued - 60 mm overlapping, horizontal strip	13,2
7	250	300	glued - 60 mm overlapping, vertical strip	10,4
8	250	310	sewed - folded in, 2 rows of stitching	12,8
9	250	325	sewed - folded in, 2 rows of stitching	10,4
10	250	340	sewed - folded in, 2 rows of stitching	13,6
11	250	317	sewed - overlapping, 2 rows of stitching	17,6
12	250	250	welded - overlapping	22,8
13	250	315	welded - overlapping	14,38
14	250	305	welded - overlapping	9,6

Table 5.2: 1<sup>st</sup> series of experiments

most of the seams in the pneumatic formwork were planned to be loaded in the same manner. Table 5.2 gives an overview of all specimens, their dimensions, types of seams and the maximal bearing load.

In the preliminary tests on seams described in the previously mentioned master thesis [70], overlapping and folded in glued seams were tested. The results show that the overlapping seams could bear a two or three times higher load than the folded in ones. Therefore only this type was tested further.

All the glued specimens are shown in Figure 5.1. The first ones - *no.1* to *no.3* - have a single seam with an overlap of 60 mm and 100 mm respectively. Moreover, it was tried to improve the joints by gluing additional strips across the seams but no real improvement could be observed.



Figure 5.2: Sewed seams - specimen 9 to 11

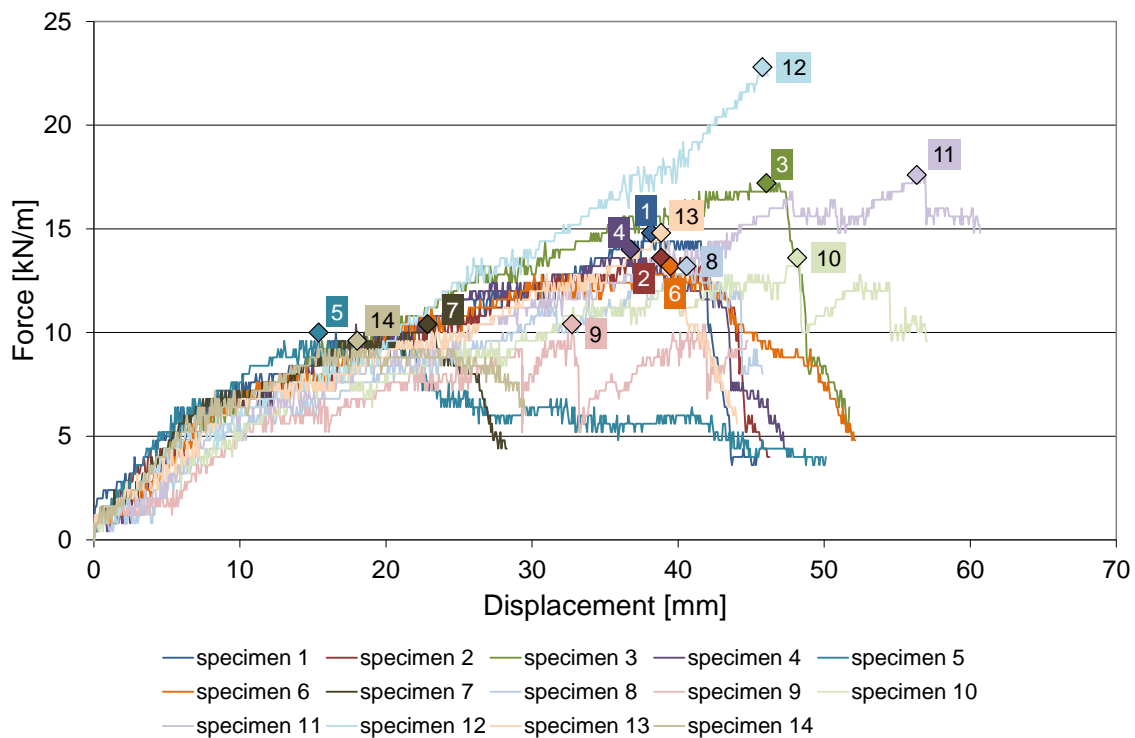
The specimens 8 to 11, with sewed seams, are shown in Figure 5.2. The stitching was made by two different companies. After having consulted these companies, it turned out that in order to make a hemispherical pneumatic formwork only folded in sewed seams could be produced. Therefore, three sewed specimens with two rows of stitching on the folded in membrane were tested and, for the sake of completeness, also one





Figure 5.3: Welded seams - specimen 12 to 14

overlapping seam was tested. That one showed the best results because both rows of stitching proved to be effective at the same time. Looking at the folded in seam, the two rows of stitches could never simultaneously carry the load. The second row didn't get any force until the first one ripped. Moreover, the air of the pneumatic formwork would escape through the stitching holes and that might lead to further problems. If sewing were chosen, additional measurements to minimize the air loss would have to be considered.

Figure 5.4: Load-displacement diagram of the 1<sup>st</sup> series of experiments

In specimen 12 to 14 welded seams were tested with varying results - see Figure 5.3. The colored print on the PVC membrane might have a negative influence on the welding process. All the welded seams were produced by two overlapping membranes. If the material is folded in for the welding, the bearable force is much lower.

Figure 5.4 shows the load-displacement diagram of all fourteen specimens. The highlighted points in every curve with the attached number symbolize the maximum load

of the respective specimen. It can be seen that in the majority of cases the ripping of the seam occurred slowly and under great deformations. Mostly, the glue or the stitches started to break in one area and then the tear increased.

In brief, glued and sewed seams can bear a load between  $10\text{ kN/m}$  to  $17\text{ kN/m}$ ; welded ones between  $10\text{ kN/m}$  to  $23\text{ kN/m}$ . This force per meter amounts to a maximum stress of  $25\text{ N/mm}^2$  to  $33\text{ N/mm}^2$  for glued and sewed seams and  $23\text{ N/mm}^2$  to  $56\text{ N/mm}^2$  for welded seams. It was decided to use PVC glue as the most appropriate fastener. More details on the production of the pneumatic formwork are shown in the chapters 5.3.

### 5.1.2.2 Determination of the tensile strength

specimen No.	width [mm]	length [mm]	thickness [mm]	direction of the force	max. load [kN/m]
1	282	320	0,41	parallel to the warp	28,7
2	282	300	0,41	perpendicular to the warp	27,3
3	282	335	0,41	parallel to the warp	33,3
4	250	345	0,41	perpendicular to the warp	28,8

Table 5.3: 2<sup>nd</sup> series of experiments

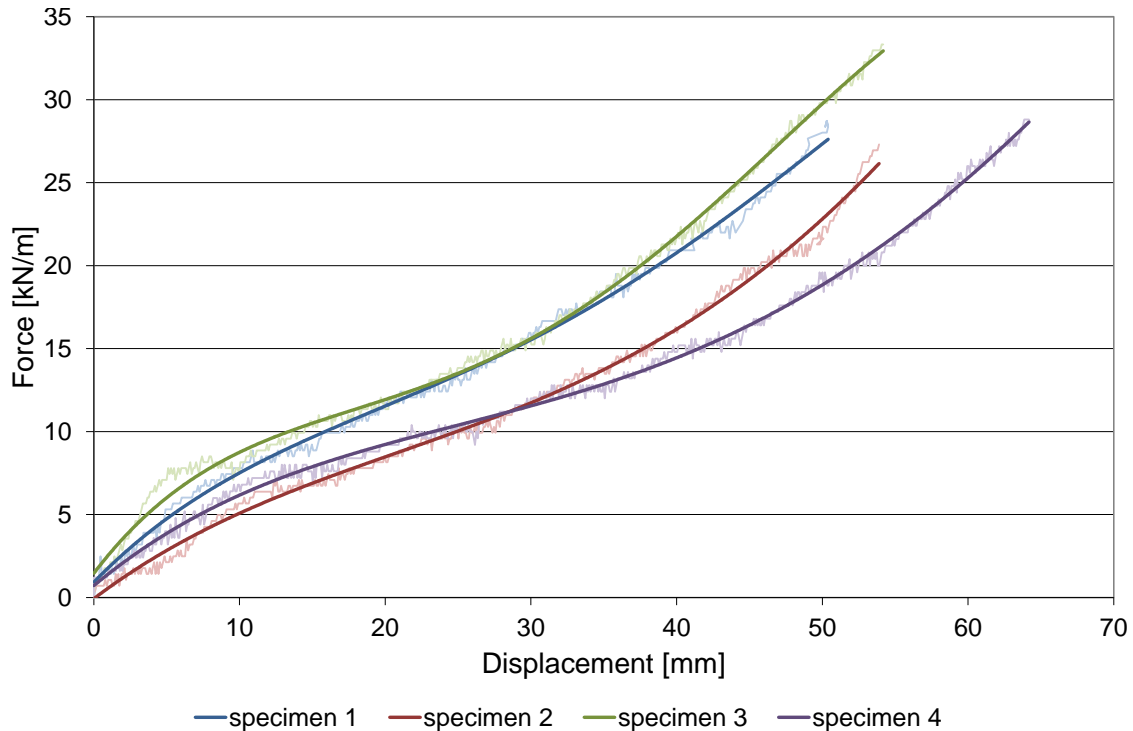


Figure 5.5: Load-displacement diagram of the 2<sup>nd</sup> series of experiments

In the second experiment series the tensile strength of the PVC membrane was determined. Table 5.3 shows the dimensions as well as the direction of the force for the four

tested specimens. The direction of the applied load compared to the warp does not influence the tensile strength significantly. But it could be observed that if the load is applied in the same direction as the warp, the PVC membrane becomes very smooth whereas a loading in the direction of the weft leads to a very uneven surface.

Figure 5.5 shows the load-displacement diagram of these specimens. The maximum load for the membrane varies between  $27,3 \text{ kN/m}$  and  $33,3 \text{ kN/m}$  which amounts to a maximum stress of  $67 \text{ N/mm}^2$  and  $81 \text{ N/mm}^2$ , respectively. In regard to the pneumatic formwork the maximal tensile strength of the PVC material is of comparatively little importance because the seams will always be the weak spot.

### 5.1.2.3 Determination of the Young's modulus and the Poisson's ratio

specimen No.	width [mm]	length [mm]	thickness [mm]	direction of the force
1	283	800	0,41	parallel to the warp
2	283	800	0,41	parallel to the warp
3	281	796	0,41	perpendicular to the warp
4	283	796	0,41	parallel to the warp
5	284	805	0,41	perpendicular to the warp

Table 5.4: 3<sup>rd</sup> series of experiment

Aiming at creating a pneumatic formwork whose shape matches exactly the shape of the shell structure, the material properties of the PVC-membrane used had to be determined. Experiments on the first pneumatic formworks showed that the stretching of the material under load must not be neglected. Therefore, experiments were carried out in order to find out the Young's modulus and the Poisson's ratio.

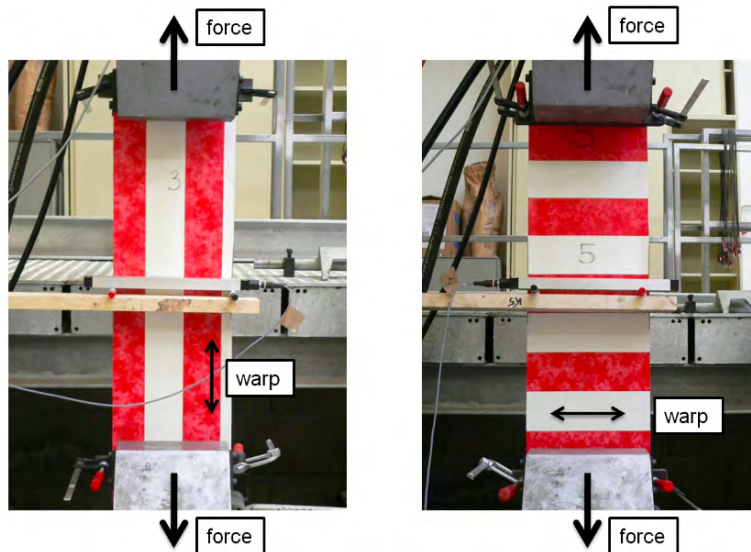


Figure 5.6: Experiment setup of the 3<sup>rd</sup> series of experiments

Five uniaxial tensile tests were carried out. The load was applied displacement controlled with a line speed of approximately  $4\text{ mm/min}$ . This slow loading rate was chosen to simulate the slow inflating of a pneumatic formwork. During the experiments the force as well as the displacement were measured in order to be able to determine the Young's modulus. Moreover, the changes in the width of the specimens were measured so that the Poisson's ratio could be calculated. In three experiments the force was applied parallel to the warp yarn, and also parallel to the painted stripes, thus the specimen had vertical stripes when it was set-up in the test frame. In two experiments the load was applied perpendicular to the warp yarn – therefore horizontal stripes appeared during testing. Figure 5.6 shows two of the specimens during testing. A greater length is chosen for the specimens in order to obtain large displacements. These experiments were not designed to test the maximum load bearing capacity; therefore the load was not increased until failure.

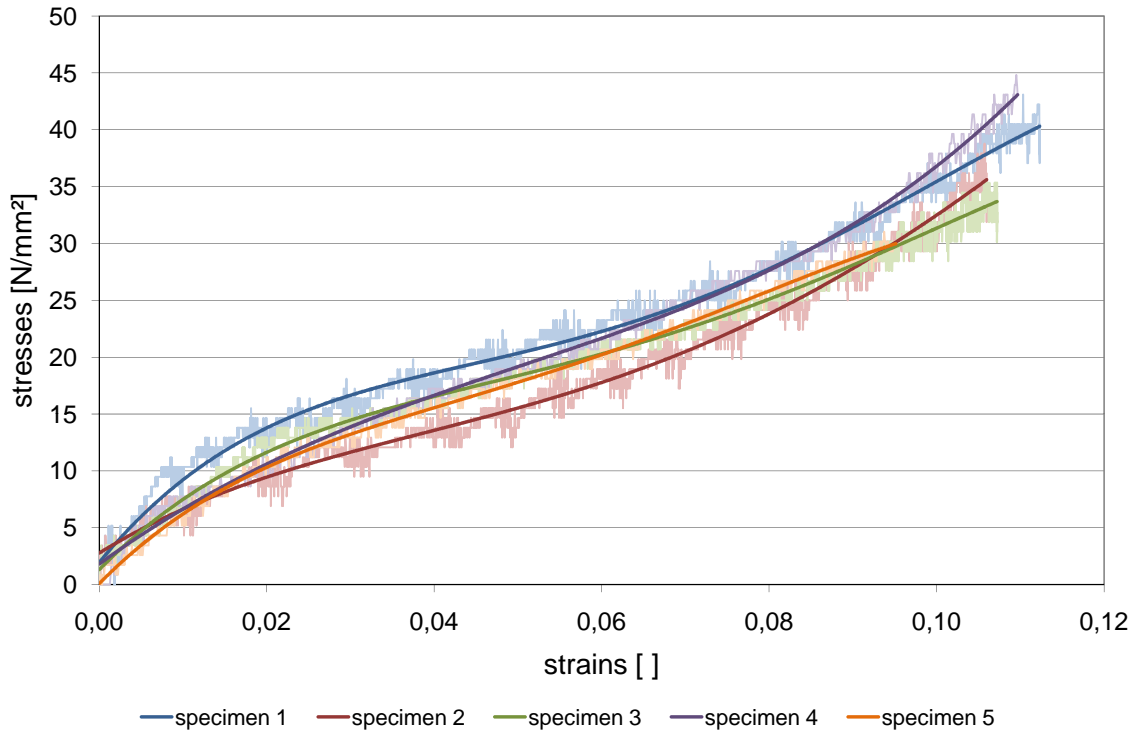


Figure 5.7: Stress-strain diagram of the 3<sup>rd</sup> series of experiments

Figure 5.7 shows the stress-strain diagram of the five specimens. As the Young's modulus is the ratio of stresses to strains, it can be seen that the PVC membrane is not linear elastic. Regarding the interval between 2% and 8% strains the mean value of the Young's moduli of all five specimens' amounts to approximately  $260\text{ N/mm}^2$ .

In the diagram in Figure 5.8 the change of the Young's modulus with the stresses is depicted. The dots in this diagram refer to the mean value of the Young's modulus in the interval of a stress difference of  $10\text{ N/mm}^2$ . At the beginning of the loading the modulus of elasticity is higher. When a stress of  $20\text{ N/mm}^2$  to  $30\text{ N/mm}^2$  is applied the Young's modulus amounts to approximately  $250$  to  $300\text{ N/mm}^2$ . This area of stresses corresponds to the maximum stresses in the pneumatic formwork. In other words, if a

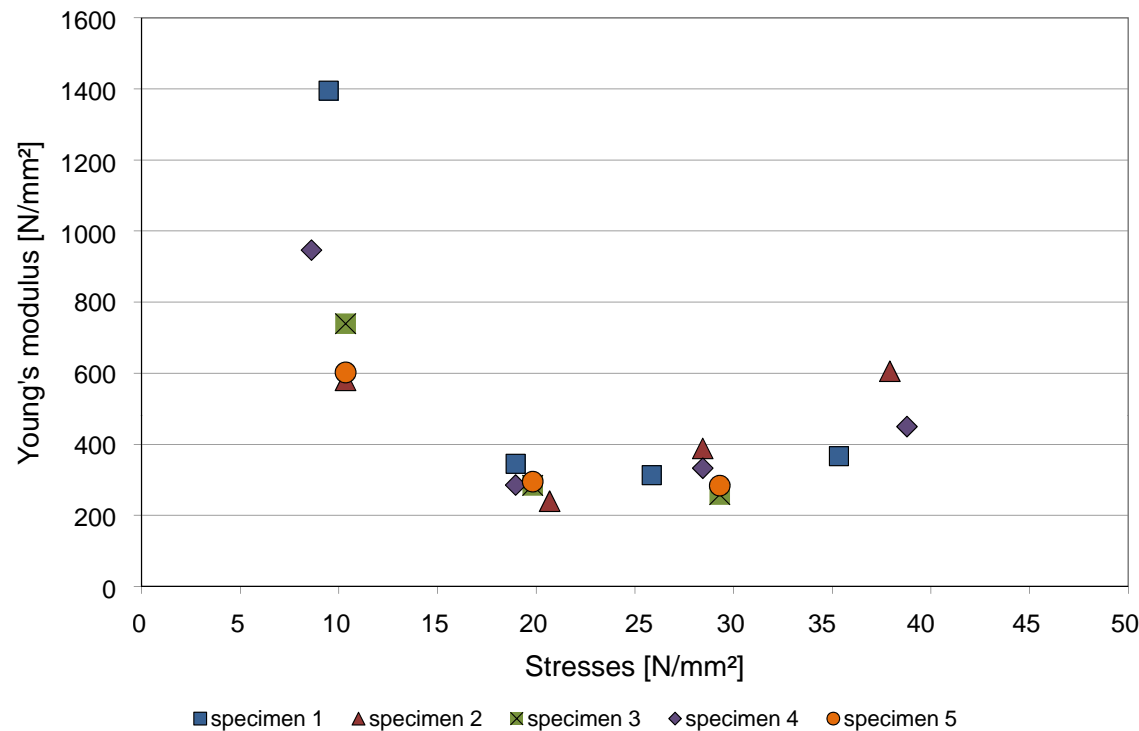


Figure 5.8: Change of the Young's modulus the 3<sup>rd</sup> series of experiments

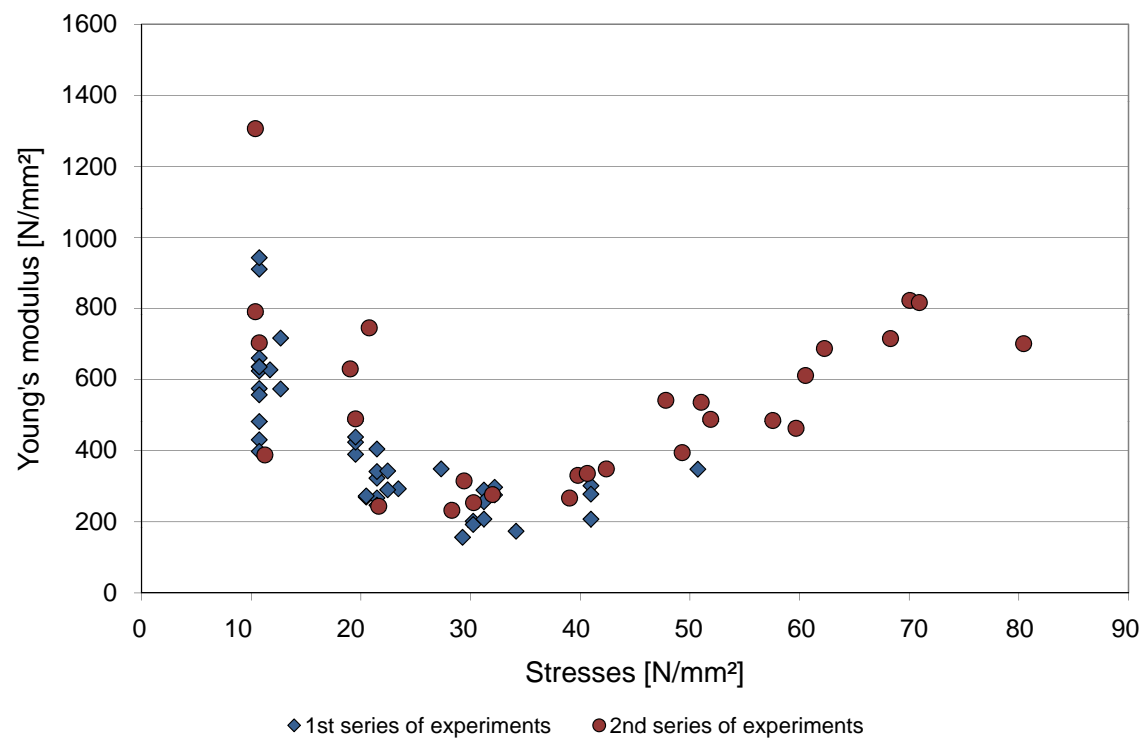


Figure 5.9: Change of the Young's modulus the 3<sup>rd</sup> series of experiments

stress of  $20 \text{ N/mm}^2$  appears in the pneumatic formwork a stretching of 5 % could be expected.

The Young's modulus of the 1<sup>st</sup> and 2<sup>nd</sup> series of experiments is analyzed in Figure 5.9. The mean value of the moduli of elasticity within an interval of  $10 \text{ N/mm}^2$  is depicted over the stresses. It can be seen that, although the modulus of elasticity differs quite strongly, these results are in accordance with the ones gained in the 3<sup>rd</sup> series of experiments. At a low stress the modulus of elasticity is higher, then, between  $20 \text{ N/mm}^2$  and  $40 \text{ N/mm}^2$  it decreases to approximately  $300 \text{ N/mm}^2$ , and with higher stresses the Young's modulus increases again.

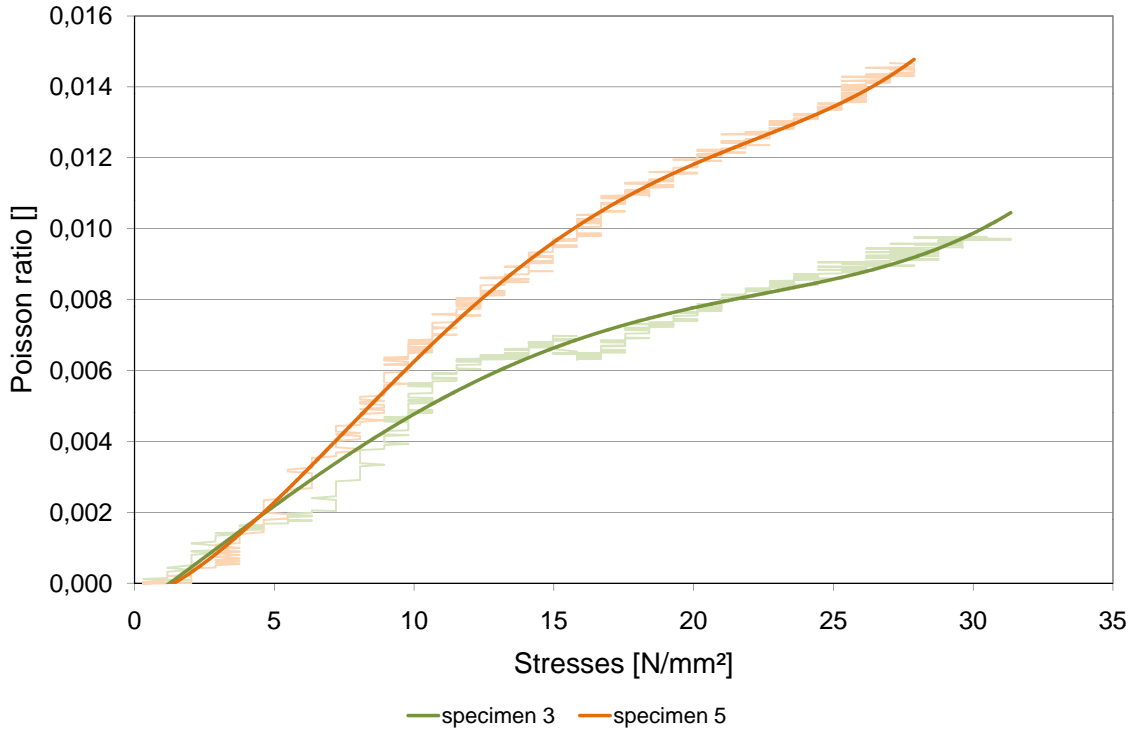


Figure 5.10: Change of the Poisson ratio the 3<sup>rd</sup> series of experiments

Furthermore, the Poisson ratio of the PVC membrane is determined. With this material property the direction of the load compared to the warp is of high importance. If the load is applied parallel to the warp no transverse strain can be measured. In Figure 5.10 the Poisson ratio changing with the stresses is depicted. When stresses of  $20 \text{ N/mm}^2$  are reached, the Poisson ratio is between 0,008 and 0,012.

### 5.1.3 Air blower

In order to generate the air pressure in the pneumatic formwork an air blower is necessary. For all the experiments, a side channel blower from the company *Ventur*, sold under the product code *SC300*, was used [82]. This air blower was connected to an air hose with a diameter of  $60 \text{ mm}$  which was plugged into the pneumatic formwork by means of a connection piece.

## 5.2 Shape of the pneumatic formwork

Building a hemispherical cupola with this construction method, a hemispherical pneumatic formwork is used. Due to the fact that a hemisphere is a non-developable surface, the shape of the pneumatic formwork has to be approximated.

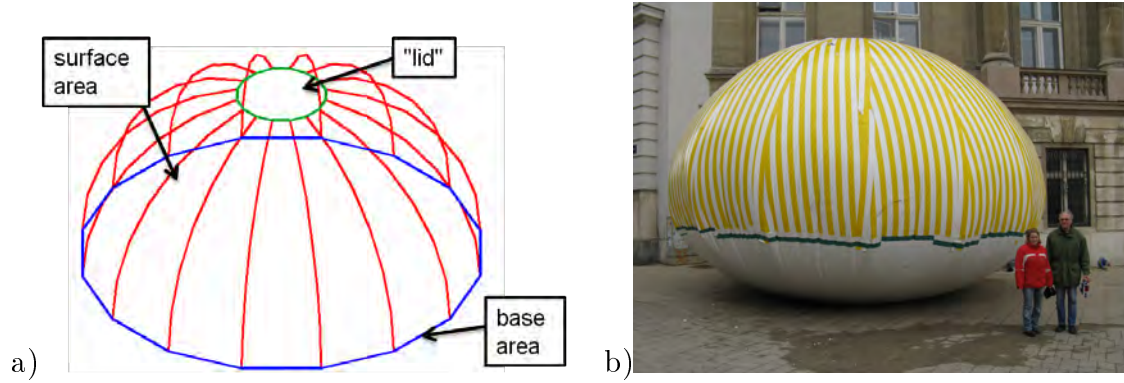


Figure 5.11: Pneumatic formwork a) schematic drawing of the main parts of the pneumatic formwork b) Picture of the inflated pneumatic fomwork

Figure 5.11 shows a schematic drawing of the component parts of the pneumatic formwork as well as a picture of the finished and inflated pneumatic formwork. The surface area is approximated with 16 segments which are glued together with an overlap of  $60\text{ mm}$ . This surface area is then connected to the base area consisting of a regular hexadecagon. To create this seam, the membrane of the surface area was folded in and glued to the base area with a connection width of  $100\text{ mm}$ . Finally, the “lid” was glued on top of the formwork in order to gain an airtight hemispherical balloon. The connection piece, which is necessary to plug in the air hose, is inserted into the lid. Thus, the air supply takes place through the oculus of the dome.

In order to define the dimensions of the pneumatic formwork, the pieces of the membrane were tailored in such a way as to create a hemisphere which inscribed the polyhedron when inflated. Furthermore, the stretching of the PVC membrane was taken into account. The circumference in the hoop direction was shortened by  $5\%$ , so that the pneumatic formwork gained its final shape when the material was stretched.

## 5.3 Producing the pneumatic formwork

The pneumatic formworks for each experiment were developed and made at the Institute for Structural Engineering at Vienna University of Technology. First, the membrane pieces were cut and then glued together in order to form the defined shape. The pictures in Figure 5.12 illustrate the production of the pneumatic formwork. The joining of two pieces of the surface area proved to be quite challenging because two curved edges had to be connected without creasing. To speed up the gluing process a wooden auxiliary structure was made which can be seen in the photo in Figure 5.12a. In the appendix A.3 the dimensions of the pneumatic formworks are given.

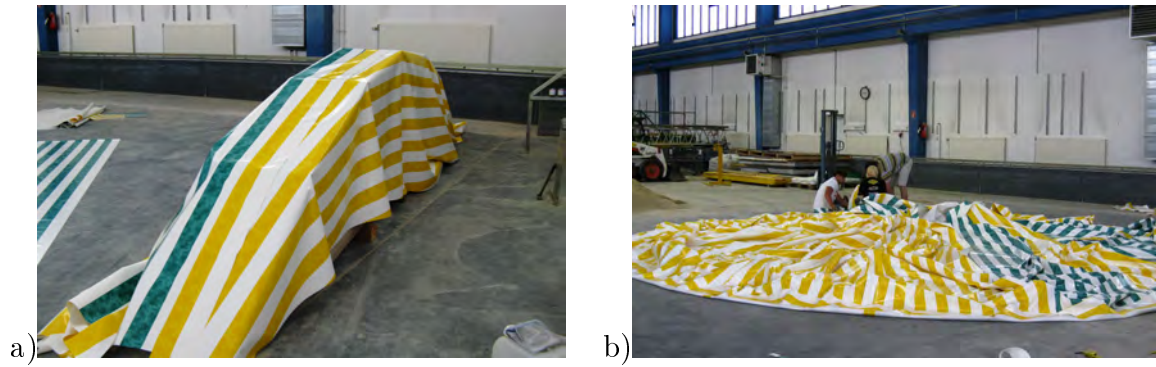


Figure 5.12: Production of the pneumatic formwork

## 5.4 Tensile forces in the membrane

In order to receive an impression of the sectional forces and stresses in the membrane, two border cases are analyzed according to the equation given by Pflüger [65]. In the following considerations only the loading caused by the air pressure in the pneumatic formwork is taken into account. Naturally, this air pressure creates a constant pressure perpendicular to the membrane.

Two different geometrical shapes are investigated; a circular cylinder and a spherical shell. The formulas provided in the equations 5.1 to 5.4 were compiled by Pflüger [65] and refer to the sketches in Figure 5.13. Both shapes are rotationally symmetric

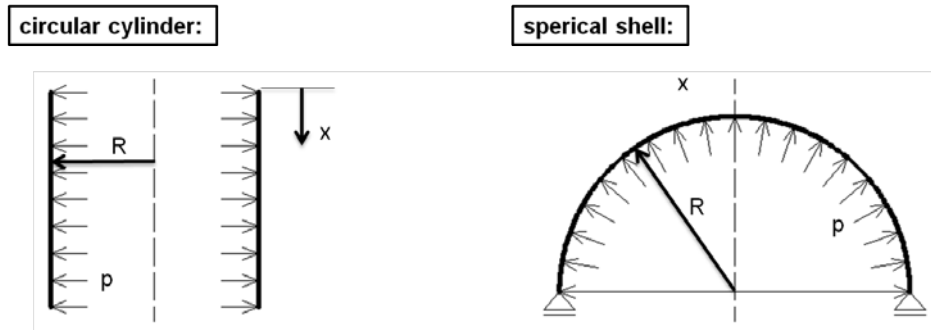


Figure 5.13: Static systems: circular cylinder and spherical shell [65]

with rotationally symmetric loading. The derived formulas are in accordance with membrane theory using the Hooke's law of elasticity.

Circular cylinder:

$$N_x = 0 \quad (5.1)$$

$$N_y = p \cdot r \quad (5.2)$$

Spherical shell:

$$N_x = p \cdot \frac{r}{2} \quad (5.3)$$

$$N_y = p \cdot \frac{r}{2} \quad (5.4)$$



As already mentioned in chapter 4.3.2, the tensile force in the membrane is proportional to the air pressure  $p$  and the radius  $r$ . A circular cylinder is a singly curved shell and the tension in the direction of the curvature amounts to  $p \cdot r$ . A spherical shell, however, is a doubly curved structure with two identical radii of curvature regarding sign and the value. In this case, the tensile force  $F_t$  caused by a constant inner air pressure amounts to  $p \cdot \frac{r}{2}$ . These equations clearly show that a doubly curved structure provides a more effective load bearing system than a singly curved one.

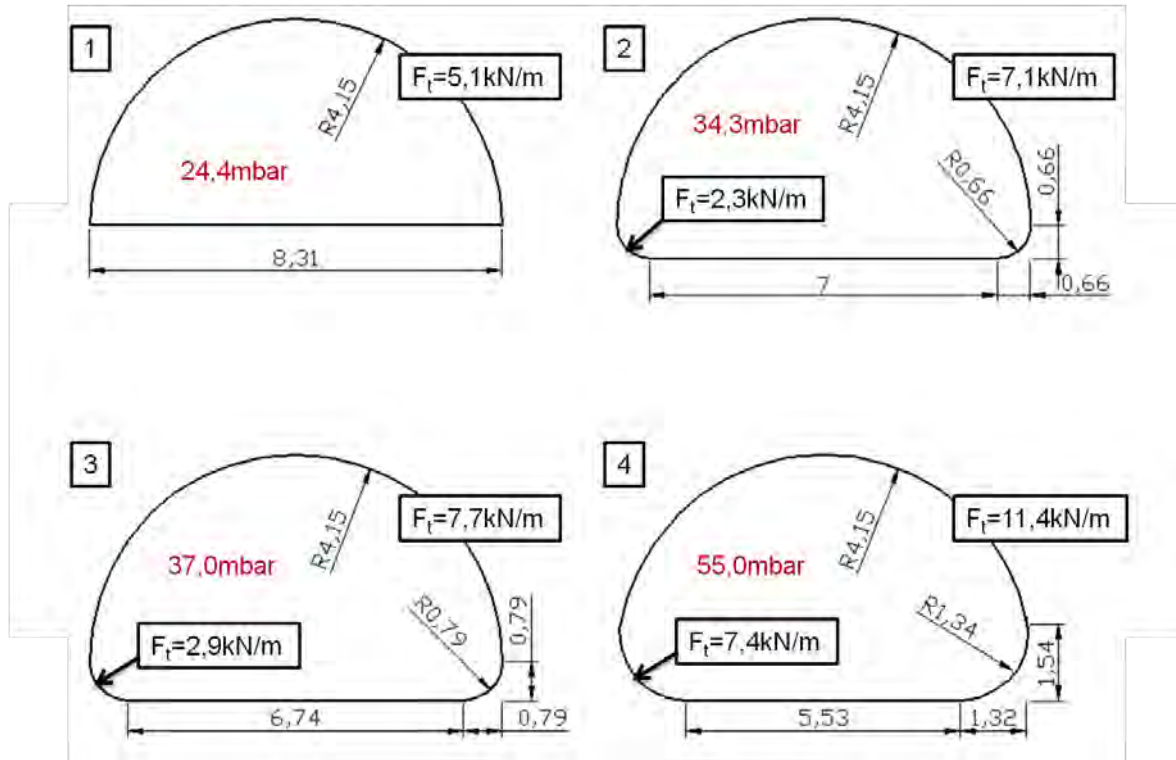


Figure 5.14: Different shapes of the pneumatic formwork

For a better understanding of the tensile forces in the membrane, different shapes of the pneumatic formwork are considered. All following calculations refer to the concrete shell built during the preliminary test – compare chapter 6.2. The weight of the hemispherical concrete shell amounts to 133 kN and the radius to 4,15 m. In Figure 5.14 four different exemplary shapes of the pneumatic formwork carrying the concrete shell are considered. In the first sketch, the membrane is completely hemispherical with a base diameter exactly twice the size of the radius. In order to lift the total weight of the concrete shell, an air pressure of 24,4 mbar is necessary. Using equation 5.3 and 5.4 for this spherical shell, the tensile force in the membrane  $F_t$  amounts to 5,1 kN/m, independent of the direction of the force. This perfectly hemispherical shape, however, only exists in theory. The shape created in the field experiments rather resembled the shapes shown in the other three sketches in Figure 5.14. The difference between the second, third and fourth drawing in Figure 5.14 is the size of the fillet radius. In all four situations, however, the entire self weight of the concrete shell has to be supported by the pneumatic formwork. The air pressure which is necessary to carry this load depends on the contact area between the pneumatic formwork and the subsoil. When

the fillet radius is increased the base diameter decreases and thus forces the air pressure to increase.

Moreover, in Figure 5.14 the tensile forces  $F_t$  in the membrane are calculated for the four exemplary situations. To identify the normal force at the upper part of the shell it is assumed that the structure is a spherical shell with a radius of  $4,15\text{ m}$  – just like the finished shell. Therefore the forces are calculated using equation 5.3 and 5.4. Since the air pressure increases, the force in the membrane increases as well.

In the base area the radius of curvature is different. In order to calculate the tensile forces  $F_t$  in the area of the fillet radius equation 5.2 is used. Of course, also in this area the pneumatic formwork is doubly curved but one radius is much larger than the other. As a simplification, only the fillet radius is taken into account and this part of the formwork is considered as a circular cylinder.

Regarding the results of the material tests on the glued seams, it can be observed that the forces in the membrane already reach the bearing capacity of the seams – see chapter 5.1.2.1. Therefore this kind of pneumatic formwork is limited to a shell structure of this size.

## 5.5 Possible solution for larger shell structures

As shown in the previous chapter, quite large tensile forces occur in the membrane due to the air pressure and the radius. In order to decrease the forces, either the air pressure or the radius has to be reduced.

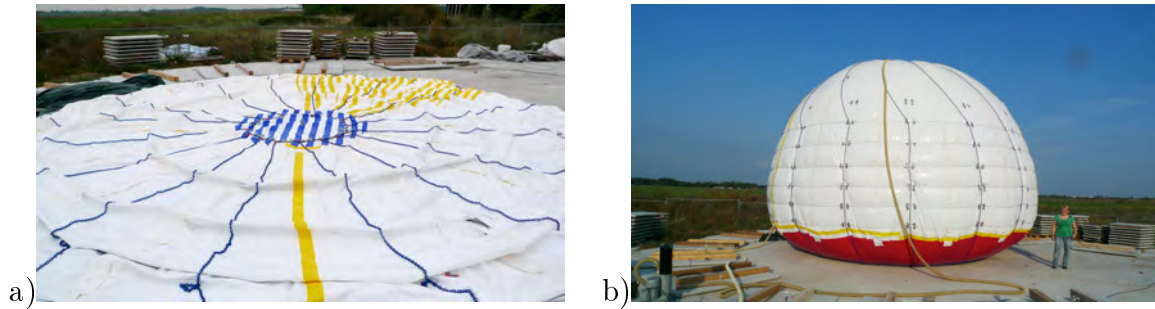


Figure 5.15: Pneumatic formwork reinforced with ropes and chains

One approach to decrease the radius is shown in this chapter. As shown in Figure 5.15, the pneumatic formwork is constricted with ropes and chains. These tendons enclose the entire pneumatic formwork, therefore no forces have to be carried by a foundation. In this way, the radius of curvature decreases dramatically. The ropes and chains, however, have to be designed in order to be able to carry the tensile force caused by the air pressure.

# Chapter 6

## Preliminary Experiments

### 6.1 Timber models

To demonstrate this new construction method, timber models were created in order to find the most suitable process to accomplish the transformation process. Different parts of the construction method could be optimized by varying construction details.

#### 6.1.1 Description of the models

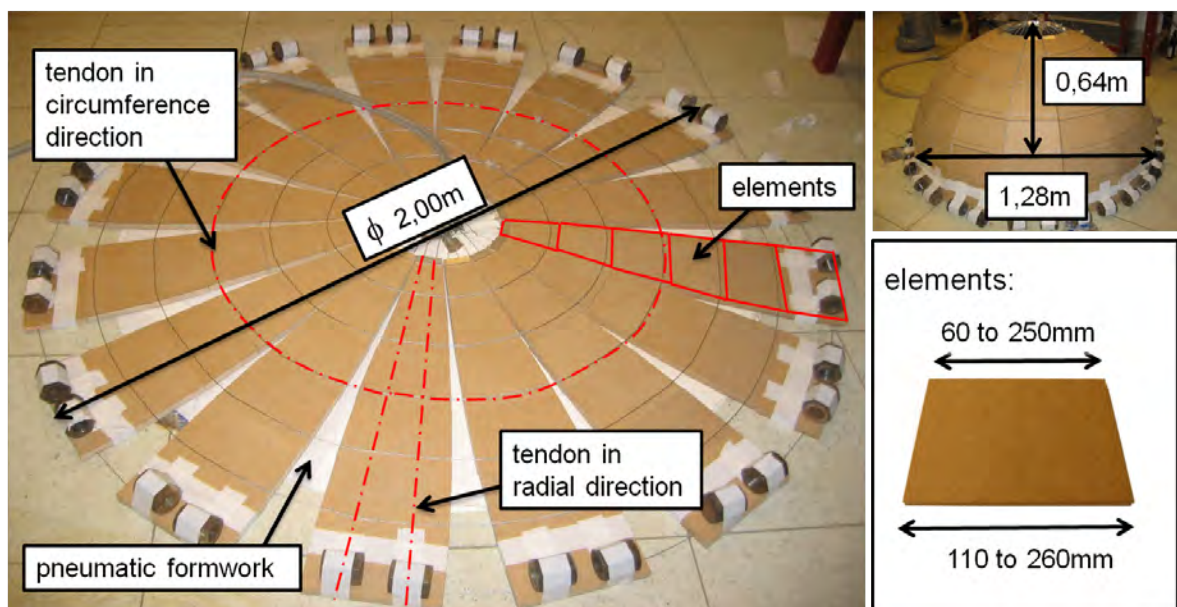


Figure 6.1: Small wooden model

Two wooden models were created – a small wooden model and a large wooden model. The shape of both shells corresponds to the example described in chapter 4.1. The shells consist of 96 individual trapezoidal shaped parts. The dimensions of the trapezoids have

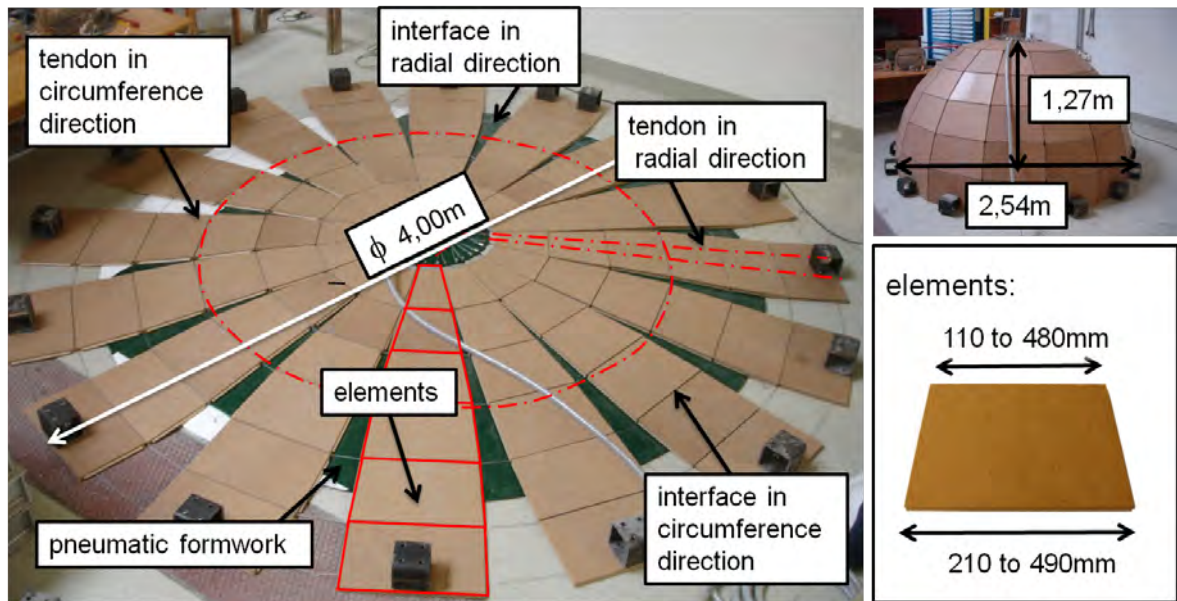


Figure 6.2: Large wooden model

to be chosen in such a way as to form a polyhedron which approximates a hemispherical dome with a diameter of  $1,25\text{ m}$  and  $2,54\text{ m}$ , respectively. The elements are formed by three layers of wooden boards glued together to form a  $20\text{ mm}$  thick element. The middle layer exists to create the necessary void for the two tendons in each element in the radial direction. Steel cables with a diameter of  $2\text{ mm}$  were used for the tendons. Additionally, every wooden trapezoid was furnished with at least one steel tendon in the circumference direction. Figure 6.1 and 6.2 show the small and the large wooden model in their initial position and as finished shells. The essential parts and dimensions are tagged.

In Figure 6.3 and 6.4 the erection process of the wooden models is displayed – the pneumatic formwork was slowly inflated with air, therefore the elements lifted and formed a shell.

### 6.1.2 Knowledge gained from the timber models

The timber models were used for experimenting with different shapes of the pneumatic formwork. Starting with a pneumatic device which only lifted the centre of the shell it soon became clear that the formwork had to support the shell on the better part of the surface area in order to obtain the desired shape. In another experiment the pneumatic formwork consisted of two concentric circles made of PVC membranes glued together on their edges. This shape of the membrane provided better results but further experiments showed that the optimal way to transform a flat plate successfully into a hemispherical shell is by means of a hemispherical pneumatic formwork.

Moreover, the necessity of the tendons in the circumference direction during the erection process became obvious. In the first experiment only the cables of the central ring and of the outer perimeter at the bottom of the shell were placed before starting the



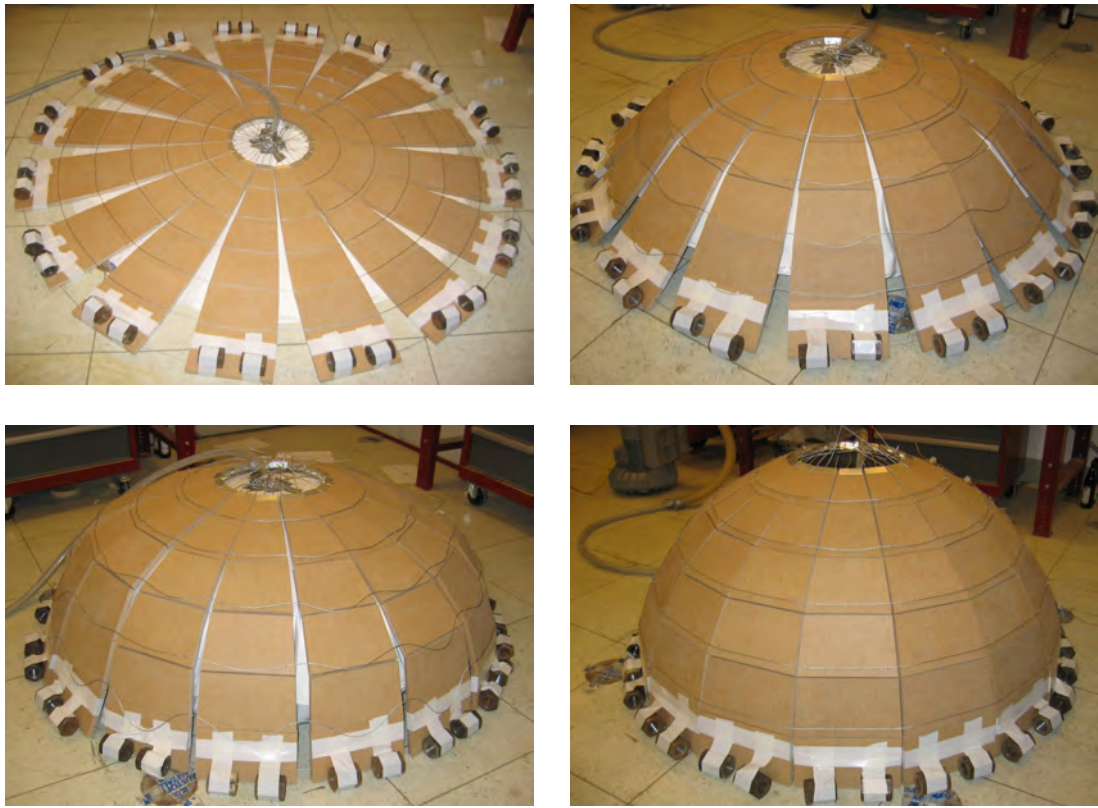


Figure 6.3: Small timber model - erection process



Figure 6.4: Large timber model - erection process

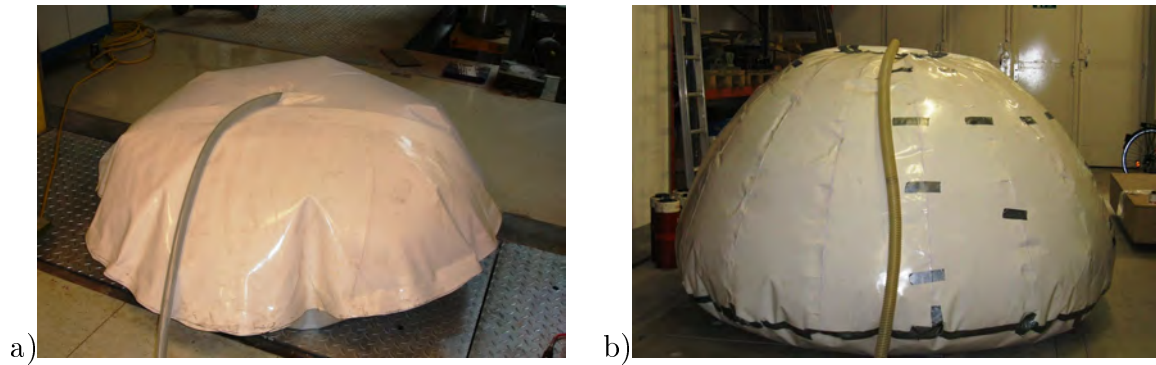


Figure 6.5: Pneumatic formwork: a) two concentric circles glued together on the their edges for the small wooden model b) hemispherical shaped membrane for the large wooden model

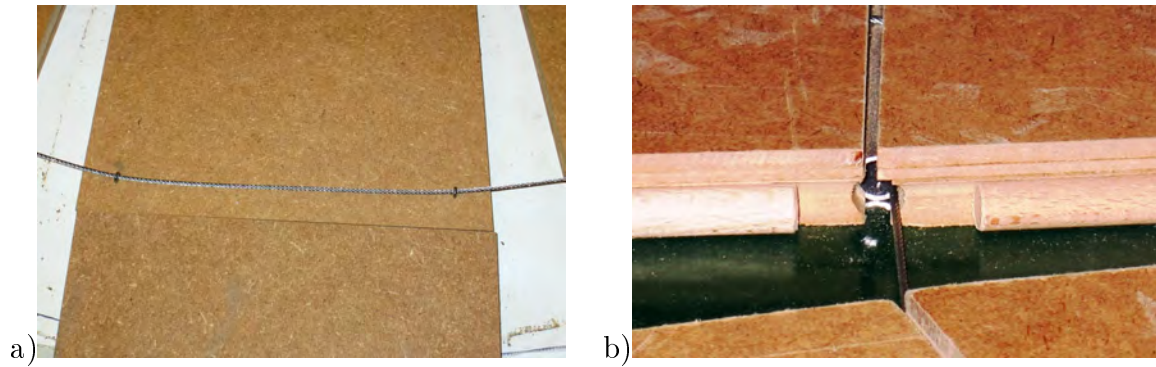


Figure 6.6: Tendons in circumference direction: a) in the small wooden model b) in the large wooden model

elevation process. The remaining cables were to be installed manually in the spaces between the pieces after the structure would have reached its final position. The shape achieved by the wooden shell was not satisfying. To make sure that the elements were aligned properly, tendons in the circumference direction were installed in every element before starting the erection process.

These tendons are only serviceable if they are tightened continuously. For the small wooden models, this can be accomplished manually but for larger structures, such as the ice shell; a suitable mechanism to tighten the tendons had to be developed.

To further improve the joining of the elements and therefore also the shape of the shell, an alternative design of the edges of each element was tested with the large wooden model. In order to guarantee that the elements obtain their proper position, tongue and groove joints were built between the elements.

*Tongue and groove* is a method of fitting similar objects together, edge to edge. Each piece has a slot - the groove - cut all along one edge, and a thin, deep ridge - the tongue - on the opposite edge. The tongue projects a little less than the groove is deep. Two or more pieces thus fit together closely. Regular tongue and groove joints allow two flat pieces to be joined strongly together to make a single flat surface. For this construction method, however, it is necessary to create a tongue and groove system which is not

only able to connect flat plates but also allows the elements to evenly change their angle between each other. Thin cylindrical elements were used for the tongues; the groove had the shape of a circular arc. This joint system was used for the interfaces in the radial as well as in the circumference direction.

In the radial direction the interfaces have to be properly joined during the erection process. When the elements are arranged on the working surface the edges of the ones in the center of the plate already touch each other, therefore in this area the tongues are already in their respective grooves. During the erection process the interfaces close continuously from the center to the edge. With the help of the cylindrical rods the elements are guided into a perfect position. The tongues in the radial direction were made of wooden rods.

The interfaces in the circumference direction are also designed as a tongue and groove system. During the erection process the angle between two neighboring elements has to decrease continuously from  $180^\circ$  to  $167^\circ$ . Therefore it is essential that the elements are allowed to roll smoothly against each other's edges. This requirement can be met by the tongues and groove system of a cylindrical rod and a circular cut. This method facilitates the transfer of forces and simultaneously creates a hinged interaction between the elements. The tongues in the circumference direction were made of aluminum pipes thus these elements could be used for the cylindrical elements as well as for the ducts for the tendons in the circumference direction.

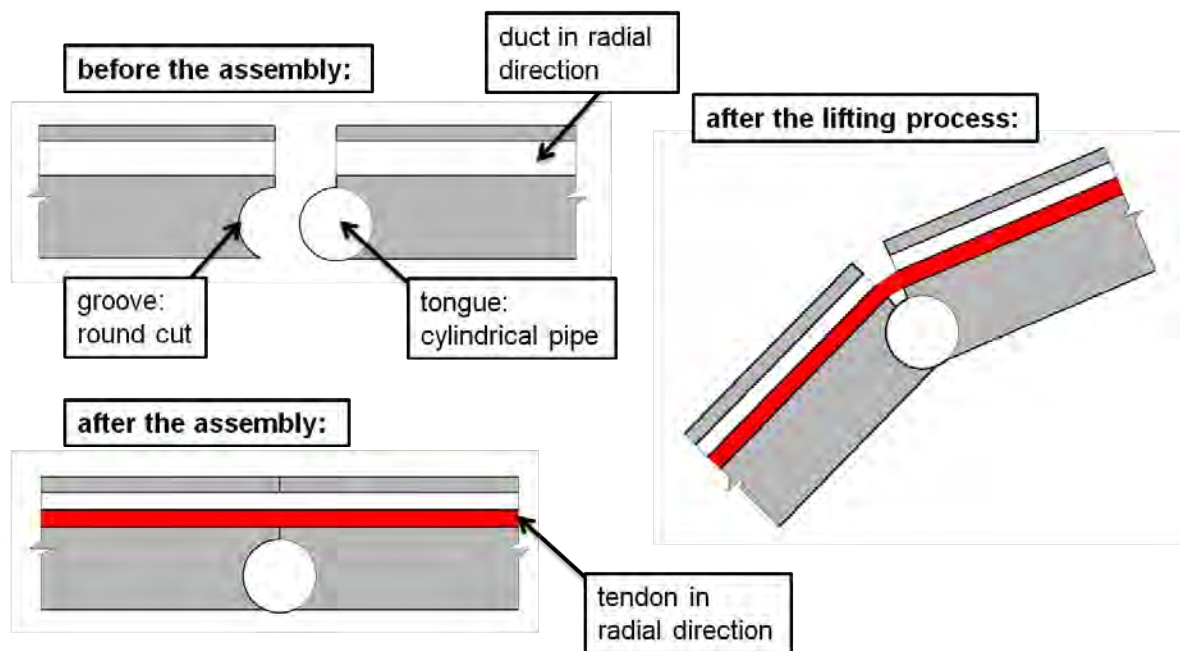


Figure 6.7: Sketch of the joint in the circumference direction

Figure 6.7 shows sketches of this kind of joint in the circumference direction before and after the assembly as well as after the transformation whereas in Figure 6.8 pictures of the actual joints in the larger wooden model are displayed.



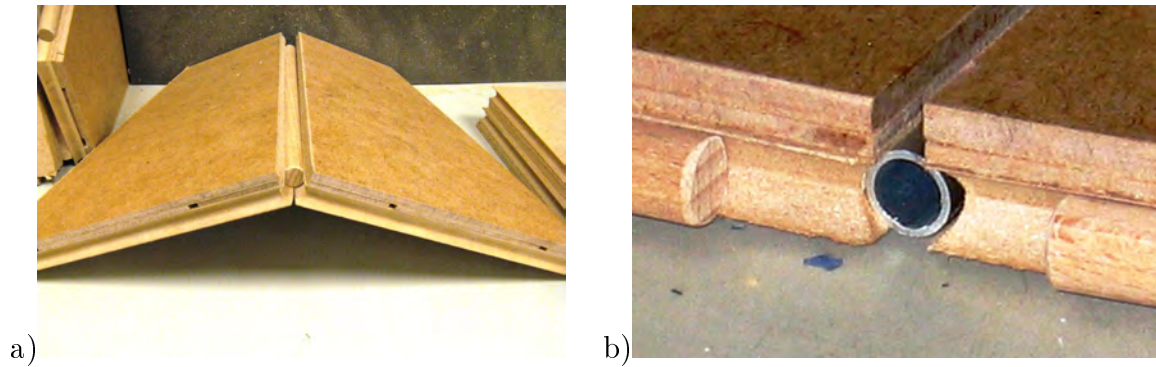


Figure 6.8: Cylindrical element a) wooden rod in the radial interfaces b) aluminum tube in the circumference direction

This tongue and groove system shows improvements in both types of interfaces. In the radial direction the elements assembled more properly without any offset in the circumference direction the elements were able to roll against each other smoothly.

Although this kind of joint worked quite well it was not further pursued. The implementation of a cylindrical ridge and round cut in the ice segments would be very complex, laborious and time-consuming. In an ice dome these joints could only be achieved by inserting built-in parts made of steel or any other material but ice, which would complicate the entire construction method and not be worth the effort. The small wooden model already shows that this construction is feasible without complicated joints.

## 6.2 Concrete shell

### 6.2.1 Preface

This preliminary experiment took place on a closed down airfield in Aspern in Vienna placed at the disposal of the Institute for Structural Engineering at Vienna University of Technology to carry out large scale experiments.

In order to be able to successfully build this experimental concrete shell more than one attempt had to be made. Problems with the pneumatic formwork led to premature terminations of the experiment so that it had to be restarted at a later date. Finally, in October 2009 this preliminary experiment could be completed successfully and the concrete shell was built.

The pictures of the concrete shell in the next chapters are from different attempts, therefore the pictures were taken in different seasons and weather conditions.



## 6.2.2 Description of the essential elements

### 6.2.2.1 Concrete Elements

Building the concrete shell the 96 elements of this shell were made of precast concrete. The usage of precast concrete is especially suitable for this construction method because the shell consists of flat individual elements. Producing large doubly curved prefabricated parts requires a complex doubly curved formwork; therefore, precast concrete is rarely used for shell structures. With this construction method, however, the elements are plane and can easily be produced on a flat working surface. The number of different shape types results from the shape of the shell. In many shell structures, such as shells of revolution, one element type is used several times. The precast factory can make use of this advantage by producing many precast concrete parts with one single mold. Moreover, the transportation to the site is unproblematic due to the low weight and size of the elements. Using precast concrete offers a variety of other advantages, e.g. high concrete quality and accuracy and a fast assembly on site.

	<b>C 25/30</b>
$f_{ck}$	$25 \text{ N/mm}^2$
$f_{ck,cube}$	$30 \text{ N/mm}^2$
$f_{cm}$	$33 \text{ N/mm}^2$
$f_{ctm}$	$2,6 \text{ N/mm}^2$
$f_{ctk,0,05}$	$1,8 \text{ N/mm}^2$
$f_{ctk,0,95}$	$3,3 \text{ N/mm}^2$
$E_{cm}$	$31000 \text{ N/mm}^2$
$\varepsilon_{c1}$	$0,21 \%$

Table 6.1: Precast concrete parts - material properties [10]

The casting of the elements necessary for this construction was entrusted to the company Oberndorfer [61], an Austrian manufacturer specialized in precast concrete. The precast concrete parts had a thickness of  $50 \text{ mm}$ . Sixteen of these 96 elements have the same dimension therefore only six different formworks were required for the production of the elements. The concrete quality *C30/37 B2 GK16 F52* was used for the production of the precast parts. The maximum grain size amounted to  $16 \text{ mm}$  and the water-cement ratio to  $0,53$ . Portland cement *CEM I 52,5R* and a polycarboxylic ether polymer superplasticiser (*BASF ACE 331*) were used. The density of the fresh concrete was  $2413 \text{ kg/m}^3$ . The material properties of this kind of concrete according to Eurocode 2 [10] are listed in the Table 6.1.

The dimensions of the precast elements are listed in Table 6.2 and shown in the appendix A.1. In order to achieve the desired polyhedron the geometric form of the elements has to be a trapezoid. The trapezoids are symmetrical with  $h$  as the height,  $a$  as the length of the shorter parallel side and  $b$  as the length of the longer parallel side - as shown in Figure 6.9. The dimensions of the six different elements are shown in Table 6.2. This table also includes the surface area  $A$  and the weight  $G$  of each element.

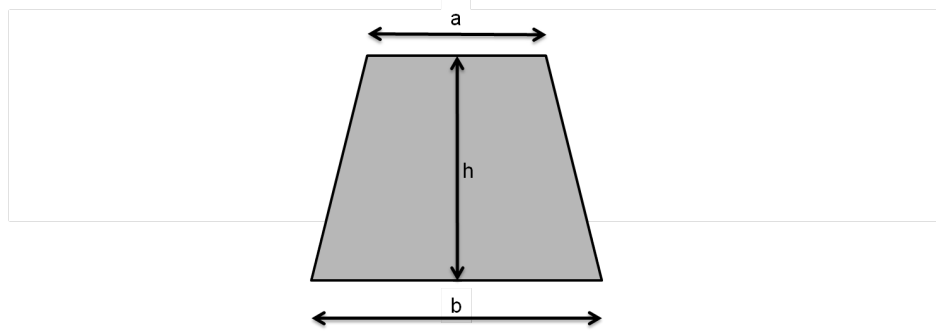


Figure 6.9: Trapezoid

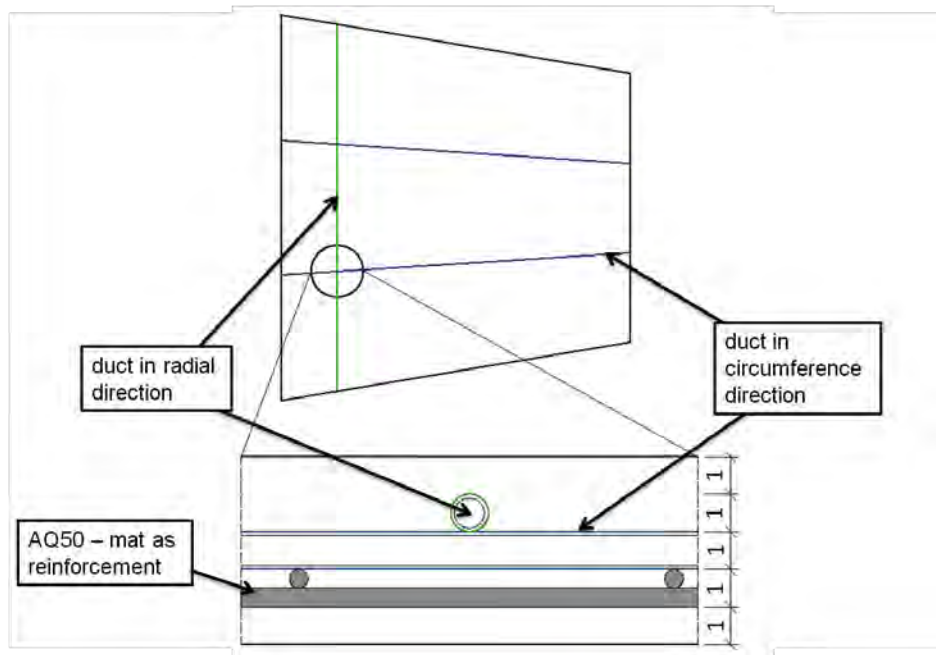


Figure 6.10: Sketch of a precast element

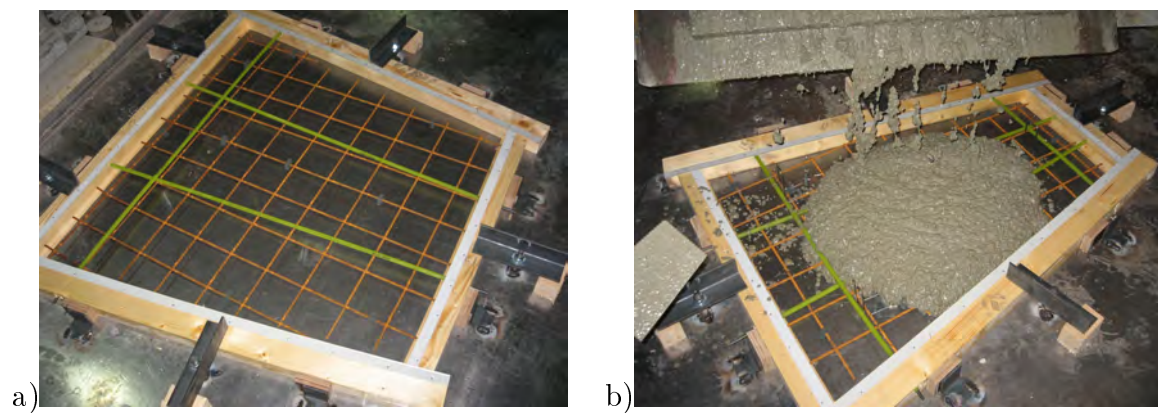


Figure 6.11: Precast concrete element - mold, reinforcement and ducts a) prior to and b) during casting

	a	b	h	A	G
Element No.	[m]	[m]	[m]	[m <sup>2</sup> ]	[kN]
1	0,367	0,717	0,93	0,504	0,630
2	0,717	1,030	0,93	0,812	1,015
3	1,030	1,272	0,93	1,080	1,350
4	1,272	1,489	0,93	1,293	1,616
5	1,489	1,611	0,93	1,441	1,801
6	1,611	1,652	0,93	1,517	1,896

Table 6.2: Dimensions of the precast elements

By summing up the weight of each element, the dead load of the entire concrete shell structure amounts to 132,95 kN.

The prefabricated parts were reinforced with *AQ 50* mats. This mat has reinforcement bars with a diameter of 5 mm ever 100 mm in the longitudinal and cross direction respectively, which equals 1,96 cm<sup>2</sup>/m in each direction. In the finished shell structure, as well as during the lifting process with the pneumatic formwork, no tensile stresses appeared in the precast concrete parts. For the transport and the assembly of the elements on the working surface, the concrete parts had to be lifted with a crane. In these situations bending moments appeared in the plates and reinforcement might become necessary. Moreover, to prevent a brittle failure, an amount of reinforcement higher than the minimum reinforcement area for beams according to Eurocode 2 [10], was chosen. The minimum of longitudinal tension reinforcement for beams is presented in equation 6.1 and is less than the chosen *AQ 50* mat.

$$A_{s,min} = 0,26 \cdot \frac{f_{ctm}}{f_{yk}} \cdot b_t \cdot d = 0,60 \text{ cm}^2/\text{m} < 1,96 \text{ cm}^2/\text{m} \quad (6.1)$$

Each of these precast elements contains ducts, so that the tendons can be pulled through afterwards. Polyethylene tubes [76] with an external diameter of 10 mm and an inner diameter of 8 mm were used for the ducts.

Figure 6.10 shows a sketch of one of these precast parts. In Figure 6.11 pictures of the casting of concrete in the factory are shown. In the pictures the mold, the reinforcement mat and the yellow ducts can be seen prior to and during casting.

### 6.2.2.2 Pneumatic Formwork

A hemispherical PVC membrane as described in chapter 5 is employed for the pneumatic formwork.

### 6.2.2.3 Tendons

Wire ropes with a fiber core produced by the Austrian company Teufelberger [78] were used for the tendons. The properties according to the catalogue of the manufacturer are shown in Table 6.3 [79].

rope diameter	5 mm
maximum breaking load	14,8 kN
nominal tensile strength	1770 N/mm <sup>2</sup>
weight	0,1 kg/m
Young's modulus	$1 \times 10^5$ N/mm <sup>2</sup>
number of wires in the outer strands	42
number of cords	6

Table 6.3: Properties of the steel ropes produced by the company Teufelberger [79]

To verify the Young's modulus a steel rope was tested. During the experiment a steel rope was loaded and released five times. The resulting load-displacement diagram can be seen in Figure 6.12. The test shows that the Young's modulus is considerably lower during the 1<sup>st</sup> load cycle compared to the following loadings. After the load had been applied and released for the first time, a lasting deformation of 15,5 mm in the rope was detected. For the calculation of the Young's modulus  $E = \frac{\sigma}{\epsilon}$  the interval between 2 kN and 10 kN was considered.

	Young's modulus	variation
	[N/mm <sup>2</sup> ]	[%]
1 <sup>st</sup> loading	41 277	—
1 <sup>st</sup> unloading	108 728	—
2 <sup>nd</sup> loading	110 628	+168,01
2 <sup>nd</sup> unloading	110 176	+1,33
3 <sup>rd</sup> loading	111 589	+0,86
3 <sup>rd</sup> unloading	111 381	+1,09
4 <sup>th</sup> loading	111 915	+0,29
4 <sup>th</sup> unloading	112 026	+0,57
5 <sup>th</sup> loading	112 194	+0,25
5 <sup>th</sup> unloading	110 960	−0,05

Table 6.4: Young's modulus of a tested steel rope with a diameter of 5 mm during 5 load cycles

In Table 6.4 the Young's moduli for each load circle are listed as well as the percentage of the variation. The variation in Table 6.4 always refers to the previous loading and unloading. The difference between the Young's modulus during the first and the second loading amounts to almost 170 %. With every further load cycle the modulus of elasticity remains quite constant - the difference is only 1 %. Comparing the results of the test with the specifications of the manufacturer in Table 6.3, it becomes clear that the Young's modulus in this data sheet refers to the reloading. The mean value of all reloadings and re-unloadings in the experiment amounts to 111 360 N/mm<sup>2</sup>.

For the anchorage of the steel ropes an appropriate anchorage system had to be found and load tests with different rope clips and cable closures were carried out. Table 6.5 shows the results of these experiments. These results don't represent general values for the strength of the anchorage systems but simulate the exact assembly of the concrete

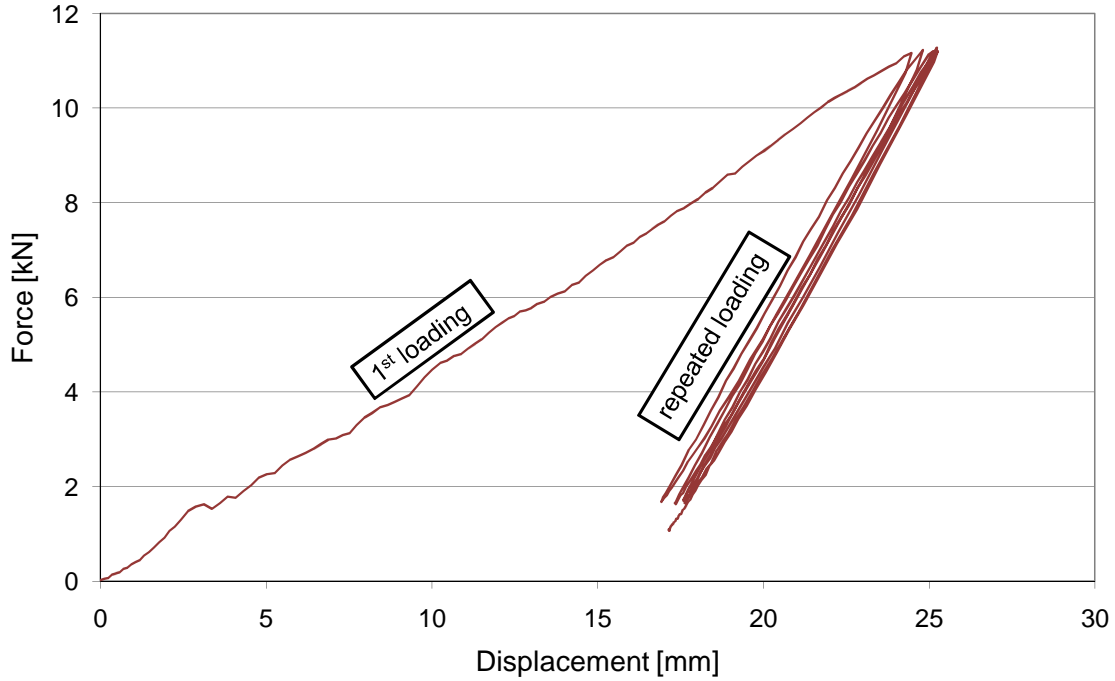


Figure 6.12: Load-displacement-diagram of a tested steel rope with a diameter of  $5\text{ mm}$

shell experiment. For all tests on the rings and clips a steel rope with a diameter of  $5\text{ mm}$  from the company Teufelberger was used. The advantage of the 2-part clamp rings is that they are designed to anchor one steel rope against a bearing whereas the cable clip only works properly when two ropes are pressed together. If a cable clip is fixed to only one cable instead of two, its bearing load is reduced dramatically.

In regard to the design of the precast concrete elements, it is not possible to press two cables against each other. Therefore the 2-part clamp rings are utilized. Some of the tendons in the circumference direction, which bear high tension, are anchored with two 2-part clamp rings.

In order to be able to tighten the steel ropes in the circumference direction during the erection process, electric winches were used. A commercially available electric winch with a  $12\text{ V}$  power supply which can apply a force of  $9\text{ kN}$  was used. The advantage of electric winches is that they can be operated from a distance to the cables. The winches are fixed to the concrete parts therefore the respective precast parts have to be adapted in order to be able to bolt the winches to the concrete. The design of these special elements is shown in the appendix A.1. By means of a circuit breaker the winches could be switched on and off depending on the tensile force in the tendons. The circuit breaker was created with a compression spring. As soon as the spring was compressed to a certain length, the electric circuit was interrupted and the winch shut down until the tension in the tendons was reduced sufficiently to elongate the spring enough to close the electric circuit again. Figure 6.13 shows these self-made switches. The desired force at the end of the tendon could be obtained by adjusting the necessary

	max. load in the experiment	manufacturer	No. of ropes in the closure
1×2-part clamp ring	8 kN	Seilerei Wüstner	1
2×2-part clamp ring arranged in series	12 kN	Seilerei Wüstner	1
1×small cable clip	1,5 kN	Stabilit	1
1×large cable clip	2,5 kN	Stabilit	1
2× small cable clip arranged in series	6,5 kN	Stabilit	1
1×large cable clip	2,5 kN	Teufelberger	2
3×large cable clip arranged in series close to each other	12,5 kN	Teufelberger	2
3×large cable clip arranged in series with distance to each other	16 kN	Teufelberger	2

Table 6.5: Results of the load tests carried out on different anchorage systems for ropes

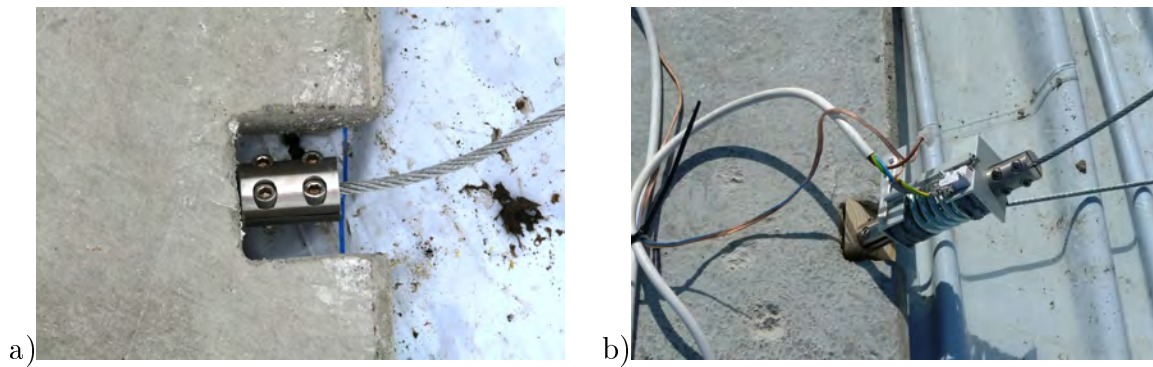


Figure 6.13: Details of the anchorage system in the concrete shell a) 2 part clamp ring on a radial tendon b) compression spring to regulate the tension in the tendons in circumference direction

shortening of the spring to turn off the switch. The used spring has a spring constant of  $35 \text{ N/mm}$  and a length of  $120 \text{ mm}$ . The position of the winches and the adjustments of the switch are described in detail in chapter 6.2.3.

### 6.2.3 Test setup

First the properly folded pneumatic formwork was placed on the plane working surface. Then it was covered with a silage film in order to protect the pneumatic formwork from possible damages and to create a sliding surface between the pneumatic formwork and the precast concrete parts allowing the elements to slide on the surface of the PVC membrane into their final position. This silage film had previously been marked with the correct position of each element of the flat plate, allowing and speeding up the

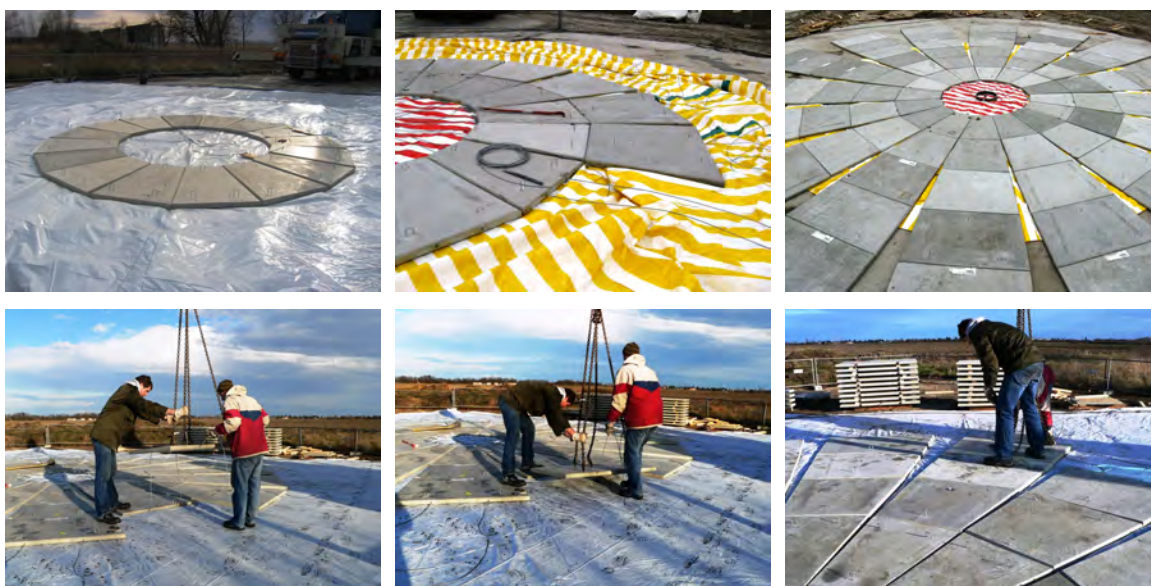


Figure 6.14: Pictures of the assembly on site

subsequent assembly of the elements. In Figure 6.14 pictures of the assembly on site are shown.

With a crane the elements are positioned on the not yet inflated pneumatic formwork and then assembled with tendons. In Figure 6.15 the arrangement of the precast parts is shown. The process started with the smallest elements (elements type 1) forming the internal ring – called *annulus no. 1* - then the next set of concrete parts (elements type 2) are positioned to create the next loop – called *annulus no. 2*. In this manner all 96 elements are positioned one after another until the flat plate is formed.

In order to inflate the pneumatic formwork the blower described in chapter 5.1.3 is used. The blower is connected to the pneumatic formwork with the help of an air tube as shown in Figure 6.16a.

The steel tendons in the radial direction are pulled through during the assembly process and anchored with 2-part clamp rings against the concrete in the element type 6. To fix the steel cables in the middle of the plate various possible approaches were chosen during the several attempts to erect the concrete shell. The most suitable solution was to place a steel ring with 32 holes for installing the steel tendons on the future apex of the shell. As shown in the picture of Figure 6.16a the tendons in the radial direction were arranged in loops. This has the advantage that in the middle of the plate no 2-part clamp rings have to be installed. All tensile forces in the radial tendons are carried by the steel ring which is designed accordingly.

The steel ropes in the circumference direction are also labeled in Figure 6.15. They were pulled through after all elements had been positioned. The theoretical lengths of these cables at the beginning of the erection process as well as in the finished shell are listed in Table 6.6. In order to tighten the tendons in the circumference direction and force them to shorten, the winches are attached to the concrete parts. The location of the winches is shown in Figure 6.15. It can be seen that in the annuli 4, 5 and 6 there



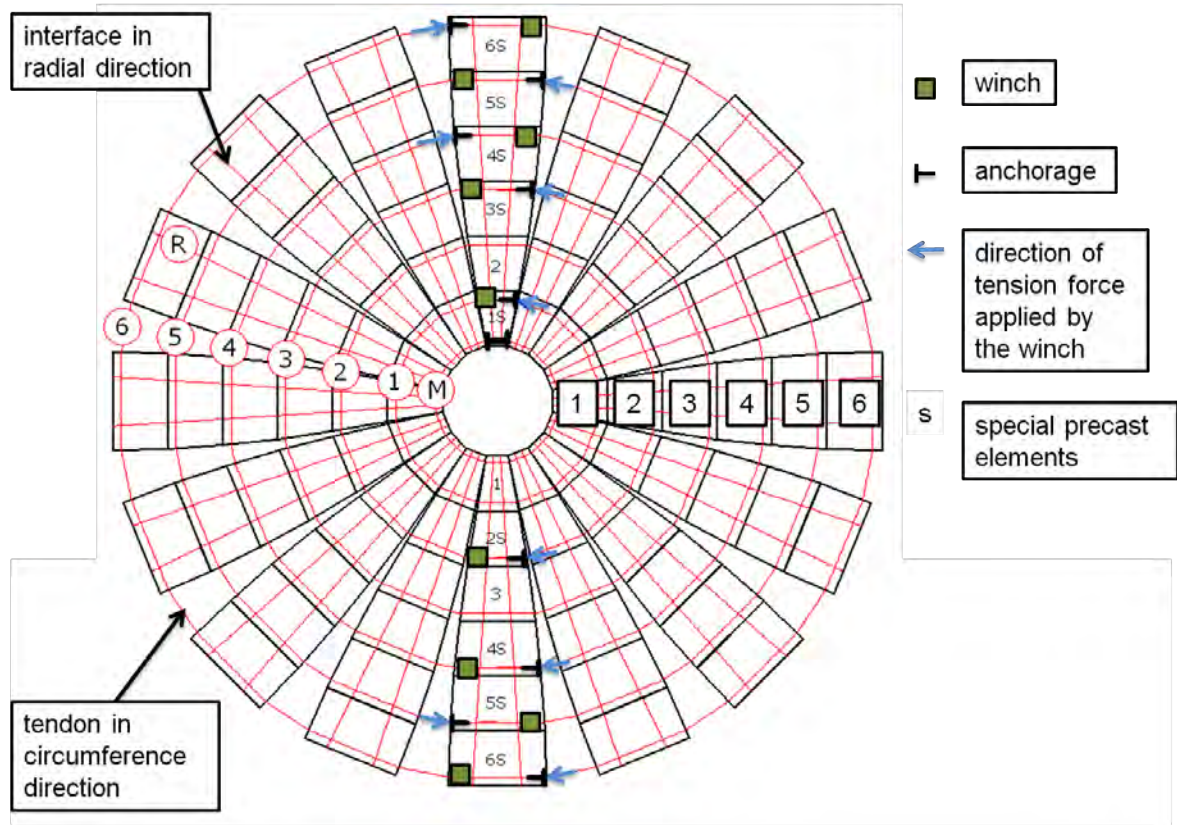


Figure 6.15: Arrangement of the 96 precast elements

are two winches, therefore every winch only has to roll half of the length difference listed in Table 6.6. The cable tagged *M* did not need a winch because the edges of the elements were already side by side from the start and thus no change of the length of the tendon is necessary.

The tensile force in the tendon at the passive end during tensioning was regulated with the help of the spring-switch system described in chapter 6.2.2. The switch was adjusted in a way so that it turned off the power supply of the winch as soon as the spring experienced a shortening of  $50\text{ mm}$ . This shortening equals a force of  $1,75\text{ kN}$ . The force, which had to be applied by the winches, however, was higher because of the losses due to friction. These losses are quite high because of the large angular displacement. The deflection of the tendons in the annuli 1 to 3 is  $360^\circ$  - a full circle.

According to Eurocode 2 [10] the losses due to friction  $\Delta P_\mu(x)$  in post-tensioned tendons may be estimated from the equation 6.2:

$$\Delta P_\mu(x) = P_{max}(1 - e^{-\mu(\theta + k \cdot x)}) \quad (6.2)$$

$\theta$  is the sum of the angular displacements over a distance  $x$ .

$\mu$  is the coefficient of friction between the tendon and its duct.



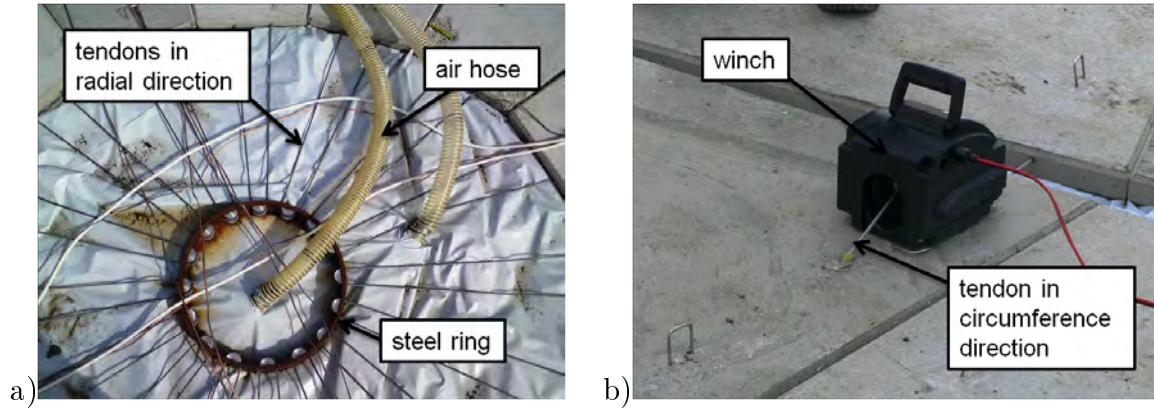


Figure 6.16: Details of the concrete shell a) steel ring to anchor the tendons in radial direction b) winch

Tendon No.	Length of the tendon in circumference direction		Difference [m]
	in the initial position [m]	in the final position [m]	
M	6, 5	6, 5	0, 0
1	10, 9	10, 5	0, 3
2	16, 8	15, 7	1, 1
3	22, 7	20, 0	2, 7
4	28, 5	23, 3	5, 2
5	34, 4	25, 5	8, 9
6	40, 2	26, 3	13, 9

Table 6.6: Length of the tendons in circumference direction

$k$  is an unintentional angular displacement for internal tendons (per unit length). In the absence of data in a European Technical Approval, values for unintended regular displacements for internal tendons generally ranged between  $0,005 < k < 0,01$

$x$  is the distance along the tendon from the point where the prestressing force is equal to  $P_{max}$  (the force at the active end during tensioning)

Table 6.7 lists the necessary tensile forces applied by the winches in order to sustain a force of  $1,75 kN$  in the passive end during tensioning. The losses due to friction are highly affected by the sum of the angular displacements  $\theta$  over the distance of the tendons. In the annuli 4 to 6 the sum of the angular displacement amounts to  $180^\circ$  whereas in the annuli 1 to 3 the tendons formed even a full circle therefore  $\theta$  amounted to  $360^\circ$ . According to examinations of friction losses with high density polyethylene ducts the coefficient of friction  $\mu$  between this type of strand and its PE duct amounts to  $0,14$  [52]. The Eurocode 2 says that in the absence of data in a European Technical Approval, values for unintended regular displacements for internal tendons generally ranged from  $0,005 < k < 0,01$  per meter. Because of the fact that this tendon-duct system does not have any technical approval, being on the safe side,

the unintentional angular displacement  $k$  was assumed to be 0,01 per meter. The distance  $x$  in the equation 6.2 describes the sum of the length of all ducts through which the specific tendon passes. The forces which had to be applied at the active end during tensioning varied between 4,9 kN and 5,1 kN and could easily be applied by the mentioned winches.

annulus no.	number of winches	necessary tensile force applied by the winch	losses due friction
		[kN]	[%]
1	1	4,9	64
2	1	4,9	64
3	1	5,0	65
4	2	5,0	41
5	2	5,1	41
6	2	5,1	41

Table 6.7: Necessary tensile force at the active end during tensioning

#### 6.2.4 The experiment



Figure 6.17: Erection processs of the concrete shell

The pictures in Figure 6.17 show how the pneumatic formwork was slowly inflated with air, the elements lifted and the plane plate was transformed into a hemispherical shell. In Figure 6.18 photos of the finished concrete shell are displayed.



Figure 6.18: The finished concrete shell

Figure 6.20 shows a series of photos of the erection process. Every five minutes a picture was taken and the current air pressure in the pneumatic formwork was measured. In this attempt to build the concrete shell, the experiment had to be terminated after  $63\text{ min}$  due to problems with the pneumatic formwork. However, approximately 87 % of the weight of the entire shell had been lifted with the pneumatic formwork therefore the pressure in the pneumatic formwork and the corresponding lifted weight could be investigated.

The pressure in the pneumatic formwork was measured with the help of a hose water level as shown in Figure 6.19. An U-shaped hose is filled with water until a certain level. One end of the tube is connected to the inside of the pneumatic formwork. Therefore, on this side of the water barrier the same pressure as in the formwork acts on the water. The other end of the hose is open and thus the atmospheric pressure is acting. Due to the difference in the degree of pressure on the two sides of the water the height of the water levels is different. A  $10\text{ m}$  high water column has by definition a hydrostatic pressure at the bottom of approximately  $1\text{ bar}$ . Therefore, a difference in the water level of  $10\text{ mm}$  describes a pressure in the pneumatic formwork of  $1\text{ mbar}$ .

Figure 6.20 shows the time span between the start of the experiment and the current measurement as well as the observed actual pressure in the pneumatic formwork  $p_{\text{actual}}$  at 14 different stages of the erection process. Moreover, during the experiment the number of elements lifted by the pneumatic formwork was permanently monitored. Therefore the weight lifted by the pneumatic formwork  $G_{\text{actual}}$  could be calculated.

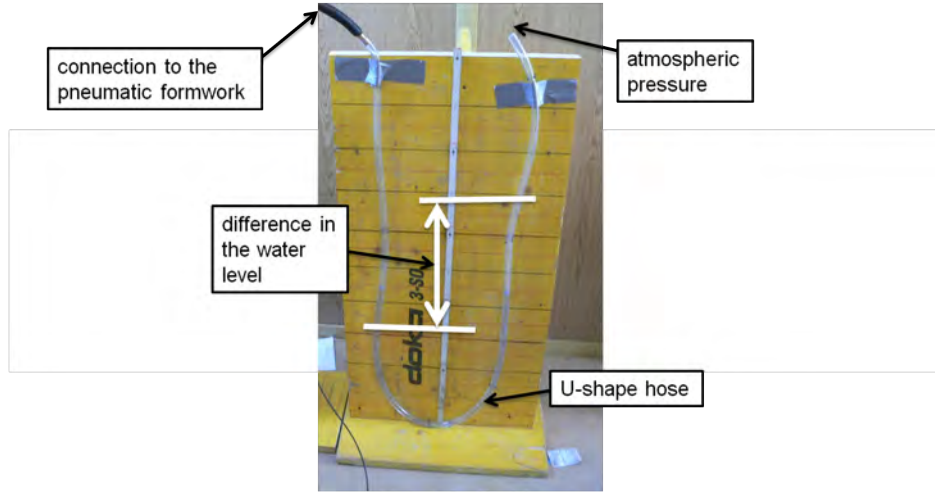


Figure 6.19: Hose water level

In the diagram in Figure 6.21 the correlation between the weight lifted by the pneumatic formwork  $G_{actual}$  and the corresponding air pressure existing in the pneumatic formwork  $p_{actual}$  is shown. Taking equation 4.2 into account, a linear correlation between the lifted weight and the pressure in the pneumatic formwork is predicted. The diagram in Figure 6.21 confirms this linear relation.

Figure 6.22 depicts the change of the air pressure in the experiment over time. With equation 4.2, the theoretical necessary air pressure in order to lift the weight of the shell at a certain time can be calculated. In this calculation it is assumed that at all times, the entire base area of the pneumatic formwork  $A_{base}$  is in contact with the ground. The surface area of the base of the formwork amounts to  $54,2 m^2$ . Therefore, the theoretical pressure  $p_{theoretical}$  in the membrane is calculated as described in equation 6.3 and depicted in the diagram in Figure 6.22.

$$p_{theoretical} = \frac{G_{actual}}{A_{base}} \quad (6.3)$$

The diagram shows that the actual pressure in the formwork is higher than the theoretical one. This can be explained by the fact that not the entire base area of the pneumatic formwork was in contact with the ground at all times. As the hemispherical pneumatic formwork tends to minimize its surface area by simultaneously maximizing its volume, its base area decreases with increasing pressure. As the experiment lasted  $50 min$  the theoretically calculated air pressure amounted to  $20,1 mbar$ ; this corresponds to a base surface area of  $39 m^2$  which is approximately 72 % of the original base area. Hence, the reduction of the base area is not a negligible factor.

### 6.2.5 Experience gained from this experiment

This field experiment showed that a concrete shell can be built with this construction method. The tendons in radial direction hold the elements together and simultaneously





Figure 6.20: Erection process of the concrete shell

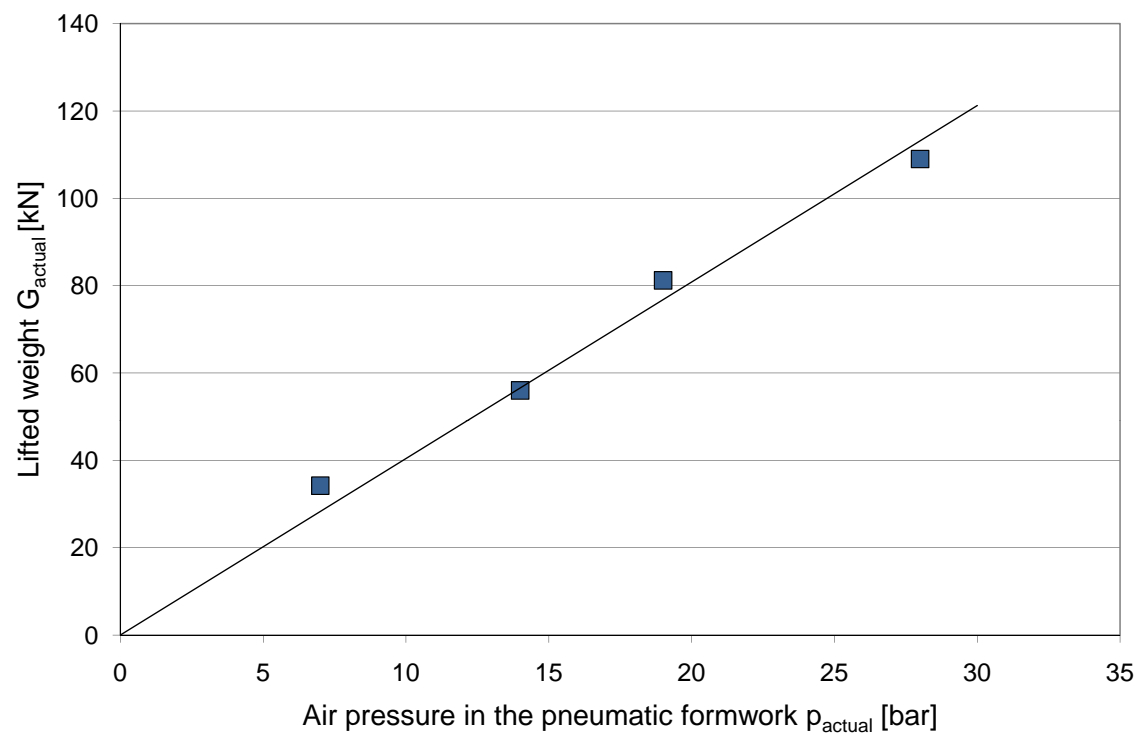


Figure 6.21: Correlation between the lifted weight and the air pressure during the erection process of the concrete shell

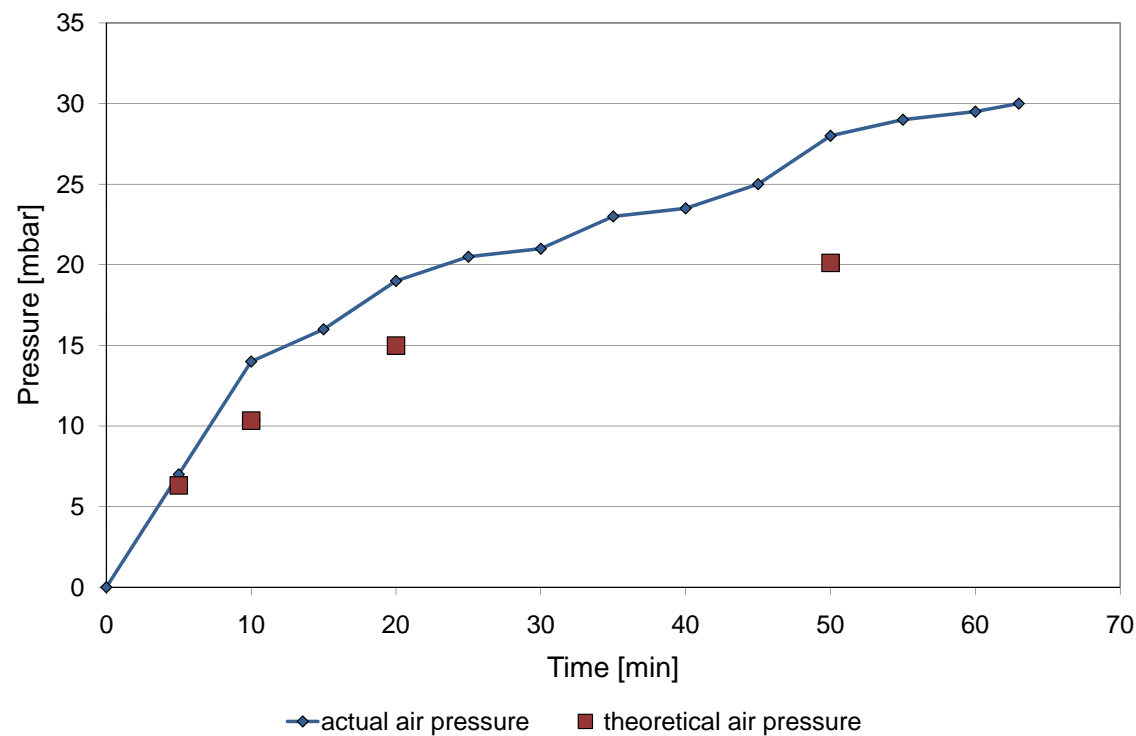


Figure 6.22: Measured and theoretically calculated air pressure during the erection process of the concrete shell

allow them to rotate around the hinge in order to move into their final position. The tendons in the circumference direction and the winches guide the elements in order to properly close the radial interfaces.

The most challenging element of this construction method is the pneumatic formwork. Although the gluing of the pneumatic formwork was carried out with special diligence, the high tensile forces could not always be borne by the seams. As long as the leakage caused by a surface defect of the glue was small, the air loss could be compensated with the air blower. When air streams out of the opening, an additional loading is applied to the edge of the leakage. Through the long term loading the opening becomes larger until the seam busts. Then a drop in air pressure in the pneumatic formwork is inevitable. This issue was even more significant since the air pressure could not be exactly determined in advance. The contact area between the pneumatic formwork and the subsoil decreased during the experiment, therefore a higher air pressure in the formwork was necessary which led to higher tensile stresses in the membrane. Calculating with the entire base area of the pneumatic formwork, the necessary air pressure for lifting the entire concrete shell would be  $24\text{ mbar}$ . When the concrete shell was lifted in the course of the field experiment, however, an air pressure of  $37\text{ mbar}$  was necessary.

If larger shell structures are to be built with this construction method, the pneumatic formwork has to be enhanced e.g. with tendons as described in chapter 5.5.

# Chapter 7

## Ice shells

### 7.1 Preface

In the winter season 2008/2009 the Pneumatic Formwork Method was tested on two ice shells. The experiment took place in Obergurgl, an alpine village in Tyrol, Austria, already mentioned in chapter 3.2.

In this winter season two ice domes were to be built. Basically the design for the construction of both shells was identical except for the different size of the two shells. The small ice shell had a plate diameter of  $6\text{ m}$  and a thickness of  $120\text{ mm}$ . The plate diameter of the large one amounted to  $13\text{ m}$  and its thickness was  $200\text{ mm}$ . In the following chapters these two experiments are described parallelly. Moreover, in the appendix A.2 drawings of the two ice shells are included.

### 7.2 Description of the essential elements

#### 7.2.1 Ice elements

The first step in building the ice shell was the producing of the ice elements which were to be subsequently lifted by the pneumatic formwork.

In the preliminary experiments with wood and concrete the respective elements were precast and then transported to the site. For the building of the ice shell, another approach was chosen. The ice elements were produced directly on site in the required position, thus avoiding any unnecessary shifting of the elements and eliminating any problems or damages caused by the maneuvering of the elements.

In order to create the elements and to make sure that they were arranged symmetrically around the center of the prospective shell an ice plate with the shape of a regular triacontakaidigon was made. At first, the working surface was prepared. A mostly even surface was crucial otherwise the thickness of the ice plate would vary due to the property of the water of leveling. Now the pneumatic formwork could be placed



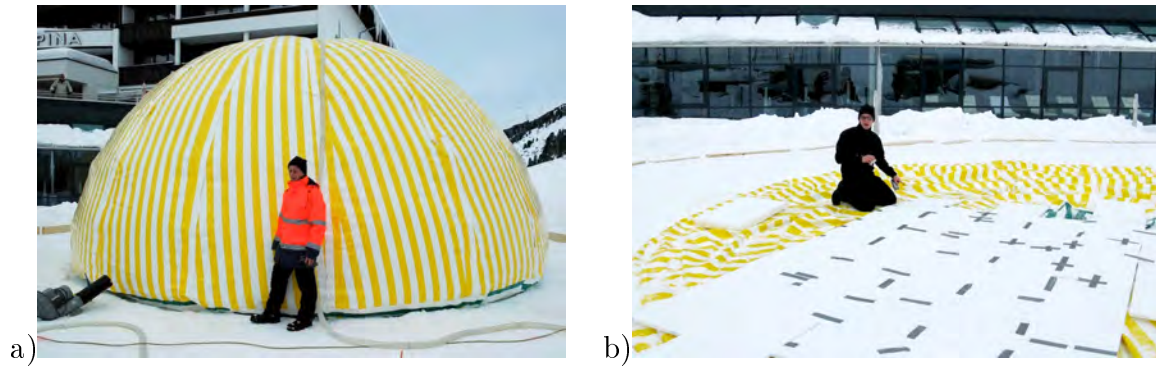


Figure 7.1: Pneumatic formwork of the large ice shell a) inflated with air b) protected with a layer of styrofoam plates

under the future ice plate. In order to fold the membrane properly, the pneumatic formwork was inflated with air – as shown in Figure 7.1a – and subsequently drained. To protect the PVC membrane, styrofoam plates with a thickness of 20 *mm* were placed on the folded pneumatic formwork. This protective layer was necessary because later on operations with chain saws were carried out. Working with a chain saw on the ice lying on top of the membrane presents the risk of cutting into the pneumatic formwork.

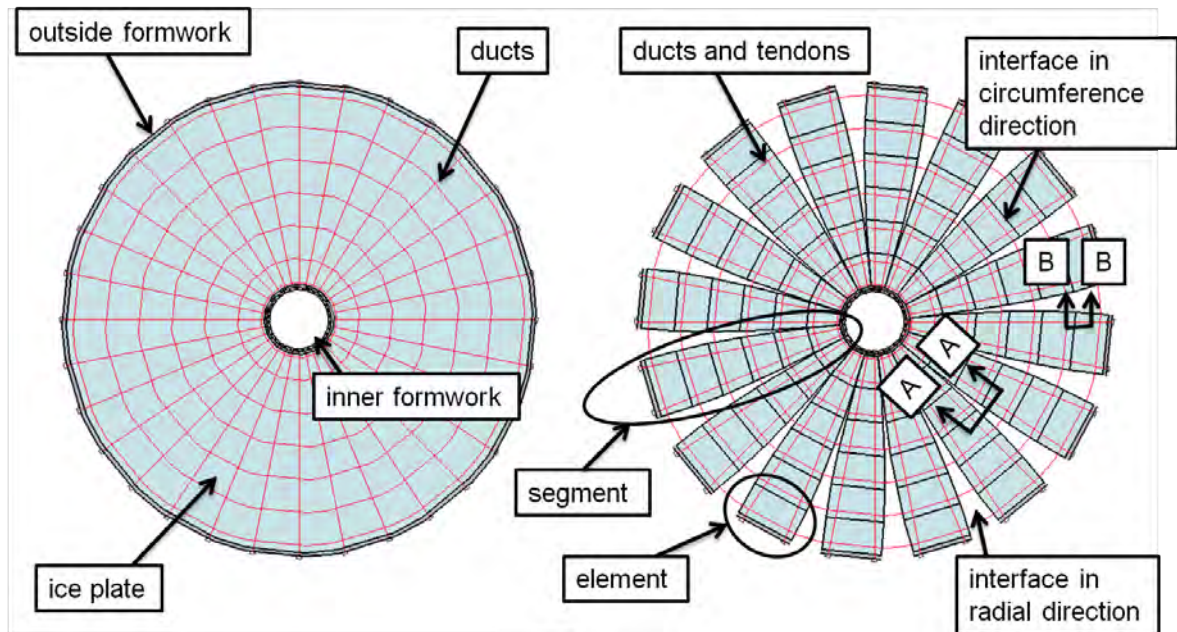


Figure 7.2: Schematic sketch of the ice plate and the ice elements

After carefully leveling and sealing the working surface, a formwork was placed in order to mold the ice plate. The formwork consisted of an outside and an inner ring for containing the water which would finally turn into ice. The outside formwork was a 32-angled polygon made of wooden boards and the inner ring consisted of 16 wooden boards. The left sketch in Figure 7.2 shows the outside and the inner formwork. In the left image in Figure 7.3 the assembly of the inner formwork is shown and the right image shows the inner and outer formwork in its final position. Water, which would

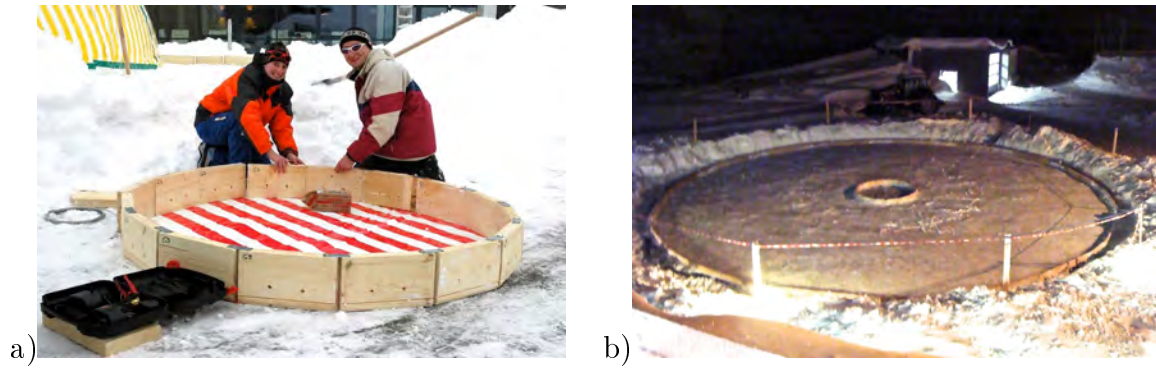


Figure 7.3: Formwork of the large ice shell a) assembly of the inner formwork b) positioned formwork

finally turn into ice, was sprayed inside the mold. The thickness of the ice plate was  $200\text{ mm}$  for the large ice shell and  $120\text{ mm}$  for the small ice shell. The ice was made by simply spraying tap water into the mold with a common garden hose. Small layers of water, with a height of only a few millimeters, were applied at the same time. As soon as this water turned into ice the next layer of water could be added. Because of the fact that the water was sprayed in thin layers, it could be ensured that the whole cross section was frozen, thus creating a good bond between the ice layers. Whenever the weather conditions would allow it, small layers of fresh snow were added to the water in order to accelerate the ice making process.

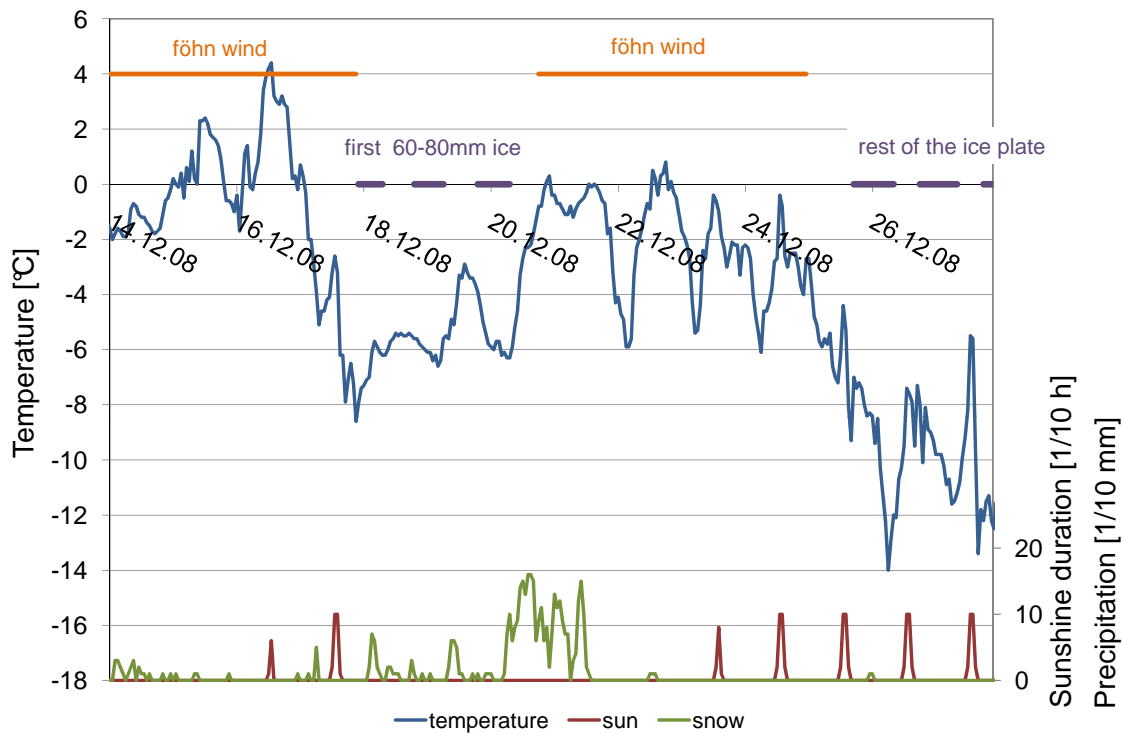


Figure 7.4: Climate data from 14<sup>th</sup> to 28<sup>th</sup> December 2008[1]

Figure 7.4 shows the climate data of the time period during which the ice was produced. In this diagram the horizontal axis shows the date and the mark on this axis always represents the beginning of the day at 00 : 00 *h*. All measurements are on an hourly basis, performed by the Central Institute for Meteorology and Geodynamics (ZAMG), Austria's national weather service agency [1].

The dark blue line shows the temperature during this time period. Moreover, the diagram presents information about the duration of the sunshine and the amount of precipitation. The red line refers to the secondary axis and shows the sunshine duration in the unit 1/10 *hour*. A value of 10 represents one full hour of unclouded sunshine. The green line shows the precipitation in 1/10 *mm* which is also depicted on the secondary vertical axis. Naturally, in winter the precipitation is always snow.

On the 14<sup>th</sup> of December 2008 the preparatory work on the working surface and the formwork was finished and the ice making process could have started. But a warm föhn wind over the next days caused the temperature to rise above freezing. After this period of warm weather three rather cold nights made it possible to produce the first 60 *mm* to 80 *mm* of the ice plate. Another föhn wind period caused another delay in the ice production. Finally, during the Christmas break, the ice plates with a thickness of 200 *mm* and 120 *mm* could be finished.

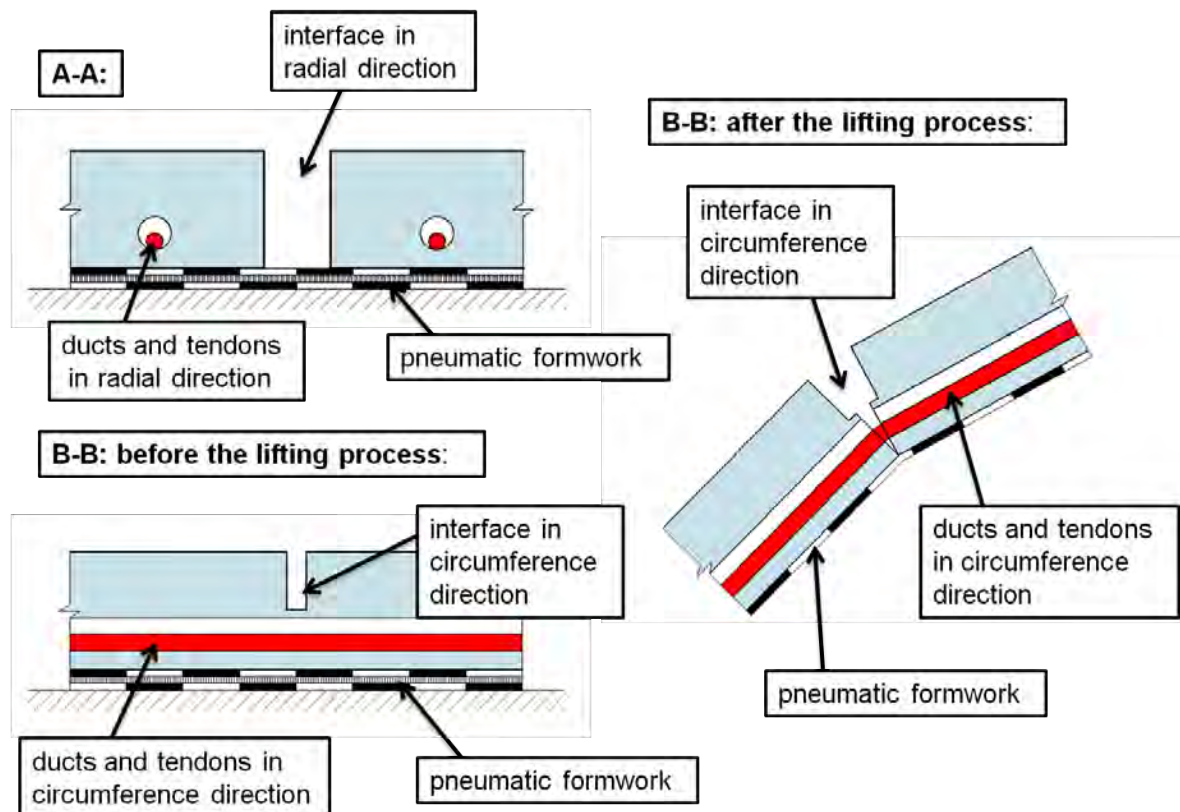


Figure 7.5: Sectional views for the basic sketch in Figure 7.2

In order to be able to pull through the tendons afterwards, ducts had to be inserted into the ice elements. For the ducts the same polyethylene tubes as for the concrete shell

were used. Their external diameter was  $10\text{ mm}$  and their inner diameter was  $8\text{ mm}$ . The red lines in the left sketch of Figure 7.2 symbolize the position of ducts. Like in the concrete shell, ducts were inserted in radial direction as well as in circumference direction.

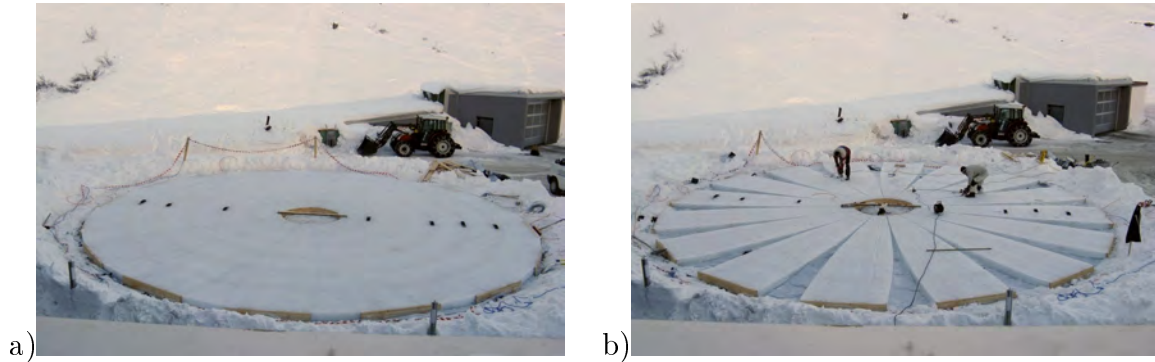


Figure 7.6: Picture of a) the ice plate and b) the individual ice elements

As soon as the ice plate had been finished, those parts of the ice which were superfluous for the transformation into a shell were removed. In order to obtain the individual elements, their shape, size and location were marked on the ice plate. With the help of a chain saw the interfaces in the radial direction were cut out of the ice plate. Thus the segments were created - as shown in the right sketch of Figure 7.2. To subdivide the ice segment into elements the interfaces in the circumference direction were produced by cutting into the ice with the chain saw. Only three quarters of the height of the cross section were cut with the saw. The last part of the interface was created by breaking these predetermined breaking points. When inserting plastic wedges into the cuts and applying an appropriate impact, the ice easily broke and small cracks appeared. This technique of cracking the ice worked well because of the soft styrofoam plates situated under the ice. In Figure 7.5 the section  $A - A$  and  $B - B$  marked in Figure 7.2 are shown. The section  $A - A$  is a sectional view in the circumference direction therefore the ducts, tendons and the interface in the radial direction are shown.

Figure 7.6 shows the ice plate of the large ice shell before as well as after cutting the elements.

### 7.2.2 Pneumatic formwork

For the large ice shell, a pneumatic formwork with the same dimensions as in the concrete experiment was used, as described in chapter 5. A picture of the inflated pneumatic formwork for the large ice shell is shown in Figure 7.1a. A hemispherical pneumatic formwork was also utilized for the small ice dome. All considerations made for the concrete shell and the large ice shell could be applied to the small ice shell, only the dimensions had to be altered accordingly. In the appendix A.3 drawings of the individual parts of the pneumatic formworks are given.



### 7.2.3 Tendons

The same stainless steel tendons with a diameter of  $5\text{ mm}$  like the ones used for the preliminary experiment with the concrete shell were employed for both ice shells. The properties of these ropes are described in chapter 6.2.2.3. The winches of the earlier shells could be reused for the tightening of the tendons.

## 7.3 Test setup

The steel tendons were pulled through the ducts of the finished ice elements. The ropes in the radial direction were placed in the previously prepared openings in the ice and the timber planks of the outer and inner formwork. To minimize the number of anchorage elements the cables were placed in loops on the outer formwork. In the middle of the plate, the radial tendons were anchored by means of the 2-part clamp rings described in chapter 6.2.2.3. To allow the tendon to vary its length, compression springs were put between the wooden boards of the inner formwork and the clamp rings. Figure

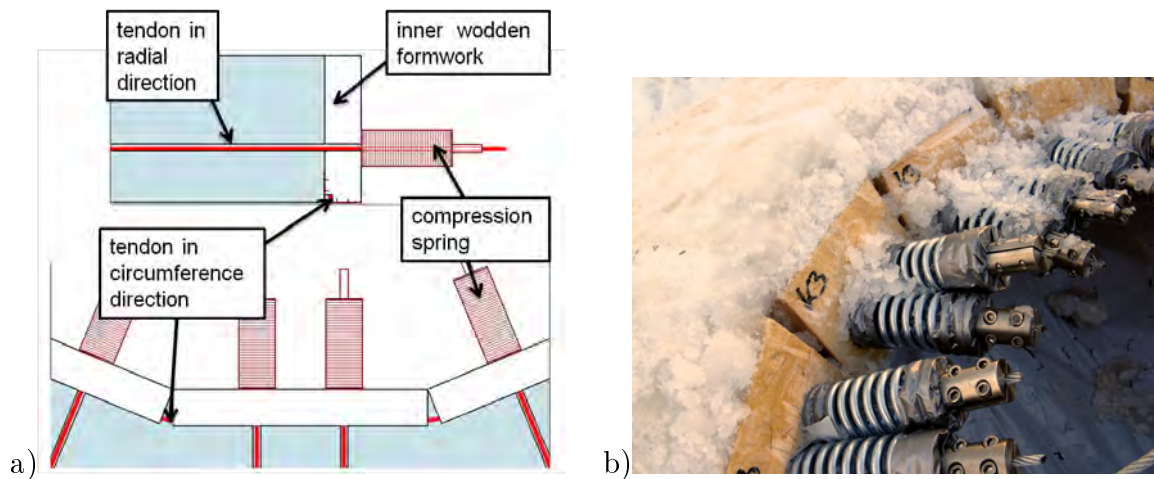


Figure 7.7: Spring - anchorages of the tendons in radial direction a) sketch of the large ice shell b) picture of the small ice shell

7.7 shows a sketch and a picture of this anchorage system. These springs had already been tested with the concrete shell but due to a thickness of only  $50\text{ mm}$ , the tendons did not experience any change of length and thus these springs did not prove to be the optimal solution for anchoring the radial steel tendons in the concrete dome. In the ice shell, however, the length of the tendons increases during the transformation process. Figure 7.8 shows a sketch of the cross-section drawn to scale in its initial position as well as after the lifting process. The center of gravity of the tendons in the radial direction is situated  $75\text{ mm}$  above the lower surface of the ice. During the lifting process the joints in the circumference direction open with the increasing deformation of the ice plate. Because of the distance of the tendon to the lower surface the length of the rope has to increase during the transformation process. In Figure 7.8 it is assumed that the ice elements have a surface of contact of  $20\text{ mm}$ . According to this assumption

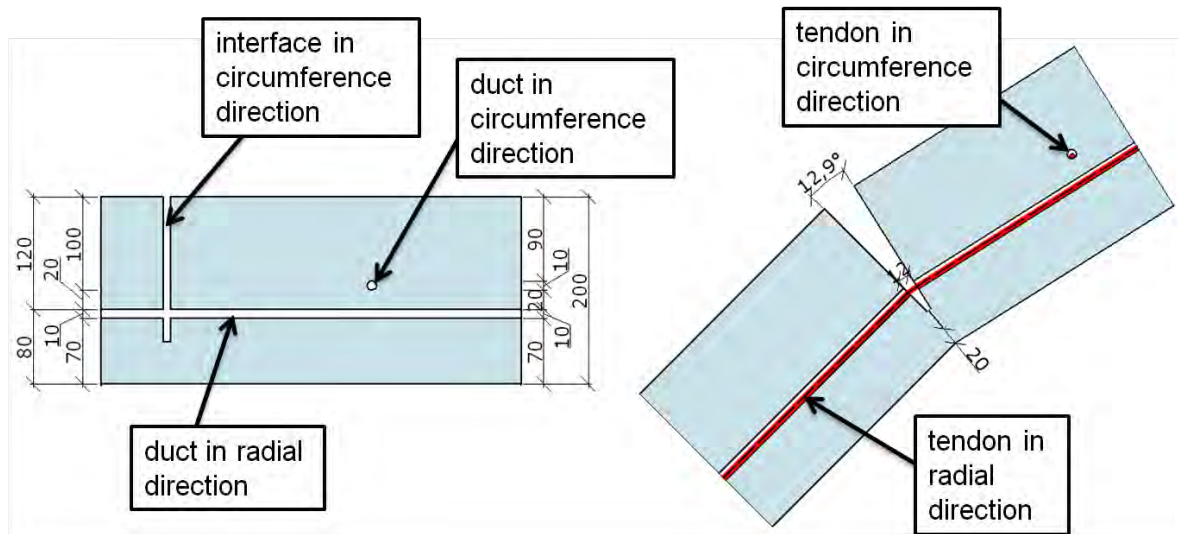


Figure 7.8: Drawing of the cross section before and after the erection process

the length of the rope has to increase about  $12\text{ mm}$ . The total necessary lengthening of the tendon therefore amounts to  $60\text{ mm}$  which is more than the stretching of the steel ropes under load. With the help of the compression springs this necessary lengthening of the tendon can be gently balanced.

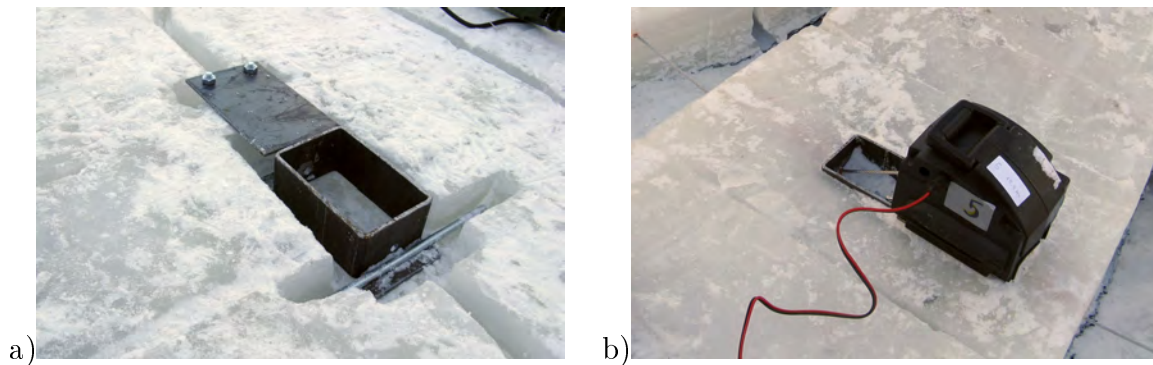


Figure 7.9: Winches a) built-in steel parts to anchor the winches b) winch

The tendons in the circumference direction have to be pulled through as well and are tightened with the same winches used for the concrete shell. To fix these winches to the ice elements and to anchor the passive end during the tensioning, built-in steel parts were used, which can be seen in Figure 7.9.

## 7.4 The experiments

### 7.4.1 Small ice shell

After all of the preparatory work had been finished, the experiments could take place. First, the small ice shell was erected. Figure 7.10 illustrates the transformation. The

pneumatic formwork was slowly inflated with air and therefore the elements lifted. As it can be seen in the pictures the elements did not lift equally. This was caused by a different thickness of the ice segments. On the right hand side of the shell, in Figure

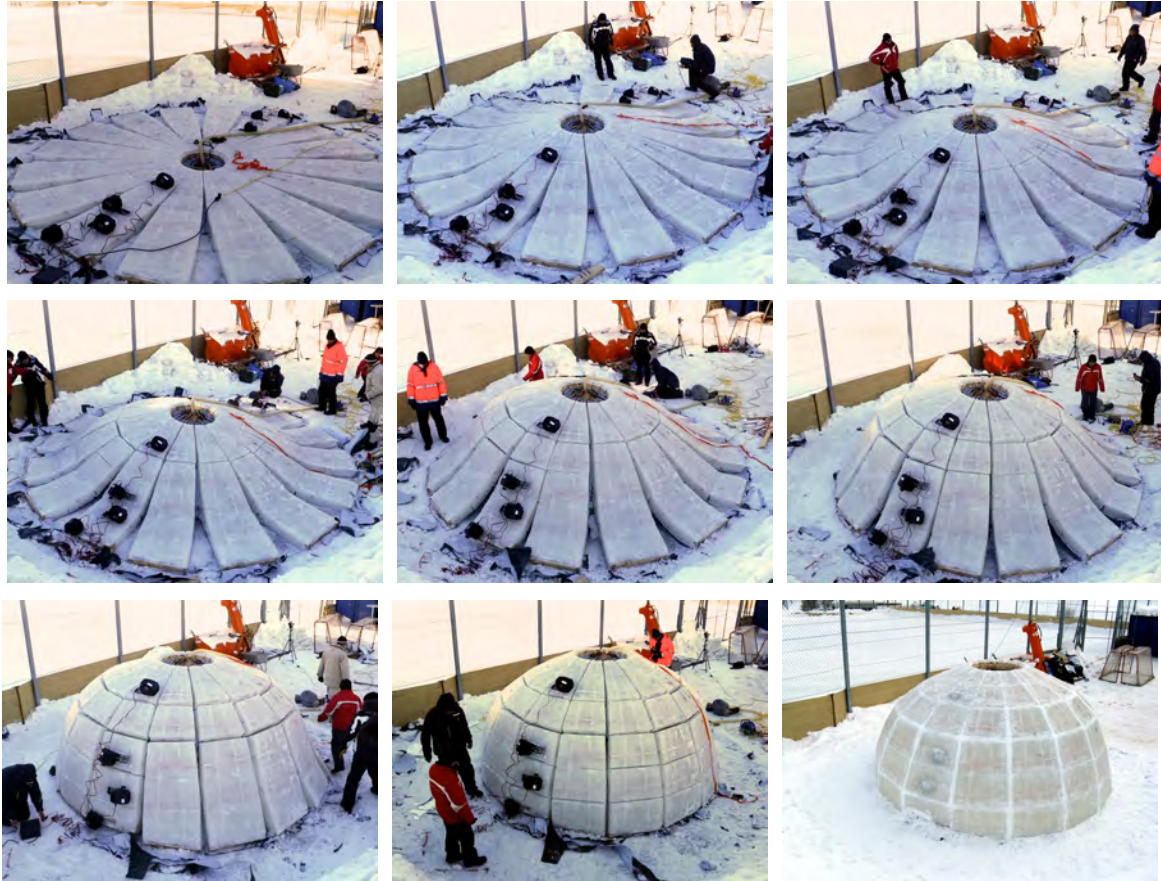


Figure 7.10: Erection of the small ice shell

7.10, the ice was approximately  $30\text{ mm}$  to  $40\text{ mm}$  thicker than on the left hand side, due to an inaccuracy during the production process. Therefore the elements with the smaller dead load were lifted first. As soon as all elements had been lifted completely from the supporting ground, this inhomogeneity dissolved. When the elements reached their final position a mixture of snow and water was filled into the gaps between the elements. After the hardening of this water-snow-mix, the pneumatic formwork was deflated and the shell structure functioned on its own.

For putting the finishing touches on the ice shell, the winches and springs were dismounted and an entrance was created. Figure 7.11 shows pictures of the finished small ice shell with a height of  $2,0\text{ m}$  and a inner base diameter of  $3,9\text{ m}$ .

#### 7.4.2 Large ice shell

The experiment of the large ice shell was also carried out by slowly inflating the pneumatic formwork. The lifting of the elements can be seen in the pictures in Figure 7.12.





Figure 7.11: Finished small ice shell

Unfortunately, the experiment with the large ice shell could not be completed since during the lifting process the wooden boards of the inner formwork collapsed and the experiment had to be aborted.

In the following section the cause of the collapse of the wooden board is investigated. The first drawing in Figure 7.13 shows the wooden board of the inner formwork in plan view. On the left hand side, the ice elements are attached to the wooden board and on the right side, the steel tendon is anchored by means of the spring and the 2-part clamp ring. The second drawing in this figure shows the section view *1-1* which is a cross section of the wooden beam. The blue arrow in this drawing shows the force acting on the wood caused by the radial tendons. The reaction force of this horizontal force is carried by the tendon in circumference direction  $M$ , displayed with the red arrow. In the third drawing in Figure 7.13 the vertical axis  $z$  of this cross section is displayed ignoring the thickness of the board. Moreover, in this simplified static system the ice segment is also neglected. Therefore it is assumed that only the wooden board takes part in this load transfer. In reality, however, the ice is supporting the wood and smaller forces will appear in the wood. By using this simplification the worst case is assumed.



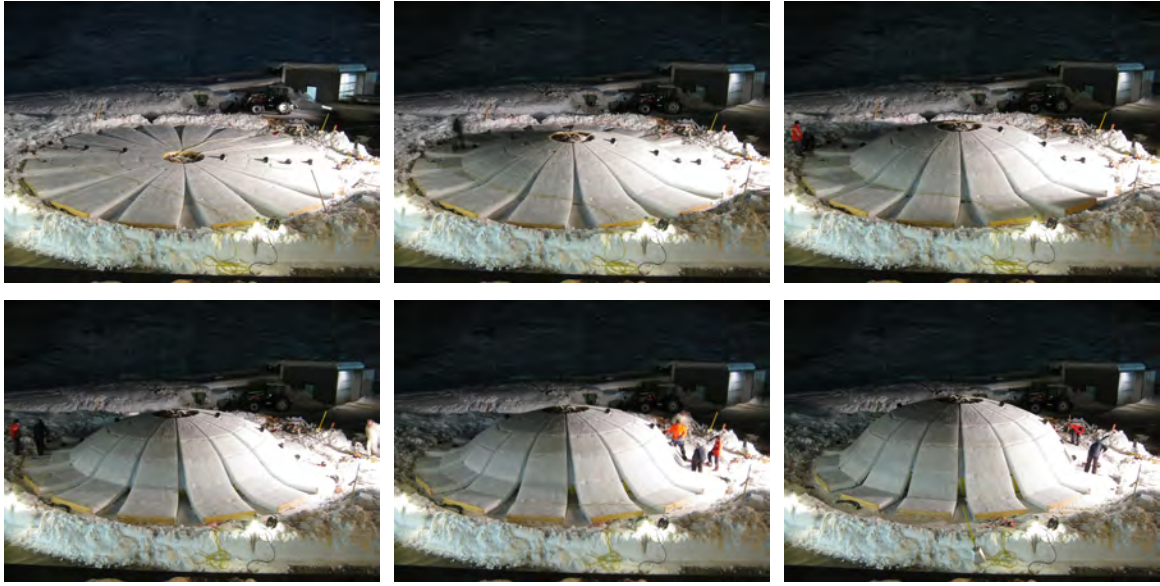


Figure 7.12: Lifting process of the large ice shell

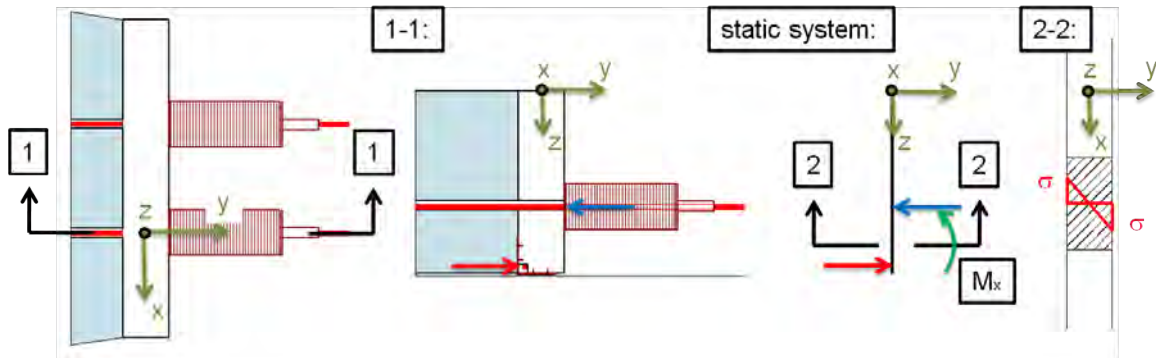


Figure 7.13: Sketches of the wooden inner formwork

It can be observed that this force couple has a distance of  $66\text{ mm}$  to each other. Therefore a bending moment  $M_x$  occurs. The last drawing shows the sectional view 2-2 with the normal stresses  $\sigma$  which are caused by the moment  $M_x$ . These stresses, however, act perpendicularly to the wood fibers. According to Eurocode 5 [60] the tensile strength of wood perpendicular to the wood fibers is much smaller than the strength parallel to the fiber. Conifer wood has a characteristic tensile strength perpendicular to the wood of approximately  $0,4\text{ N/mm}^2$  and a characteristic compressive strength of  $2,2\text{ N/mm}^2$  to  $2,9\text{ N/mm}^2$  depending on the strength class.

By using this simplified static model, the tensile and compressive stresses in the wooden board can be estimated. Figure 7.14 shows the absolute value of the stresses according to different forces in the radial tendons, assuming that the participating cross section is  $100\text{ mm}$  wide and  $50\text{ mm}$  high. If an entire ice segment is lifted by the tendons only, each of the tendons would have to carry a force of  $6\text{ kN}$ . In this field experiment, however, part of the vertical force is also carried by the pneumatic formwork. The exact size of the loading in the tendons during the collapse remains unknown because no measuring

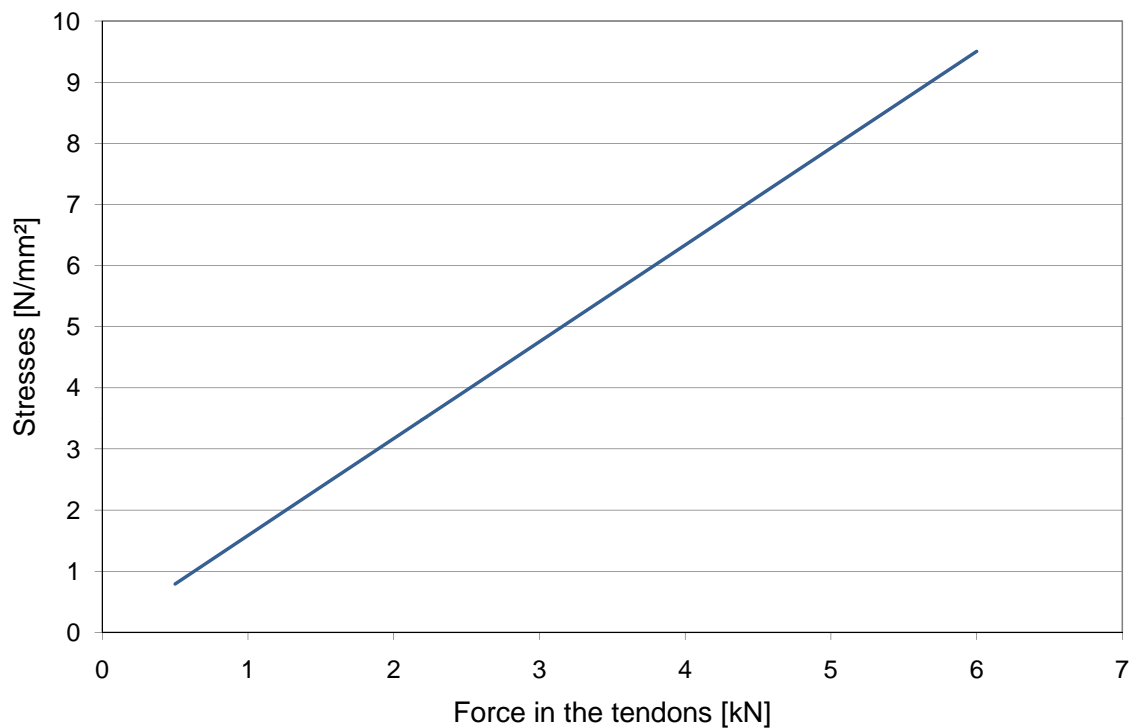


Figure 7.14: Stresses in the wooden board

devices had been installed. But the collapse in the wooden board proves that the tensile strength of the timber had been exceeded which led to an early termination of the field experiment of the large ice shell.

This failure of the inner formwork that caused the collapse of the shell during the erection process could be avoided by designing this specific detail in a different way. One possibility is to use a material with a higher strength, e.g. steel, for the inner formwork. Another solution would be to separate the anchorage of the radial tendons from the wooden formwork. A steel ring like the one used for the concrete shell could be employed to anchor the tendons. A picture of this steel ring used for the concrete shell is shown in Figure 6.16 in chapter 6.2.3.

## Part III

### Segment Lift Method

# Chapter 8

## Basic principle

### 8.1 General description of the method

The key elements of the segment lift method are distorting individual ice segments and subsequently lifting them in order to form a shell.

According to this construction method the shell structure is composed of uniaxially deformed ice segments fitting together in order to create an ice dome. Strictly speaking, the geometry of this structure resembles a cloister-vault with a regular hexadecagon as base area.

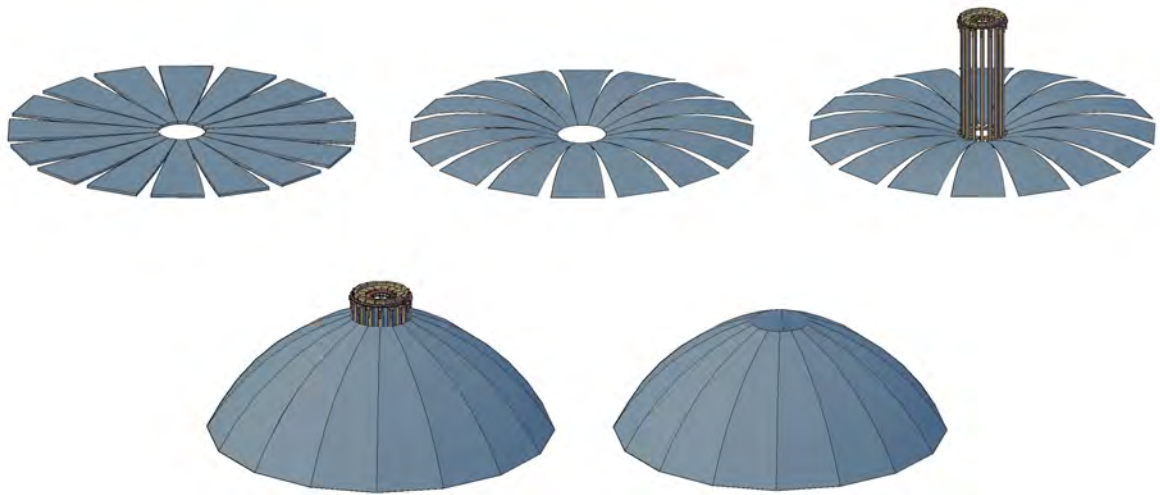


Figure 8.1: Key elements of the segment lift method

In the first step, plane segments made of ice are produced, illustrated in the first drawing of Figure 8.1. To obtain these elements, an ice plate is produced by spraying water on a previously leveled and sealed working surface. Afterwards the parts of the ice, which are superfluous for forming a shell, are removed. In the next step, the segments are distorted uniaxially; this curvature is produced both by elastic deformation

and creep deformation. These deformations generate high tensile stresses, thus tensile reinforcement is placed inside the ice segments during their production.

In order to distort the ice segments, these elements have to be lifted. Subsequently, this working step is referred to as 1<sup>st</sup> lifting process. One way is to lift them by means of a pneumatic formwork which has to be placed underneath the ice elements before producing the ice plate. Another option is to lift the ice segments with a crane or a lifting device and then rest them on stands. In both methods the end parts of each element are bent down.

By maintaining this condition, creep deformations are added to this instant deformation caused by dead load. The second drawing in Figure 8.1 illustrates the distorted ice segments. Then the distorted segments are equipped with temporary tension chains and afterwards lifted and assembled in order to form a shell. Therefore, a temporary mounting tower is created. The distorted ice segments as well as the mounting tower can be seen in the third picture of Figure 8.1.

Then the ice segments are lifted individually either by means of the mounting tower or a crane and fixed to the mounting tower. This lifting process is subsequently called 2<sup>nd</sup> lifting process. The fourth picture in Figure 8.1 shows the segments in their final position. In the last step, the gaps between the segments are filled with a snow-water mix and a tension cable carrying the horizontal thrust is attached. Thus, these individual segments work together as a shell structure. So the mounting tower and the temporary tension chain can be removed - shown in the fifth sketch in Figure 8.1.

## 8.2 Field experiments

Two experiments according to this construction method have been carried out. In the winter seasons of 2009/10 as well as 2010/11 a team from the Institute for Structural Engineering experimented in building an ice shell with an inside base diameter of approximately 10 m and a height of almost 3,7 m. In both cases the ice domes were designed to consist of sixteen individual ice segments which had to be distorted before they could be assembled to form a shell structure.

Many of the individual production steps were similar in both ice shell experiments and are described in a single chapter (chapter 10). One big difference in regard to the construction process is that in the winter of 2009/10 a pneumatic formwork was used for the 1<sup>st</sup> lifting process and the distortion of the ice segments, whereas in season 2010/11 a lifting device, which placed the segments on stacks of wood so that the deformation process could take place, was utilized. To distinguish the two variations of this construction method, they will subsequently be referred to as *Segment Lift Method with Pneumatic Formwork* and *Segment Lift Method without Pneumatic Formwork*.

### 8.3 Considerations regarding the shape

#### 8.3.1 Stresses during the construction process depending on the rise

In the process of building an ice shell with the segment lift method, the lifting of the segments is an important and also precarious procedure. In the 2<sup>nd</sup> lifting process, the ice segments are lifted and rotated in order to place them into their final position. During this lifting process the ice segments are already distorted and temporary tension chains are fixed to each segment. Therefore the static system consists of a compression arch, represented by the ice segment and a tension tie modeled by the temporary tension chain. This static system is depicted in Figure 8.2. The rise of the arch is defined as the maximal distance between the tension tie and the compression arch measured perpendicular to the tension tie.

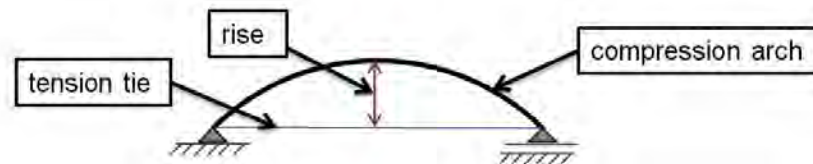


Figure 8.2: Static system during the lifting process

It is important that during the lifting process the stresses in the ice do not exceed the strength of the ice reduced by a partial safety factor. Therefore the occurring stresses while lifting the segments need to be taken into account and analyzed in detail. As described in chapter 10.5.4 the highest stresses occur in the initial position of the lifting process, depicted in Figure 10.58 in chapter 10.5.4. Under the assumption that the ice segment is always of the same length, its maximum tensile and compressive stresses depend on the shape of the arch. If the geometry of the arch resembles an inverted catenary arch, only compression stresses appear in the cross section. Due to the fact that the ice segment is lifted and rotated it is impossible to find a specific shape which will act as an inverted catenary arch during the entire lifting process.

Moreover, the distortion of the ice segment is produced by deflection due to dead load and creeping of the ice which only allows a low accuracy of the final shape. Therefore tensile stresses are accepted in the ice segment during the lifting process. These tensile stresses, however, must not exceed the tensile strength.

The diagram in Figure 8.3 shows the correlation between the size of the rise of an arch and the occurring tensile and compressive stresses for one particular ice segment. This particular ice segment was modeled according to the ice segments used in the field experiments – see chapter 10. The ice segments have an arch length of  $5,54\text{ m}$  and a thickness of  $200\text{ mm}$ . The width of the ice segments is calculated in order to form a closed three-dimensional shell structure with sixteen individual segments. The Young's modulus of ice is set to  $400\text{ N/mm}^2$  and the specific weight to  $9\text{ kN/m}^3$ , as described

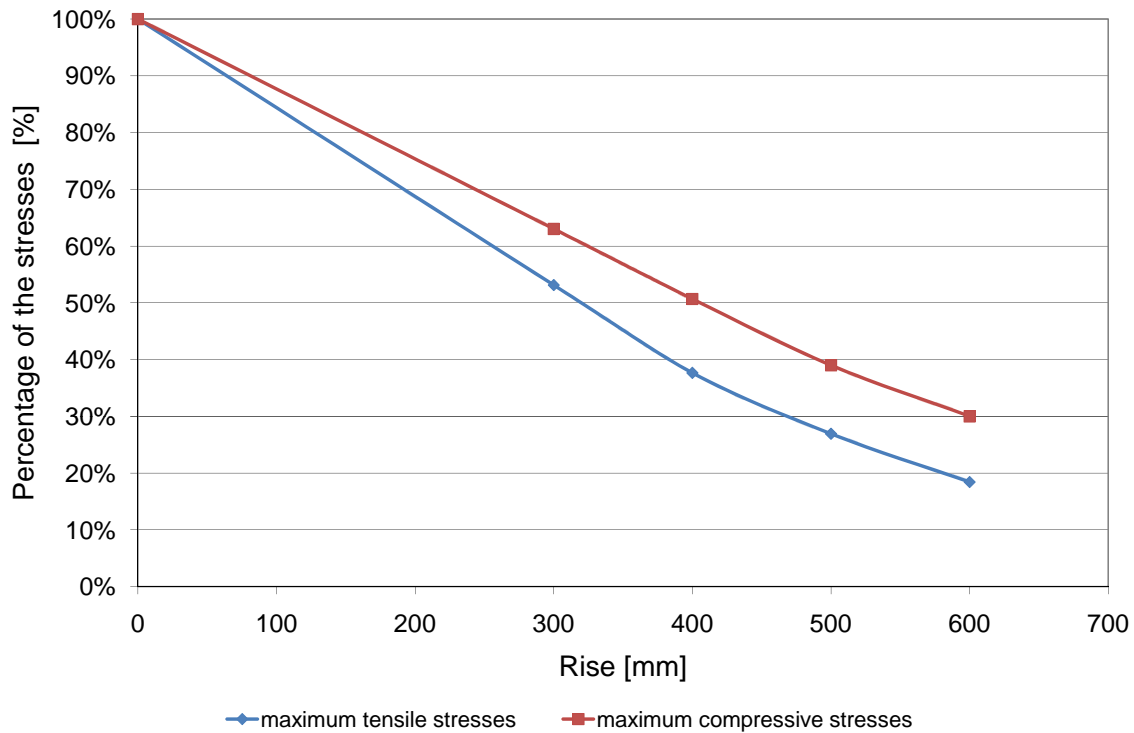


Figure 8.3: Correlation between the stresses and the size of the rise

in chapter 2.2.2. The material properties of the tension tie correspond to the tension chains used in the field experiments described in chapter 10.5.4.

The maximum tensile and compressive stresses of five different shapes are calculated. As a reference, the maximum stresses which would appear in a straight single span girder - the rise equals zero – with the described properties is determined. Of course, in this case, the tensile and the compressive stresses are of the same absolute value because no normal forces occur in the entire beam. These stresses are defined as 100 % and all other calculated values are expressed as a percentage of these stresses. The diagram in Figure 8.3 shows the maximum stresses of the described ice segment with a rise of 300 mm, 400 mm, 500 mm and 600 mm, respectively. It can be seen that especially the tensile stresses decrease as the rise increases. If an ice segment has a rise of 500 mm, its maximum tensile stress is only 30 % of the tensile stress of a straight beam.

The diagram in Figure 8.3 should only give an impression of how the stresses are influenced by the rise of the ice segment. Therefore the values are based on an approximate calculation in which several simplifications are assumed. The shape of the segment is always a circular arc which is approximated by a strut-and-tie model consisting of eight straight beams. The calculation was carried out by means of the framework program *RStab 7* created by *Dlubal Software* [15], assuming a linear elastic behavior.

### 8.3.2 Stresses in the finished structure

In this chapter the stresses in the finished shell structure are discussed by means of the membrane theory [21]. Therefore only membrane stress resultants, which all act in the plane of the shell, occur. By applying the membrane theory it is assumed that the displacement due to stress resultants does not cause perceptible bending. Moreover, all boundary conditions can support the reaction forces and simultaneously permit the displacement required by the membrane stress resultants. The third condition for the usage of the membrane theory is a smoothly distributed load over the surface of the shell, which is perfectly met by considering dead load.

Similar to chapter 4.3.2, different shapes are taken into account and the basic dimensions correspond to the ice shell built in the field experiment.

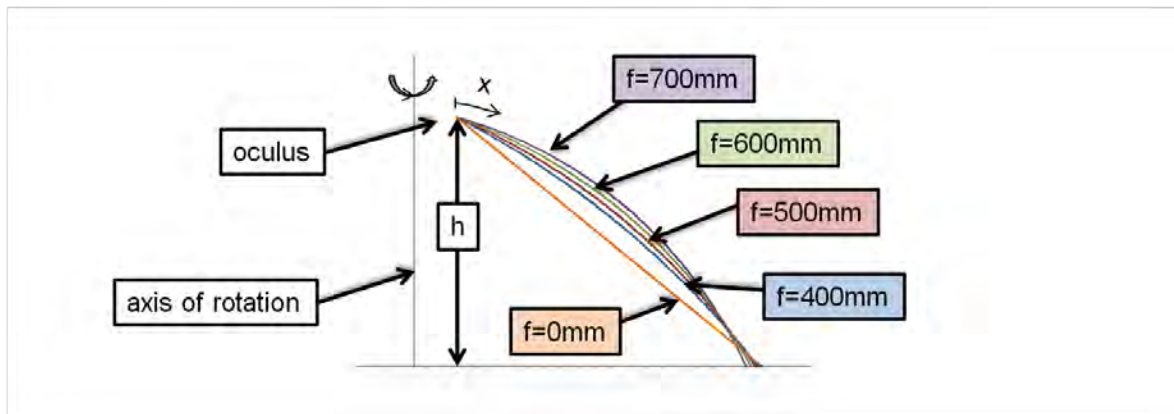


Figure 8.4: Variation of the rises taken into account in Figure 8.7

First, the membrane stress resultants of a shell structure which was produced by rotating a pointed arch with an arc length of  $5,56\text{ m}$ , a rise  $f$  of  $500\text{ mm}$  and a height  $h$  of  $4,13\text{ m}$  are shown - see Figure 8.4. By rotation of a circular arch a pointed dome is formed. The rise is defined - as shown in Figure 8.2 - as the maximal distance between the chord and the arch measured perpendicularly to the chord. The plotted forces occur due to the self weight of the shell. The dome has a constant thickness of  $200\text{ mm}$  and the specific weight of the ice is set to  $9\text{ kN/m}^3$ . In Figure 8.5 the distribution of the hoop forces is depicted whereas in Figure 8.6 the meridian forces of the described structure are shown. These results are gained by a numerical simulation carried out with the 3D finite element analysis program *RFEM 4* created by *Dlubal Software* [13], assuming a linear elastic behavior. The line support is chosen in order to satisfy the requirements of the membrane theory.

In the diagram in Figure 8.7 the section forces in meridian and hoop direction are shown considering different shapes of the shell structure. In order to illustrate the design of the shell structures discussed in Figure 8.7, Figure 8.4 is created. In this figure circular arches with different rises  $f$  are depicted. By rotating this arch around the rotational axis, a rotationally symmetric dome is created. All curves have the same arch length of  $5,56\text{ m}$ . The height as well as the dimension of the oculus are identical for all dome structures. As a consequence, the base diameter of the shell varies depending on the



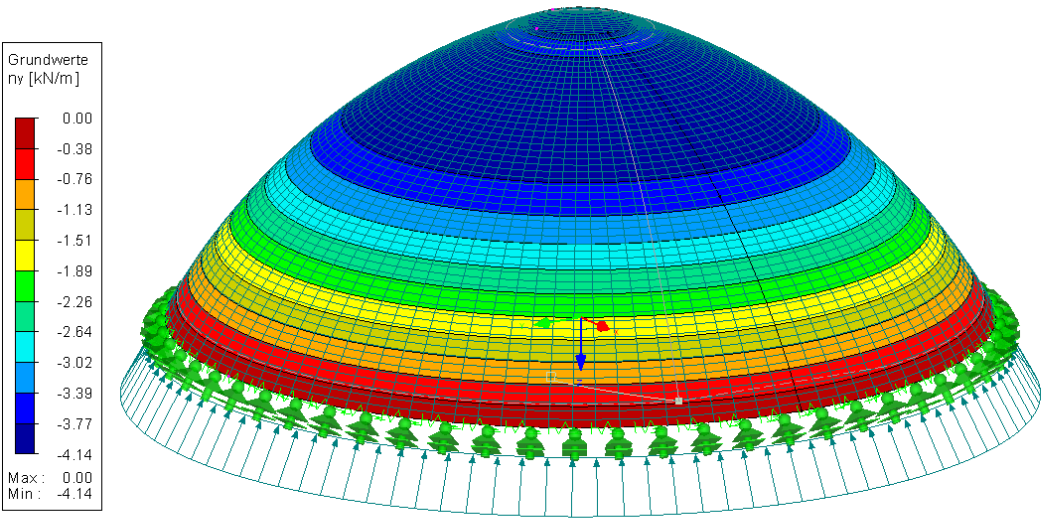


Figure 8.5: Distribution of the hoop forces

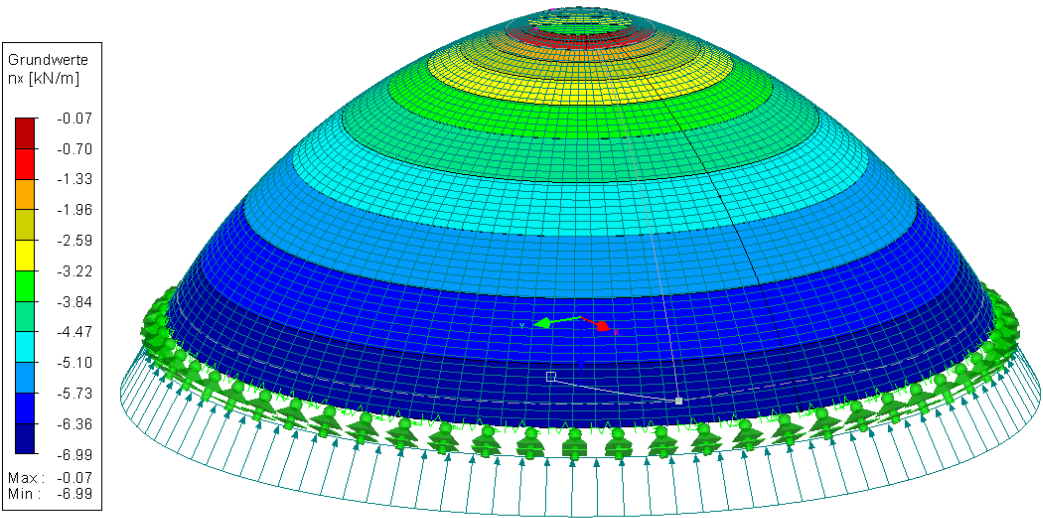


Figure 8.6: Distribution of the meridian forces

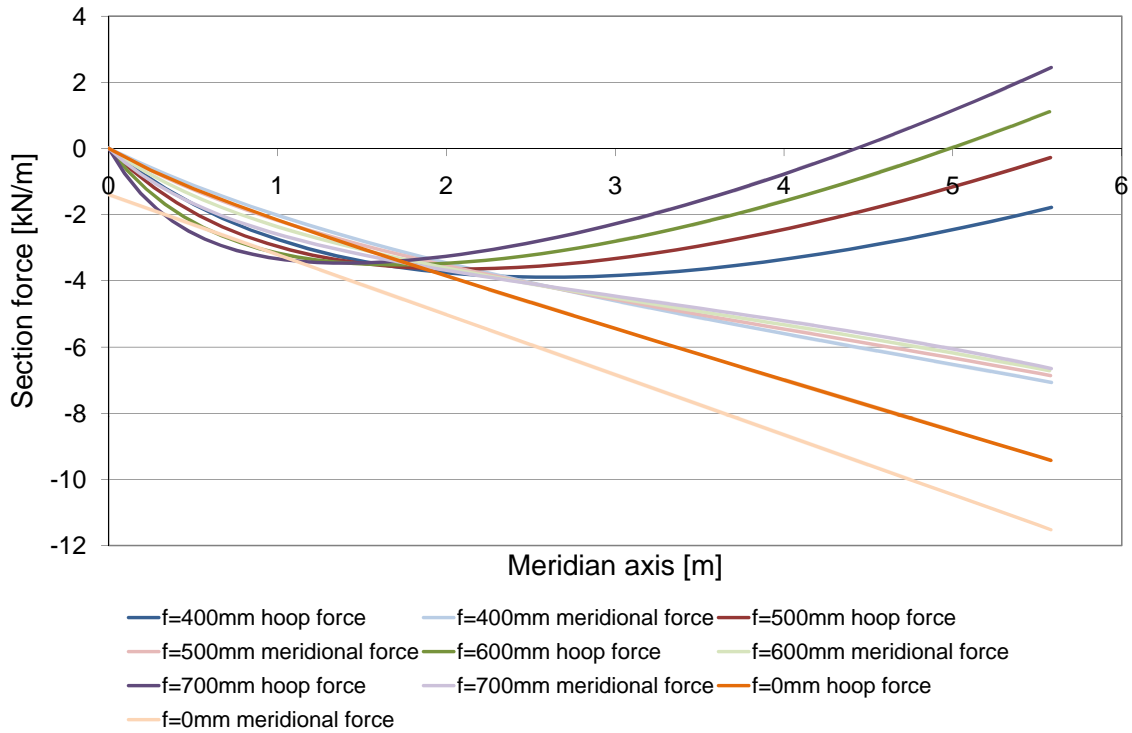


Figure 8.7: Section forces of the finished dome considering different sizes of the rise

size of the rise. The horizontal  $x$ -axis in Figure 8.7 represents one meridian axis of the surface of rotation. The index  $x$  originates at the oculus of the dome structure.

The forces shown in Figure 8.7 are determined analytically by means of the set of formulae provided by Pflüger [65]. The used formulae are all based on membrane theory. First, the size of the rise is set to  $400\text{ mm}$  – shown with the blue curves in Figure 8.7 and 8.4. In this case only compression forces act in the entire shell structure, both in meridian and hoop direction.

The red curves show the section forces occurring if the rise is  $500\text{ mm}$ . This is the same situation as the one calculated with the finite element program *RFEM 4* and depicted in the Figures 8.5 and 8.6 showing that the results obtained are very similar. The largest difference occurs at the edge of the oculus. In the analytic solution, all forces amount to zero at this free edge. In the numerical finite element analysis, however, the values do not reach zero. This is a phenomenon of the finite element analysis mainly depending on the size of the mesh. Rotating an arch with a rise of  $500\text{ mm}$ , all hoop forces have negative values, representing compressive forces. At the very bottom of the shell structure, the hoop force, however, almost amounts to zero. If the size of the rise is further increased, e.g.  $600\text{ mm}$  or  $700\text{ mm}$ , the hoop force at the bottom becomes tension. In order to maintain only compressive forces in the ice structure, the rise must not exceed  $500\text{ mm}$  under the given circumstances.

The orange lines in Figure 8.7 show the sectional forces of a conoidal dome, which obviously has a rise  $f$  of  $0\text{ mm}$ . In a conoidal dome, however, the highest compression forces appear.

### 8.3.3 Cloister vault versus dome

Strictly speaking, the geometry of the shell structure which will be received by using this construction method resembles a cloister-vault with a regular hexadecagon as base area. It is a vault resulting from the intersection of eight barrel-vaults crossing at an angle of  $22,5^\circ$ . Every segment, however, is only uniaxially curved. Therefore, when assembled, they connect to each other at an angle of  $157,5^\circ$ .

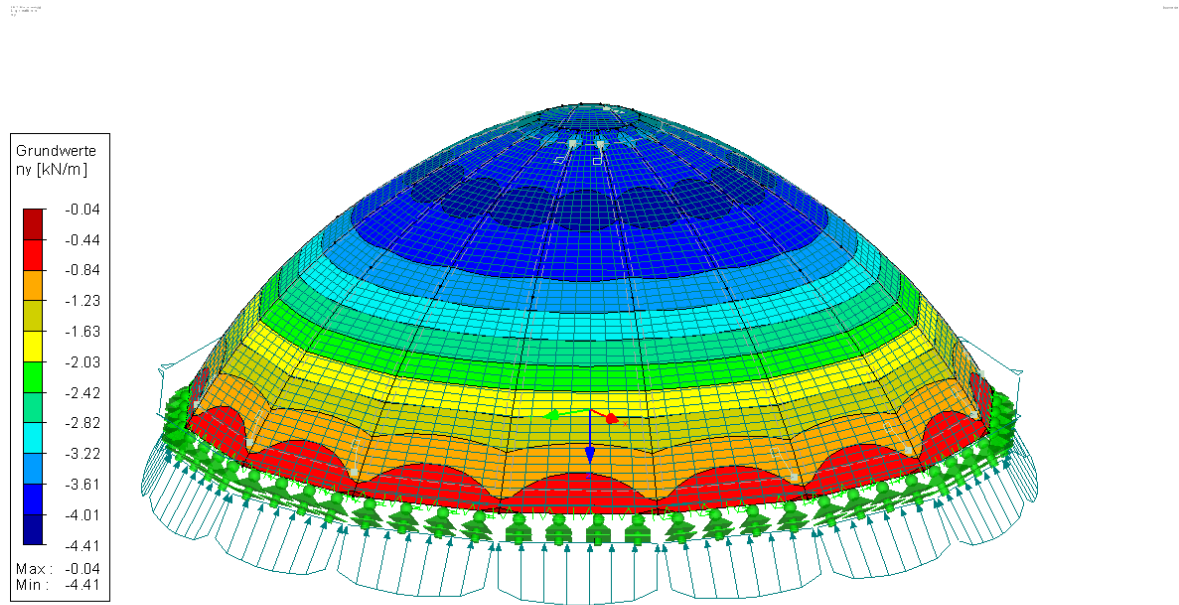


Figure 8.8: Distribution of the hoop forces

In order to compare the resulting stresses of this cloister-vault with a regular hexadecagon as base, to the ones of a pointed dome, a finite element model is created. The model shown in Figure 8.5 and 8.6 is created by rotating a pointed arch therefore a rotationally symmetric pointed dome develops. The model shown in Figure 8.8 and 8.9 consists of sixteen uniaxially curved segments. Aside from the shape, all other parameters are identically for both models. Figure 8.8 shows the hoop forces and Figure 8.9 the meridian forces of this structure. It can be seen that, when building a dome out of sixteen segments, the boundary conditions cannot completely satisfy all requirements of the membrane theory. But the reaction forces perpendicular to the shell edge only have a maximum value of  $0,12\text{ kN/m}$  in this model. Moreover, it can be seen that through the contact edges between the segments, the hoop and meridian forces are not rotationally symmetrical anymore. Comparing the values of the forces of these two models, however, it is obvious that these discontinuities do not influence the general size of the loading significantly. Also the bending moments obtained by the more precise model have only a maximal absolute value of  $0,06\text{ kNm/m}$ . Therefore, subsequently, no distinction between these two models is made and as an approximation and simplification, the static system of the pointed dome will be considered.

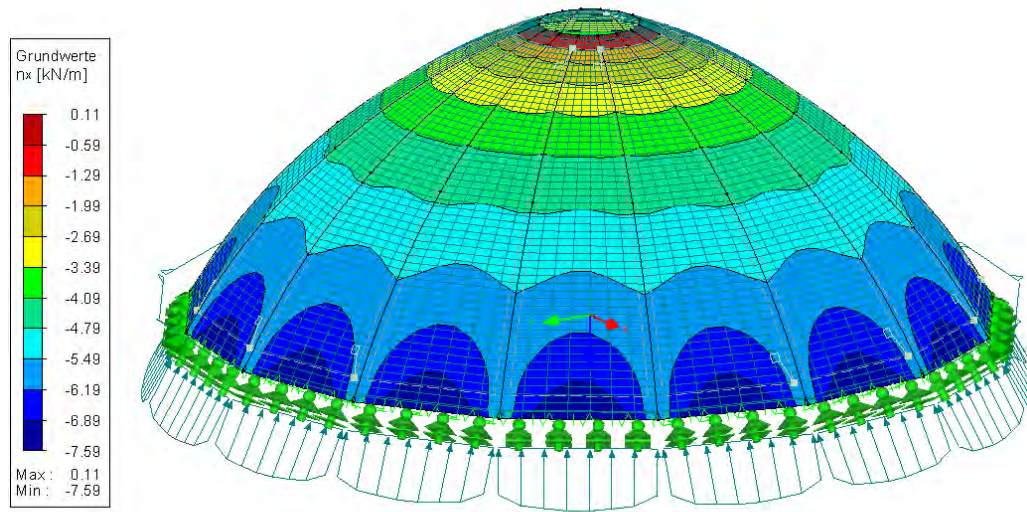


Figure 8.9: Distribution of the meridian forces

This construction method can also be carried out with a larger or smaller number of ice segments. When more segments are used, the finished shell resembles more a dome structure, optically and statically speaking. By using fewer segments, the finished structure becomes more discontinuous. Moreover, the size and weight of the individual elements also have to be taken into account when defining the number of segments.

# Chapter 9

## Preliminary experiments

### 9.1 General

One of the key elements of this method is to lift the elements and keep them in an elevated position in order to allow the creeping process to take place. This working procedure is referred to as 1<sup>st</sup> lifting process. Therefore this part of the segment lift method for ice shells was investigated more closely with the help of preliminary tests. To get a better understanding of the deformation due to dead load and the creep behavior of ice, specimens were made to study their behavior. Moreover different possibilities to lift the ice segments could be tested with these experiments.

### 9.2 Test setup

A total of four ice specimens were made, lifted and their deformations over time were measured. Three of these tests took place in fall of 2009 and one specimen was tested in summer 2010 at a location belonging to the Vienna University of Technology in the city of Vienna. The experiments were carried out inside of a refrigerated container which could keep any inner air temperature between  $+20^{\circ}C$  and  $-20^{\circ}C$ .

specimen no.	length [m]	width [mm]	thickness [mm]	no. of ropes	reinforcement per width [cm <sup>2</sup> /m]
1	5	550	225	2	0,45
2	5	550	210	4	0,90
3	5	550	215	3	0,67
4	5	1000	200	5	0,62

Table 9.1: Dimensions of the four specimens

In order to produce the ice specimens, formwork was laid down to shape the respective specimen. After the formwork was screwed into place, a plastic layer was laid on top of the formwork to prevent the leakage of water from the ice beam mold. The

specimens had a length of  $5\text{ m}$ , limited by the dimensions of the refrigerated container, and a thickness of approximately  $200\text{ mm}$ . The width varied from  $55\text{ cm}$  to  $1\text{ m}$ . The dimensions of all specimens are listed in Table 9.1.

To reinforce the ice beams steel ropes with a diameter of  $5\text{ mm}$  were used. These ropes were manufactured by the same company which created the steel tendons for the concrete and ice shells built with the pneumatic formwork method. Their properties are identical to the ones described in chapter 6.2.2.3. The number of ropes used in the respective specimen as well as the reinforcement ratio per meter width are also listed in Table 9.1.

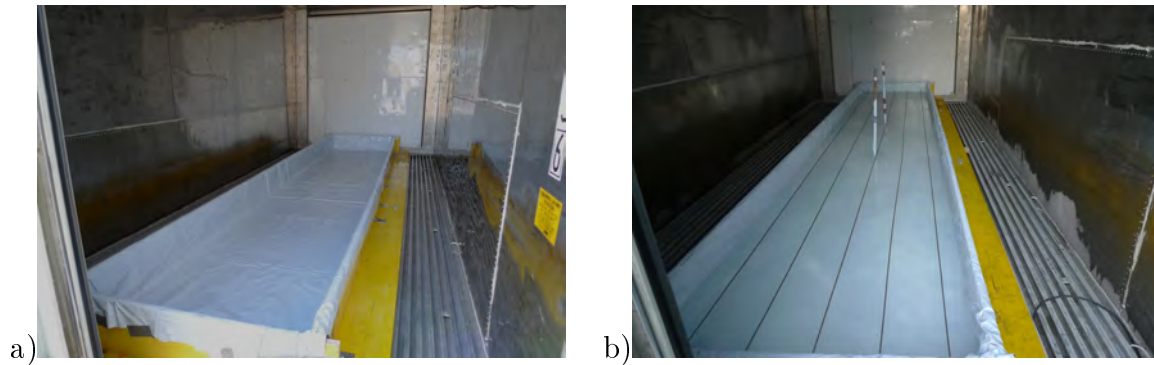


Figure 9.1: Specimen number 4 a) mold b) reinforcement

Once the formwork was placed, water, at about  $10^{\circ}\text{C}$ , was poured into the mold with a water hose at a rate of about  $15\text{ mm}$  twice a day until the approximate  $200\text{ mm}$  height was reached. During the ice production process the temperature in the refrigerated container amounted to  $-20^{\circ}\text{C}$ . As soon as half the height of the ice beam was produced, the steel reinforcement was inserted. Just like in the previously described pneumatic formwork method 2-parted clamp rings were used to anchor the steel ropes. Pictures of the mold and the reinforcement are shown in Figure 9.1.

Two of the four specimens were equipped with cuts which served as predetermined breaking points in order to weaken the cross section and force the ice beam into a cracked state. Once the complete height of  $200\text{ mm}$  was reached, cuts of about  $50\text{ mm}$  to  $70\text{ mm}$  depth were cut horizontally with a chain saw. In Figures 9.2b, 9.4a, 9.4c and 9.4d these cuts can be seen. The impact of these cuts on the deformation will be discussed in chapter 9.3 and 9.4.

Different methods were used to lift the ice segments. In the experiments carried out in fall 2009 – prior to the ice shell experiment carried out with the segment lift method with pneumatic formwork – the ice beams were lifted with pneumatic devices. The used pneumatic lifting devices had to be placed under the ice beam before creating the ice. Then the ice beams could be lifted by slowly inflating the pneumatic devices.

The specimen number 4 was lifted by means of a hydraulic jack. Lifting the  $5 \times 1 \times 0,2\text{ m}$  specimen required a hydraulic jack that could lift a load of about  $1\text{ ton}$ . The jack was positioned as illustrated in Figure 9.2. The ice beam was lifted by attaching the jack to two threaded steel rods which had been previously anchored in the ice segment. Tests

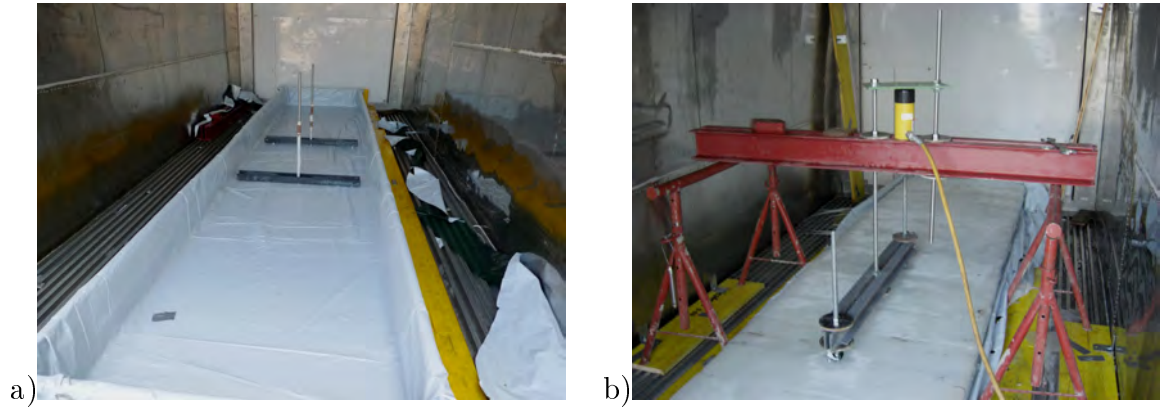


Figure 9.2: Lifting devices for the ice beams a) U-shaped line supports b) lifting device with hydraulic jack

on this anchorage system showed that with this kind of line support, the ice beam can be lifted from the ground. Both threaded steel rods were anchored by means of a 900 mm U-shaped steel beam with a nut welded to its inner surface. The threaded rod was then screwed into the nut. These two U-shaped steel beams had to be placed in the mold before pouring in the water.

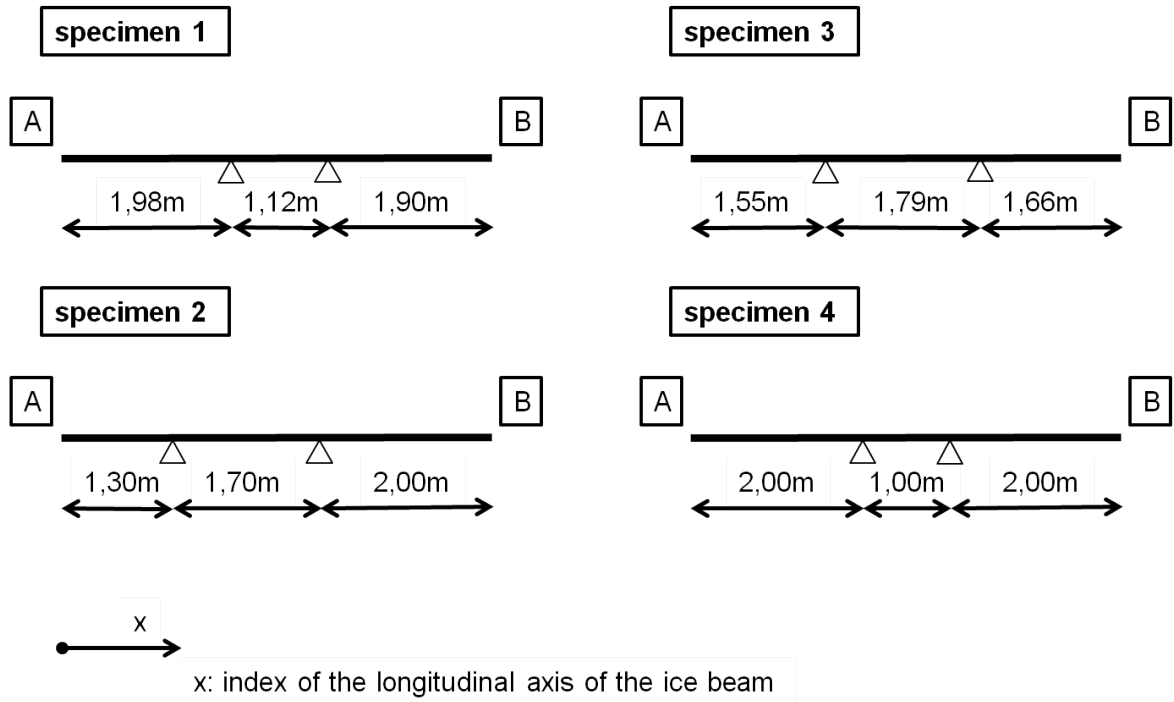


Figure 9.3: Setup of the specimens 1 to 4

Independent of the lifting method used, all specimens were placed on stacks of wood in order to experience creep deformation. The spans and cantilevers of all specimens were different and are summarized in the sketch in Figure 9.3. The lifting processes were carried out at an ice temperature between  $-10^{\circ}\text{C}$  and  $-5^{\circ}\text{C}$ .



specimen No.	moments / width		stresses	
	A [kNm/m]	B [kNm/m]	A [N/mm <sup>2</sup> ]	B [N/mm <sup>2</sup> ]
1	3,96	3,65	0,85	0,79
2	1,60	3,78	0,40	0,95
3	2,33	2,67	—	—
4	3,87	3,87	—	—

Table 9.2: Moments and stresses in the specimen 1-4

In Table 9.2 the bending moments per width above the supports during the creeping process are cited. These moments are calculated under the assumption of line supports in the area of the stacks of wood. For specimen 1 and 2 which do not have cuts, the normal stresses due to these moments are also calculated. Calculating the stress distribution of specimen 3 and 4 the cuts have to be taken into account therefore additional considerations with a finite element model would have to be carried out. The influence of the cuts is going to be discussed in chapter 10.4.2.5.

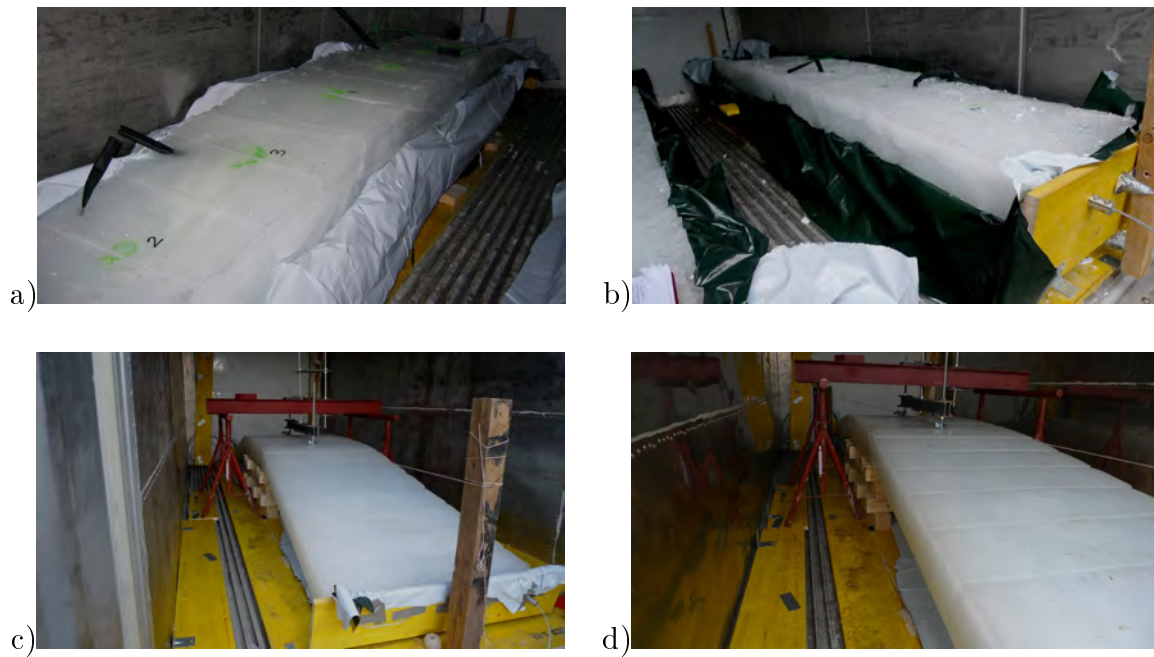


Figure 9.4: Specimens during the creep process a) specimen no. 1 b) specimen no. 2 c) specimen no. 4 d) specimen no. 4

In order to monitor the deformation of the ice beam, measuring points were defined every 500 mm where the distance to a reference height could be measured. Figure 9.4 shows additional pictures of the specimens after the lifting process.



### 9.3 Results

The deformations of the ice beams are depicted in Figures 9.5 to 9.8. The blue lines symbolize the values measured on the specimen. Immediately after the lifting process the initial deformations were identified. After the lifting the ice segment experienced a few cracks but the specimens did not reach the final cracking state. The 1<sup>st</sup> and 2<sup>nd</sup> specimen were lifted at an ice temperature of  $-10^{\circ}\text{C}$  and then situated on the stacks of wood for 98 hours. As soon as the creeping process started the temperature in the refrigerated container was adjusted to  $-5^{\circ}\text{C}$  therefore the ice temperature also increased to this level. The dark blue lines in Figure 9.5 and Figure 9.6 show the deformations occurring after 98 hours.

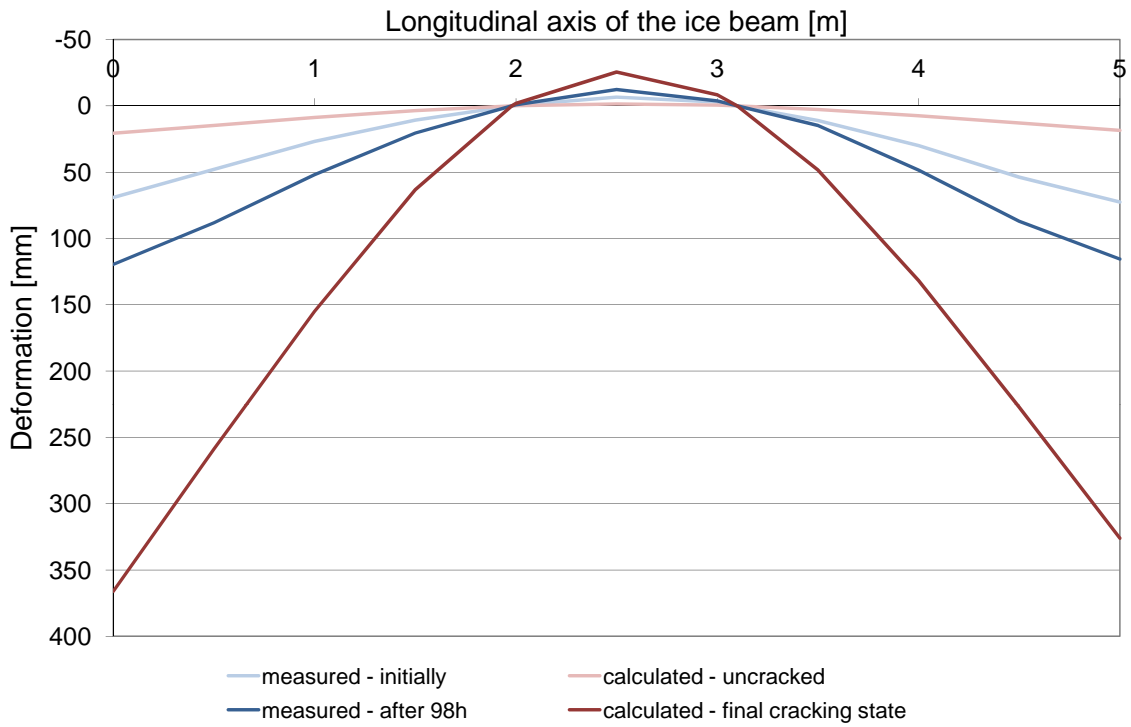


Figure 9.5: Deformations of specimen 1

The ice temperature of the 3<sup>rd</sup> and 4<sup>th</sup> specimen during lifting and creeping was approximately  $-5^{\circ}\text{C}$ . Moreover, a big difference between the first two specimens and the specimens 3 and 4 were cuts which worked as predetermined breaking points. In specimen 3 cuts with a depth of approximately 50 mm were produced at intervals of 250 mm. Specimen 4 was also equipped with cuts at intervals of 250 mm, but these cuts were approximately 70 mm to 80 mm deep. The ice beam number 3 experienced creeping for 149 hours. After this time period the end of the beam labeled with B in Figure 9.3 rested on the ground. Specimen 4 showed the largest deformation; after less than 27 hours the end part B of the beam reached the ground situated 425 mm below the supports in this specimen. After 50 hours of creeping the other end of the specimen rested on the ground as well. Because of the test setup, the creeping after that period could not be examined.

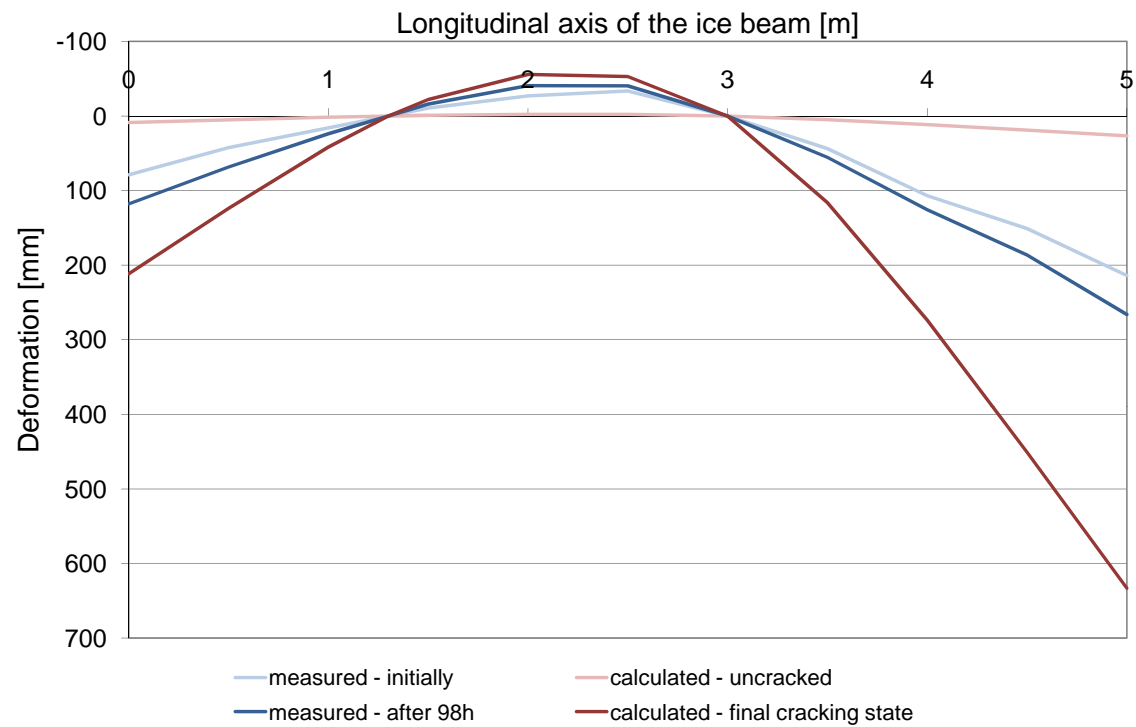


Figure 9.6: Deformations of specimen 2

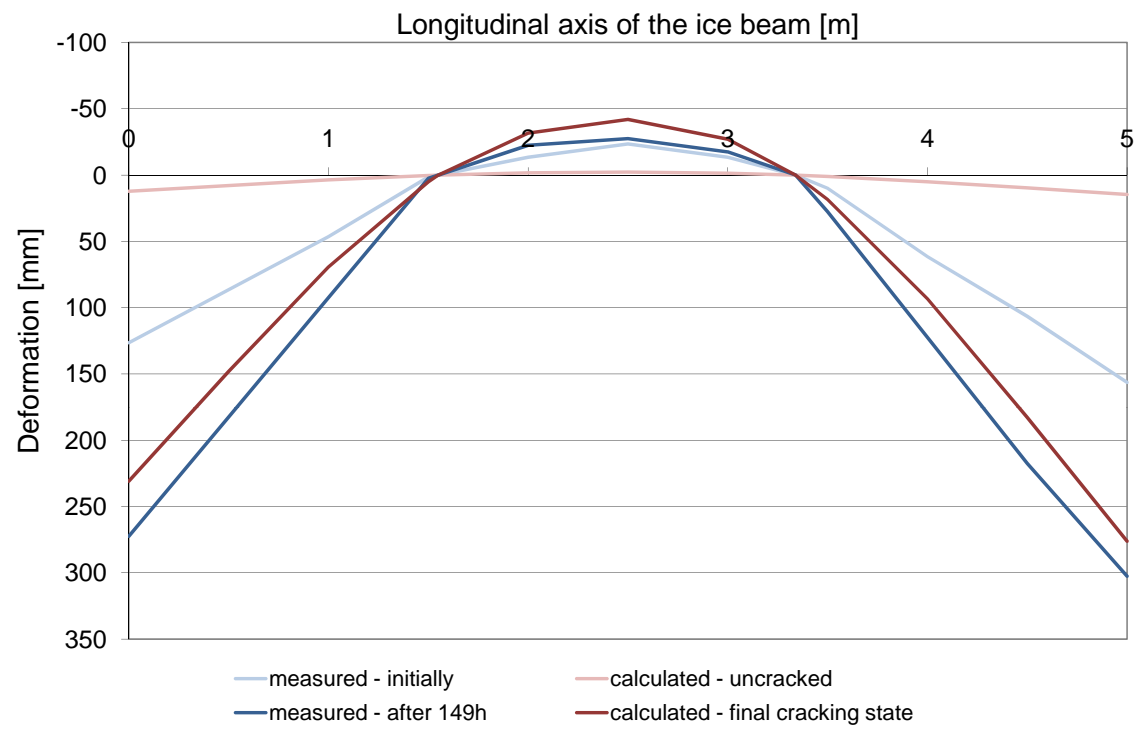


Figure 9.7: Deformations of specimen 3

The red lines in Figures 9.5 to 9.8 present calculated values. The light red line shows the theoretical deformations under the assumption that the whole cross section of each specimen is uncracked. For specimen 3 and 4 even the cuts are neglected. The dark red line shows the calculated deformation of the respective specimen in the final cracking state, neglecting the tension stiffening effect due to participation of the ice between the cracks. For this calculation the position and quantity of the reinforcement is taken into account. The steel ropes have a cross sectional area of  $12,7 \text{ mm}^2$  each and a Young's modulus of  $41300 \text{ N/mm}^2$  for their first loading – see chapter 6.2.2.3. A Young's modulus of  $400 \text{ N/mm}^2$  is assumed for ice - see chapter 2.2.2.

In Figure 9.9 the results are summarized and normalized. Because of the fact that the specimens had different thicknesses, cantilevers, widths and amounts of reinforcement, the measured deformation of the ends A and B are depicted in Figure 9.9 as percentage of the calculated deformation in the final cracking state of the respective specimens, neglecting the tension stiffening effect due to participation of the ice between the cracks. Specimen 1 and 2 only experience an initial deformation of 20% to 40% of the value which would be reached if the specimens were in mentioned final cracking state. It can be assumed that due to the cuts in specimen 3 and 4 the amount of cracks in these ice beams are more similar to the final crack pattern. The red columns show the deformation after 100 hours or 50 hours of creeping as a percentage of the calculated deformation in the final cracking state. For specimens 1 to 3 the values after 100 hours are taken into account. Both ends of the ice beam of specimen 4 reached the ground after only 50 hours, therefore only this deformation can be depicted.

In Figure 9.10 the height difference  $\Delta H$  between the end points of the ice beams and their supports is depicted over the time. It can be seen that most of the creep deformation occurs in the first 24 to 48 hours; afterwards the deflection doesn't change much. The ends of the beams reaching the ground are marked with an orange triangle.

## 9.4 Insights gained from the preliminary tests

The main purpose of these preliminary tests was to be able to design ice segments matching the needs of an ice shell created with the segment lift method. As described in chapter 10.2 a rise of  $500 \text{ mm}$  for these  $5,54 \text{ m}$  long elements was planned. The ice beams of the preliminary tests only had a length of  $5,0 \text{ m}$ , limited by the geometry of the refrigerated container. Under the assumption of a circular arc shaped deformation, the corresponding rise for the specimen would be  $410 \text{ mm}$ . As shown in Figure 9.11 specimen 1 and 2 were far away from reaching the desired rise. Therefore when designing the segments for the ice shells specimen 3 and 4 were taken as a model. It became obvious that it was important to prepare the ice beams in such a way that they were as close to the final cracking state as possible, thus the cuts and additional possibilities to crack the ice were planned for the shell structures – see chapter 10. Moreover, to determine the spans and cantilevers for the creeping process of the ice shell segments the loading and the stress resultants of specimen 3 and 4 could be used as a reference.

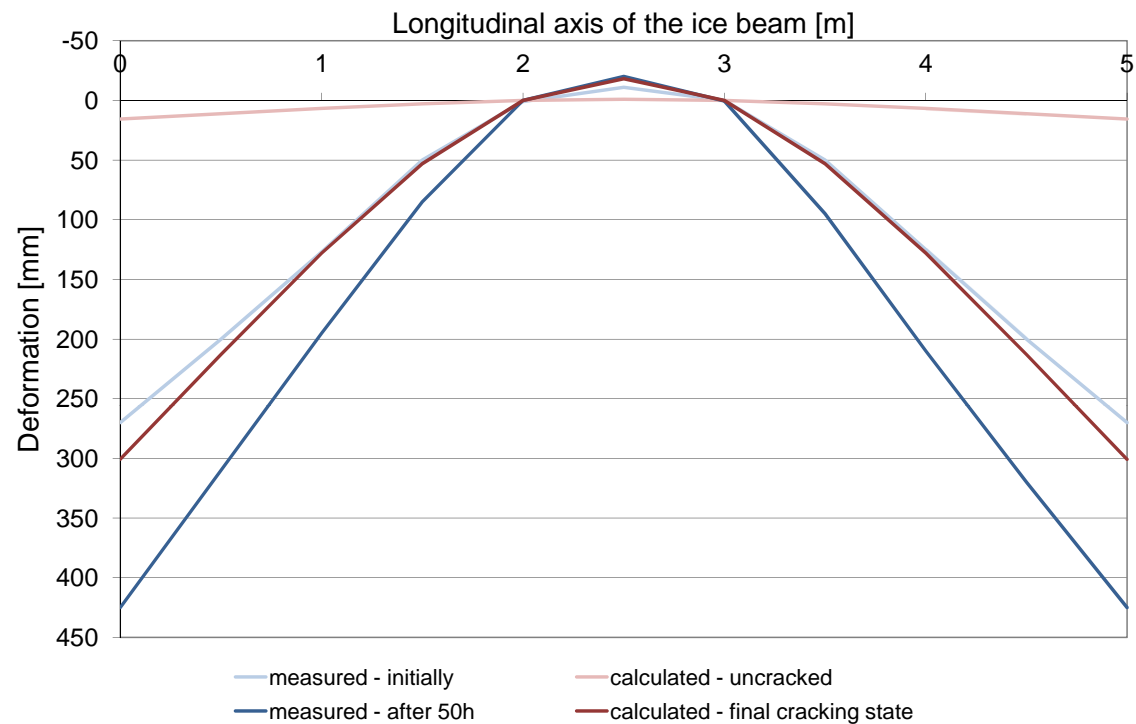


Figure 9.8: Deformations of specimen 4

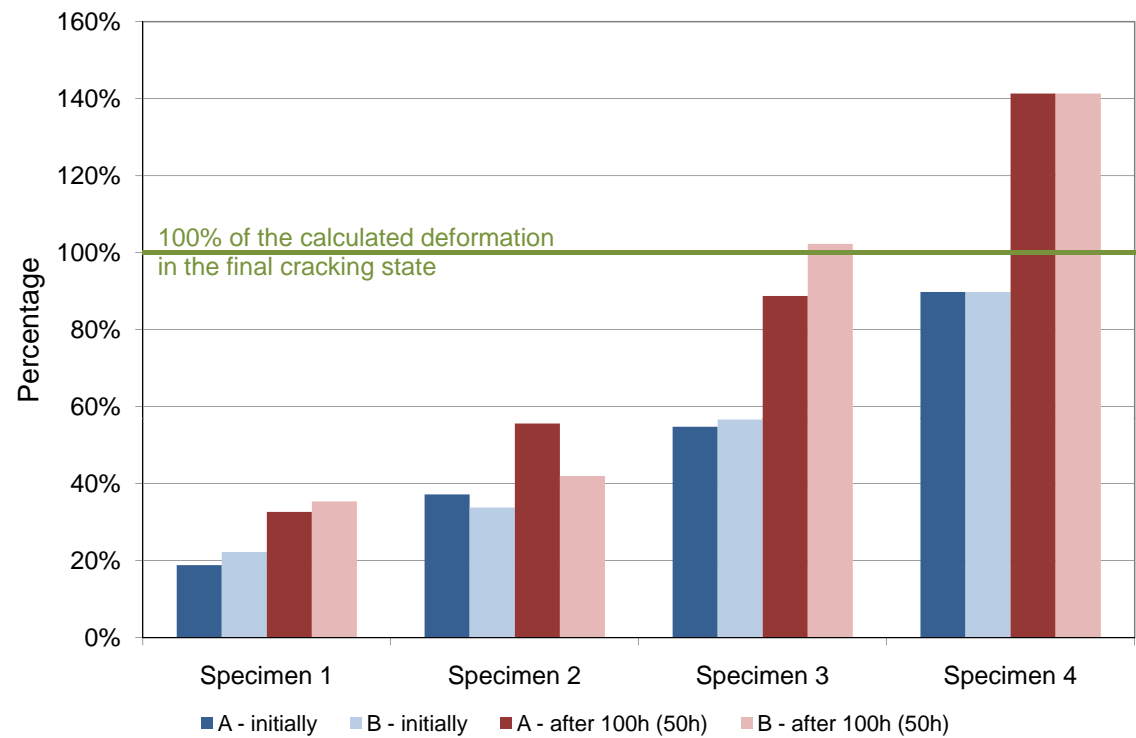


Figure 9.9: Percentage of the measured deformation of the calculated deformation in the final cracking state for specimen 1 to 4

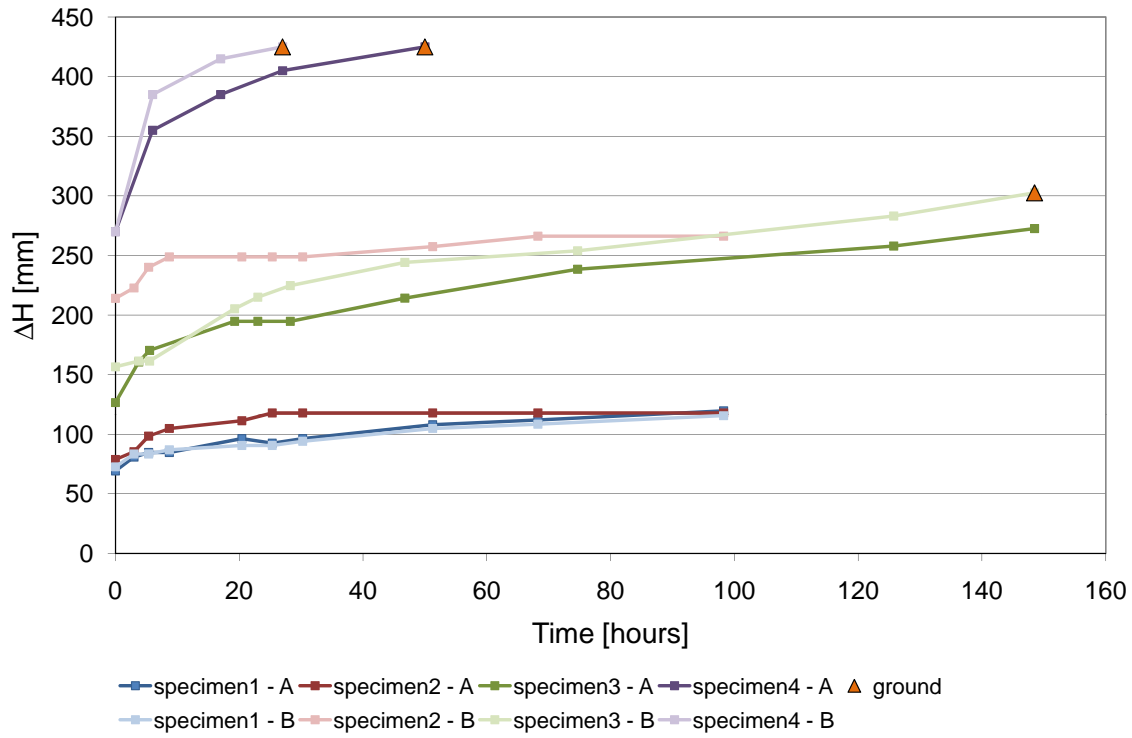


Figure 9.10: Height difference between the ends of the beams and their supports over the time

After carrying out the preliminary tests, the reinforcement for the actual ice shell was chosen on the basis of the reinforcement in the specimens. As the steel ropes with a diameter of  $5\text{ mm}$  proved to be applicable, the same steel ropes were used for the ice shell. Figure 9.12 shows a diagram of the reinforcement normalized with the width. The specimens had a constant cross section whereas the widths of the segments of the ice shell varied with the longitudinal axis of the segment. In order to compromise between having an uniform reinforcement rate and simultaneously keeping the laying of the reinforcement simple, the quantity of reinforcement was chosen according to Figure 9.12. In chapter 10.3 the arrangement of the steel ropes in the ice segments will be discussed.

Observing the crack width of the cracks directly above the supports, it can be asserted that the bond between the steel ropes and the ice is not optimal. The cracks in the area of the maximum bending moment are significantly larger than other cracks of the specimen. A possibility to improve the bond between the reinforcement and the ice is to attach additional elements to the steel ropes. This improvement will be further discussed in chapter 10.3.3.

Another important piece of information gained from the 4<sup>th</sup> specimen of these preliminary tests, is the use of a lifting device with the hydraulic jack. This way of lifting an ice segment without a pneumatic formwork was adapted for the segment lift method without pneumatic formwork.

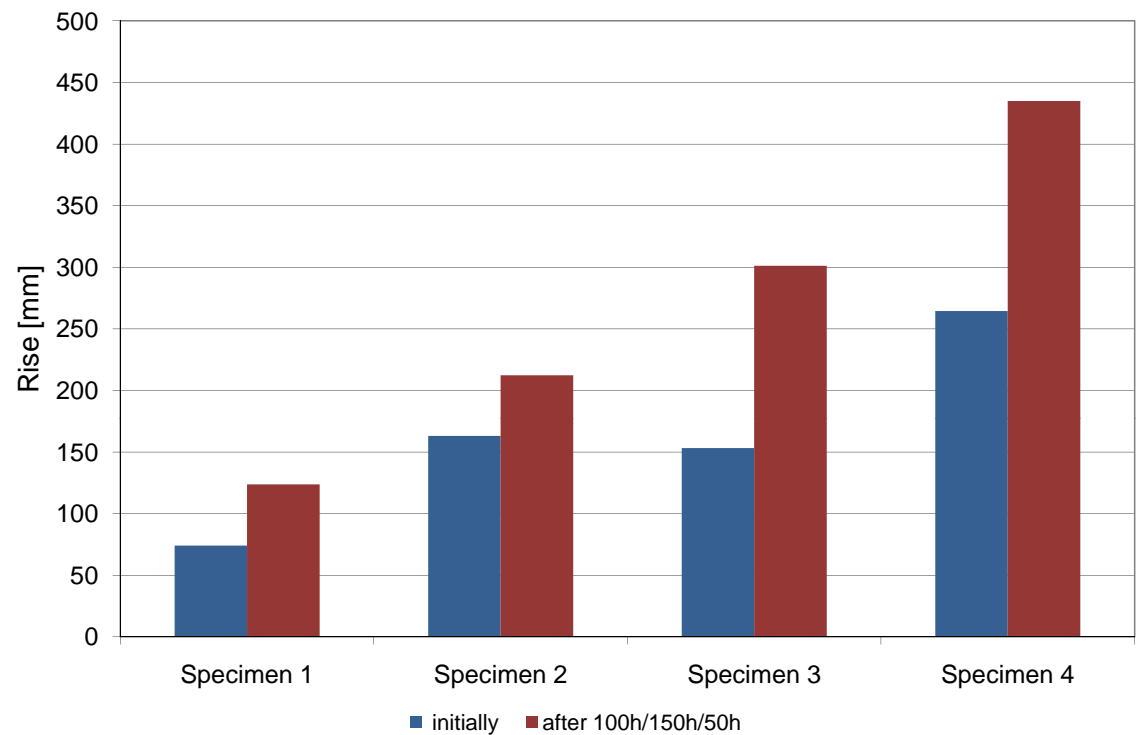


Figure 9.11: Rise of the specimen 1 to 4 before and after the creeping process

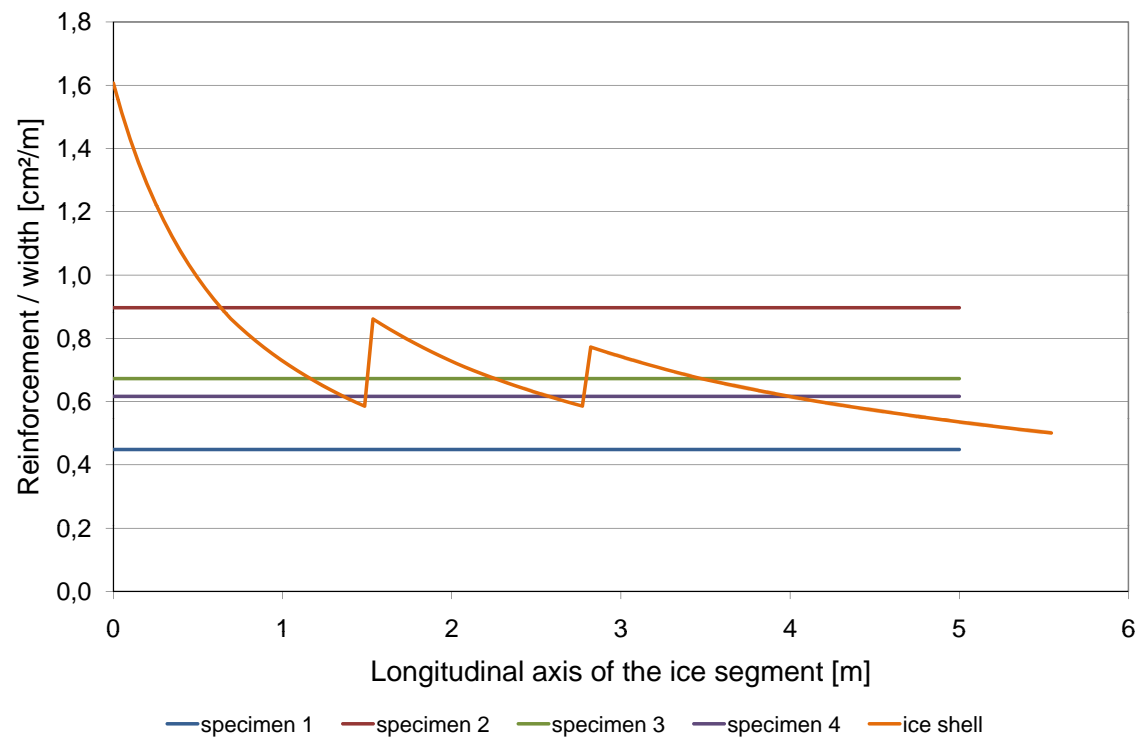


Figure 9.12: Reinforcement ratio of the specimens 1 to 4 and the segments of the ice shell

# Chapter 10

## Ice shell

### 10.1 Preface

The following chapters describe the two field experiments carried out in order to build an ice shell - one in winter 2009/10 using the segment lift method with pneumatic formwork and one in winter 2010/11 using the same method but without the pneumatic formwork. In the appendix B drawings of all essential parts are provided.

Unfortunately, due to problems with the pneumatic formwork, the ice shell which was intended to be built with the segment lift method with pneumatic formwork could not be finished successfully. However, many construction steps of this ice shell could be carried out and important knowledge was gained from this test. The successful experiment in winter 2010/11 proves that building an ice shell with the segment lift method is feasible.

### 10.2 Design of the ice segments

In order to build an ice shell from individual ice segments the design of the segments has to be chosen carefully. The curvature of the segments not only defines the appearance of the finished shell but also the stresses which occur during the construction process as well as in the finished structure. As shown in chapter 8.3.1 the stresses in the ice during the lifting of the ice segments decrease with a higher rise of the curved segment. Considering this construction step, the higher the rise the better. Regarding the stresses in the final dome structure, however, a rise of the ice segments larger than 500 *mm* generates tensile hoop forces, shown in chapter 8.3.2. As the tensile strength of ice is relatively low, it was decided to avoid large tensile stresses in the ice of the finished shell structure. Consequently, the designed size of the rise for the two shell structures amounts to 500 *mm*.

This large curvature has to be obtained by a combination of elastic and plastic deformations due to dead load as well as additional deflections due to the creep behavior of ice. For both types of deformation a higher level of stress in the segment is advantageous.

The higher the stresses in the cross section due to self weight, the higher the strains and therefore the deformation. As creep deformation can be defined as a multiple of the elastic deformation, the creeping process also benefits from a higher stress level.

At the same time, it is very important to prevent a collapse of the ice due to too high stresses. As described in chapter 2.2.2 ice is a very inhomogeneous material with varying strength. Due to the fact that its material properties depend on many factors, for example temperature, density and crystal structure developed during the particular way of producing the ice, a high variation of the bearing strength of the ice may occur. Thus, the stress level had to be chosen in such a way that the ice can withstand the applied force under all circumstances.

Due to the fact that the tensile strength of ice is much lower than the compressive strength, the ice segments are improved by means of steel reinforcement. Several requirements are placed on the reinforcement: Besides having a high tensile strength, the reinforcement must also be able to experience large strains and distortions due to the desired curvature of the ice beams.

By inserting reinforcement into the ice, the material of these segments can be referred to as reinforced ice. Similar to reinforced concrete, reinforced ice can also be considered as a composite material, since the ice carries the compression forces and the reinforcement bears the tensile forces. The ice, however, can only pass the tensile stresses to the reinforcement if cracks occur in the ice. Just like in reinforced concrete construction, the stiffness behavior of ice can be classified in uncracked, initial cracking and final cracking state. As long as the cross section is uncracked the stiffness is higher and mainly depends on the Young's modulus of ice. As soon as cracks appear, the state of stress changes in the cross section and the deformations increase considerably. By increasing the loading, the number of cracks also increases until the final cracking state is reached. The distance between the cracks depends on the bond stresses between the reinforcement and the ice. In this state, however, the ice between the cracks still participates on the resistance of the cross section due to the tension stiffening effect.

Contrary to most of the concrete structures where a high stiffness is required, the ice segments for the ice shell should feature low stiffness. Therefore it is advantageous for the reinforced ice segments to be in the final cracking state. Possibilities and arrangements to approach this state are described in chapter 10.4.

Apart from the ability of the reinforcement to be able to bend, a good bond between the ice and the reinforcement is necessary. To obtain an evenly curved ice segment many small cracks have to occur instead of a few wide ones. By providing a good bond and a large number of thin reinforcement bars, a small crack width can be achieved.

To satisfy all requirements on the reinforcement, steel ropes were chosen. They have a high tensile strength, a relatively low extensional stiffness compared to steel bars or rods and almost no bending stiffness. To avoid corrosion, stainless steel is the optimal choice.

Ice has a brittle behavior with a low rotation capacity if the load is applied impulsively. Therefore, impact loading which leads to a sudden increase of force must be avoided. Moreover a sudden cracking of the ice can also lead to a high rotation in the compression



zone and destroy the ice. If the crack pattern is already fully developed and the ice is in the final cracking state a sudden cracking is virtually impossible.

The durability of the finished ice shell is mainly depending on the thickness of the ice. The thicker the ice, the longer the sun needs to melt and eventually destroy the shell. The thickness of the ice shell was determined to  $200\text{ mm}$ . The bending stiffness of the cross section, however, increases by the  $3^{\text{rd}}$  power of the height. The thinner the beam, the larger its deformations. In order to have an ice thickness of  $200\text{ mm}$  but still showing a smaller effective depth of the cross section, the reinforcement is placed in the middle of the cross section. In this way the lever arm of internal forces only extends from the compression zone on the edge of the beam to the reinforcement in the middle of the cross section. As soon as the beam is in a cracked state, only half of the height is statically effective which increases the deformation of the ice segments dramatically.

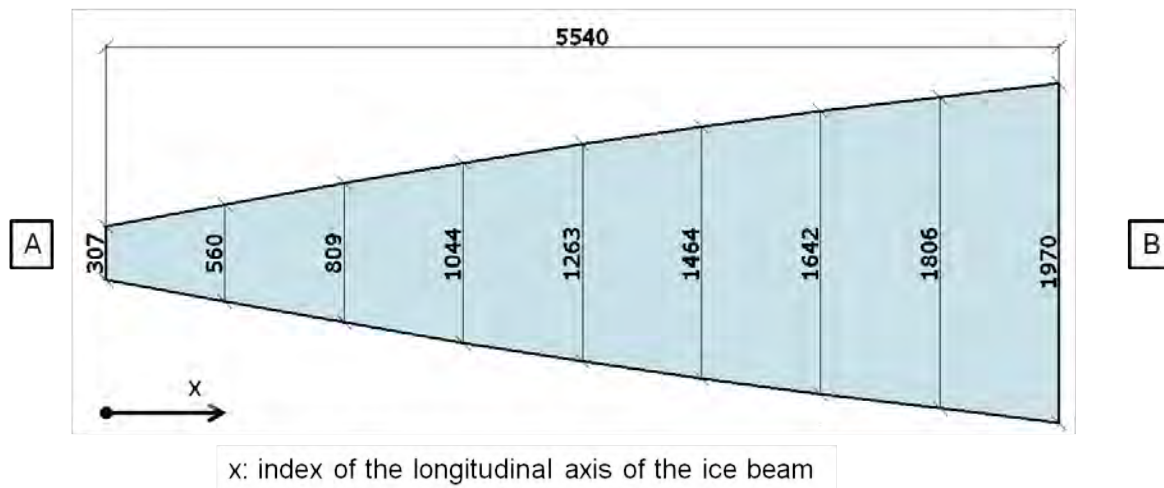


Figure 10.1: Plan view of the ice segments

Moreover, due to this arrangement of the reinforcement, negative as well as positive bending moments can be carried by the cross section. If a negative moment is applied the compression zone develops on the bottom of the cross section whereas a positive bending moment creates the compression zone on the top of the beam. In both cases the tensile force can be carried by the reinforcement situated in the center of the cross section.

The ice shell was made of sixteen individual ice segments. The length of these segments was determined by the size of the available construction site and was defined to be  $5,54\text{ m}$  in their undistorted state. By choosing the inner height of the ice shell to be  $3,5\text{ m}$  and taking the required rise of  $500\text{ mm}$  into account, the width of the ice segment can be calculated in every cross section in order to form a complete shell structure.

In Figure 10.1 a sketch of one ice segment for the ice shell with its respective widths is shown. In all following descriptions, diagrams and calculations the index  $x$  describing the longitudinal axis of the segment starts at the smaller cross section of the ice segment, labeled with  $A$ . The edge with the wider cross section on the location  $x = 5,54\text{ m}$  is called  $B$ .

Obviously, the width of the ice segment varies in every single cross section. In Figure 10.1, however, the cross section is divided into eight equally long parts and the width of the cross section is only marked on the edges of these parts. Due to the fact that the accuracy on the construction site is in the region of  $\pm 10\text{ mm}$ , a more precise shape of the segment is only of theoretical interest.

## 10.3 Creating the ice segments

### 10.3.1 Preparing the formwork



Figure 10.2: Preparations for making the ice plate a) leveling the working surface, winter 2010/11 b) mold for the ice plate, winter 2009/10 c) pneumatic formwork folded and positioned under the future ice plate, winter 2009/10 d) U-shaped steel beams with rods in order to lift the future ice segments with the lifting device, winter 2010/11

The first step to build an ice shell with the segment lift method was to create the ice segments. Therefore the construction site had to be prepared accordingly in order to be able to create a plane ice plate. The surface had to be leveled and sealed with multiple layers of waterproof silage films to separate the ice plate from the subsoil.

Using the segment lift method with pneumatic formwork, the membrane of the formwork had to be situated under the silage films so that it would be available underneath the future ice segments. To ensure an even thickness of the ice segments, the area where the pneumatic formwork had been situated was lowered to gain a plane surface after positioning and folding the membrane. Moreover, those parts of the sensitive formwork which might get in contact with a chain saw were protected by a layer of styrofoam plates.

After preparing the working surface, the mold for the ice plate could be built. The formwork on the outside circumference was made of 32 wooden boards with a height of 200 mm, corresponding to the thickness of the ice segments. 16 boards defined the end part of each segment and another 16 boards were situated in between. The center of this regular triacontakaidigon is identical to the center of the base area of the finished shell. The inner formwork consisted of 16 steel elements. These *assembly brackets* are shown in Figure 10.7d. They are situated to form a regular hexadecagon. The center of this polygon is also identical to the center of the base area of the finished shell. The inner as well as the outer mold stayed connected with the ice and became a part of the ice segment. In the Appendix B.1 detailed drawings of the wooden boards used as outside mold, as well as of the steel assembly brackets which are utilized as inner formwork, are shown.

The ice segments used for the segment lift method without formwork had to be equipped with mounting parts which enabled the ice segments to be lifted later on with a lifting device. These mounting parts consisted of two U-shaped steel beams with nuts welded to the inner surface and threaded steel rods screwed in. The steel beams had a length of 0,85 m and 1,55 m, respectively, and were positioned according to Figure 10.26 in chapter 10.4.2. In Figure 10.2 the mold, the not yet inflated pneumatic formwork and the steel mounting parts are shown.

### 10.3.2 Producing ice



Figure 10.3: Producing ice, winter 2010/11

Finally the mold was prepared for the ice making process. The first step in this procedure involved the production of the 1<sup>st</sup> half of the ice thickness by spraying water into the mold and simultaneously adding small layers of fresh snow to accelerate the ice making process.

In order to produce ice, the air temperature is very important. Experience gained showed that it is virtually impossible to make ice efficiently during the day, when the sun is shining or the temperatures are above  $-5^{\circ}\text{C}$ . The best conditions are during the night at a temperature below  $-10^{\circ}\text{C}$ . The tap water used had a temperature of approximately  $5^{\circ}\text{C}$  to  $7^{\circ}\text{C}$  and was slowly sprayed into the mold. When exclusively working with water, only very thin layers of water with a thickness of a few millimeters were applied at the same time. As soon as this water had turned into ice, another layer

was applied. If very fine snow was available, a small amount of snow was put inside the mold as well. The thickness of the snow never exceeded 5 mm. Then this snow was completely soaked with water, in order to gain a high density and strength of the ice. After adding same snow, a few layers of water only were always sprayed into the mold before another dose of snow was added.

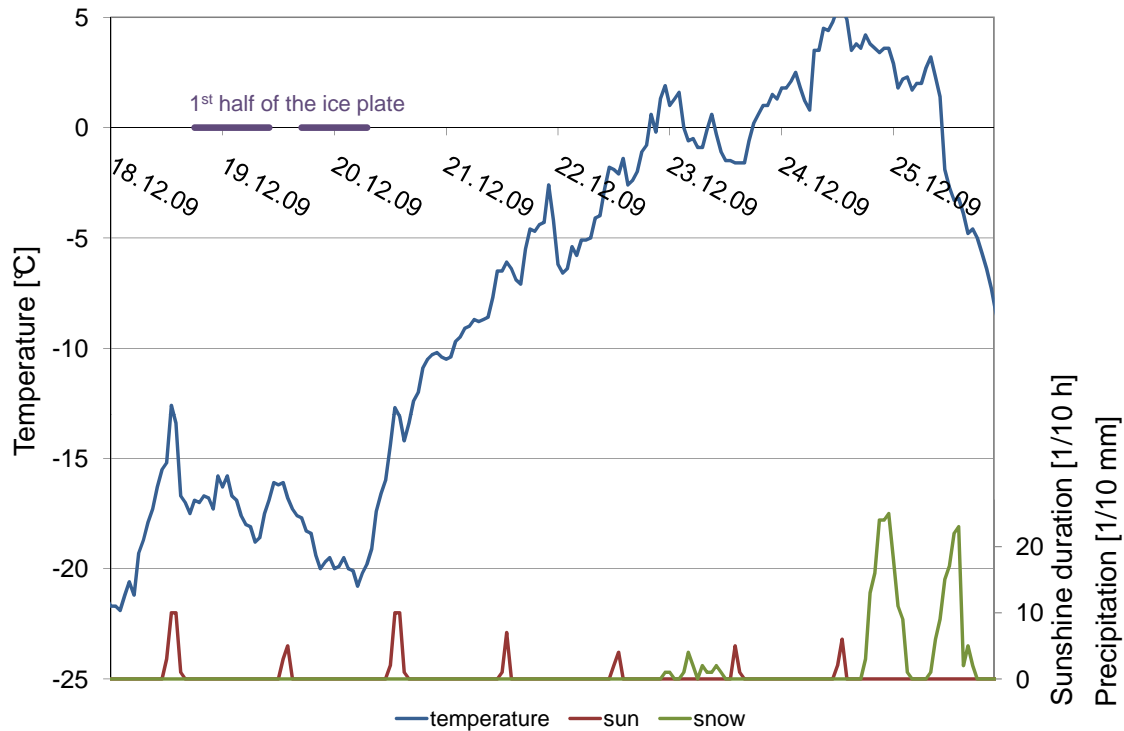
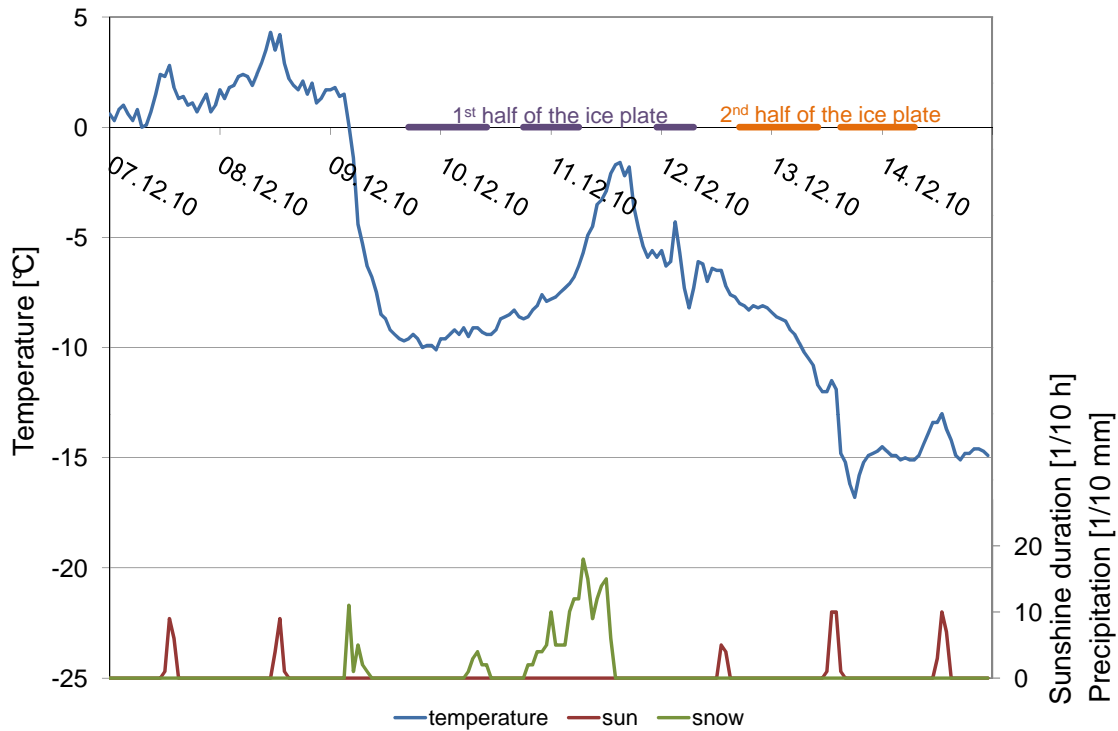


Figure 10.4: Climate data from 18<sup>th</sup> to 25<sup>th</sup> December 2009

Figures 10.4 and 10.5 show the climate data of the time period in which the ice was produced. In these diagrams the horizontal axis shows the date and the mark on this axis always represents the beginning of the day at 00 : 00 h. All measurements are on an hourly basis, performed by the *Central Institute for Meteorology and Geodynamics (ZAMG)*, Austria's national weather service agency [1].

The dark blue line shows the temperature in this time period. Moreover, information about the duration of the sunshine and the amount of precipitation is also available. The red line refers to the secondary axis and shows the sunshine duration in the unit 1/10 hour. A value of 10 represents one full hour of unclouded sunshine. Due to the fact that Obergurgl is situated in a deep valley, even on a cloudless day the sun only shines for a few hours in winter. The green line shows the precipitation in 1/10 mm which is also depicted on the secondary vertical axis. Naturally, in winter the precipitation is always snow.

Figure 10.4 shows the climate data of the time period in December 2009 when the first half of the ice plate for the ice shell made with the segment lift method with pneumatic formwork, was produced. It can be seen that during the night the temperature reached  $-16^{\circ}\text{C}$  to  $-20^{\circ}\text{C}$ , optimal conditions for making ice. Therefore, it was possible to

Figure 10.5: Climate data from 7<sup>th</sup> to 14<sup>th</sup> December 2010

produce 100 mm of ice within only two nights. The purple line shows the time period in which water was sprayed into the mold. In 2009 fresh snow was scarce, therefore the ice was almost exclusively made with tap water.

The temperatures as well as the sunshine duration and the amount of precipitation in the time period of the 7<sup>th</sup> to the 14<sup>th</sup> of December 2010 are shown in Figure 10.5. It can be seen that between the 7<sup>th</sup> and 9<sup>th</sup> it was impossible to produce ice due to warm weather. In 2010 it took three nights to produce the 1<sup>st</sup> half of the ice plate because even during the nights the temperature did not drop below  $-8^{\circ}\text{C}$  to  $-10^{\circ}\text{C}$ . The second half of the ice plate, however, could be produced quite fast due to low temperature and a sufficient amount of fresh snow.

### 10.3.3 Inserting the reinforcement

As soon as 100 mm of ice had been produced, the reinforcement could be inserted into the ice segment. The chosen amount of reinforcement has already been discussed in chapter 9.4 and was defined by taking the insights gained from the preliminary tests into consideration. The arrangement of the 5 mm steel ropes is shown in Figure 10.6. As described in chapter 6.2.2.3 rope clips connecting two ropes is the best option to anchor steel ropes. Therefore the steel ropes were placed in loops and connected with rope clips inside the ice segment. Figure 10.6 shows the reinforcement pattern and the location of the rope clips.



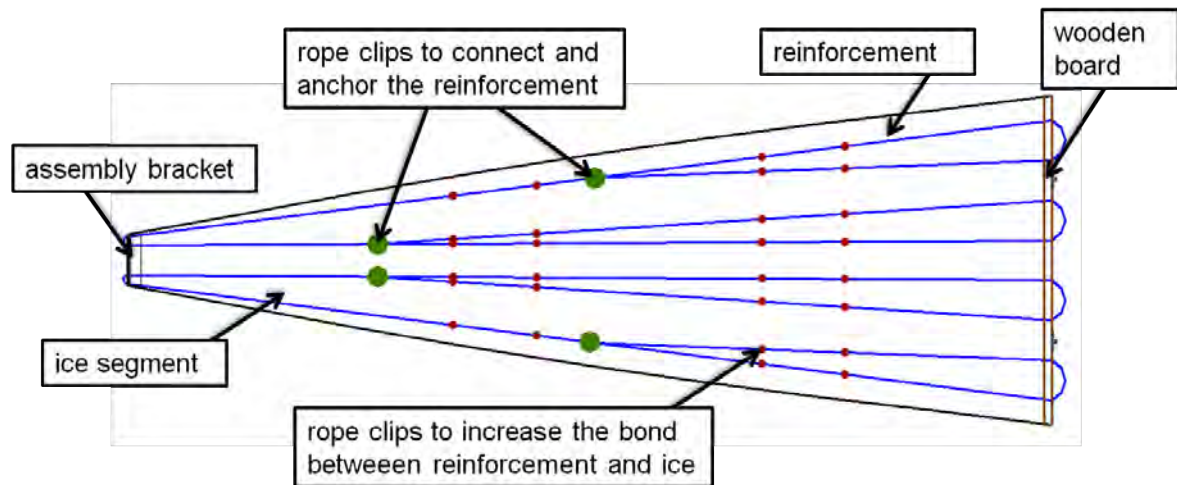


Figure 10.6: Arrangement of the reinforcement in an ice segment

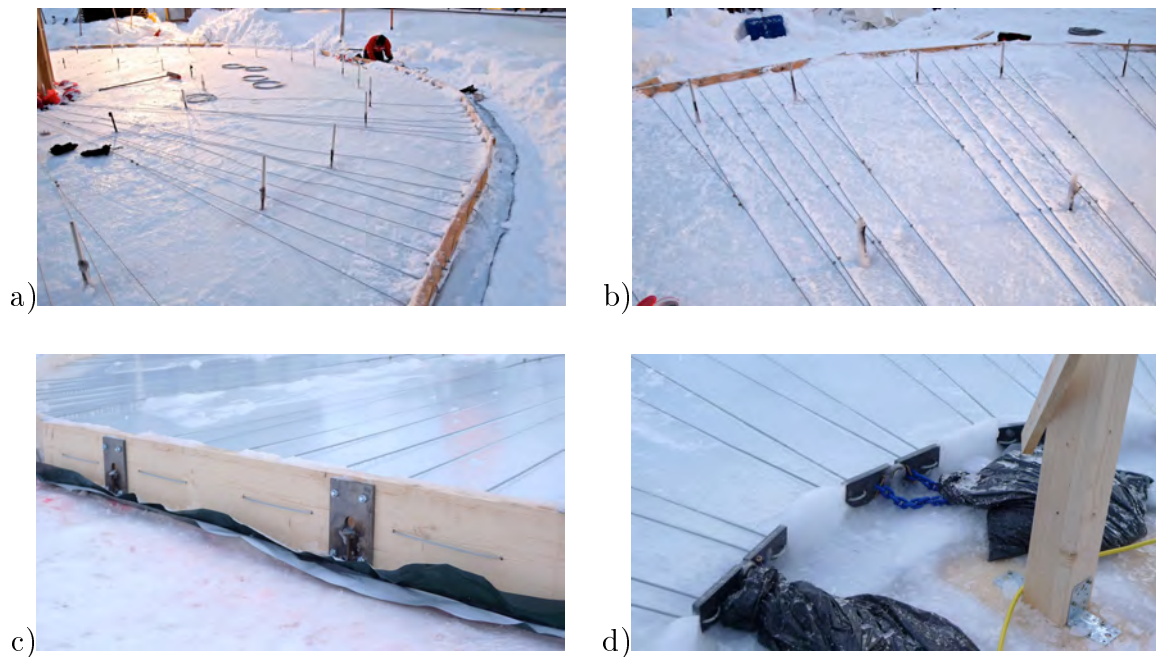


Figure 10.7: Reinforcement in the middle of the cross section of the ice segments a) inserting the reinforcement, winter 2010/11 b) arrangement of the reinforcement and the rope clips, winter 2010/11 c) reinforcement and outside formwork, winter 2009/10 d) reinforcement and assembly brackets of the inner formwork, winter 2009/10

As described in chapter 9.4, the cracks directly above the supports bearing the ice segments during the creeping process widened considerably. This phenomenon can be traced back to the fact that the bond between the steel ropes and the ice is not strong enough in the area of high bending moments. By using a pneumatic formwork during the creeping process, the bending moments created by self weight are distributed more smoothly therefore this is not an issue for this lifting method. In the segment lift method without pneumatic formwork the ice beams are situated on stacks of wood just like in the preliminary tests. To avoid large crack widths in the ice segments, additional rope clips were fixed to the steel ropes in order to increase the bond behavior. The rope clips are placed on the steel ropes only in the area of the maximum stresses – see Figure 10.6. Figure 10.7 shows pictures of the reinforcement inserted into the middle of the cross section.

After placing the reinforcement, the second half of the ice layer could be produced in order to create an ice plate with a thickness of 200 *mm*.

#### 10.3.4 Cutting the ice segments

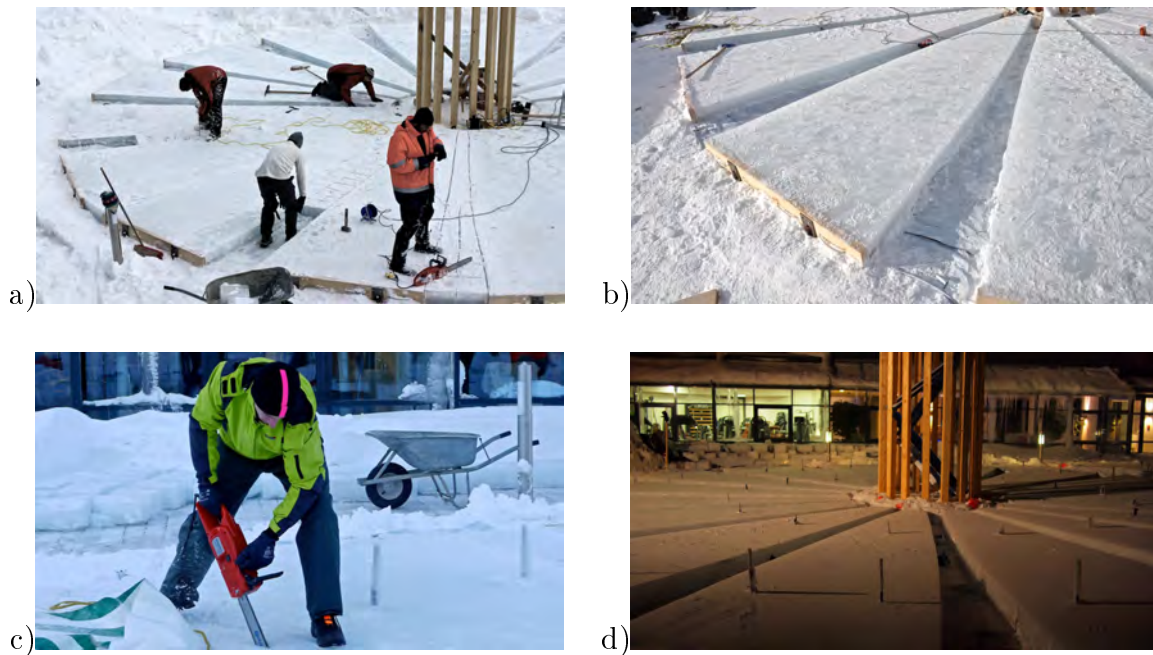


Figure 10.8: Cutting the ice segments a) winter 2009/10 b) winter 2009/10 c) winter 2010/11 d) winter 2010/11

In the next step, the ice plate was cut in order to create the ice segments with their predefined shape, as shown in Figure 10.1. One segment after another was cut out of the plate with the help of a chain saw. In the winter 2009/10, when the pneumatic formwork was placed underneath the ice plate, special diligence was required when working with the chain saw because the membrane must not be damaged. Photos of this process can be seen in Figure 10.8.

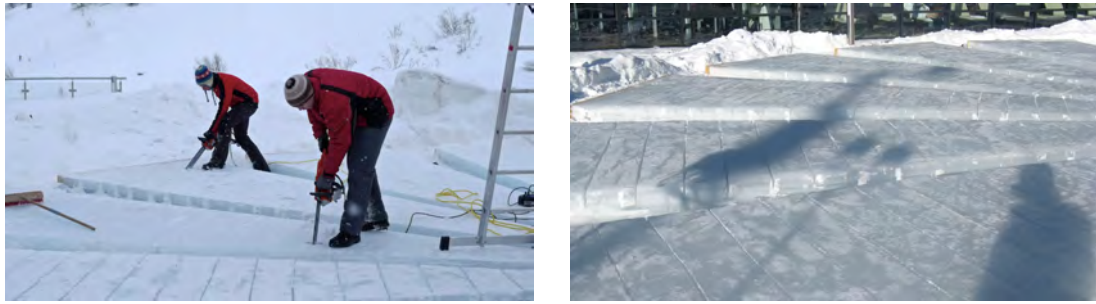


Figure 10.9: Creating the cuts which served as predetermined breaking points, winter 2009/10

As the preliminary tests have shown, the deformation of the ice beams increases considerably when weakening the cross-section with predetermined breaking points. Therefore, in both winter seasons, all of the ice segments were provided with cuts serving as predetermined breaking points. The cuts were created in an interval of  $250\text{ mm}$  perpendicular to the longitudinal axis of a segment and had a depth of  $70\text{ mm}$  to  $80\text{ mm}$ . These kind of cuts could easily be produced with a chain saw. Figure 10.9 shows pictures of the cuts and their production process.

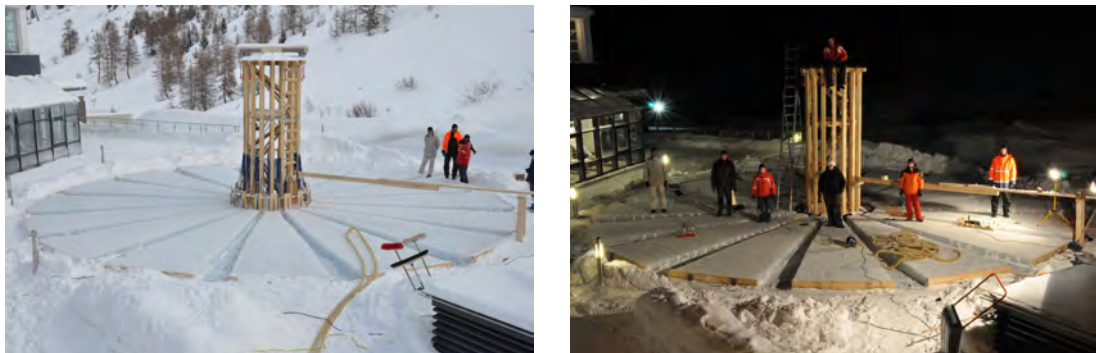


Figure 10.10: Sixteen individual ice segments, winter 2009/10

In Figure 10.10 two pictures of the sixteen flat ice segments prior to the lifting process are shown.

## 10.4 Deforming the ice segments

The next step to build an ice shell with the segment lift method is to distort the ice segments. This was done by lifting the ice segments and keeping them in an elevated position in order to allow the creep process to take place. This working procedure is called 1<sup>st</sup> lifting process. This step presents the main difference between these two methods with and without formwork.



### 10.4.1 Deforming the ice segments with a pneumatic formwork

#### 10.4.1.1 Lifting the ice segments with the pneumatic formwork

Pneumatic formworks provide a gentle way to lift the ice segments. The air pressure can be increased slowly and the pneumatic formwork supports the ice in a large area instead of a few isolated points, which decreases the stress peaks.

The pneumatic formwork used to lift the ice segments was approximately shaped like a donut with sixteen individual tailored membrane pieces glued together to form the airtight pneumatic formwork.

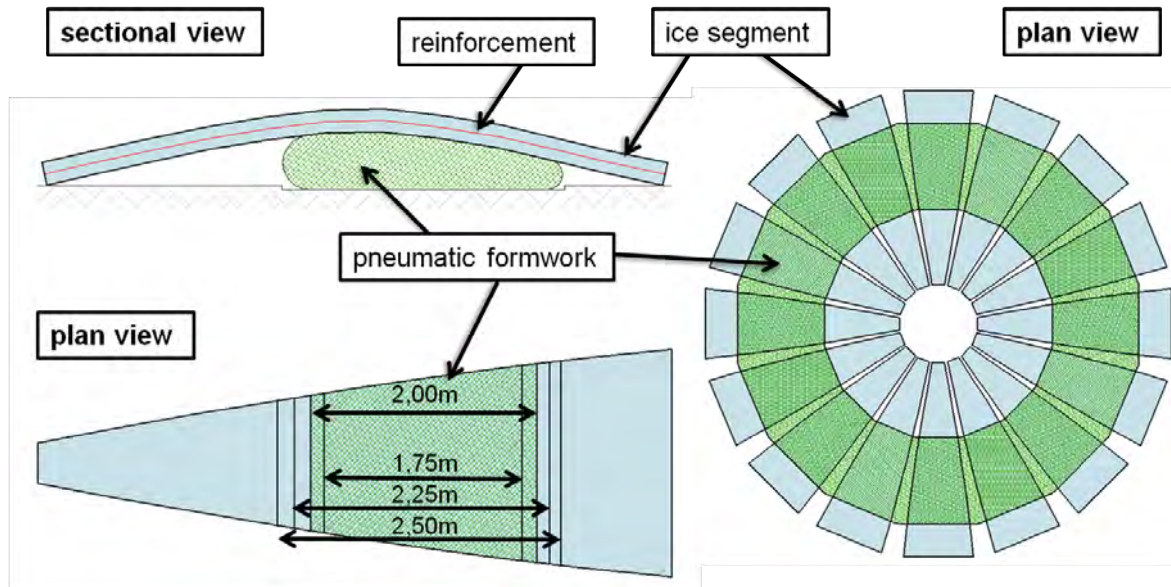


Figure 10.11: Position of the pneumatic formwork

In order to find the desired shape, the following requirements were taken into account. As already described in chapter 10.2, on the one hand, the stresses in the specimen must remain low enough to prevent the ice from collapsing. On the other hand, certain stresses are necessary in order to gain the desired rise. As a compromise, the maximal bending moment per meter to which the shape of the pneumatic formwork was tailored accordingly was determined to  $3,2 \text{ kNm/m}$ . This moment per meter corresponds to a contact area of the pneumatic formwork with an ice segment of  $2,0 \text{ m}$  length in the direction of the longitudinal axis of the specimen. The resulting vertical force generated by the pneumatic formwork has to be located at the center of gravity of the ice segment. To be able to receive the designated rise of  $500 \text{ mm}$  the pneumatic formwork must be at least this high. The formwork has to support the whole width of the ice segment. As shown in the right drawing of Figure 10.11, one pneumatic formwork extends over all sixteen ice segments. The membrane parts glued together in order to form this formwork were tailored accordingly.

In Figure 10.12 pictures of the production process of the pneumatic formwork are shown. For the PVC-membrane, as well as for the glue, the same materials as for the experiments on the pneumatic formwork method, described in chapter 5.1.1, were used.



Figure 10.12: Production of the pneumatic formwork

In the next step, the pneumatic formwork could slowly be inflated. Two air hoses were connected to the airtight membrane by means of two connection pieces which had been installed in the membrane during its production. One of the air hoses was used to inflate the pneumatic formwork and with another one, the air pressure could be measured by means of a hose water level. To fill the membrane with air the same air blower, as described in chapter 5.1.3, was used. The number of revolutions of the blower was regulated manually with an electrical AC converter. During the whole creeping process the air pressure was regulated regarding the following terms: On the one hand, the calculated stresses in the ice could only develop when all edges of the ice segments were unsupported. On the other hand, it was avoided to lift the segments too far above the ground to minimize the damage in case of a brittle failure of the ice segment. Therefore the air pressure was regulated by eye in such a way as to lift almost all edges of the ice segments off the ground and at the same time avoiding large distances between the end parts of the segments and the subsurface.

#### 10.4.1.2 Stresses in the ice segment and the membrane

One advantage of the pneumatic formwork is that the stresses in the ice can be regulated by changing the air pressure in the inflated membrane. At the beginning, only as much air as necessary in order to lift the ice segments slightly, was applied. In this configuration, the contact area between the pneumatic formwork and the ice segments had a length of more than the planned  $2,0\text{ m}$ . In the diagram in Figure 10.13 the vertical axis shows the bending moments per meter width of the ice segments and on the horizontal axis the longitudinal axis of the ice segments are depicted. Four different situations were considered. At the beginning, when the rise of the segments is still low, the length of the contact area between the pneumatic formwork and the ice can be estimated with  $2,5\text{ m}$ . By increasing the air pressure in the pneumatic formwork, the vertical extension increases because the formwork aspires toward maximizing its cross-sectional area while keeping the lateral area constant. In Figure 10.13 the bending moments per meter with a theoretical contact area of  $2,5\text{ m}$ ,  $2,25\text{ m}$ ,  $2,0\text{ m}$  and  $1,75\text{ m}$  are depicted. These contact areas are marked in the left drawing in Figure 10.11. By comparing these moments per meter depicted in Figure 10.13 with the ones generated

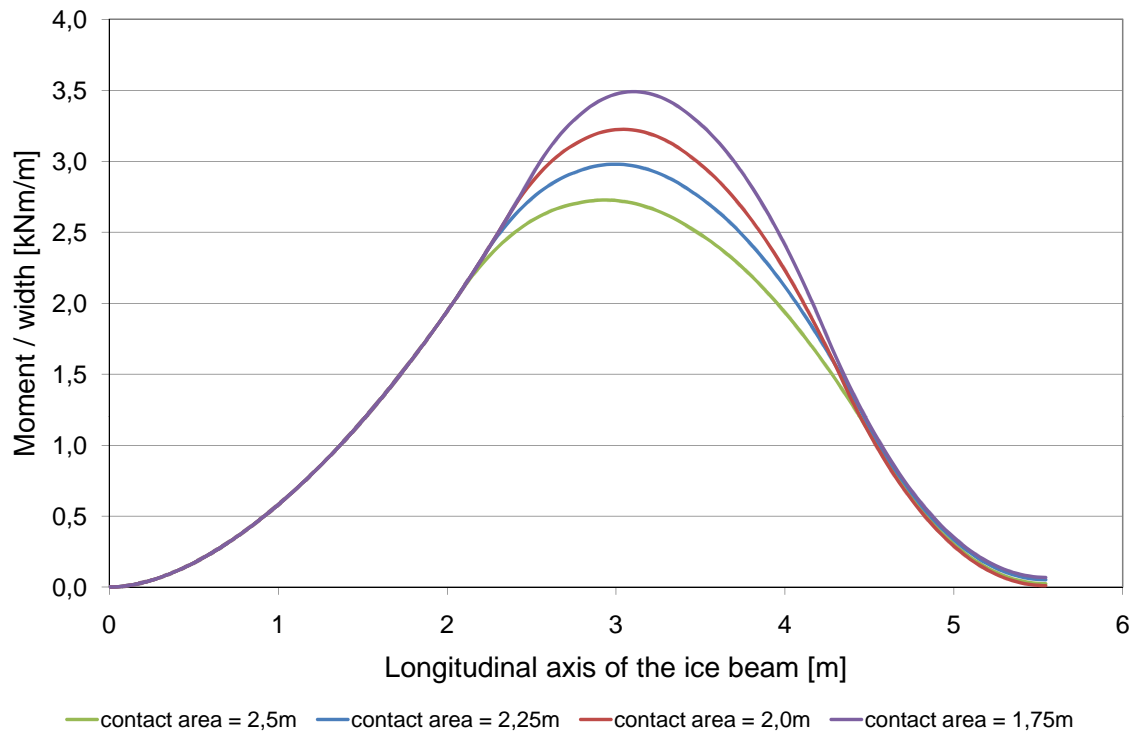


Figure 10.13: Bending moments per width in the ice segment for different contact areas of the pneumatic formwork

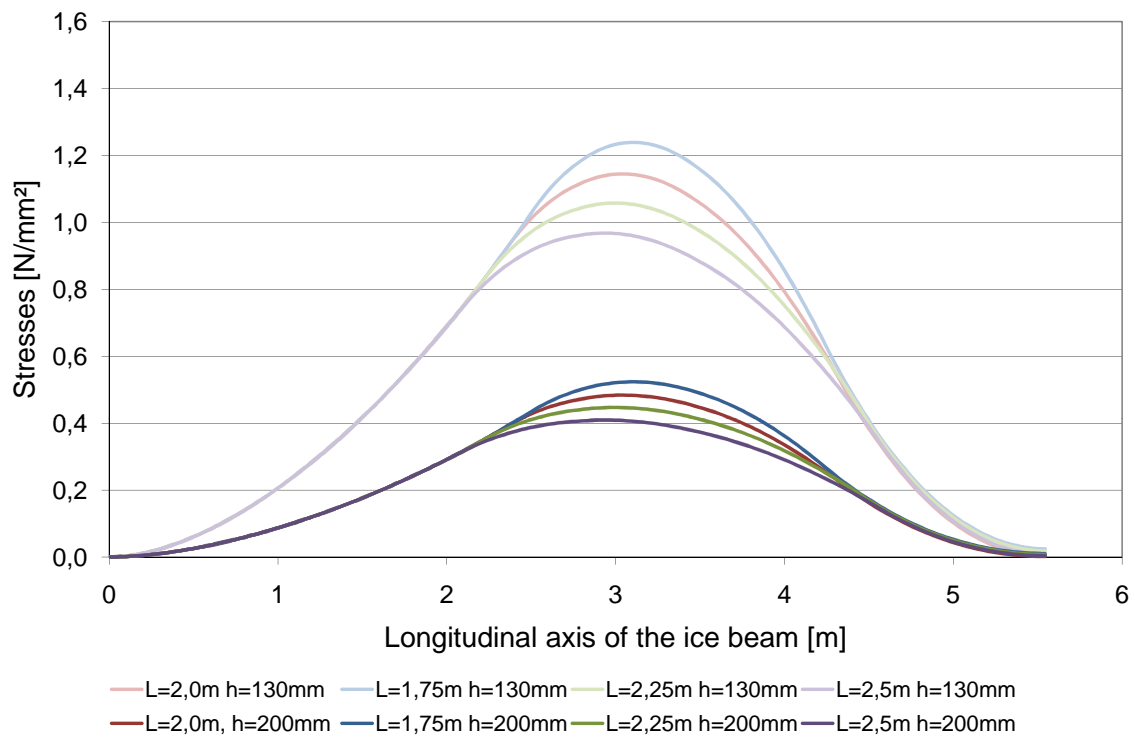


Figure 10.14: Stresses in the ice segment during lifting and creeping

in the preliminary experiments (Table 9.2), it can be assumed that the ice can bear these forces.

The calculated air pressure in the pneumatic formwork for these contact areas amounts to  $34\text{ mbar}$ ,  $38\text{ mbar}$ ,  $43\text{ mbar}$  and  $49\text{ mbar}$ , respectively. The larger the contact area, the lower the air pressure in the membrane. These values of air pressure are similar, concerning the range, to the ones necessary with the pneumatic formwork method. The forces in the seams, however, are considerably lower using this donut-shaped pneumatic formwork because the radius of this shape is much smaller and the force in the membrane behaves accordingly to equation 4.3 and 4.4, described in chapter 4.3.2. Therefore, no problems in the seams of this type of formwork are to be expected.

The stresses in the ice are presented in Figure 10.14. On the horizontal axis, the longitudinal axis of the ice beam is shown and on the vertical axis the maximum absolute value of the stresses in the cross section is depicted. Like in Figure 10.13 it is assumed that the length of the contact area between pneumatic formwork and ice can vary. The designed value of this length  $L$  is  $2,0\text{ m}$  but the stresses for the contact lengths  $L$  of  $1,75\text{ m}$ ,  $2,25\text{ m}$  and  $2,5\text{ m}$  are also shown. Due to the cuts made by the chain saw of an interval of  $250\text{ mm}$ , the height of the cross section is not constant. Every  $250\text{ mm}$  the cross section was weakened, so that in this section the height only amounted to  $130\text{ mm}$ . In the areas between the cuts, the cross section had the designed height of  $200\text{ mm}$ . In Figure 7.14 analytical results of those two settings are presented. On the one hand, the stresses are calculated with a theoretical cross section height  $h$  of  $130\text{ mm}$ , representing the cross section in the areas of the cuts. On the other hand, the stresses are calculated for the entire height  $h$  of  $200\text{ mm}$ . In those calculations the cross section is rectangular and only bending moments occur, thus the tensile stresses on the top and the compression stresses on the bottom of the cross section are of the same absolute value.

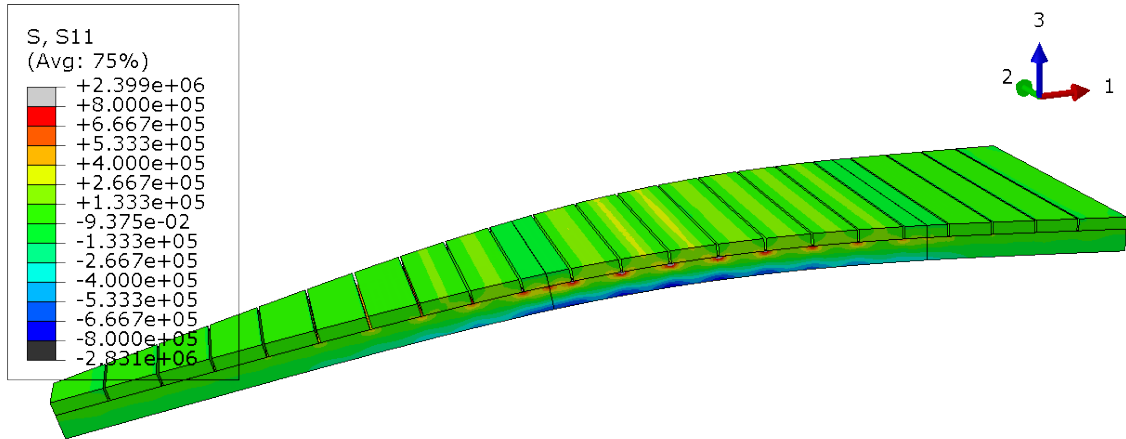


Figure 10.15: Normal stresses  $S_{11}$  in  $N/m^2$

In order to get an impression of the actual stress distribution in the ice segments, which have an abruptly changing cross section, a 3D finite element model was created by means of the finite element program *ABAQUS* [14]. The cuts were modeled with a thickness of  $10\text{ mm}$  and a depth of  $70\text{ mm}$ . In Figure 10.15 results of this linear elastic

numerical simulation are shown. It can be seen that the stress distribution are strongly influenced by the cuts. But due to the fact that the edges of the cuts are singularities, the exact value of the stresses at this point cannot be determined with this model. This problem will also be discussed in chapter 10.4.2.5.

### 10.4.1.3 Initial deformation

Measurements of the deflection of two ice segment were taken immediately after the pneumatic formwork was inflated as well as after 63 hours of creeping. Figure 10.16 shows a comparison between calculated deflections and measured ones. The horizontal axis depicts the chord between the two end points of the ice segments starting with the end point *A*. The vertical axis shows the deflection perpendicular to the chord. The blue and the red curves show the deformation of the segment 1 and 16 immediately after the lifting as well as after 63 hours of creeping. Moreover, this diagram also shows theoretical deflections. The dark green line presents the calculated shape of the ice segments under the assumption that the whole cross section is in the final cracking state and the tension stiffening effect due to participation of the ice between the cracks is neglected. The length  $L$  of the contact area between the pneumatic formwork and the segments amounts to  $2,0\text{ m}$  and the Young's modulus of the ice is assumed to be  $400\text{ N/mm}^2$ . Because of the fact that the modulus of elasticity of ice is very diversified, the light green lines show the deflection according to the same assumptions accept that the Young's modulus was set to  $300\text{ N/mm}^2$  and  $500\text{ N/mm}^2$ , respectively. The dark purple curve was calculated with a length  $L$  of the contact area of the pneumatic formwork and the ice of  $2,5\text{ m}$ . Because of the larger support area of the segment, the deformations resulting from the self weight are smaller compared to the ones with a contact length of  $2,0\text{ m}$ . The influence of the Young's modulus is also shown for this boundary condition. The light purple curves show the deformation occurring when the modulus of elasticity is defined to  $300\text{ N/mm}^2$  and  $500\text{ N/mm}^2$ , respectively.

The actual initial deflection of the ice segments has to be equal or lower than the calculated deformation in the final cracking state. If the ice segments experience a lot of cracks the deformation approximates to this upper limit. If no cracks appear at all, the cross section is only weakened by the  $70\text{ mm}$  to  $80\text{ mm}$  deep cuts, previously made by the chain saw in an interval of  $250\text{ mm}$ . To calculate the deflection of this lower limit, a 3D linear elastic finite element model of the ice segments with a modulus of elasticity of  $400\text{ N/mm}^2$  was created by means of the finite element program *ABAQUS* [14]. For this calculation the length of the contact area between formwork and ice was defined to the designed  $2,0\text{ m}$ . The orange triangle in Figure 10.16 shows the rise of the modeled ice segment, taking the cuts into account but assuming that the segment stays in an uncracked state. The actual initial deformation of the ice segments ranged between these two limits: the uncracked and the final cracking state. After the creeping process, however, the deformation can extend the one occurring under the final cracking state.

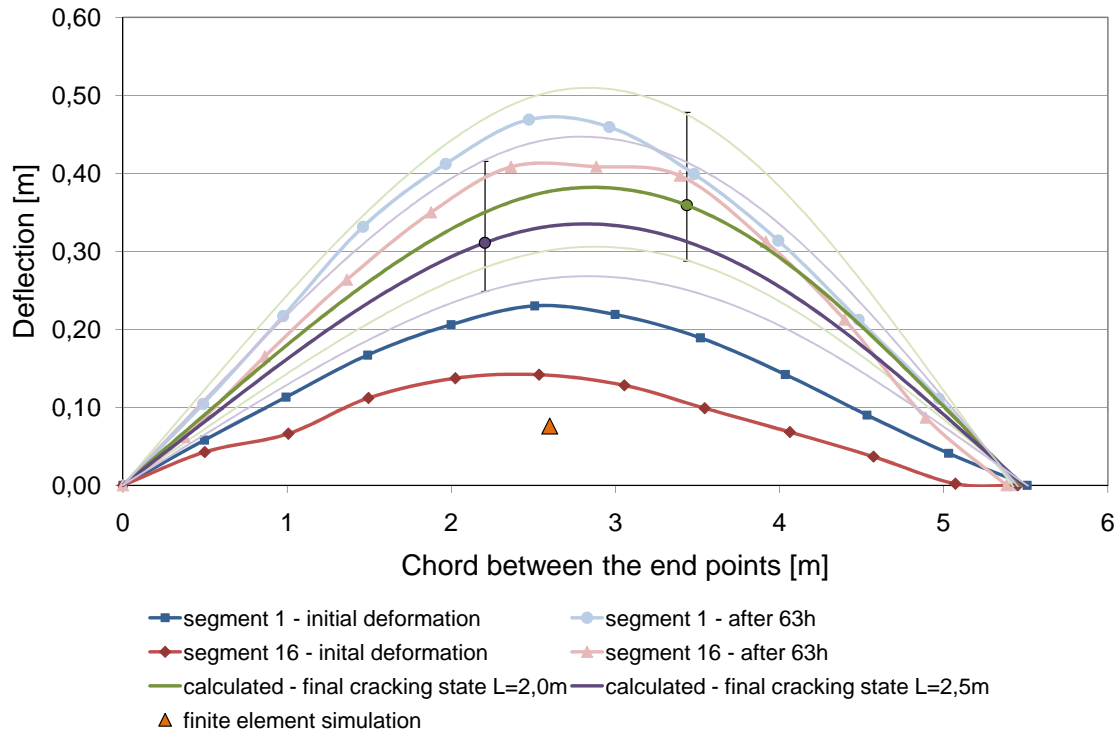


Figure 10.16: Measured and calculated deformations

#### 10.4.1.4 Creeping behavior of the ice segments

In the Figures 10.17 and 10.18 pictures of the ice segments undergoing the creeping process are shown.

The deformation of two ice segments was detected during the first 63 hours of the creeping process by measuring the height difference between twelve evenly distributed points alongside the longitudinal axis of the ice segment and a fixed reference point with a theodolite. The results are shown in Figure 10.19 and 10.20. In order to be able to compare the change of the rise over a certain time period, the horizontal axis of these diagrams represents the chord between the end points  $A$  and  $B$  of each segment; the index  $x$  starts at the end point  $A$ . In other words, the points of the curved segments are rotated and translated in such a manner that the edges of the segment are always situated on the ground, represented by the horizontal axis with  $y = 0$ . Moreover, the point  $A$  of the segments is moved to the point of origin of the diagrams. Figure 10.19 shows the deformation of segment 1, as labeled in Figure 10.18, and Figure 10.20 refers to the segment 16. The blue lines on the very bottom show the initial deformation directly after inflating the pneumatic membrane. The light orange line on the very top shows the deflection of the segments 1 and 16 after 63 hours. During this time span the rise of segment 1 and 16 increased by 2,1 and 2,9, respectively.

The segments experienced creeping for almost 100 hours. The detailed measurements on segment 1 and 16, however, could only be performed during the first 63 hours.



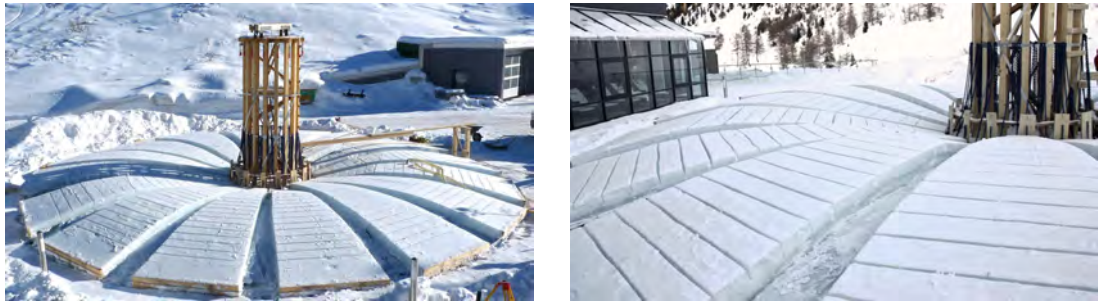


Figure 10.17: Creeping process of the ice segments, winter 2009/10

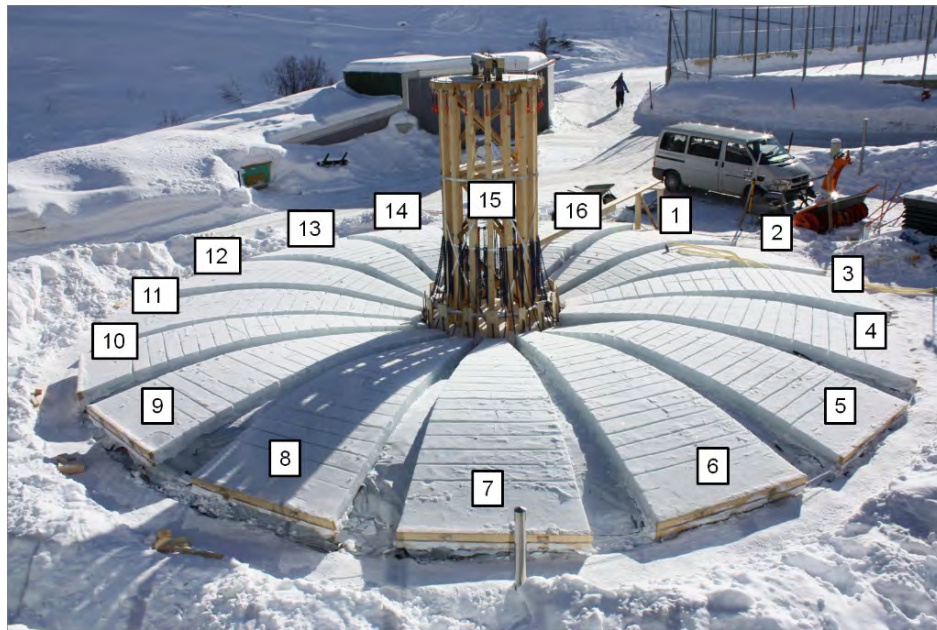


Figure 10.18: Creeping process of the ice segments, showing their respective number, winter 2009/10

Figure 10.21 shows the development of the rise of the segments during the creeping process. The rise is defined in Figure 8.2 in chapter 8.3.1. With a small angle between the vertical and the rise, which is by definition perpendicular to the tension tie, the following approximation holds:  $\cos \alpha = 1$ . The respective rise for each segment is depicted in Figure 10.21 and labeled with the according specimen number, defined in Figure 10.18. The vertically primary axis on the left side of the diagram in Figure 10.21 shows the rise of the segments in meters. In the first 38 hours only segment 1 and 16 were measured. Later on, data for the other segments were available as well. It can be observed that the variation of the rises of the different segments is quite large and amounts to approximately  $100\text{ mm}$ . Moreover, the rise also increases and decreases over time. This phenomenon might appear inexplicable at first but can be explained by the change of air pressure in the pneumatic formwork. Therefore the air pressure is also depicted in this diagram. The orange line on the very top refers to the air pressure and relates to the secondary vertical axis which shows the air pressure in the membrane in millibar. As described previously, the air pressure was varied constantly

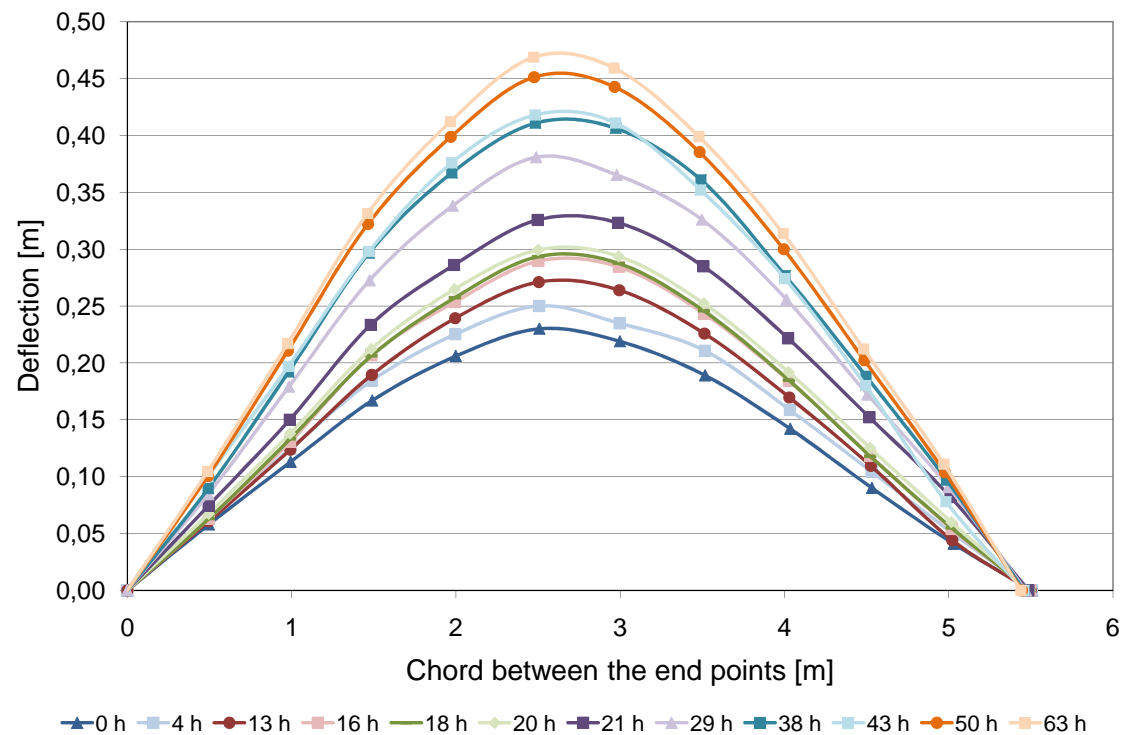


Figure 10.19: Deflection of the ice segment 1 due to creeping in a certain period of time

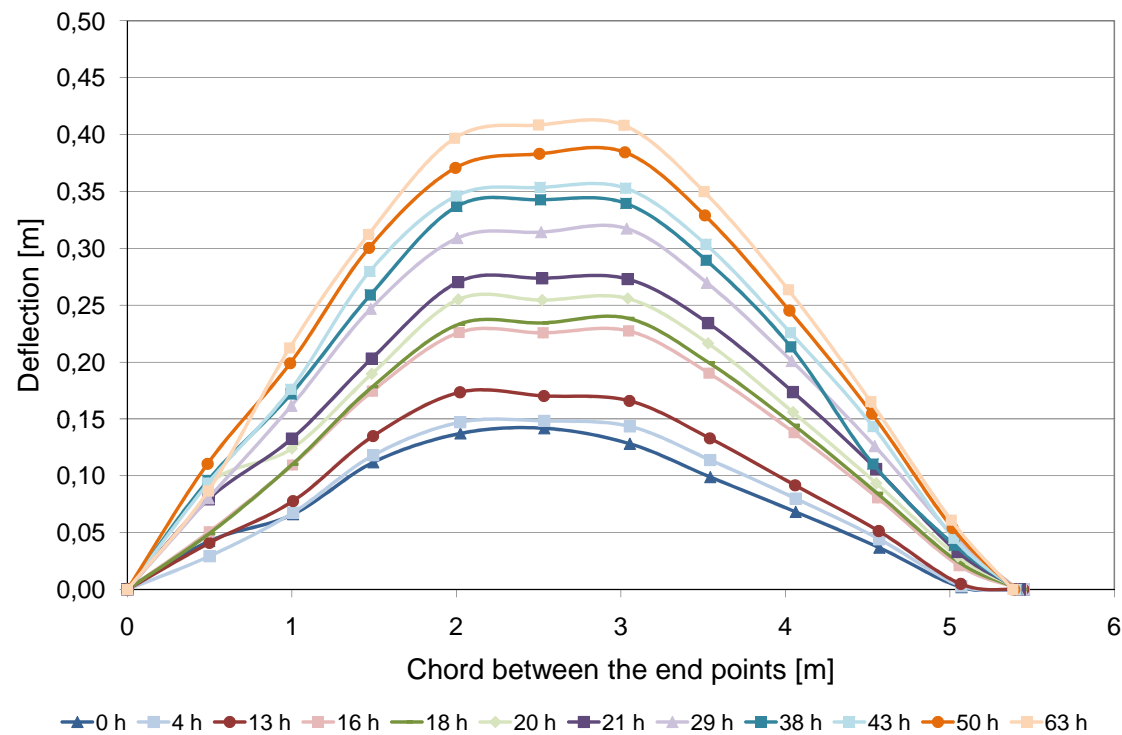


Figure 10.20: Deflection of the ice segment 16 due to creeping in a certain period of time



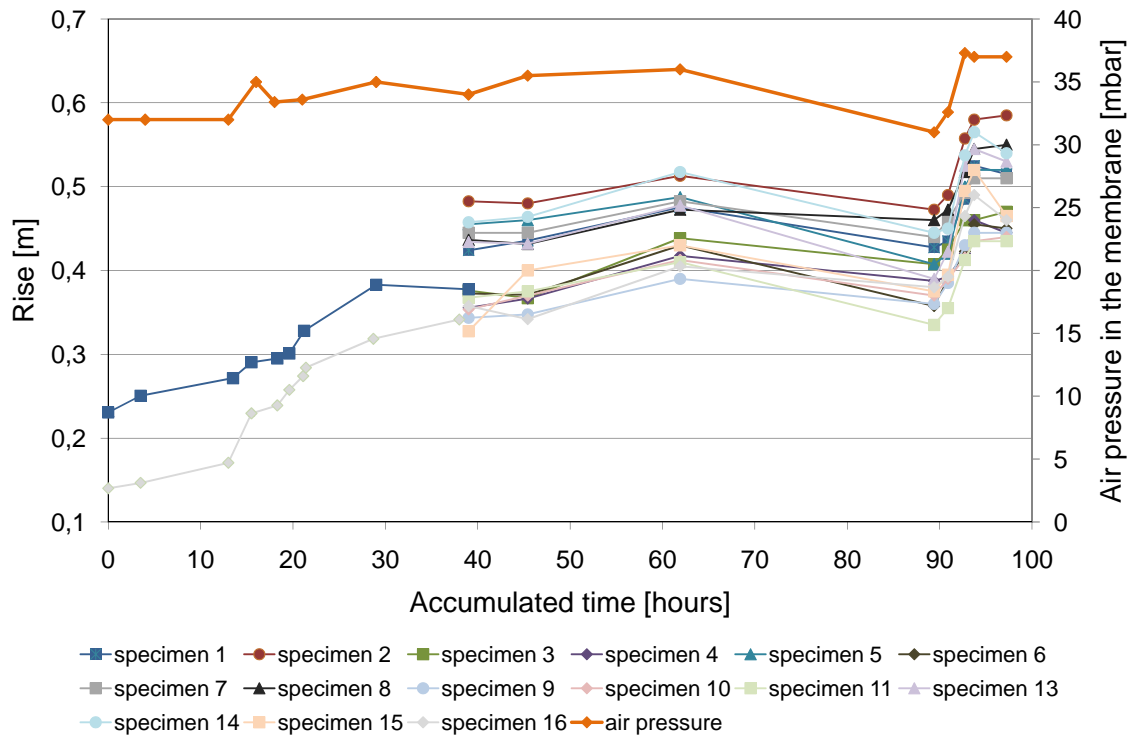


Figure 10.21: Change of the rise of all 16 segments and the air pressure in the first 100h after inflating the formwork

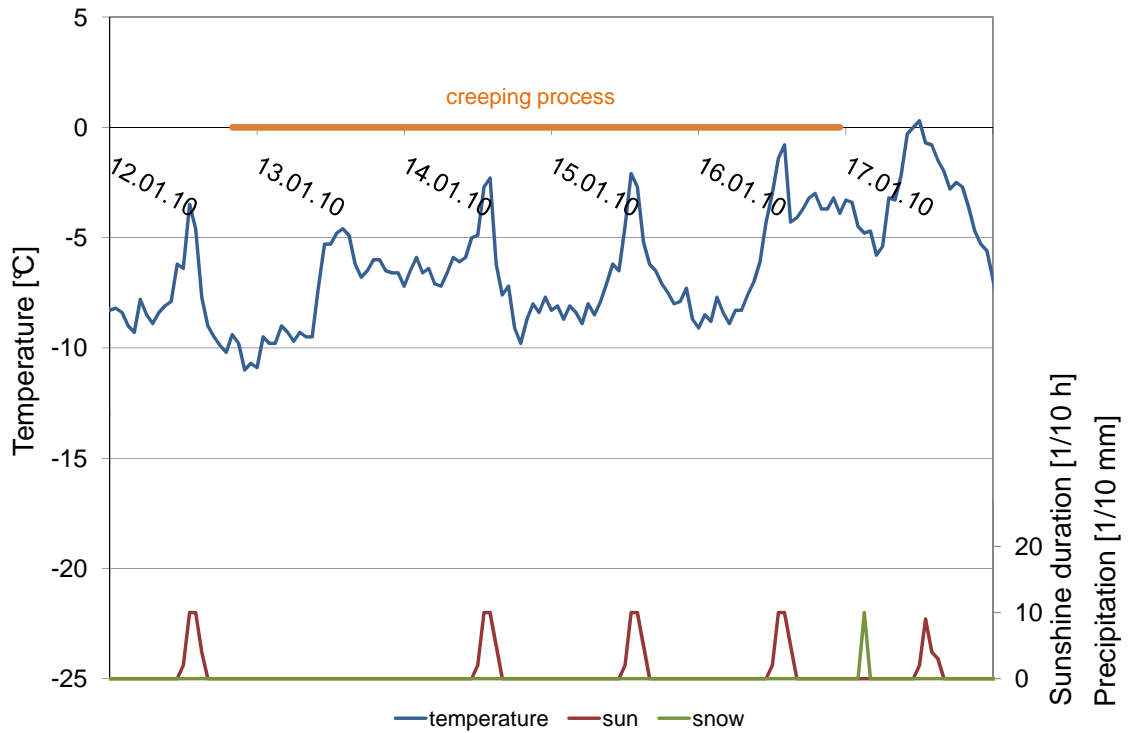
with the intention of lifting the edges of the segments only slightly. Due to the fact that the properties of the ice segments were not totally identical, some segments were lifted from the ground while others still had contact to the support. This led to different deformations and changing rises.

After 90 hours the air pressure was lowered in order to be able to work on the temporary tension chains. This lower air pressure immediately caused lower rises in the segments because all ends had contact to the ground. By increasing the air pressure the rises increased once again.

It has to be pointed out that the displayed development of deformation in this certain period of time cannot be understood as universally valid values describing the creep behavior of ice. All measurements only refer to the specific circumstances of this experiment.

As described in chapter 2.2.2, the creep behavior of ice is highly dependent on the temperature. Due to the fact that these ice segments were situated outside, the air temperature as well as the solar radiation had an important impact on the creep deformation. Therefore Figure 10.22 shows the air temperature curve over the time period of the creeping process [1].

With this construction method large creep deformations are required, therefore selective measures were accomplished in order to maximize the deflection. For example, the pneumatic formwork was inflated with warm air of approximately  $+15^{\circ}\text{C}$ . Therefore,

Figure 10.22: Climate data from 12<sup>th</sup> to 17<sup>th</sup> January 2010

the compression zone of the ice segments was warmed which accelerated the creeping process.

Another endeavor to increase the creep deformation of the ice segments was to drive wedges into the cuts which served as predetermined breaking points in order to crack the ice. If the cross section is in a cracked state, the deformation increases. Moreover additional weight was added to the ends of those segments which showed less deformation, in order to increase the stresses and subsequently the creeping. By applying all these measures and by varying the air pressure in the membrane, the specific curves were achieved as shown in the Figures 10.19 to 10.21.

## 10.4.2 Deforming the ice segments without a pneumatic form-work

### 10.4.2.1 Lifting the ice segments with the lifting devices

Using the segment lift method the segments need to be lifted and placed in an elevated position in order to allow the creeping process to take place. For the lifting of the ice segments two lifting devices were used. Figure 10.23 shows the components of the lifting devices in schematic drawings. Each lifting device consists of a hydraulic center hole jack, a jack chair, a stand, a threaded steel rod and a U-shaped anchorage beam. The hydraulic jacks were bought from the international company *ENERPAC®* and are sold under the labeling *RCH-123* [26]. This hydraulic jack can easily be operated

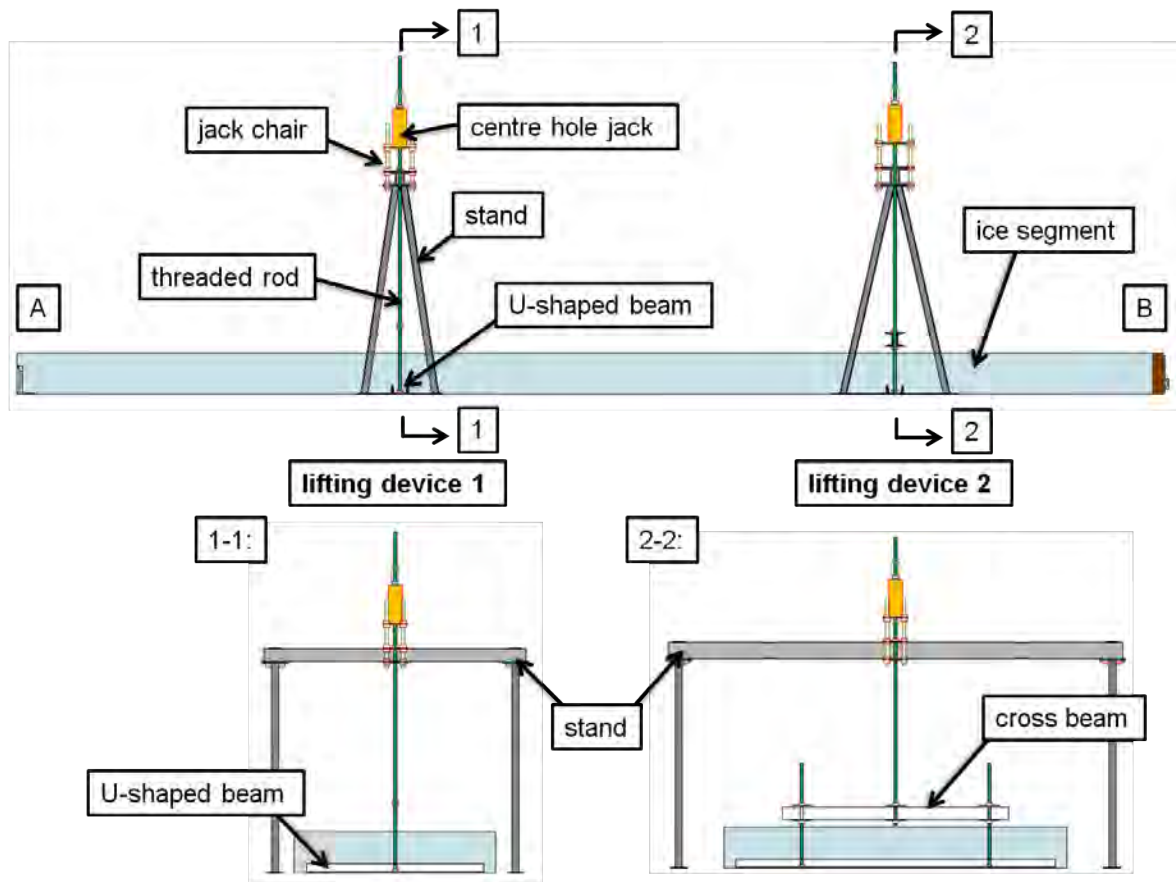


Figure 10.23: Lifting device

with a lightweight hand pump; the model used had the model number *P-202*. The hydraulic jacks as well as the hand pumps were fixed to steel stands. These steel stands were purpose-built for this lifting operation. They were designed to bear the load resulting from the self weight of the ice segments while being light enough to be handled manually. Drawings containing detailed dimensions and materials used for all parts of the lifting device are attached in the appendix B.2. The nomenclature in these drawings is in accordance with ÖNORM EN 1993-1-1 [12].

In order to lift the ice segments, the threaded steel rods were passed through the center hole of this hollow plunger cylinder and connected to the ice segment on their other end. The rod used had a *M16* screw thread according to DIN 13-1 [11]. Several strokes with the hydraulic jack were necessary to lift the ice segments into their final position, therefore the jacks were placed on so-called *jack chairs*. With every stroke, the plunger of the jack could be extended *76 mm*. Figure 10.24 explains how one stroke is carried out. The threaded rod is anchored with a nut above the hydraulic jack, labeled *nut 1*, in Figure 10.24. Then the plunger is extended by means of the hand pump which lifts the ice segment. When the plunger is completely extended, a second nut (*nut 2*) - fixed to the threaded rod inside of the jack chair - has to be manually screwed down to the base plate of the jack chair in order to carry the weight of the ice segment. As the force is carried by the second nut, the plunger can be retracted and the nut situated

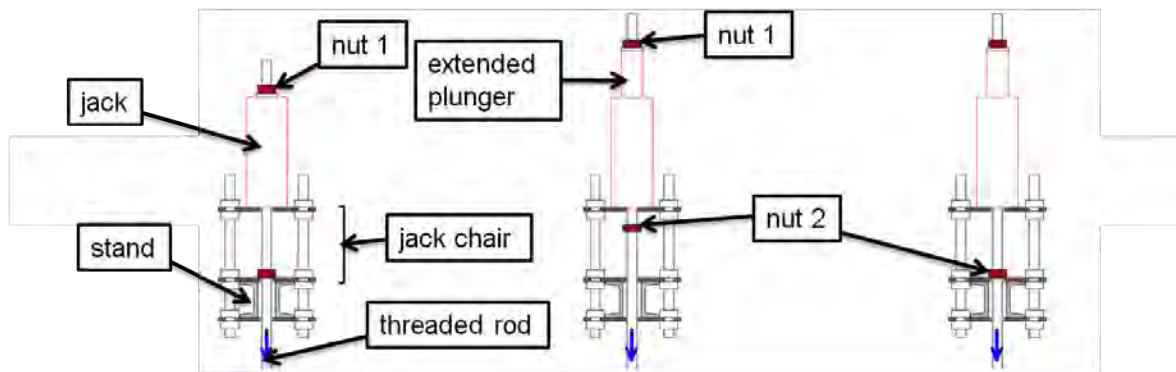


Figure 10.24: Description of a stroke with the lifting device

above the jack can be made to follow up. In this manner the number of necessary strokes can be executed in order to lift each ice segment into its final position.

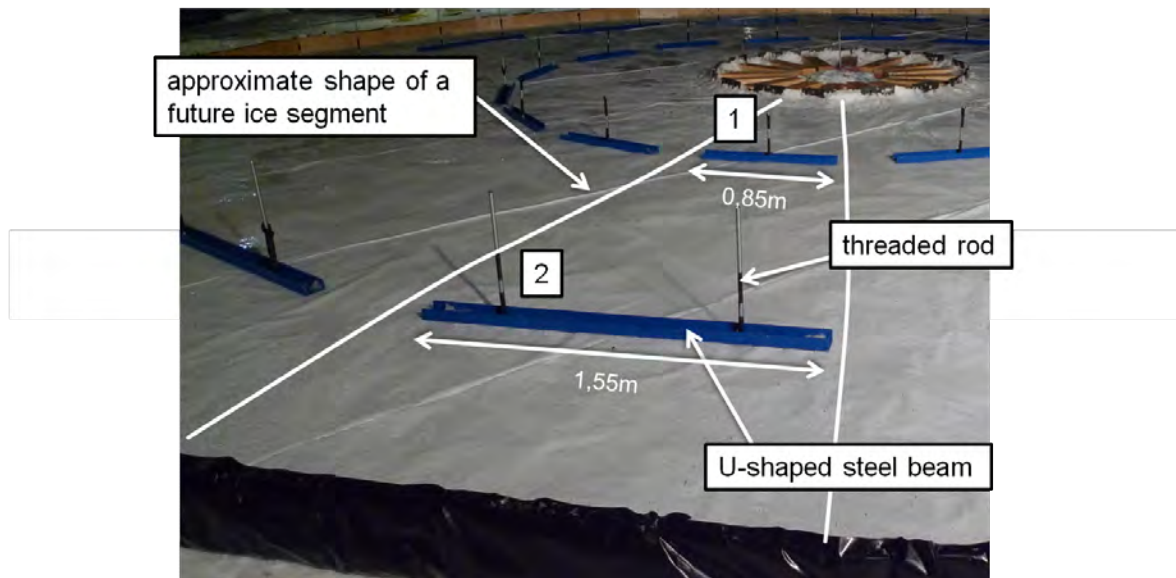


Figure 10.25: U-shaped steel beams and threaded rods situated in the ice segment

To anchor the threaded steel rods to the ice, U-shaped steel beams were inserted into the ice segment. The nuts had been welded onto the steel beam in order to connect the threaded rods with the U-shaped steel beams. This assembly of rod and steel beam had been placed into the mold of the ice plate before the ice producing process started – as described in chapter 10.3. A detailed picture of the steel rods is shown in Figure 10.25. The U-shaped steel beam, which is connected to lifting device 1 according to Figure 10.23, is  $0,85\text{ m}$  long and equipped with one rod. On the  $1,55\text{ m}$  long U-shaped steel beam two nuts were welded to the inner surface, so that in this area the ice segment could be lifted with two rods. The steel beams can only function as line supports for the ice segments if their stiffness is high enough to distribute the supporting force uniformly. For the shorter steel beam, this is not an issue. If the longer steel beam, however, is only lifted in the middle with one rod, the deflection of the steel beam

could be larger than the one of the ice in cross direction. To reduce the deflection of the steel beam, two rods are anchored to the beam. Above the ice segments these two rods are connected with a cross beam. Thus, the ice segment could be lifted on both lifting points with one hydraulic jack each.

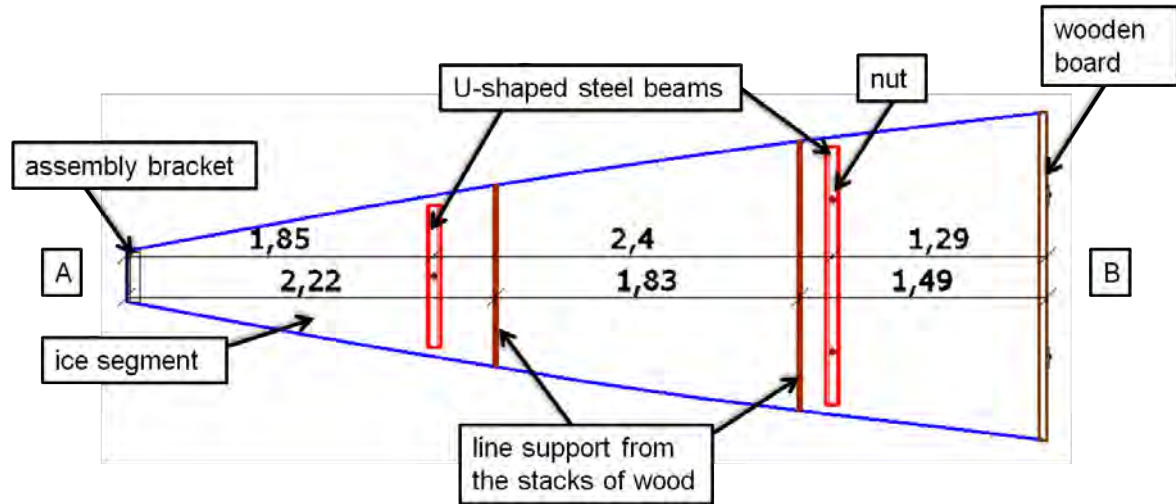


Figure 10.26: Position of the U-shaped steel beams and the line supports from the stacks of wood

The position of these lifting points of the ice beam was chosen according to the following considerations. On the top face of the ice segments, the cross section is weakened by the 70 mm to 80 mm deep cuts, therefore no compression zone can be created. Hence, the location of the lifting points is chosen in such way that the self weight only causes negative bending moments and no compression arises on the top face. Moreover, to prevent the ice from collapsing during this lifting process, the position of the steel beams is defined in order to minimize the stresses.

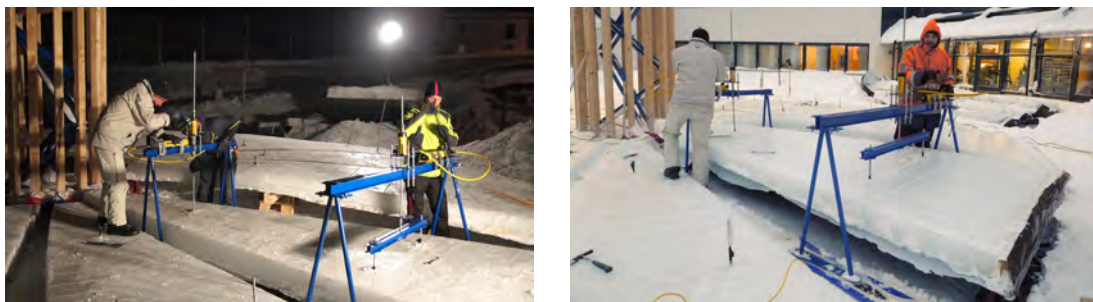


Figure 10.27: Lifting the ice segments by means of the lifting devices

Figure 10.26 shows the location of the U-shaped steel beams which form line supports for the ice segments. The resulting bending moments per width occurring during the lifting process with the lifting device can be obtained from Figure 10.34. The maximum bending moment during the lifting process amounts to  $1,64 \text{ kNm/m}$ . In the preliminary tests (chapter 9), specimen 4 was lifted with a very similar lifting device and the bending moment in this specimen was  $3,87 \text{ kNm/m}$  which is a 2,4 larger value.

Therefore, it can be assumed that the loading during the lifting of the ice segments is unproblematic. In Figure 10.27 pictures of the lifting process by means of the lifting devices are shown.

#### 10.4.2.2 Triggering cracks

Cracks in the tension zone of the ice are requested in order to obtain large deflections. As soon as the ice segment has been lifted a few millimeters from the ground, the tensile stresses can cause the first cracks. In these cracks the tension force is no longer carried by the ice but by the reinforcement. Naturally the cracks appear in the areas of the cuts, which are supposed to be predetermined breaking points. The number of cuts in which cracks occur depends on the tensile strength of ice. As already discussed in chapter 2.2.2, the tensile strength varies strongly and depends on many parameters such as temperature, crystalline structure, density of the ice and strain rate.

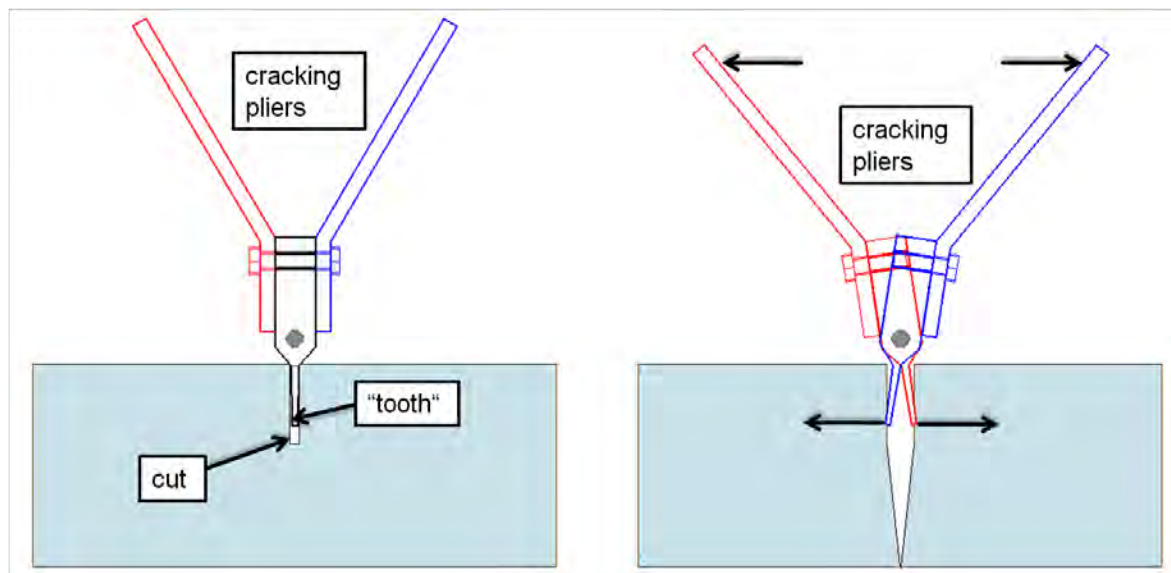


Figure 10.28: Exaggerated sketch of the cracking pliers

To maximize the deflections a state similar to the final cracking state is requested. Therefore cracks were triggered in every single cut. In order to trigger the cracks, a special tool – named *cracking pliers* – was designed. Figure 10.28 shows a highly exaggerated sketch of the mechanism of these cracking pliers. The basic idea of this tool was that by opening the pliers an additional horizontal load is applied to the weakened cross section. Through this horizontal force, tension occurs on the base point of the crack. To use this tool, the teeth are placed into the cuts and by pushing apart the upper end parts of the cracking pliers, the teeth apply a horizontal force at the base of the crack. In theory, the pushing apart of the upper ends of the pliers can be done by a combination of a threaded rod and nuts or by a hydraulic jack.

Using the cracking pliers on the real ice segments showed that in most cases a crack appeared as soon as the tool was placed into the crack. This phenomenon can be explained by the fact that the cracking pliers have a self weight of approximately 25 kg



Figure 10.29: Usage of the *cracking pliers*

which produced a jerkily additional load. Moreover, the teeth of the cracking plies could not be inserted into the cut totally parallel to the cut's axis. Due to this additional excentricity, cracks appeared easily in every single cut. In the majority of cases, one could actually hear the cracking of the ice and visible cracks always appeared on the edge of the ice segment. Figure 10.29 shows how the cracking pliers were used.

#### 10.4.2.3 Placing the ice segments on stacks of wood

After the cracks were triggered in the cuts, the ice segments were lifted high enough to place the woodpiles under the ice segments. In Figure 10.30 a schematic drawing of

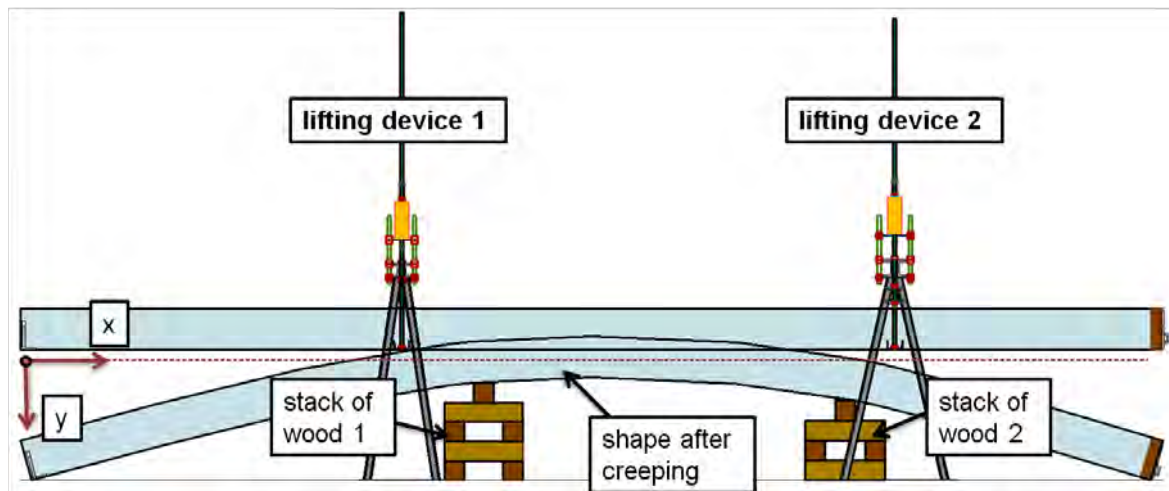


Figure 10.30: Placing the ice segments on stacks of wood

the stacks of wood as well as the lifting devices is shown. The stacks of wood define a line support for the ice segment during the creeping process. The position of these line supports was optimized in order to gain large stresses which increase the initial deformation and the creep but simultaneously keep the stresses low enough to prevent the ice from collapsing. The location of the line supports created by the stacks of wood is depicted in Figure 10.26, which also shows the position of the U-shaped steel beams.

Figure 10.31 shows the ice segments placed on the stacks of wood. The stacks of wood consisted of squared timber with a cross section of  $100 \times 100 \text{ mm}$ . Several wooden



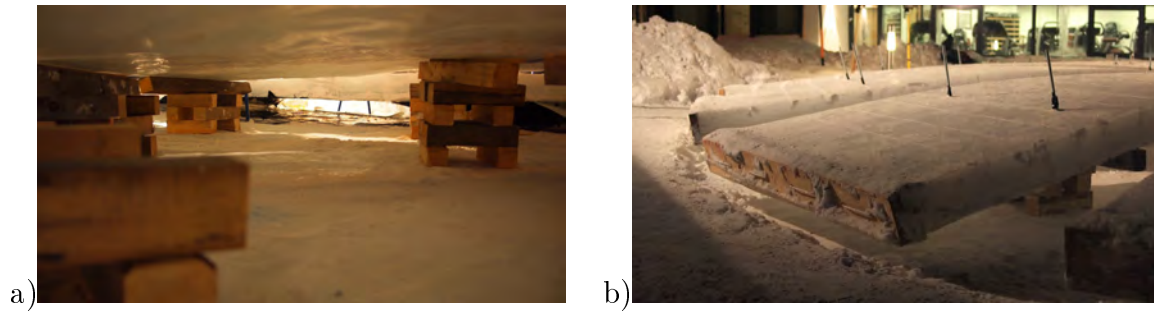


Figure 10.31: Ice segments after lifting a) positioned on the stacks of wood b) ends of the ice segments without support

beams with different lengths were put on top of each other in order to gain the desired height. The dimensions of the squared timber used is shown in appendix B.2. Timber was chosen as construction material because in this particular region of Austria where the ice shell was built, wood is easily and cheaply available.

#### 10.4.2.4 Initial deformation

Measurements of the deflection of the ice segments were taken immediately after they had been put on the stacks of wood as well as during the creeping process. The diagram in Figure 10.32 compares actual deformations with analytically and numerically predicted ones. The values shown in this figure relate to the middle axis of the ice segment.

As shown in Figure 10.30, the two stacks of wood did not have the same height. The stack of wood 1 – as labeled in Figure 10.30 – amounted to  $500\text{ mm}$ , consisting of five layers of squared timber, whereas the other woodpile only had a height of  $400\text{ mm}$  composed of four layers of timber beams. This design was chosen in order to gain the desired final deflection of the ice beam. The position of the woodpiles was chosen in order to create the same bending moments per width above both line supports. This requirement leads to different cantilevers on the thinner and wider end of the ice beam. Because of the fact that the thinner end part of the ice segment had a larger cantilever, it was also going to experience larger deformations than the wider end part. The final shape of the ice segment is reached when both ends touch the ground due to deflection. To create the necessary conditions so that both ends of the segment reach the subsoil after a similar long period of time, their initial starting positions have to differ in height.

The vertical and the horizontal axis in Figure 10.32 refers to the coordinate system plotted in Figure 10.30. The horizontal axis  $x$  represents the projected longitudinal axis of the ice beam. The vertical axis  $y$  shows the deflection in vertical direction with its origin at the same height as the middle axis of the ice segment in the area of woodpile 1. The positive direction of the  $y$ -axis points downwards. To be able to plot deformations of the ice segment in the diagram in Figure 10.32 clearly, the deflections are vertically oversized. For orientation, the positions of the two stacks of wood are

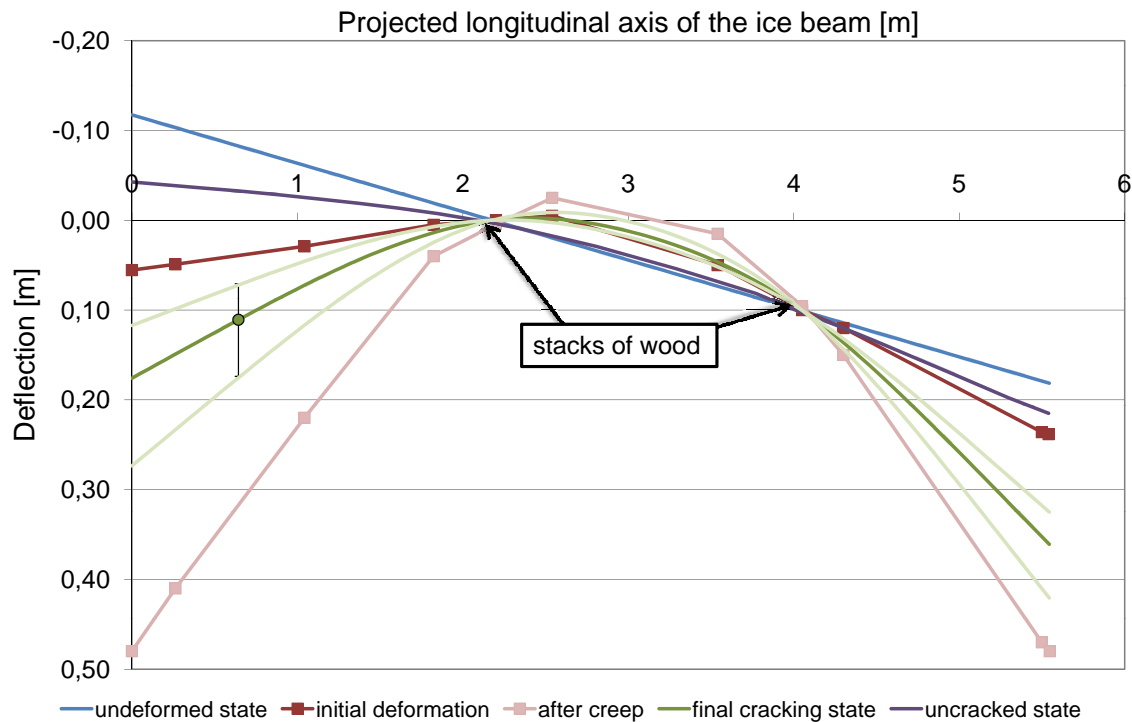


Figure 10.32: Measured and calculated deformations

marked in the diagram. The blue line shows the undeformed state of the ice segment, which is of course only theoretical because deflections always occur.

The red line shows the mean values of the initial deformation of the ice segments directly after being placed on the woodpiles. Nine points were measured represented by the data markers in the red line. The data markers are connected with linear lines in order to give an impression of the shape of the ice segments. By comparison, the light red line shows the deformation after the creeping process. Again, only the data markers represent measurement data. If the deflection curve reaches the  $500\text{ mm}$  mark, the bottom of the cross section of the end parts touches the defined working surface. Therefore it can be observed that the thinner part of the segments had to bend down approximately  $450\text{ mm}$ , additional to the initial deformation in order to reach the final shape. The wider end part of the ice had to lower itself another  $380\text{ mm}$  after experiencing the initial deformation.

The green lines show the calculated deformation of the beam under the assumption that the whole cross section is in the final cracking state and the tension stiffening effect due to the participation of the ice between the cracks is neglected. Therefore, in this theoretical calculation only the compression zone of the ice and the cross section of the steel reinforcement have an influence on the moment of inertia. In the final cracking state the cuts do not have any influence on the deformation because they are only in the tension zone, which is not conducive to the resistance of the cross section anyway. The dark green line shows the deformation calculated with a Young's Modulus of  $400\text{ N/mm}^2$ . The two light green lines surrounding the dark green one,

show the same deformations with the exception that the modulus of elasticity is set to  $300 \text{ N/mm}^2$  and  $500 \text{ N/mm}^2$ , respectively.

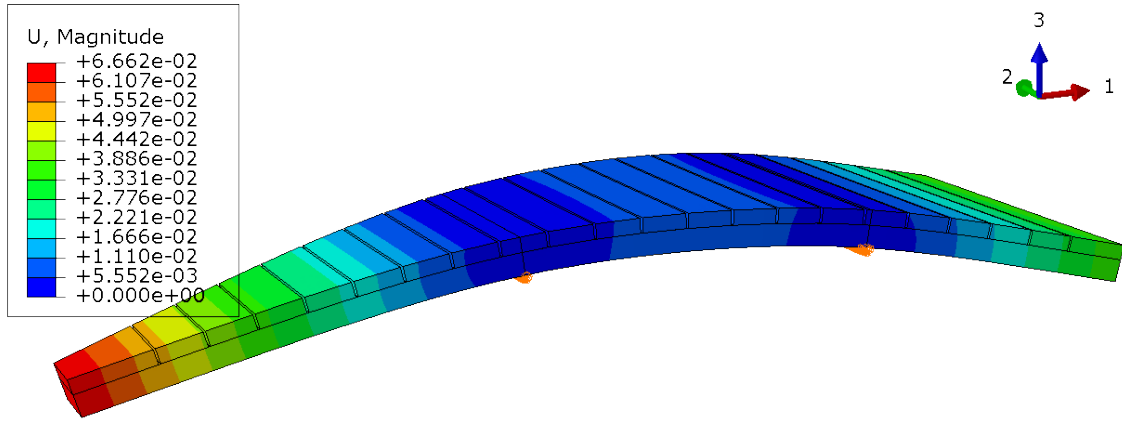


Figure 10.33: Initial deformation of the ice segment [m]

The purple line shows the theoretical deformation of an uncracked ice segment considering the cuts. For the calculating of these deformations a 3D finite element model was created using the FE-program *ABAQUS* [14]. The cuts were modeled on their respective position with a depth of  $80 \text{ mm}$  and a width of  $10 \text{ mm}$ . The mass density was set to  $900 \text{ kg/m}^3$  and the Young's modulus to  $400 \text{ N/mm}^2$ . As boundary conditions, line supports on the location of the stacks of wood were chosen and the segment was loaded only with self weight. A linear elastic finite element analysis was carried out using this input. The resulting deformations are shown in Figure 10.33 where the different heights of the woodpiles are also taken into account.

These two calculated deformations represent limit values. If no cracks appeared at all, the shape of the ice segment would be in accordance to the purple line. Because of the high stresses and the usage of the cracking pliers, however, cracks can certainly be assumed. The other limit is shown in the green line. If the whole cross section was in the final cracking state and the ice in the tension zone had no impact on the stiffness, the deformation would be as shown in the green line. The actual initial deformation – the red line – is in between those two limits.

#### 10.4.2.5 Stresses in the ice segment

Figure 10.34 compares the occurring bending moment per width during the lifting process of the ice beam with the lifting device as well as laying them on the stacks of wood. This diagram shows that the moments during the lifting with the lifting device are only 60 % of the maximal moments during the creeping process. Due to the fact that higher maximal stresses develop during the creeping process than during the lifting process, only this load case is analyzed in detail. Moreover, in the diagram of Figure 10.34 the moments per width, which were experienced by the ice segments in winter 2009/10 when using the segment lift method with pneumatic formwork, are also depicted. It can be seen that in winter 2009/10 even higher loads had been applied

to the ice segments during the creeping without causing damage to the ice during this construction phase.

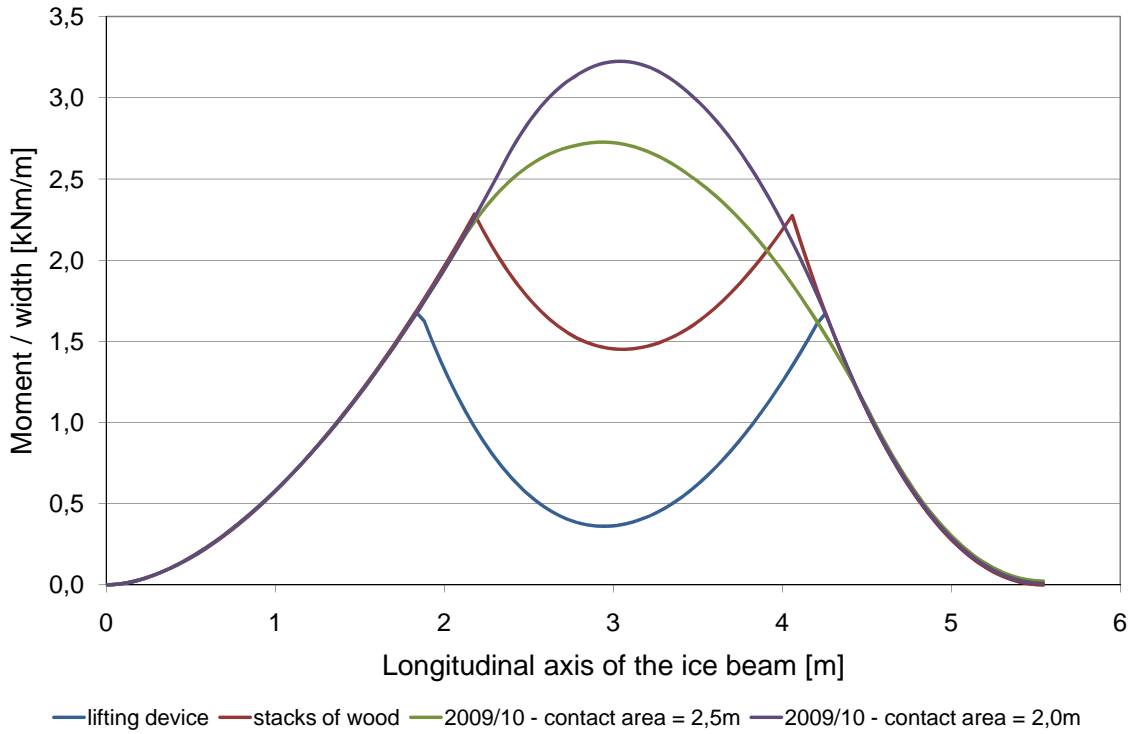
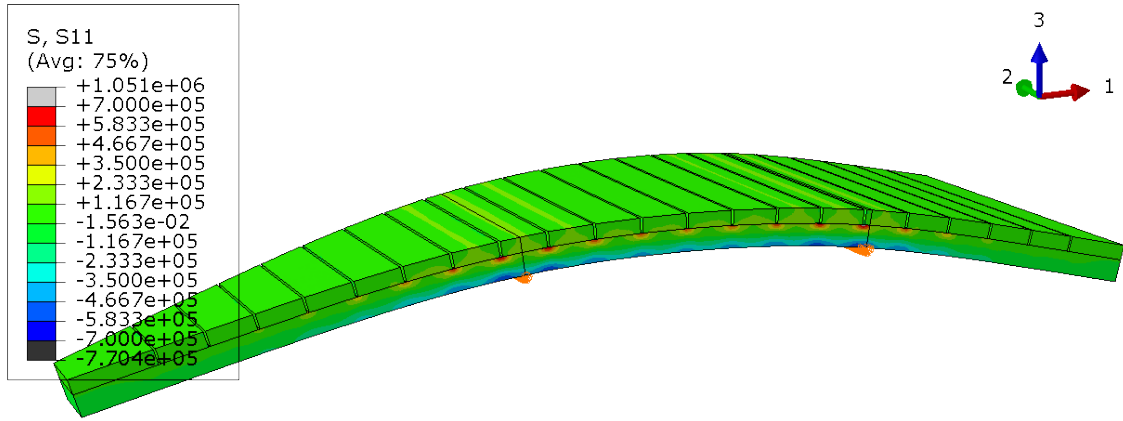
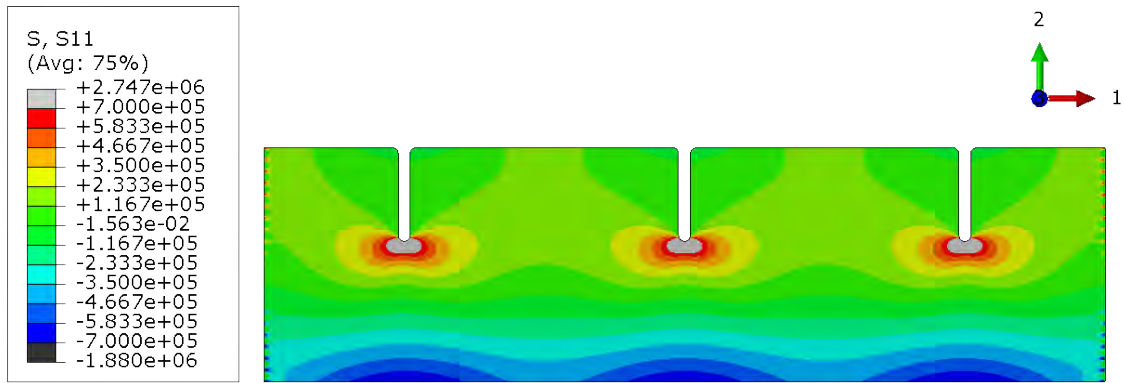


Figure 10.34: Moments per width in the ice segment

As already mentioned before, the maximal stresses in the ice regarding the whole construction process occur during the creeping process. Therefore the stresses in this state are examined more closely. For this purpose, a finite element analysis was carried out with the FE-program *ABAQUS* [14]. The same model with identical properties as described in chapter 10.4.2.4 was used. In Figure 10.35 the normal stresses  $S_{11}$  in  $N/m^2$ , which act in the direction of the longitudinal axis of the ice segment, are depicted. This model is three dimensional and with an approximate global size of the meshes of  $0,02\text{ m}$ . This simulation shows the overall distribution of the stresses over the entire ice segment. Obviously, the highest stresses occur in the areas of the supports, where the highest bending moments arise and the influence of the cuts is visible. The highest tensile stresses appear on the bottom of the cuts.

In order to study the effect of the cuts more closely, a second finite element model was created. This model is only two dimensional and shows the part of the ice segment with the highest stresses. In Figure 10.36 the normal stresses  $S_{11}$  in  $N/m^2$  of this model are depicted. Like in the three dimensional model, the axis 1 represents the direction of the longitudinal axis of the ice segment. In this model, the loading is chosen in order to reproduce the stresses occurring due to the maximal bending moment. An important difference between these two models is the density of the mesh. In the two dimensional model the approximate global size is set to  $0,001\text{ m}$ , which makes the mesh 400 times denser.

Figure 10.35: Normal stresses  $S_{11}$  in  $N/m^2$ Figure 10.36: Normal stresses  $S_{11}$  in  $N/m^2$ 

This model illustrates that a peak occurs in the area of the cuts. The absolute value of these maximal stresses, however, cannot be detected by this linear elastic model. If more information about the actual stresses is required, a non-linear calculation with a suitable non-linear material model has to be carried out and more detailed information about the exact geometry of the bottom of the cut would be necessary. Due to the fact that the properties of the ice are subject to high variations and the exact dimensions of the bottom of the cut are unknown, even a more detailed and improved model would not provide the precise distribution of the real stresses.

Considering the results gained from this model, it can be observed, that in the area of the cuts high stresses occur which will finally lead to cracks and plasticizing of the material in this area. Moreover, it can be seen that in the middle areas between two cuts, the entire cross section takes part in the load transfer. But, due to the fact that the cuts are quite close to each other, there is no equal distribution of the stresses over the entire height of the cross section.

Assuming that the whole ice segment had a uniform thickness of  $200\text{ mm}$ , the tensile stresses on the top and the compressive stresses on the bottom would amount to the

same absolute value;  $0,3 \text{ N/mm}^2$ . According to the stress distribution shown in Figure 10.36, the tensile stress in the very middle between two cracks amounts only to  $0,16 \text{ N/mm}^2$  whereas the compressive stress on the bottom of the same cross section reaches  $0,43 \text{ N/mm}^2$ . In a cross section of a cut, the compressive stresses as well as the tensile stresses are significantly higher due to the smaller height and the abruptly changing cross section.

Analytical solutions of similar problems are discussed by Girkmann [28]. He shows an example of an infinite panel with a circular hole. This panel is loaded with uniaxial uniformly distributed tensile stresses. Girkmann demonstrates that in this case the maximal normal stresses are three times higher than the stresses in a panel without a hole. Although the geometrical and static boundary conditions in this example are not identical with the ones in the ice segment, it can be assumed that the stresses on the bottom of the cut are considerably higher than the ones in the remaining areas of the ice segment.

#### 10.4.2.6 Creep behavior of the ice segments

As soon as an ice segment is placed on the stacks of wood, the creeping process starts. Due to the lifting method the segments are lifted one after the other. Therefore, the

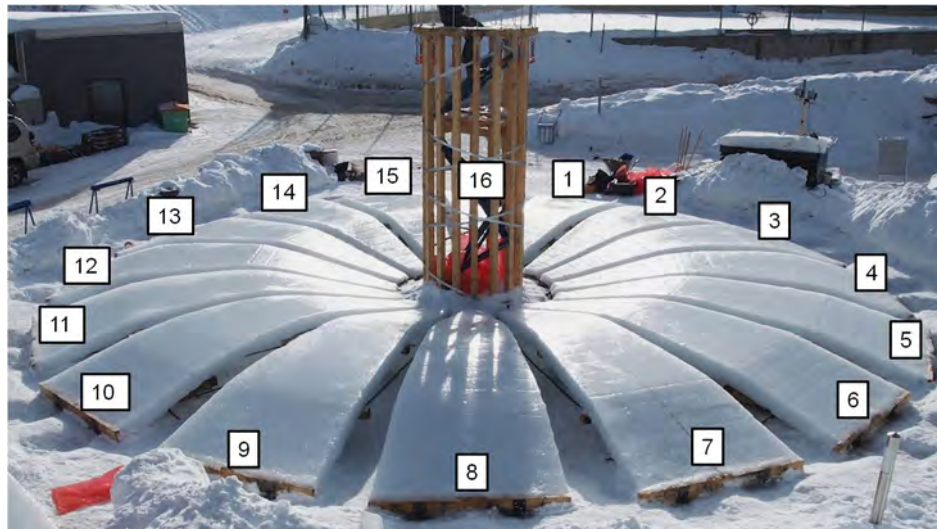


Figure 10.37: Creeping process of the ice segments

start of the creeping process cannot be determined to one single generally valid point of time for all the segments - each segment has its own starting time. To be able to compare the creep behavior, on the horizontal axis of the diagram in Figure 10.38, the age of the segments is depicted. The age stands for the time period between the starting of the creeping process and the respective measurement, i.e. two measurements which were both taken at the same age of two different ice segments, could be accomplished even on different days. The vertical axis shows the rise of the ice segments as defined in Figure 8.2 in chapter 8.3.1. With a small angle between the vertical and the rise, which is by definition perpendicular to the tension tie, the following approximation

holds:  $\cos \alpha = 1$ . The diagram in Figure 10.38 shows the development of the rise of all

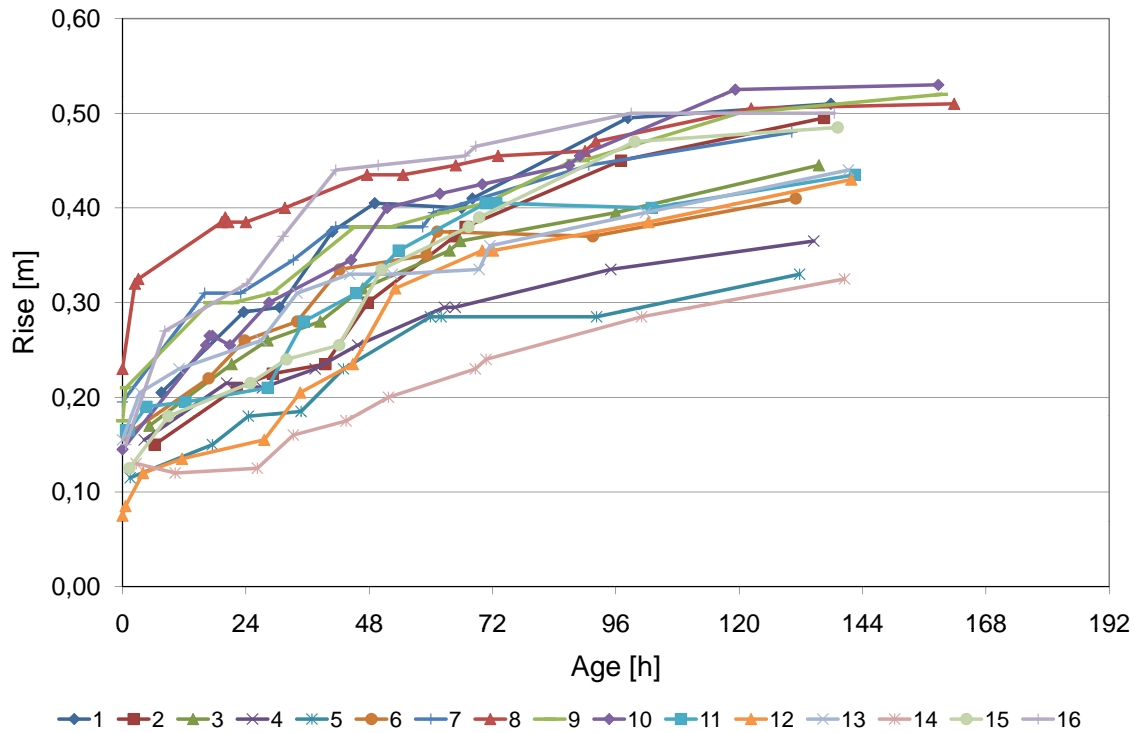


Figure 10.38: Development of the rise with age of all sixteen segments

sixteen segments during their first days of creeping. The numbers of the segments is according to Figure 10.37. It can be seen that the variation of the deflection is quite high. Some segments already have higher initial deflections due to many different influencing factors. First of all, the numbers of cracks is different in every segment, which has a high impact on the deformation. Also the location of the stacks of wood may differ a few centimeters. Moreover, the ice segments were lifted under different



Figure 10.39: Creeping process of the ice segments

environmental conditions, like temperature and sun radiation, which influences the Young's modulus and subsequently the deformation. Additionally the ice segments are not identical, as they were made under site conditions. Their crystalline structure varies due to the different conditions during the ice making process. The thickness and



the length of the ice segments have a range of tolerance of  $\pm 10\text{ mm}$  and the natural inhomogeneity of the material ice may not be underestimated.

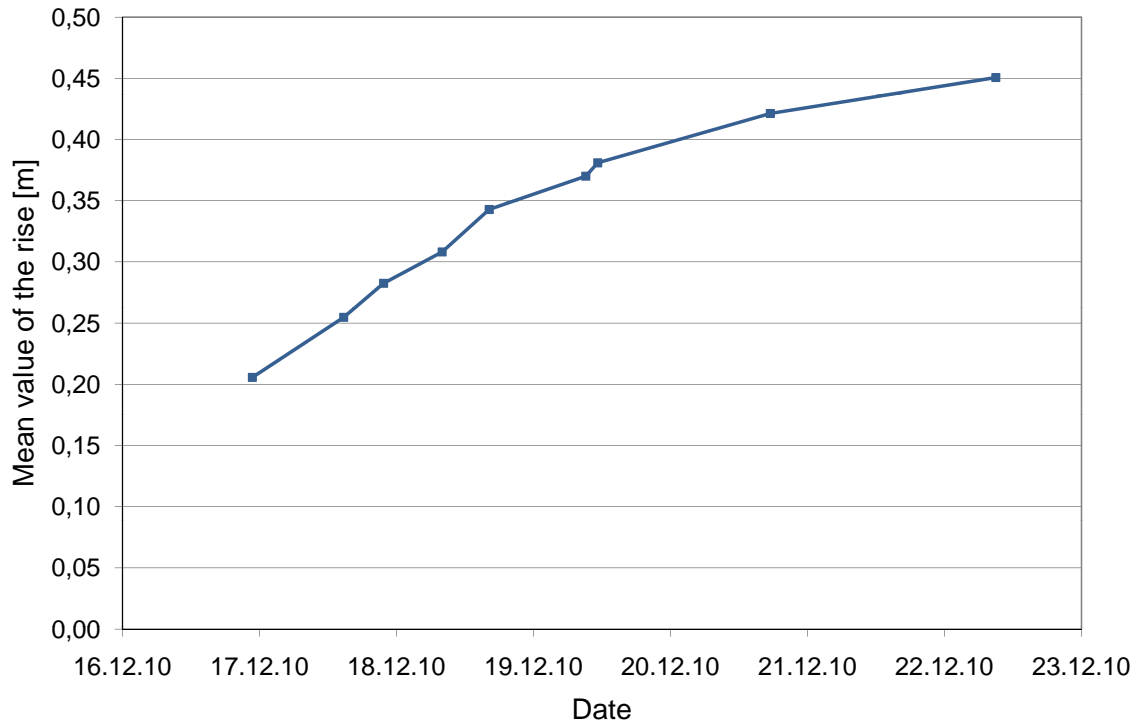
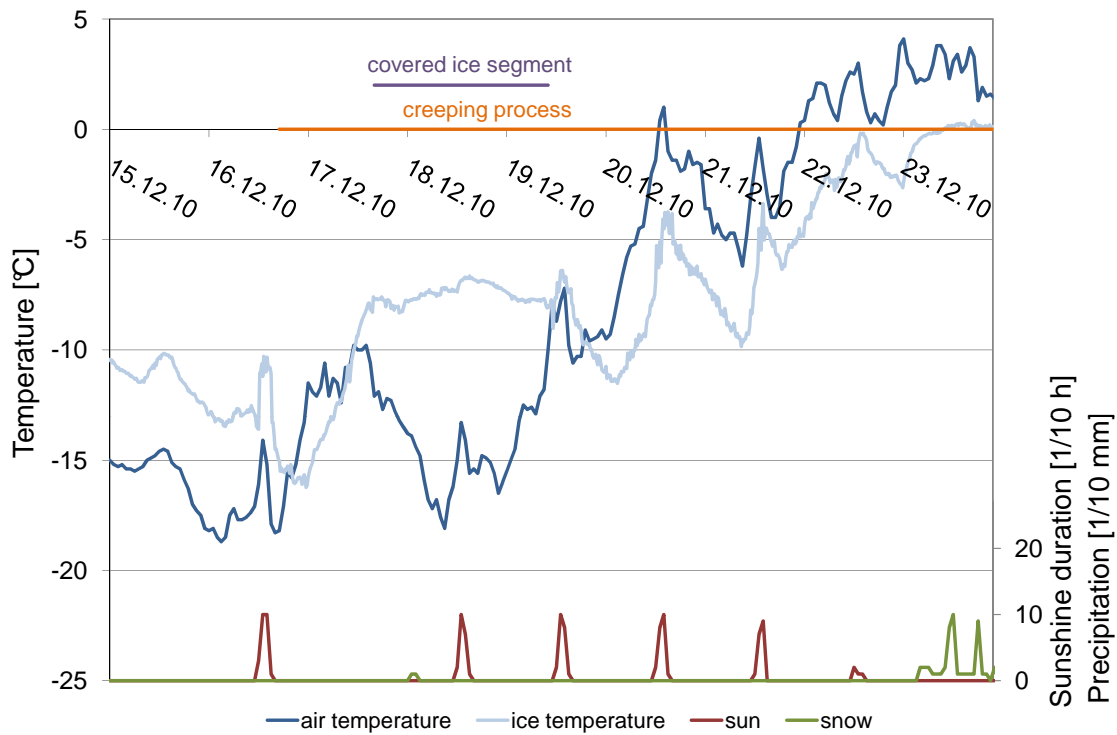


Figure 10.40: Mean value of the rise

Figure 10.40 shows the arithmetic mean of all rises at a certain time. This measurement started on the 16<sup>th</sup> of December 2010 at 10 *pm*. At this time the ice segments had experienced creep between 0 and 30 hours. These values are available until the 22<sup>nd</sup> of December 2010 at 9 *am*. During this time period the air temperature was quite low as shown in Figure 10.41.

Figure 10.41 not only shows the air temperature (dark blue line, [1]) but also the temperature in the ice. The ice temperature was measured every 15 *min* on four different positions. The mean value is depicted in Figure 10.41. It can be seen that the change of the ice temperature is quite inert compared to the air temperature. In order to accelerate the creeping process of the ice, it was tried to increase the temperature in the ice. For this purpose, the ice segments were covered with silage foil and warm air with a temperature of approximately 15°C was blown under the ice segments. The result of this action can be identified in Figure 10.41. Between the 17<sup>th</sup> and the 19<sup>th</sup> of December 2010 the air temperature was approximately −15°C, the temperature in the ice, however, never dropped below −8°C.

On the 22<sup>nd</sup> of December 2010, after the creeping process of the ice segment had taken place for 130 to 160 hours under extremely unfavorable conditions concerning the creep behavior, the shapes of the ice segments were measured and can be seen in Figure 10.42. The axes of this figure are identical to the ones in Figure 10.32. This measurement

Figure 10.41: Climate data from 15<sup>th</sup> to 23<sup>rd</sup> December 2010

showed that the deformations of some of the segments were still quite low and therefore the experiment could not be finished before the Christmas holidays.

Figure 10.43 shows the deflections measured on the 11<sup>th</sup> of January 2011. At this time, all the end parts of the ice segments already touched the ground. Unfortunately, the specific point of time when all segments reached their desired shape could not be determined because no measurements were taken during the Christmas break. But a visual inspection on the 2<sup>nd</sup> of January 2011 showed that already at that time both ends of each segment touched the ground.

Even though both end parts of all sixteen segments had reached the ground, the deflections depicted in Figure 10.43 do not always equal  $0,5\text{ m}$ . This phenomenon can be explained by the fact that the stacks of wood had sunk into the subsoil which consisted of compressed snow. Because of the long term and concentrated loading the squared timber beams were pressed a few centimeters into the ground.

The temperature in the ice was also measured while the experiment was on hiatus. In Figure 10.44 these measurements are compared to the climate data provided by the ZAMG [1]. On the 23<sup>rd</sup> of December 2010 heavy snowfall covered the ice segments with a layer of approximately  $120\text{ mm}$  of snow. This snow blanket practically acts as an insulation. The temperature in the ice during the following days stayed quite constant compared to the air temperature. On the 9<sup>th</sup> of January 2011, the snow was removed from the ice segments. Afterwards, the temperature in the ice responded more sensitively to the changing environmental conditions.

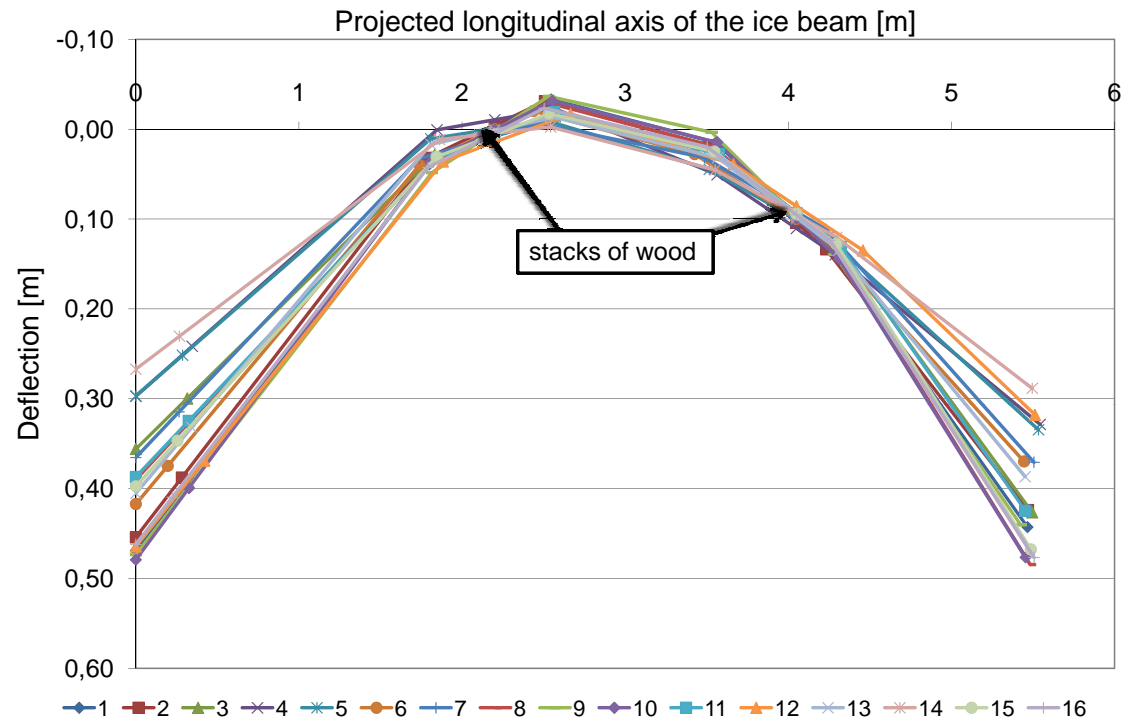


Figure 10.42: Deformation measured on the 22<sup>nd</sup> of December 2010

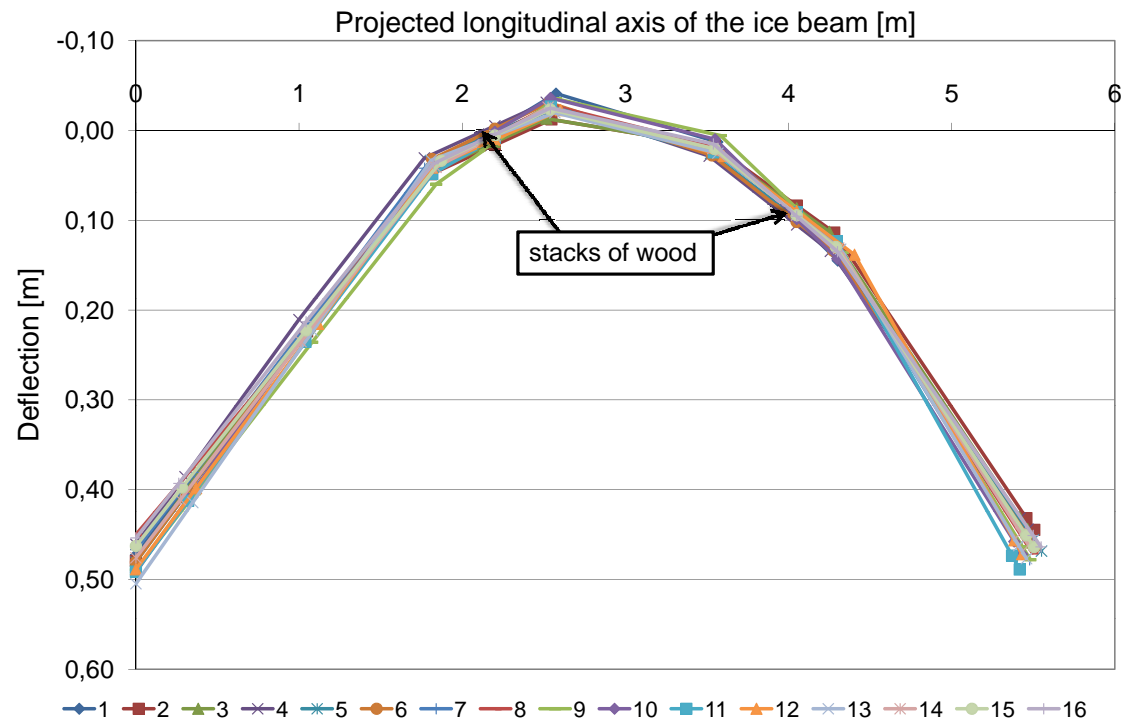


Figure 10.43: Deformation measured on the 11<sup>th</sup> of January 2011

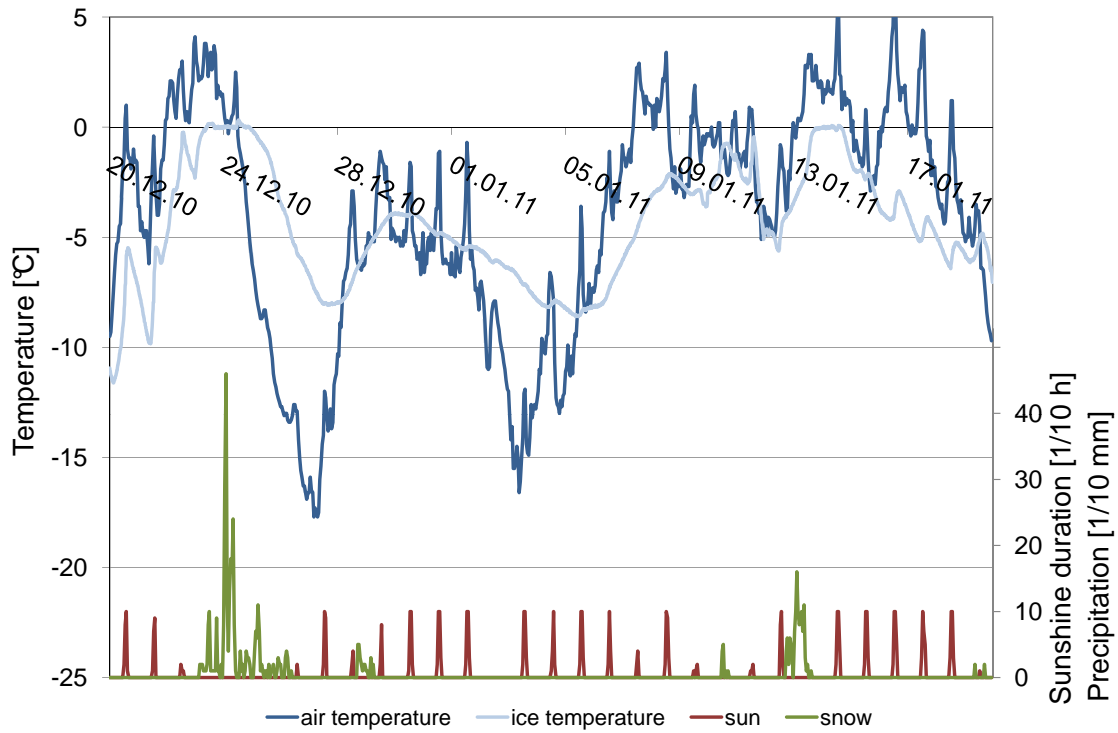


Figure 10.44: Climate data from 20<sup>th</sup> December 2010 to 17<sup>th</sup> January 2011

## 10.5 Lifting the ice segments

### 10.5.1 The mounting tower

By using the segment lift method, every ice segment is lifted individually. Only if all ice segments are in their final position, the individual ice beams can be joined together to form a shell structure, which can carry the load mainly through normal forces in meridian and hoop direction. As the segments are lifted one after the other, they have to be fixed to an auxiliary construction, until all segments have reached their final position. No special requirements are necessary for this auxiliary construction as long as it can carry the self weight of the ice segments during this construction phase.

A mounting tower made of wood was used in the field experiments. Timber was chosen due to its good availability. The schematic 3D drawing in Figure 10.45 shows the main elements of this mounting tower. The wooden columns as well as the horizontal beams are made of glued laminated timber beams with a cross section of  $100 \times 100 \text{ mm}$ . To prevent the columns from buckling, steel diagonals, wooden cross beams and bracing straps act as strengthening for the wooden tower.

In order to connect the horizontal beams with each other and to enable the tower to carry a certain horizontal force, inner and outer steel rings are reinforcing the top of the tower. Each of the sixteen horizontal beams is equipped with a *mounting bracket*, which was designed to connect the ice segments to the wooden tower. More detailed

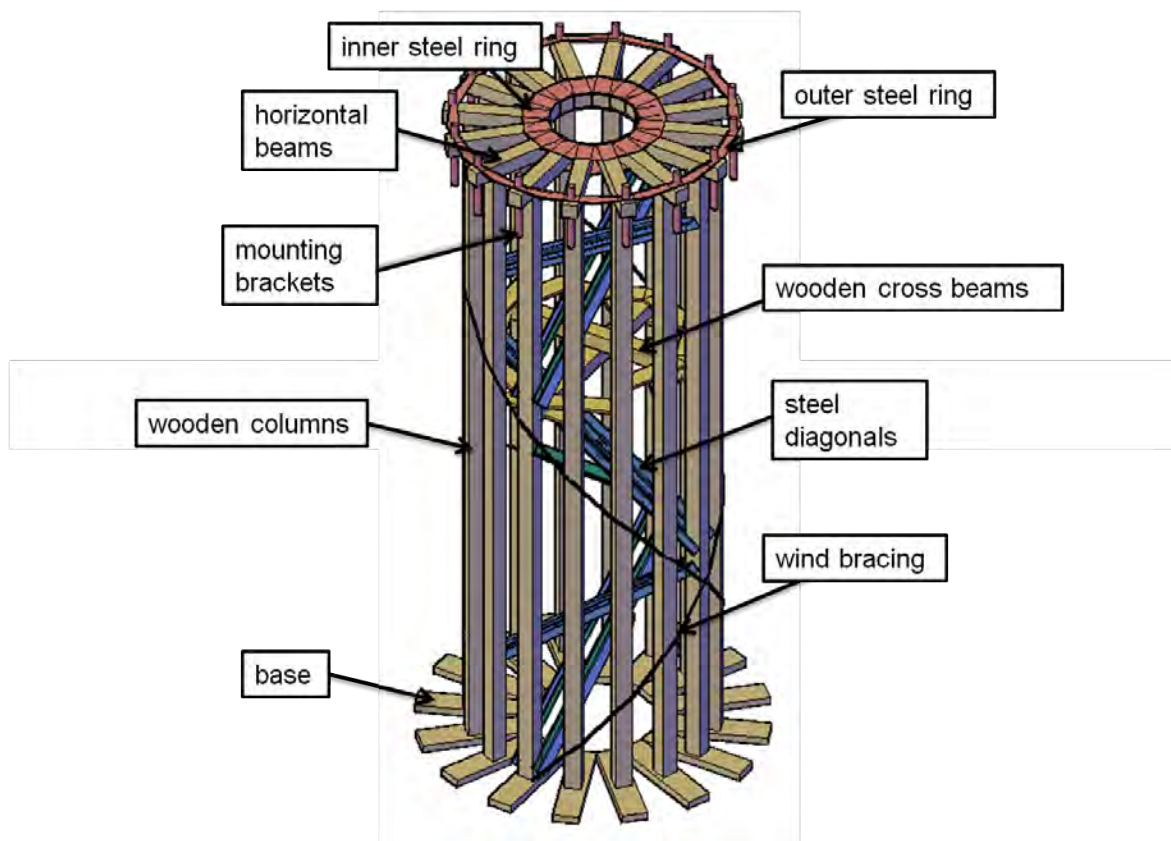


Figure 10.45: Schematic drawing of the mounting tower

drawings as well as the main dimensions of the mounting tower can be found in the appendix B.3.

The building of the mounting tower was done simultaneously to other working procedures. For example, the wooden boards which were used as a base for the tower were placed while preparing the working surface. The majority of the mounting tower was built simultaneously to producing the ice plate whenever idle time existed. Figure 10.46 shows three pictures of the assembly of the mounting tower.

## 10.5.2 Preparing the ice segments for the lifting process

### 10.5.2.1 Compression arch with tension tie

During the lifting process the static system of a compression arch with a tension tie is chosen, as already described in chapter 8.3.1. In Figure 8.2 in chapter 8.3.1 a schematic drawing shows this principle. In Figure 10.47, however, it is shown how this compression arch – tension tie – system is adopted for the ice segments. The distorted ice segment functions as compression arch and two steel chains take the part of the tension tie.

As the ice segments already are in their final shape as little further deflection as possible is desired. Therefore, the cuts which weaken the cross section and promote the

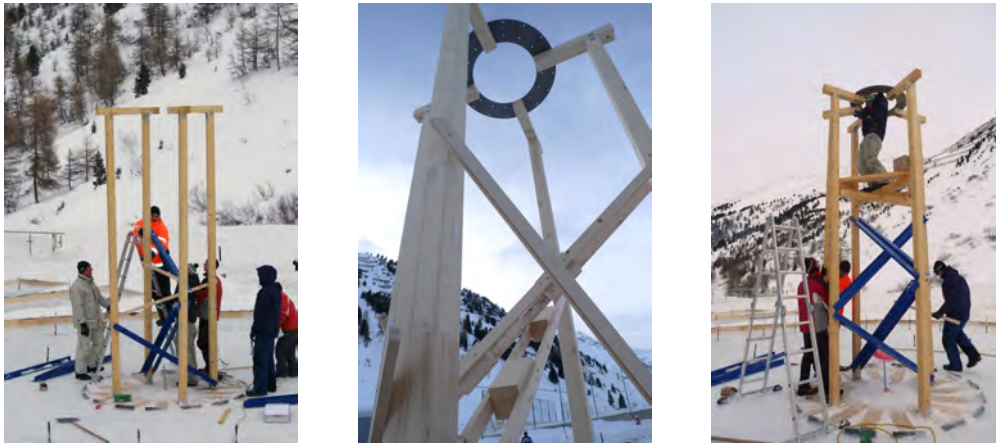


Figure 10.46: Building the wooden mounting tower

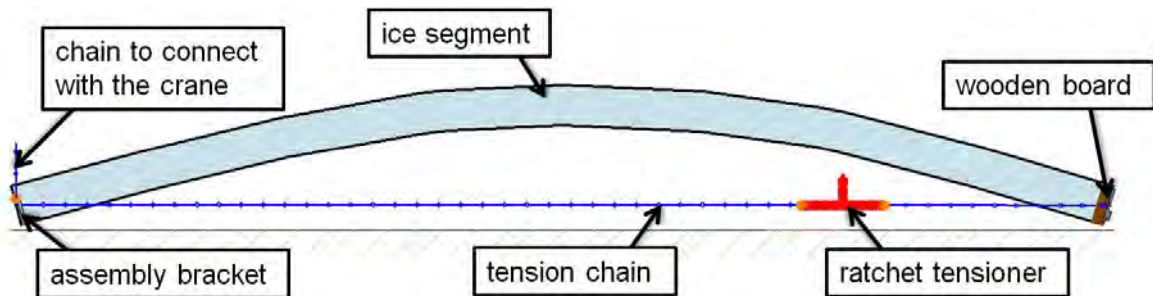


Figure 10.47: Compression arch with tension chain

distortion were closed again. These gaps were filled with small layers of water which would freeze to ice. Thus, again, the cross section of the ice segment had a uniform and continuous thickness of  $200\text{ mm}$  along the entire longitudinal axis.

In order to be able to tighten the chains, a ratchet tensioner is integrated in each chain. Figure 10.48 shows how the chains are anchored to the ice segment. At the smaller end point *A*, the chain runs in a loop through the assembly bracket. When designing the assembly brackets, it was made sure that these brackets were stiff enough to equally distribute the load coming from the chain in order to avoid loading the ice with a concentrated force. On the wider end part *B* of the ice segment, two holes have been drilled through the ice segment in order to pull the chains through and anchor them against the wooden board. In Figure 10.48 the anchorage plate fixed to the wooden board is shown. Moreover, Figure 10.49 shows additional pictures of the chains and the ratchet tensioner.

#### 10.5.2.2 Properties of the chains

The chains as well as the ratchet tensioner and all connecting links are produced by the international company *pewag*. Chains from the product line WINNER 400 with the code *WIN 7 400* which have a breaking force of  $77\text{ kN}$  were used.

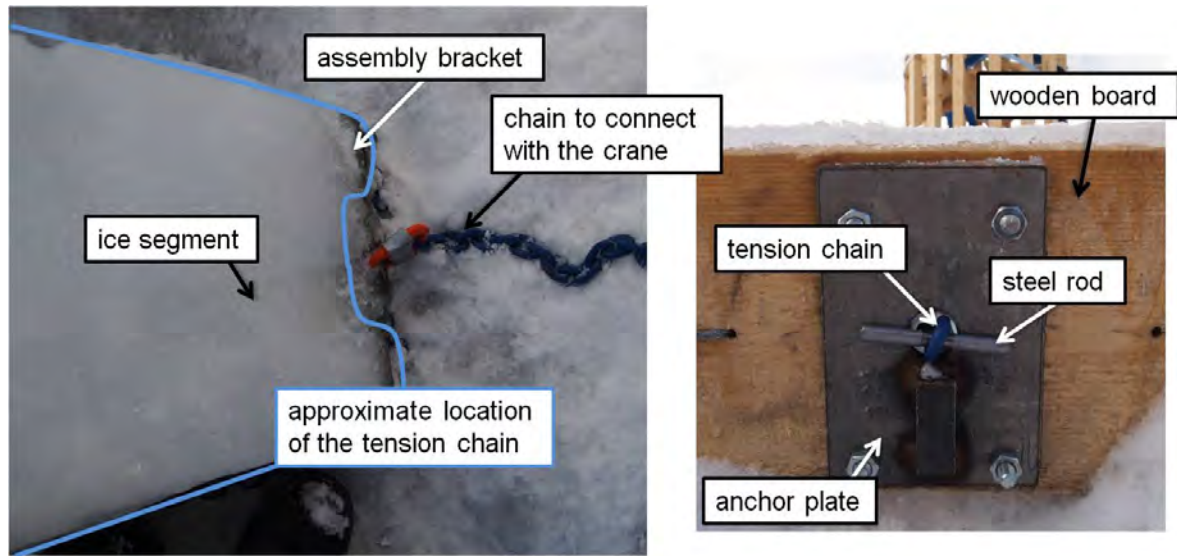


Figure 10.48: Connection between the tension chain and the ice segment



Figure 10.49: Tension chains

Due to the fact that the arch-tension tie assembly is a system that is statically indeterminate even though its reactions are determinate - the stiffness of the individual members is very important. Therefore, the extensional stiffness  $EA$  was experimentally determined. For this purpose, an approximately  $1\text{ m}$  long piece of chain was tested in a displacement controlled tensile test by means of a testing machine in the laboratory of the Institute for Structural Engineering. The measured forces and strains are depicted in Figure 10.50. The force was increased until a load of approximately  $55\text{ kN}$  was reached. This load step, however, lies below the breaking load, therefore the chain did not collapse. Due to the fact that the purpose of this experiment was to find out the extensional stiffness of the chain, failure was not intended. As described in chapter 10.5.4, the load range which is being experienced by one chain does not exceed  $10\text{ kN}$ . Therefore, in order to calculate the extensional stiffness of the chain, only the area between  $2\text{ kN}$  and  $12\text{ kN}$  is taken into account. In this area, the strain increases from  $0,0011$  to  $0,0055$ . In equation 10.1 the extensional stiffness  $EA$  is calculated.

$$EA = \frac{\Delta F}{\Delta \varepsilon} = 2273\text{ kN} \quad (10.1)$$



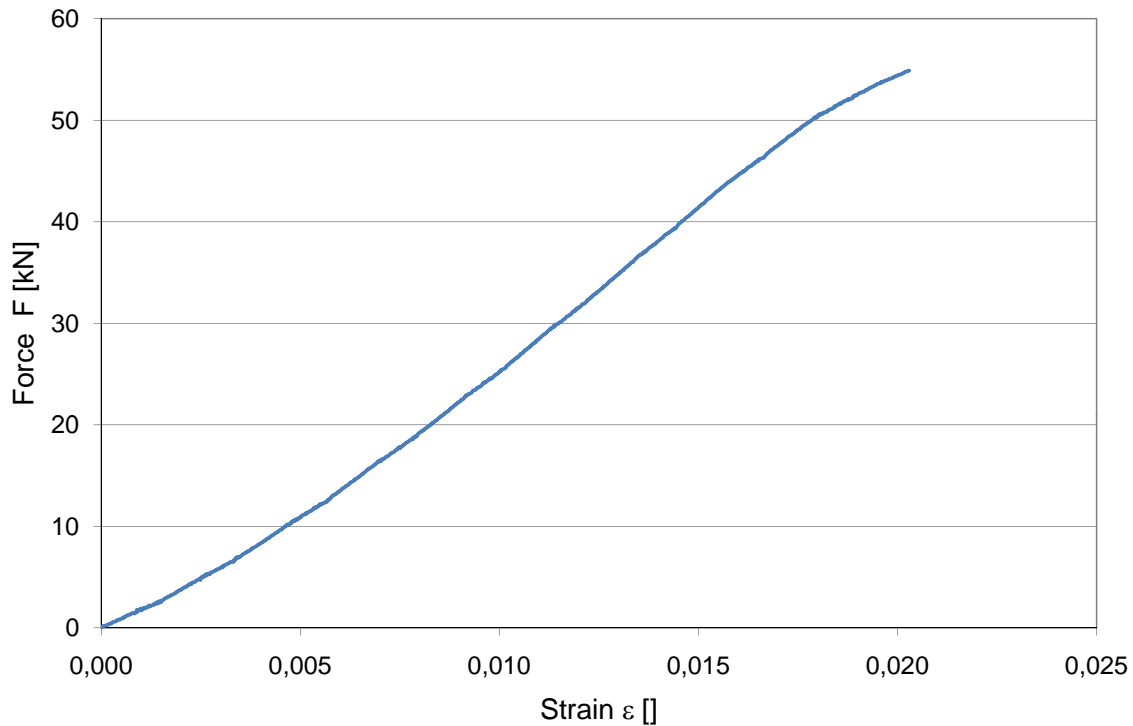


Figure 10.50: Force - strain diagram of the chain

### 10.5.2.3 Problems with the assembly of the chains in winter 2009/10

When testing the segment lift method with pneumatic formwork the assembly of the chains turned out to be problematic due to the pneumatic formwork. The chains were to be pulled through between the inflated pneumatic formwork and the ground by means of ropes which had been placed underneath the membrane before-hand. Due to the air pressure in the pneumatic formwork it was not possible to move the steel chains with a diameter of approximately  $20\text{ mm}$  underneath the inflated membrane by hand. Therefore the air pressure in the membrane was reduced while part of the weight of the segments was supported by stacks of wood, which had been placed under the ice before. In Figure 10.21 the decrease of the air pressure can be seen. At an air pressure of approximately  $31\text{ mbar}$  it was possible to pull through the chains underneath the pneumatic formwork. This was done in the area between the segments.

In Figure 10.51 the brown line shows the location of the chain after it had been pulled through. While the air pressure was reduced it was tried to guide the chains into their defined position. At this point, the chains could only be pulled by hand because the ratchet tensioner had not been installed yet. Due to the fact that the air pressure was still quite high it was not possible to straighten the chains under the segments. The blue line in Figure 10.51 shows the assumed position of the chain while assembling the ratchet tensioner. As soon as all chains had been pulled through, the air pressure was increased again. Before the ratchet tensioner had been installed, it was not possible to tighten the chains permanently, therefore at this point the chain was lying on the ground, clenched between the pneumatic formwork and the ground.

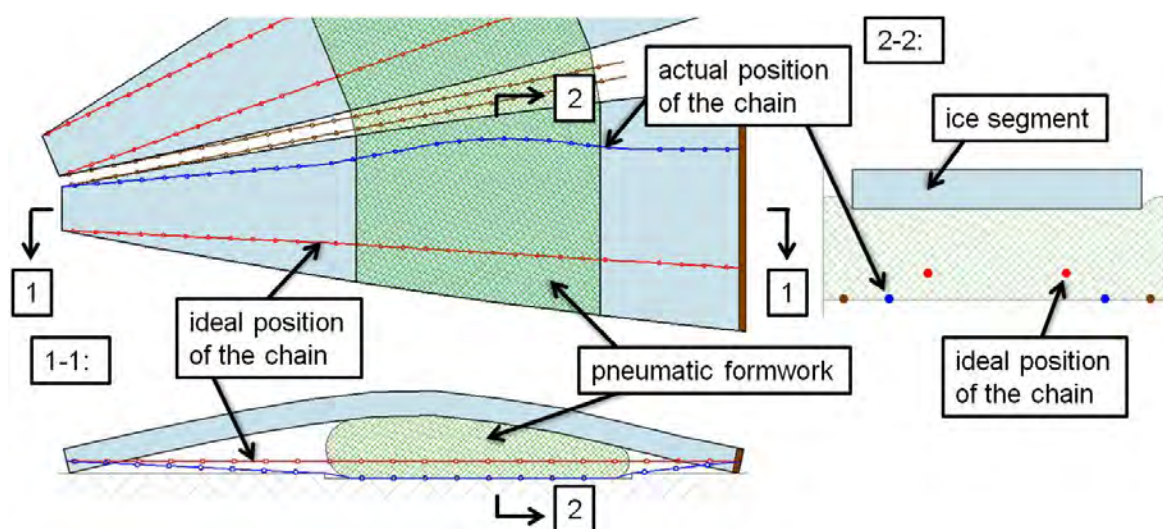


Figure 10.51: Position of the chain

In section view 1-1 in Figure 10.51, the assumed position of the chain in the vertical direction is shown with the blue line. The red line in the same figure shows the ideal position of the chain. As soon as the ratchet tensioners had been installed, they were used to tighten the chains. A tension force of approximately  $1\text{ kN}$  was introduced to each chain.

The night before the lifting and assembling procedure was to take place, problems with the pneumatic formwork occurred. The connection piece between the air hose and the pneumatic formwork broke and the air pressure decreased rapidly. Although the chains had already been tightened with the ratchet tensioner, the self weight of most ice segments could not be carried by means of a compression arch and a tension tie. When the air pressure decreased, eleven of the sixteen segments collapsed. The ice segment was supposed to carry the load by means of a compression arch and a tension tie. The chains, however, can only serve their purpose when they are totally straight and tightened. As long as the chains are loose, the end parts of the ice segments move apart until the chains are tightened.

This horizontal displacement of the supports is a very unfavorable load case for the ice segment. Figure 10.52 shows the impact on the ice segments due to an imposed horizontal support displacement. On the horizontal axis the displacement of the support is depicted. The blue and the red line show the maximum compressive and tensile stresses in the ice after the superposition of the stresses due to self weight and due to the load case *imposed support displacement*. It can be seen that the stresses in the ice increase rapidly due to the displacement of the supports. The green line in Figure 10.52 refers to the secondary vertical axis which shows the reduction of the rise. By moving apart the two end parts of an ice segment the size of the rise inevitably decreases and the radius of curvature increases simultaneously. If the ice segment has a rise of  $500\text{ mm}$ , the radius of curvature amounts to  $7,6\text{ m}$ . With a rise of  $430\text{ mm}$  or  $360\text{ mm}$ , the radius increases to  $8,4\text{ m}$  and  $10,7\text{ m}$ , respectively. Obviously most of the ice segments were not able to carry these stresses caused by the change of geometry.

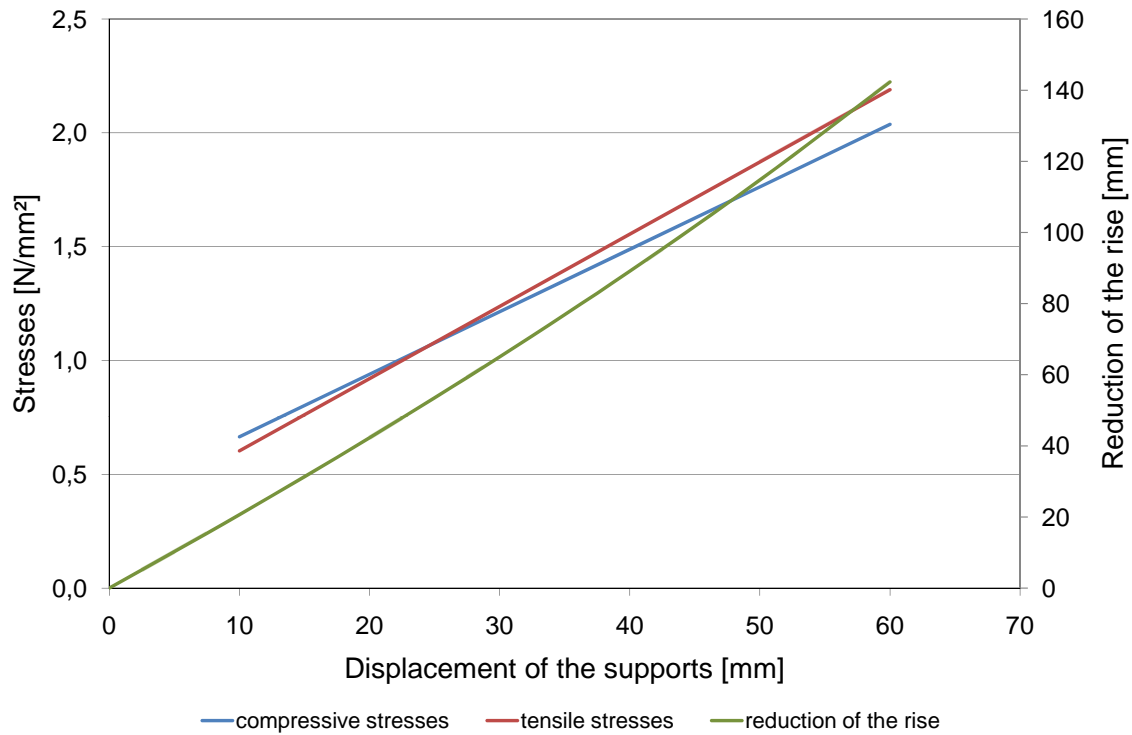


Figure 10.52: Impact on the ice segments due to an imposed horizontal support displacement

The following calculation intends to give an impression of the amount of force necessary to force the chains into their ideal position when pushing against the air pressure. The following model is strongly simplified and many assumptions are made. Nevertheless, it can be shown that a great amount of tension force in the tension chain is necessary in order to approach the ideal position of the chain.

The tension in the chain, however, cannot be increased arbitrarily because the chains are anchored to the ice segments which have to be able to carry this anchorage force. Before the tension ties were tightened, the cut on the top of the ice segments had been closed. Therefore the entire cross section had a height of  $200\text{ mm}$ . According to the diagram in Figure 10.14, the maximum tensile stress due to dead load of the ice segment while resting on the pneumatic formwork amounts to approximately  $0,5\text{ N/mm}^2$ . If the chain is stressed with a tension of  $1\text{ kN}$ , this anchorage force gives rise to an additional tensile stress of almost  $0,1\text{ N/mm}^2$  on the top of the ice segment. In order to prevent the ice from collapsing while stressing the chains, the combined tension in the pair of chains of each ice segment must not exceed  $2\text{ kN}$  or  $3\text{ kN}$ .

In the following simulation, the force in the chain, which is necessary to lift the chain in the vertical direction, is determined. Figure 10.53 shows the simplified static system derived from the sectional view of a segment. One position of the chain is considered, shown by the black line. In the center area of the pneumatic formwork the chain is still lying on the ground and on the edge of the formwork the middle axis of the chain has a distance of  $60\text{ mm}$  from the ground.

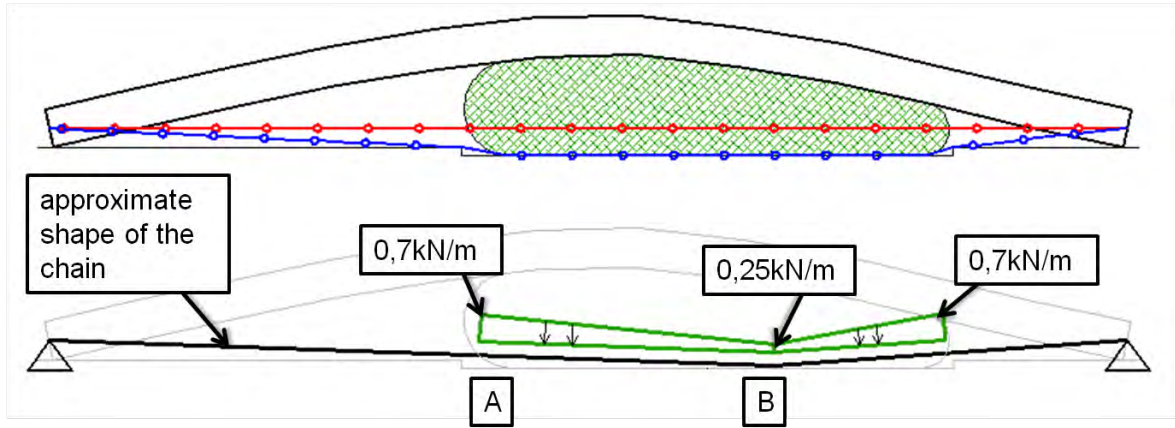


Figure 10.53: Simplified static system of chain subjected to line load

The chain is loaded with a line load, simulating the pressure of the pneumatic formwork. Naturally, a chain is only able to carry tensile forces. In this calculation, the tension force in the chain that is supposed to carry the applied load, is determined.

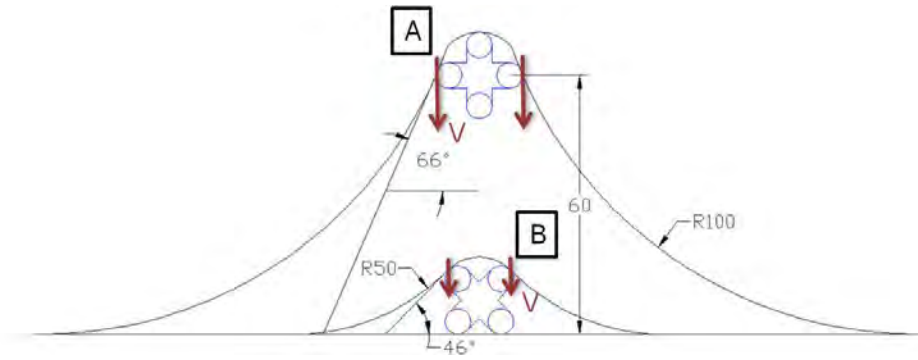


Figure 10.54: Assumed shape of the membrane in the area of the chains

The size of the load was approximated by the use of the following assumptions. The air pressure  $p$  in the membrane is  $37 \text{ mbar}$  and the assumed shape of the formwork is shown in Figure 10.54. It is assumed that at the location  $A$ , the radius of the membrane, is  $100 \text{ mm}$  whereas the radius of the membrane at  $B$  amounts to  $50 \text{ mm}$ . When defining these radii  $R$ , the tension force in the membrane  $F_t$  can be calculated approximately with equation 10.2

$$F_t = p \cdot R \quad (10.2)$$

The tension force in the membrane  $F_t$  for the radius of  $100 \text{ mm}$  and  $50 \text{ mm}$  amounts to  $0,37 \text{ kN/m}$  and  $0,17 \text{ kN/m}$ , respectively. The vertical force  $V$  which is applied to the chain equals the vertical component of the force in the membranes  $F_t$ . Therefore,  $V$  can be calculated with equation 10.3

$$V = F_t \cdot \sin \alpha \quad (10.3)$$

The angle  $\alpha$  is depicted in Figure 10.54 and equals  $66^\circ$  and  $46^\circ$ , respectively. Due to the fact that the chain is pulled down on both sides, the vertical loading of the chain

amounts to  $2 \cdot V$ . The resulting size of the loading in the points  $A$  and  $B$  are shown in Figure 10.53. The line load in between these two points is approximated linearly.

The tension force which is necessary to carry the described load is calculated to approximately  $10 \text{ kN}$ . Due to the fact that each ice segment is equipped with two tension chains, a horizontal force of  $20 \text{ kN}$  will be applied to each end part of the ice segment if the described position of the chain is reached. This force cannot be carried by the ice.

This calculation shows that the force necessary to even move the chains from the ground would force the ice to collapse. Therefore it is impossible to straighten the chains when they are blocked by the pneumatic formwork.

Due to the fact that the chains cannot be straightened when blocked by the pneumatic formwork, another solution has to be found to guarantee that the tendons are perfectly straight. It is necessary to create a void in the area where the temporary chains are to be placed. This void could for example be created by means of a wooden auxiliary construction or plastic tubes which are placed beneath the pneumatic formwork and are strong enough to resist the pressure of the inflated membrane.

### 10.5.3 The lifting process



Figure 10.55: Lifting ice segments, winter 2009/10

The lifting process of the ice segments can be carried out with different methods. In the winter of 2009/10 it was planned to lift the segments with two mechanical hoists fixed to the top of the mounting tower. To minimize asymmetric loading, the two ice segments which were situated opposite each other were planned to be lifted simultaneously. Due to the collapse of most of the ice segments in the winter of 2009/10, this lifting device could not be tested. During this field experiment, it came to knowledge that in the village of Obergurgl a loader crane is easily available. The ice segments which were left undamaged after the incident with the pneumatic formwork, were lifted by means

of the loader crane in order to gain information about this working step. Pictures in Figure 10.55 prove that it was possible to completely lift the ice segment from the ground with a crane. The ice segments were only fixed to the crane by means of a chain connected to the assembly bracket and hanging freely. The stresses occurring during this load case are mentioned in Figure 10.59.

Although lifting the ice segments with only one crane on the assembly bracket proved to be possible, it still was a risky undertaking. As long as the static model is consistent with the previously described compression arch and tension tie, the maximal tension stresses in the ice due to the lifting do not amount to more than  $0,26 \text{ N/mm}^2$  – as shown in Figure 10.59. Because of the fact that the ice segments dangle freely on the crane hook, there is no guarantee that the tension is carried mainly by the tension chains. If the position of the ice segments change in such a way that the chains receive compression and the ice beam tension, neither of them can carry these forces and a collapse is inevitable.

In order to be able to move the ice segments in a controlled manner one needs two lifting points, therefore two loader cranes were used. One of the cranes lifted the ice segment on its thinner end point *A* where the assembly bracket bordered the segment. The assembly bracket had already been previously equipped with an attachment point for connecting the ice segments to the crane. On the wider end part *B*, the segments were lifted with the second crane by means of two lifting slings.



Figure 10.56: Lifting the ice segments, winter 2010/11

Pictures of the lifting process with two cranes are shown in Figure 10.56 and Figure 10.57. The lifting process was carried out very slowly to avoid stress peaks in the segment. Moreover, it had to be ensured that the end parts of the ice segments were not tied positively to the subsoil. The end point *A* was slowly lifted until it could be fixed to the mounting tower at the predefined height. Simultaneously, the second crane lifted the wider end part *B* a few centimeters above the ground allowing it to move freely. As soon as the ice segment was connected to the mounting tower the crane connected to the assembly bracket was released and the force was transferred to the tower. Then the wooden board of the wider end part was positioned in its predefined position and the second crane was also released. The height of the end point *A* was defined by the length of the chain which connected the ice segments to the tower. On



end point  $B$ , potential length differences of the ice segments could be compensated by putting wooden boards underneath the segment.



Figure 10.57: Lifting process of an ice segment

#### 10.5.4 Stresses in the segments

Lifting the ice segments with a crane is a crucial step when the ice dome is built with the segment lift method. Therefore the stresses in the cross-section are calculated. The diagram in Figure 10.59 shows the stresses during different positions of the lifting process. The horizontal axis in this figure shows the longitudinal axis of the ice segment. Of course this axis is curved, but in this diagram the axis is developed into a horizontal line. The vertical axis in this diagram shows the stresses in the segments. Positive stresses describe tension and negative stresses compression. Four different situations are considered, see Figure 10.58.

The sectional forces in the segments were calculated with the framework program *RStab 7* [15]. In this simulation the ice segment is modeled as a series of straight beam elements approximating the actual shape of the segments. The width of the individual beams is also chosen in order to represent the ice segment. In this analysis, the ice has a Young's modulus of  $400 \text{ N/mm}^2$  and a specific weight of  $9 \text{ kN/mm}^3$ . Due to the fact that the cuts have already been filled, the ice segment is calculated with a constant thickness of  $200 \text{ mm}$ .

To simulate the material properties of the tension chains the experimentally determined extensional stiffness  $EA$  is taken into account - see chapter 10.5.2.2. In the simulation one tension tie represents the two chains. Defining the Young's modulus of the steel chain  $E_{steel}$  to  $210\,000 \text{ N/mm}^2$ , an equivalent cross section area  $A'$  for the tension tie can be calculated with equation 10.4.

$$A' = \frac{2 \cdot EA}{E_{steel}} = 22 \text{ mm}^2 \quad (10.4)$$



Choosing a circular cross section, an equivalent diameter of  $5,3\text{ mm}$  represents the two chains.

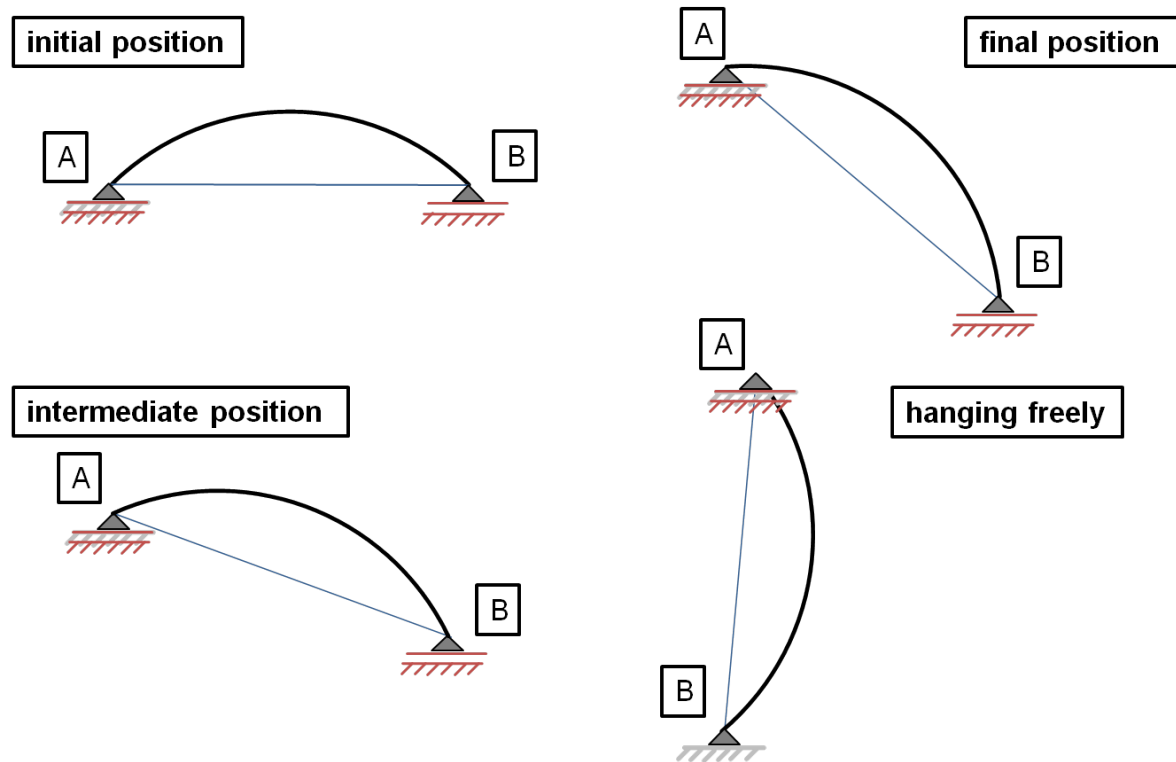


Figure 10.58: Statical systems of the different positions

When an element is lifted by a crane only vertical forces can be applied to the element. Therefore, the red bearings, shown in Figure 10.58, are all moveable supports, showing the boundary conditions induced by the cranes. But the system must neither be unstable nor partially constrained when it is calculated with a framework program. Thus for the simulation with *RStab 7* the boundary conditions are chosen in a such manner that its reaction forces are determinate – shown with the gray symbolic supports in Figure 10.58. The reaction forces of those additionally added boundary conditions are not in conflict with the actual conditions of support. The system consisting of a compression arch and a tie member, however, is statically indeterminate even though its reactions are determinate. Therefore, the stiffness of the single members influences the distribution of the section forces.

The curves in Figure 10.59 show the stresses on the top of the cross section (dark colors) and on the bottom (light colors). These stresses are calculated based on the section forces gained from the framework program under the assumption of a linear elastic material behavior of the ice in an uncracked state. These curves represent the stresses occurring due to dead load in the respective position, shown in Figure 10.58. Eigenstresses which might be in the cross section of the ice segments are not taken into account.

First the initial position of the ice segment is examined. In this position both end parts are lifted off the ground but the supports are still at the same level. This represents

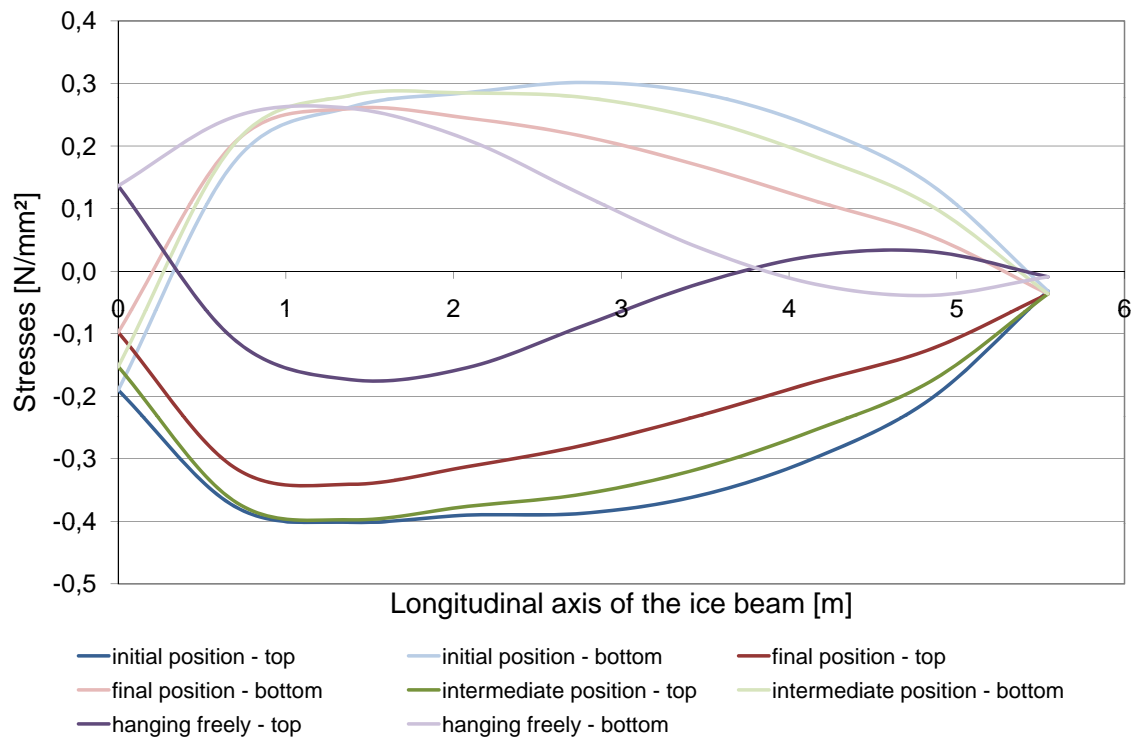


Figure 10.59: Stresses in the ice segment during the lifting process with the crane

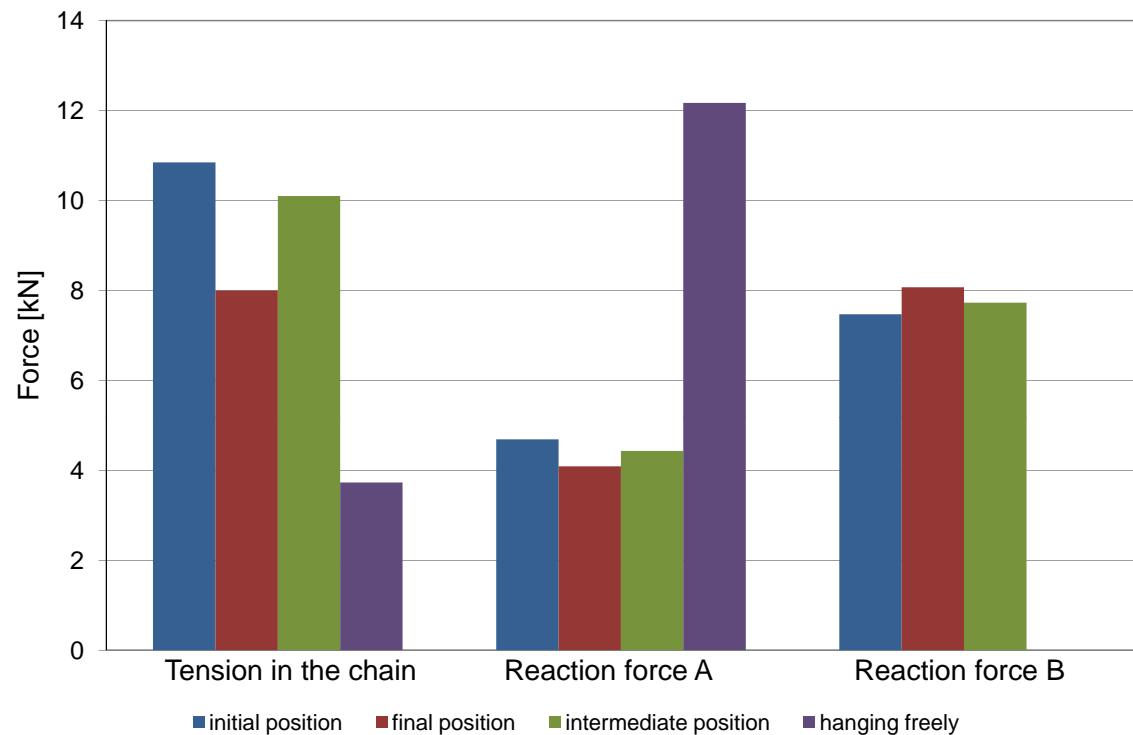


Figure 10.60: Forces in the chains and the cranes during the lifting process

the situation at the very beginning of the lifting process when both cranes just lift the ice segments a few millimeters only. In the final position the end part  $A$  of the ice segment is fixed to the mounting tower and the other end rests on the ground. The intermediate position represents a situation in between. It can be seen that the maximal tension stress of all three situations is  $0,3 \text{ N/mm}^2$ , which is definitely below the tensile strength of ice. The maximal compression stress occurs on the top of the cross section and amounts to  $0,4 \text{ N/mm}^2$ . The stress distribution of the initial and the final position does not show major changes during the lifting process with the cranes and the loading tends to decrease during the lifting process with the two cranes.

The purple curves show the stresses which occur if the ice segment is hanging freely on one crane hook. The diagram shows that, in theory, this method of lifting the ice segments also creates no stresses which are higher than the strength of the ice.

The diagram in Figure 10.60 shows the dimension of the forces carried by the tension chains and the cranes. The tension in the chains is highest in the initial position and decreases when the position of the ice beam changes to vertical. Due to the fact that each ice segment is equipped with two chains, the maximal force in one steel chain does not exceed  $5,5 \text{ kN}$ . The necessary lifting force of the cranes is slightly higher than the vertical reaction forces of the ice segments. During the positioning of the ice segment, the lifting force stays quite constant and the dimension of the force is absolutely unproblematic for a loader crane even when a large jib length is necessary. Moreover, the reaction force  $A$  in the final position which amounts to approximately  $4,0 \text{ kN}$ , is the force which has to be carried by the mounting tower. If the ice segment is hanging freely on one crane hook, its whole weight is obviously carried only by the one crane situated at the end point  $A$ .

## 10.6 Creating a shell structure

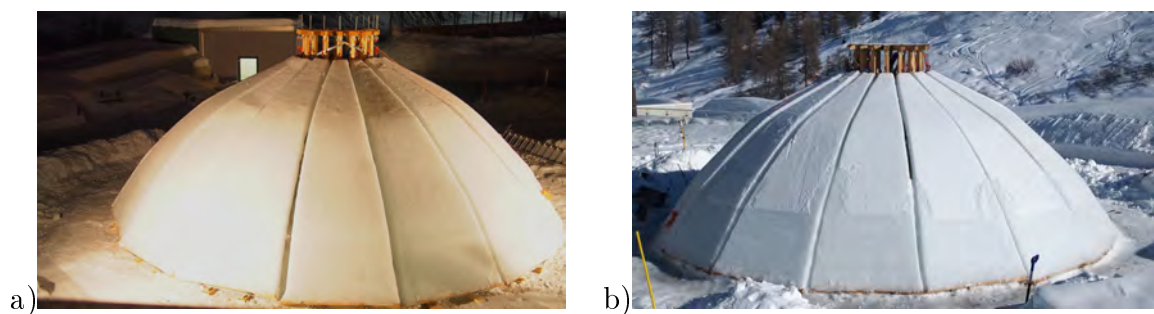


Figure 10.61: Ice segments fixed to the mounting tower a) immediately after lifting b) with gaps already partly filled

In Figure 10.61, all sixteen ice segments are in their final position fixed to the mounting tower. Speaking from a static point of view, this structure is not yet a shell. Every ice segment carries its load individually. Basically, sixteen single span girders or arches with tension ties are situated next to each other. To create a shell structure, hoop forces have to be able to develop. Therefore, the gaps between the individual segments

have to be filled in order to connect the elements and allow sectional forces to run from one segment to the adjacent one.

Moreover, in order to create a shell structure, the horizontal thrust at the bottom of the shell has to be carried by a tension ring. This tension ring is created by means of three steel ropes with a diameter of  $5\text{ mm}$  – the same ropes as the ones used for the reinforcement, described in chapter 10.3. Together they have a minimal breaking strength of  $44\text{ kN}$  according to the producer. After assembling the tension ring, a snow - ice mix was also put around the contact area between dome and subsoil so that the shell was connected to the ground.

Taking a look at the boundary conditions of this actual dome structure, it can be seen that they are not according to membrane theory. In chapter 8.3.2 a numerical simulation of a pointed dome with boundary conditions according to membrane theory was carried out by means of the 3D finite element analysis program *RFEM 4* [13]. In order to simulate the supports of the actual ice dome, the same model was used except that fixed line supports were used as boundary conditions. Also under these conditions the bending moments stay negligibly small and the size of the normal forces is also almost identical. The main difference is the reaction force. Using the same parameters as described in chapter 8.3.2, a horizontal reaction force  $u_{hor}$  of the size of  $3,5\text{ kN/m}$  occurs. This horizontal force gives rise to a tensile force of approximately  $17\text{ kN}$  in the rope. This force can easily be carried by the three steel ropes. The tensile force in the rope  $F_{t,rope}$  is calculated using equation 10.5 where  $r$  is the radius of the base diameter of the ice dome and  $u_{hor}$  is the horizontal reaction force acting in direction of the normal vector on the bottom of the shell.

$$F_{t,rope} = r \cdot u_{hor} \quad (10.5)$$

In order to fill the gaps a mixture of snow and water was used. The size of each gap depends on the accuracy of the assembly of the segments. Moreover, each ice segment was narrowed  $10\text{ mm}$  on each edge in order to have a tolerance of  $20\text{ mm}$  for each interface during the assembly process. When making the ice for these gaps, particular attention was paid to adding great amounts of water to the snow-water mixture in order to create an ice quality with a similar density to the one of the ice segments.

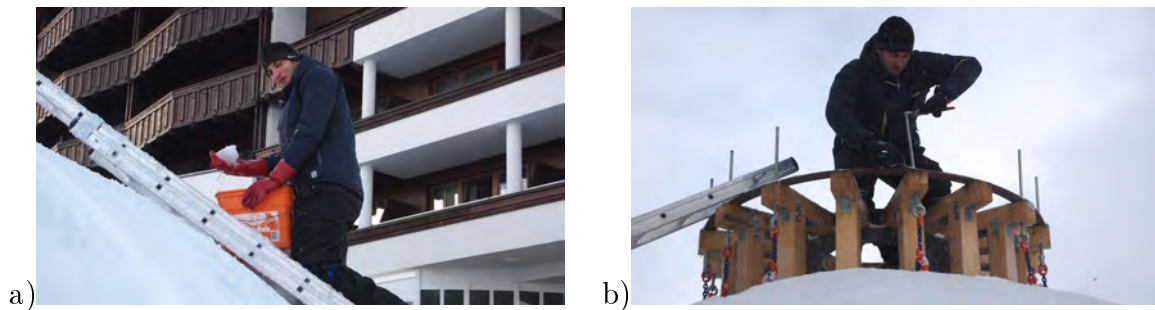


Figure 10.62: Last working stage a) filling the gaps b) detaching the ice shell from the mounting tower

As soon as the gaps have been filled with solidified material, hoop forces can develop and the ice dome acts like a shell structure. Therefore the mounting tower which acted

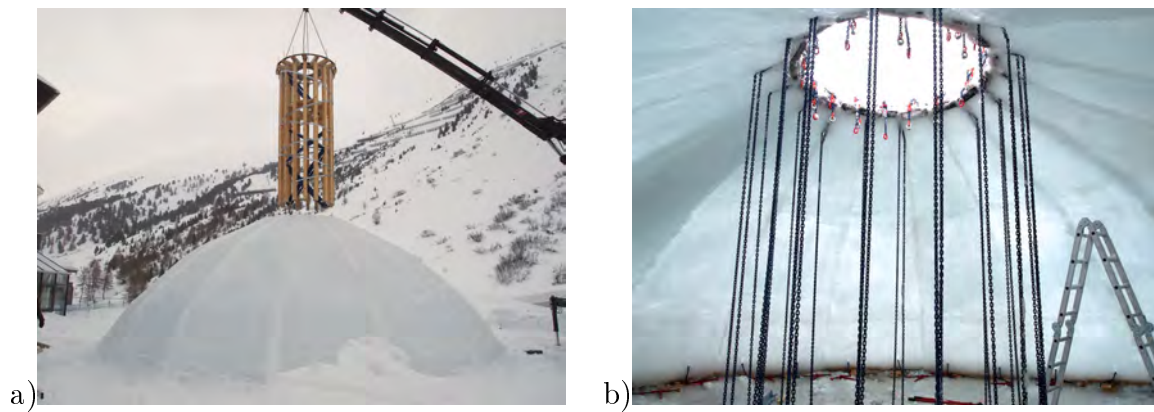


Figure 10.63: Last working stage a) dismantling the mounting tower b) removing the temporary tension chains

as a support for the single span girders, is no longer necessary. The ice segments are fixed to the tower by means of a mounting bracket – a detailed drawing of this mounting bracket is shown in the appendix B.4. Part of this connection between the segment and the tower is a threaded rod anchored with a nut. Through turning this nut, the ice segments can be lowered in order to reduce the force on the support *A* and thus force the structure to function as a shell. Figure 10.62b shows how the ice segments were lowered. One only had to turn the nuts between  $180^\circ$  and  $360^\circ$  to free the mounting tower from the entire load. For the threaded rods a *M* 16 screw thread was used [11]. One turn with this *M* 16 thread equals a pitch of  $2\text{ mm}$ . Therefore only a distance of  $1\text{ mm}$  to  $2\text{ mm}$  was necessary to remove the entire reaction force from the tower and the mounting tower could be dismantled.

After removing the tower, the temporary tension chains could also be dismantled unproblematically because they had become stress-free as soon as the reaction force which was carried by the tower was removed. Figure 10.62 and 10.63 show pictures of this last working stage.

## 10.7 The finished ice shell

### 10.7.1 Characteristics of the ice dome

The finished ice dome has an inner base diameter between  $9,96\text{ m}$  and  $10,14\text{ m}$  depending on whether the measurement is taken in the middle of an ice segment or in the contact area between two segments. Strictly speaking, the base area of this dome forms a hexadecagon.

The highest point of the inside surface of the shell measured  $3,5\text{ m}$ , whereas the highest point of the ice on the outside measures  $3,67\text{ m}$  from the ground. The thickness of the finished shell amounted to  $190\text{ mm}$  to  $200\text{ mm}$ . If considering the actual measured distortion of the ice segment determined on the 11<sup>th</sup> of January 2011, and approximating a mean value of the radius of curvature, the radius will amount to  $7,85\text{ m}$ . The

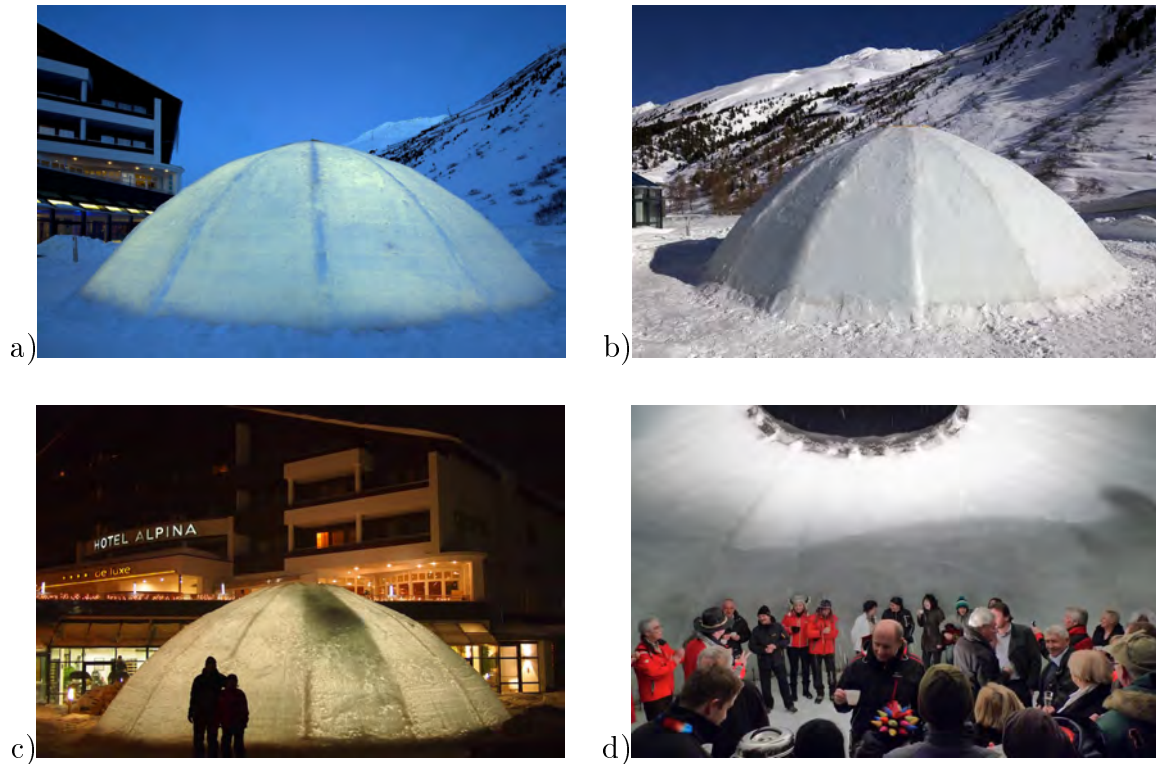


Figure 10.64: Finished ice shell a) and b) picture: Günter R. Wett

slenderness of an arch or dome is defined as ratio of radius to thickness and amounts to approximately 40. By comparison, the slenderness of an egg shell is 60. However, it was not the intention to build a very slender dome because a higher thickness extends the durability significantly. In chapter 10.8, it is shown that the shell is also functional with a far smaller ice thickness.

The oculus has a diameter of approximately  $1,6\text{ m}$  and it remained open during the whole lifetime of the ice shell. If the middle axis of the pointed dome is extended to the axis of rotation, the apex will be at a height of  $3,83\text{ m}$  above the ground.

Figure 10.64 shows pictures of the finished ice dome.

### 10.7.2 Numerical simulation

A numerical simulation of the finished ice dome was carried out. Before the ice segments were lifted, their shape had been measured with a theodolite. The results of this measurement are almost identical to the deformations detected on the 11<sup>th</sup> of January 2011, depicted in Figure 10.43. The maximum difference between these two measurements amounted to  $10\text{ mm}$ , which could also be caused by measurement uncertainty.

Seven points of each segment were measured in order to define its final shape. With this data set a 3D finite element model was created with the program *RFEM 4* [13]. In this model, the ice dome consists of the sixteen segments, each of them modeled with its respective shape and placed on its respective position. The segments were modeled



with their designed width and a thickness of  $200\text{ mm}$ . To connect the ice segments, the ice in the gaps was also modeled using the same thickness. Like in most of the simulations before, the Young's modulus of ice was set to  $400\text{ N/mm}^2$  and the specific weight to  $9\text{ kN/mm}^3$ . The results of this linear analysis are shown in the Figures 10.65 to 10.68. Due to the fact that there are discontinuities in the shape of the segments and small areas of ice between the gaps, a quite dense mesh has to be used. In order to make the output files readable, the mesh is not displayed. All ice segments and the ice in the gaps are supported by fixed line supports and therefore they cannot experience a deflection in any of the three dimensions. This boundary condition represents the real situation where a tie strap carries the horizontal thrust and the base of the dome is thicker and connected to the subsoil through additional snow and ice.

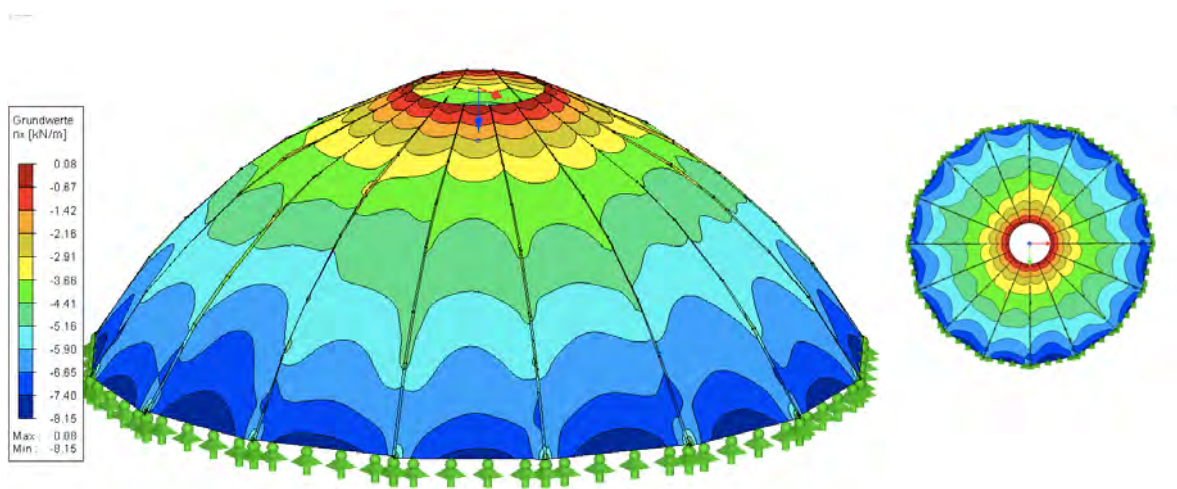


Figure 10.65: Meridional forces in the actual shell structure

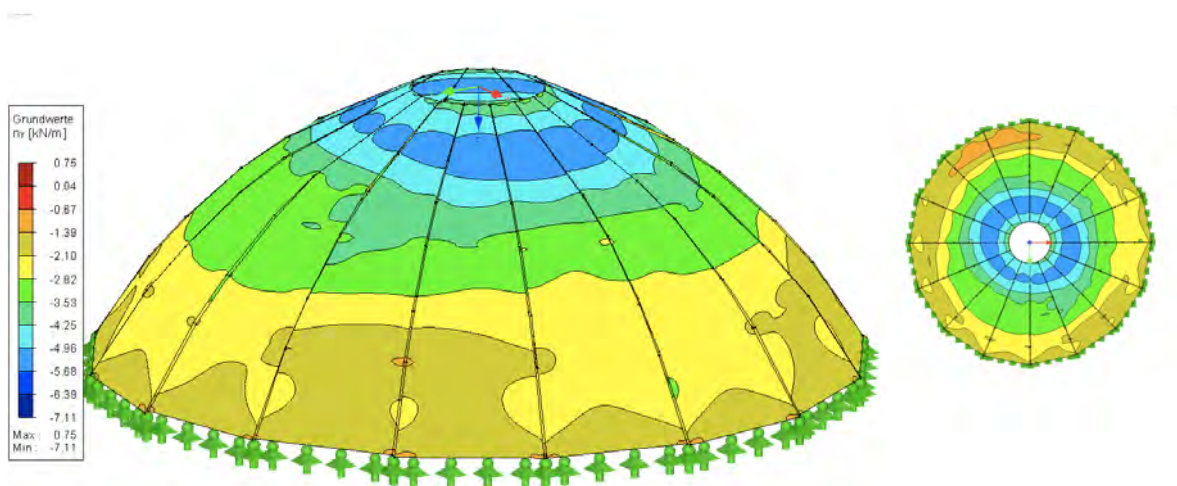
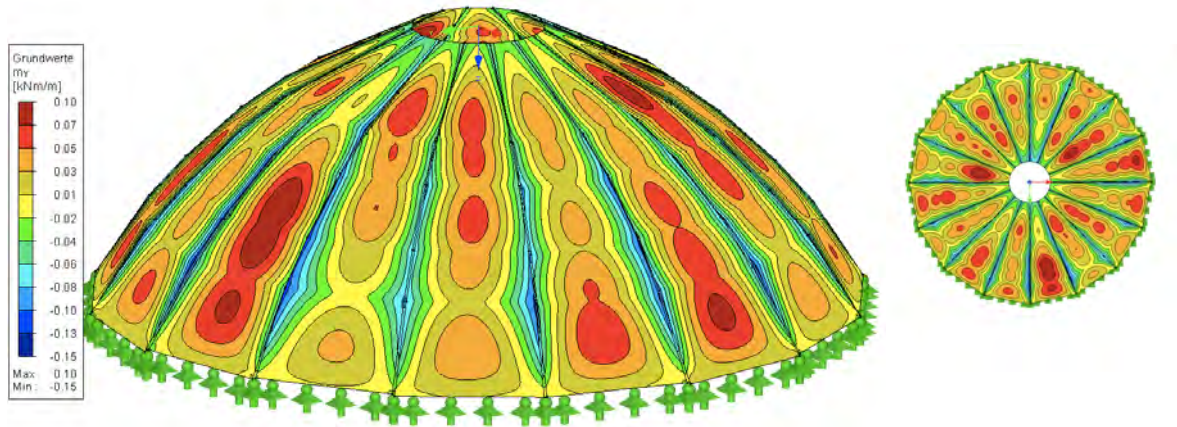
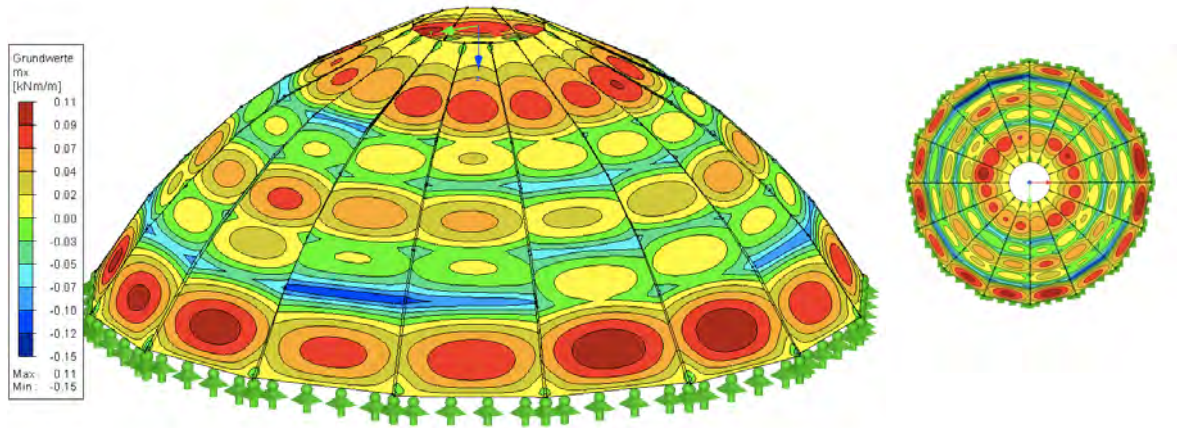


Figure 10.66: Hoop forces in the actual shell structure

Figure 10.65 to 10.68 show the normal forces and bending moments due to dead load. In all figures it can be seen that the section forces and moments are not rotationally



Figure 10.67: Moments  $M_y$  in the actual shell structureFigure 10.68: Moments  $M_x$  in the actual shell structure

symmetrical and not even identical in every segment. This, of course, is a result of the different shapes of the segments. Taking a closer look at the distribution of the forces and moments, it can be noticed that the imperfections do not cause large additional forces or bending moments. This simulation can be compared to the predicted forces in a pointed dome or a cloister vault with a regular hexadecagon as base, shown in the Figures 8.5 to 8.6 and 8.8 to 8.9 in chapter 8.3.

Figure 10.65 shows a perspective view and a plan view of the normal forces acting in meridian direction. Even though these forces are not completely evenly distributed, they are about the same size as the predicted normal forces in Figure 8.6 and 8.9. At the base of the ice dome the normal forces range from  $6 \text{ kN/m}$  to  $8 \text{ kN/m}$  which gives rise to normal compressive stresses with magnitude of  $0,03 \text{ N/mm}^2$  to  $0,04 \text{ N/mm}^2$ , which can easily be carried by the material ice.

Figure 10.66 shows that also in the circumference direction almost exclusively compressive stresses occur. The areas where tension might appear, however, are at the very bottom of the dome where the tension strap is situated.

The bending moments are depicted in Figure 10.67 and 10.68. The direction of the moments is according to the definition in Figure 2.5, in chapter 2.1.3.3. The moments in Figure 10.67 are given rise to by the joints between the segments. If one cross section of an ice segment is fictively cut out of the segment it can be seen that the ends of the cross section are partly clamped in the joins and a negative bending moment occurs. In the area between these “supports” a positive bending moment acts due to the vertical loading. The moments in Figure 10.68 are mainly influenced by the curvature of the ice segments. If the curvature of the ice segment resembles an inverted catenary arch, these moments will disappear. Due to the fact that the segments were situated on two stacks of wood during their creeping process, there are two noticeable discontinuities - like kinks - in the curvature. These kinks produce bending moments spinning around the circles of latitude. Moreover, these bending moments are also influenced by the modeling. Seven different points of each segment were measured. In the 3D model these points were connected linearly which produced additional kinks to the existing ones. According to this simulation the moments occurring in the finished shell have a maximal absolute value of  $0,15 \text{ kNm/m}$  which equals stresses in a range of  $0,02 \text{ N/mm}^2$  which can easily be carried by the ice.

## 10.8 Monitoring the ice shell until collapse

Measuring points were installed in order to gain information about the behavior of the ice dome during its lifespan. Altogether, five monitoring visits took place at different times.



Figure 10.69: Opening in the ice dome on the side facing the sun

The collapse of the ice dome took place in two steps. First, an opening appeared due to the strong solar radiation. The part of the ice which was facing the sun became thinner

and thinner. The last few millimeters of the ice broke off and a hole of approximately  $4\text{ m} \times 3\text{ m}$  developed. This hole, however, did not lead to an overall collapse. In the following days, this opening became larger until the dome was finally destroyed for safety reasons. Figure 10.69 shows pictures of the opening on the side facing the sun.

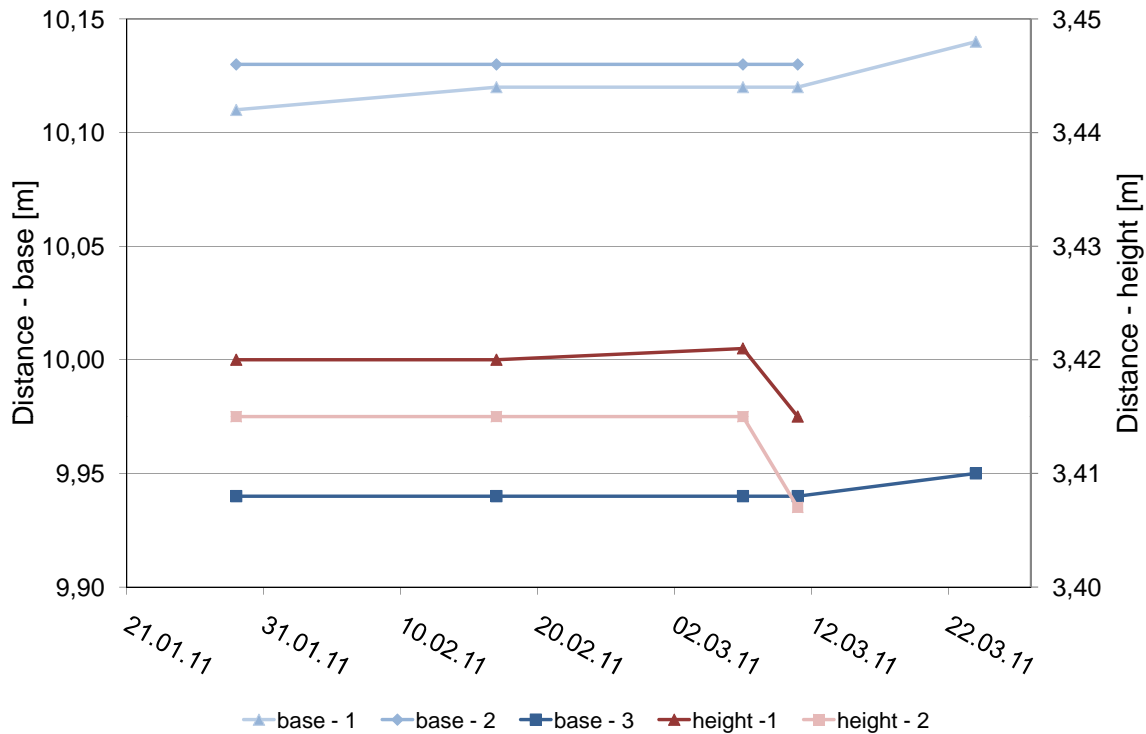


Figure 10.70: Monitoring the base diameter and the height of the ice dome

Various measurements were taken during the monitoring visits. First, the base diameter of the ice shell was monitored by measuring the distance between two opposite wooden boards which used to be the outer formwork for the ice segments. For this purpose six points were marked and the distance between the two opposite marks were measured. The three blue lines in the diagram of Figure 10.70 show the measured results. These blue lines refer to the primary axis, which shows the distance between points in the base of the ice dome. It can be seen that during the first weeks, the base diameter of the ice dome did not change at all. At the last monitoring visit, which took place after the opening in the ice shell appeared, a small increase of the base diameter of the ice shell is noticeable.

Moreover, the height of the ice dome was measured at two different points. The red lines in Figure 10.70, referring to the secondary axis of the diagram, show the results. It is important to note that the scale on the two axes is different. In the first weeks the height did not change at all. On the last but one measuring visit, however, a slightly lower height could be measured.

Another parameter measured was the thickness of the shell. Measurements on different locations of the shell were taken. A very large difference could be detected between the side of the shell facing the sun and the one averting the sun. Therefore, the diagram

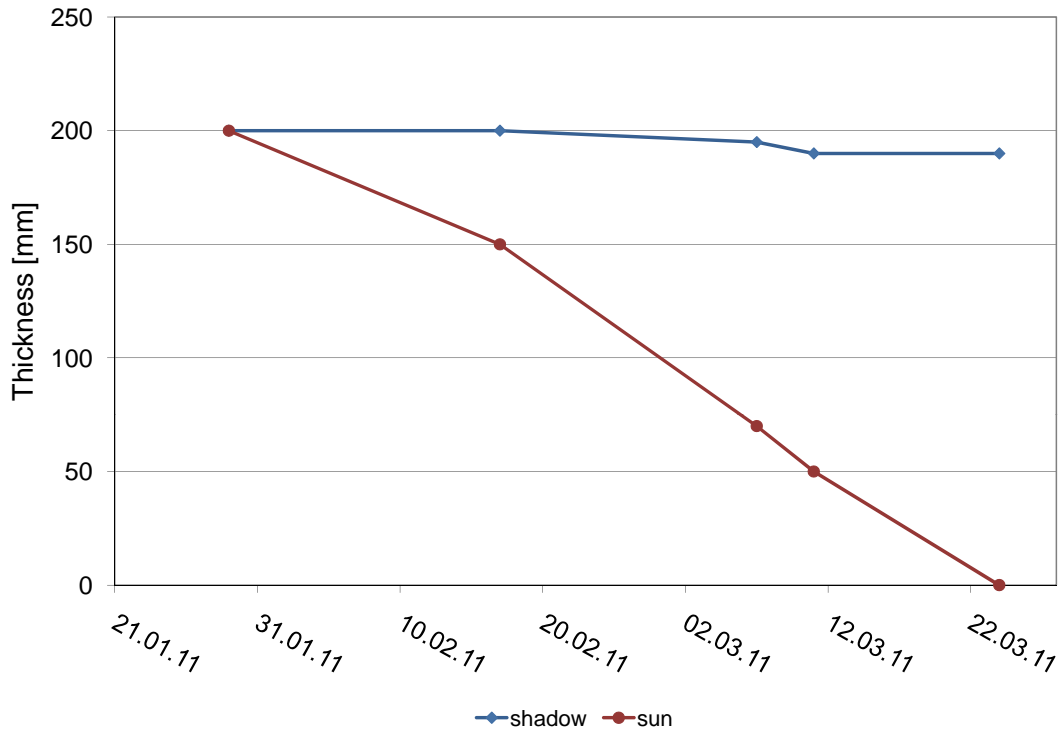


Figure 10.71: Monitoring the thickness of the ice dome

in Figure 10.71 shows the minimum thicknesses of the shell on both sides. On the side averted to the sun, called “shadow” in Figure 10.71, the thickness remained almost constant during the entire time. On the side facing the sun, the thickness of the ice decreased rapidly due to sun radiation. On the 21<sup>st</sup> of March a hole appeared on the side facing the sun and therefore the thickness reached zero. The side of the shell which was situated in the shade, maintained its thickness during all five monitoring visits.

Date	base			height		thickness	
	1	2	3	1	2	shadow	sun
	[%]	[%]	[%]	[%]	[%]	[%]	[%]
29.01.2011	reference						
17.02.2011	0,00	0,00	0,00	0,00	0,00	0,00	−25,00
07.03.2011	0,00	+0,10	−0,10	0,00	0,00	−2,50	−65,00
11.03.2011	0,00	+0,10	−0,10	−0,15	−0,23	−5,00	−75,00
24.03.2011	+0,10	+0,30	-	-	-	−5,00	−100,00

Table 10.1: Percentage of the changes

Table 10.1 shows an overview of the change in the measured values. The measurement on the 29<sup>th</sup> of January always served as reference and the changes of the parameters are expressed as a percentage and are based on the reference. It can be seen that the base diameter of the shell only increased by 0,3 % and the height only decreased by 0,23 %. These differences could also be a result of the measurement uncertainties. Major changes took place regarding the thickness of the ice on the side of the shell

facing the sun. The thickness constantly decreased until the loss reached 100 %. This effect is caused by melting of the ice as well as sublimation. Regarding these results, it becomes obvious that the sun radiation has a significant impact on the durability of the shell.

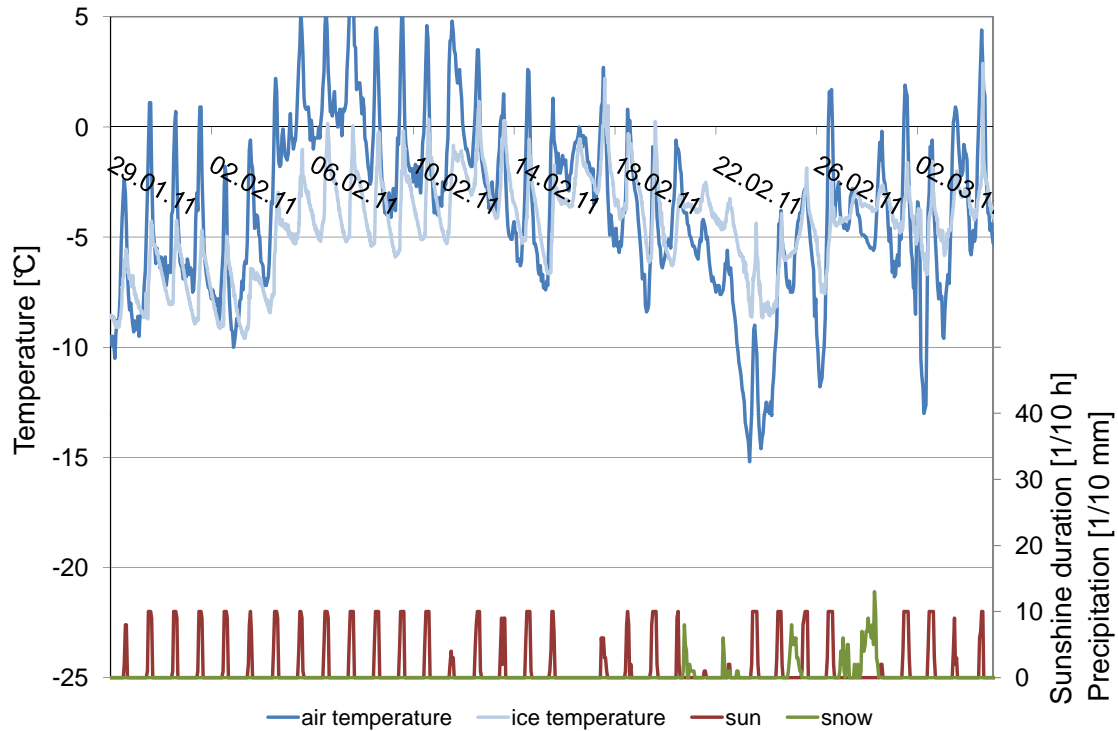


Figure 10.72: Temperature in February 2011

Figure 10.72 compares the air temperature to the ice temperature in February 2011. The temperature of the ice was measured by 4 different temperature sensors, placed inside the ice. Figure 10.72 shows the calculated mean value. The air temperature was measured by the ZAMG [1], Austria's national weather service agency with a weather station in Obergurgl. This weather station, however, is situated in another part of the village. Therefore, the measured air temperatures may differ from the ones in the immediate vicinity. Generally speaking, the inner temperature of the ice remained quite constant and overall changes in the ambient temperature will only have an effect on the ice after a few days.

As discussed previously, the direct sun radiation has a strong impact on the ice. The sunshine duration per day is depicted in Figure 10.73. Moreover, the blue vertical line in Figure 10.73 shows the day when the opening appeared in the ice dome.

The World Meteorological Organization uses the term "sunshine duration" to indicate the cumulative time during which an area receives direct irradiance from the sun of at least  $120 \text{ W/m}^2$  [23]. The number of hours in which this value is exceeded is summed up over one day and shown in the diagram. It is obvious that during December and January the maximal sunshine duration cannot exceed 2,5 hours per day. When winter turns into spring the sun shines longer every day, so that at the end of March the sun

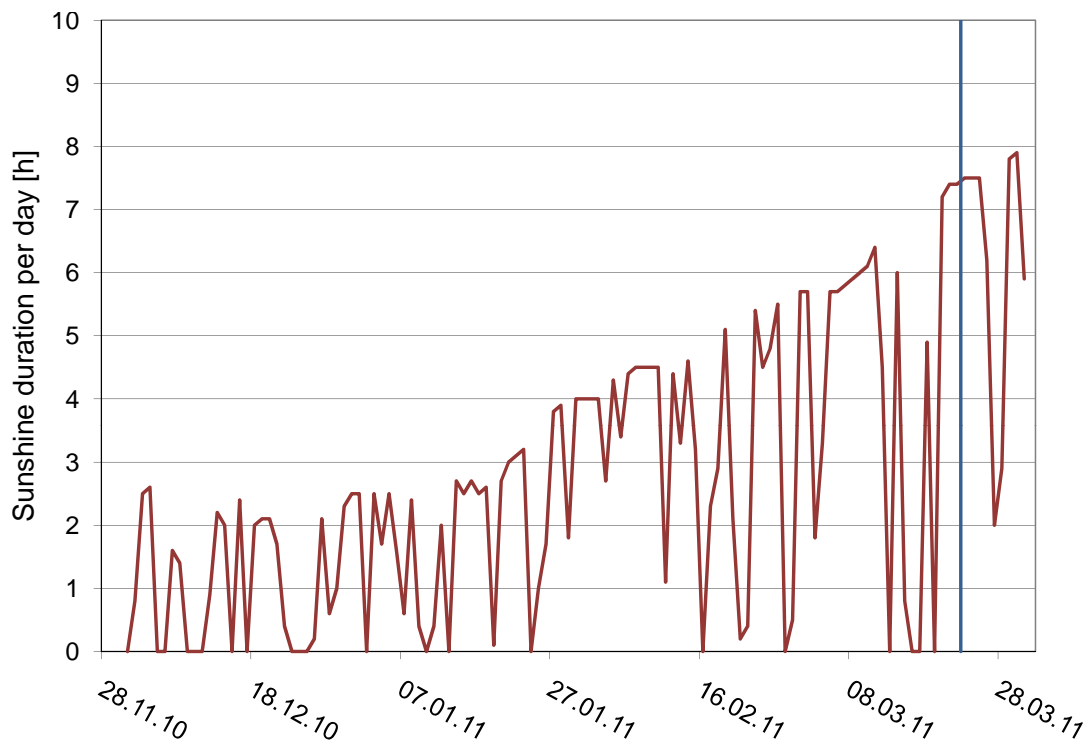


Figure 10.73: Sunshine duration from December 2010 to March 2011

might shine continuously up to 8 *hours* per day. This longer period of sun radiation encouraged the sublimation and also constantly melted the ice.

# Part IV

## Conclusion



# Chapter 11

## Achievements and limitations

In this thesis two new construction methods for ice domes have been presented. The basic concept is similar for both construction methods: In the initial position the intended shell structure consists of a plane plate which is subsequently transformed into a shell structure. Both construction methods have been described in detail in the parts II and III. In order to gain a better understanding of these techniques both newly developed construction methods were tested in large scale field experiments. In the following two chapters the achievements and limitations as well as the advantages and disadvantages of the two methods are summarized.

### 11.1 Pneumatic formwork method

The pneumatic formwork method is characterized by building a shell consisting of individual plane elements shaped in order to create a continuous structure. In this method, the individual elements are placed on a planar working surface and are assembled by means of tendons. In order to transform the flat plate into a shell a pneumatic formwork is used to lift the elements into their final position.

In addition to theoretical investigations and considerations, large-scale field experiments were carried out in order to verify the feasibility of this construction method. The preliminary test on the concrete shell – described in chapter 6.2 – proved that this construction method is suitable to build hemispherical dome structures with a diameter of at least  $8,4\text{ m}$ . This field experiment indicated that the pneumatic formwork, and especially the seams of the membrane, are the crucial factor of this method. As described in chapter 4.3.2, the tensile force in the membrane is directly proportional to the radius of the membrane at a certain point. Using the materials and techniques for creating the seams as described in chapter 5.1 this construction method is limited to a shell with a radius not significantly larger than the one tested with the concrete and ice shell. Research and experiments on the techniques of producing seams for pneumatic formworks did not reveal any solutions for improving the seams suitable in these circumstances. If larger dome structures are to be built with this method, a reduction of the radius of the membrane proves to be the most suitable approach. One

possible method to reduce the radius of the membrane locally is suggested namely by constricting the foil with ropes and chains - see chapter 5.5. In this thesis, however, developing and testing of the pneumatic formwork method was limited to hemispherical dome structures with a maximum radius of 8 *m* to 9 *m*. In order to build larger structures, additional investigation would be necessary.

It could also be demonstrated that ice is a suitable construction material in regard to this method. By successfully completing the small ice shell, it could be proven that an ice shell structure can be built with this newly developed technique. This method was also tested on a larger scale with a hemispherical ice dome originating from a ice plate with a diameter of 13 *m*. Unfortunately, the design of one detail proved to be unsuitable which led to a premature termination of this experiment. Apart from this local failure of the wooden boards, the pneumatic formwork method seemed to be applicable for ice shells this size as well.

Theoretically, this construction method is not limited to hemispherical dome structures. Different types of shells could be built using this very method. When other shapes are to be created, then the pneumatic formwork as well as the dimensions of the individual elements have to be chosen according to the final shape of the shell.

## 11.2 Segment lift method

The key elements of the segment lift method are the deformation of the individual plane ice segments and the subsequent lifting of the segments in order to form a shell. In order to distort the ice segments, these elements have to be lifted and kept in an elevated position so that the curvature produced both by elastic deformation and creep deformation can develop. For this purpose two different lifting methods were presented in this thesis – the *segment lift method with pneumatic formwork* and the *segment lift method without pneumatic formwork*. One way to lift the segments is by means of a pneumatic formwork which has to be placed underneath the ice elements prior to producing the ice plate. Another option is to lift them with a lifting device. Except for this part of the construction both methods are identical.

The segment lift method with pneumatic formwork was tested on an ice dome in the winter of 2009/10. Using the pneumatic formwork proved to be a very gentle way of lifting the ice segments because the pressure in the membrane, and therefore the stresses in the ice, could be varied continuously. The disadvantage of the pneumatic formwork is that the membrane presents an additional source of defect. During the field experiment, the membrane in the area of the connection piece between the pneumatic formwork and the air hose failed which led to an air loss which could not be compensated by the air blower. Moreover, the pneumatic formwork interferes with the assembly of the chains which are essential when the segments are lifted into their final position. On the one hand, when a pneumatic formwork is used in this method, then the membrane must be built in a way so that the air pressure can be kept constant at all times. On the other hand, a smooth assembly of the chains must be ensured.

Although the experiment could not be finished successfully in winter 2009/10, the completed ice dome built in the following winter proved that this construction method is feasible when the formwork is applied accurately.



Figure 11.1: Ice Dome built within this thesis (pictures: Günter R. Wett)

In the winter of 2010/11 the version of the segment lift method without pneumatic formwork was tested. For this purpose a lifting device for placing the ice segments on stacks of wood had been designed. The problems with the pneumatic formwork were basically solved by omitting the pneumatic formwork altogether. During this field experiment it could be also shown that the last working steps of this construction method, especially the lifting of the ice segments with a crane, are not only theoretically but also practically possible.

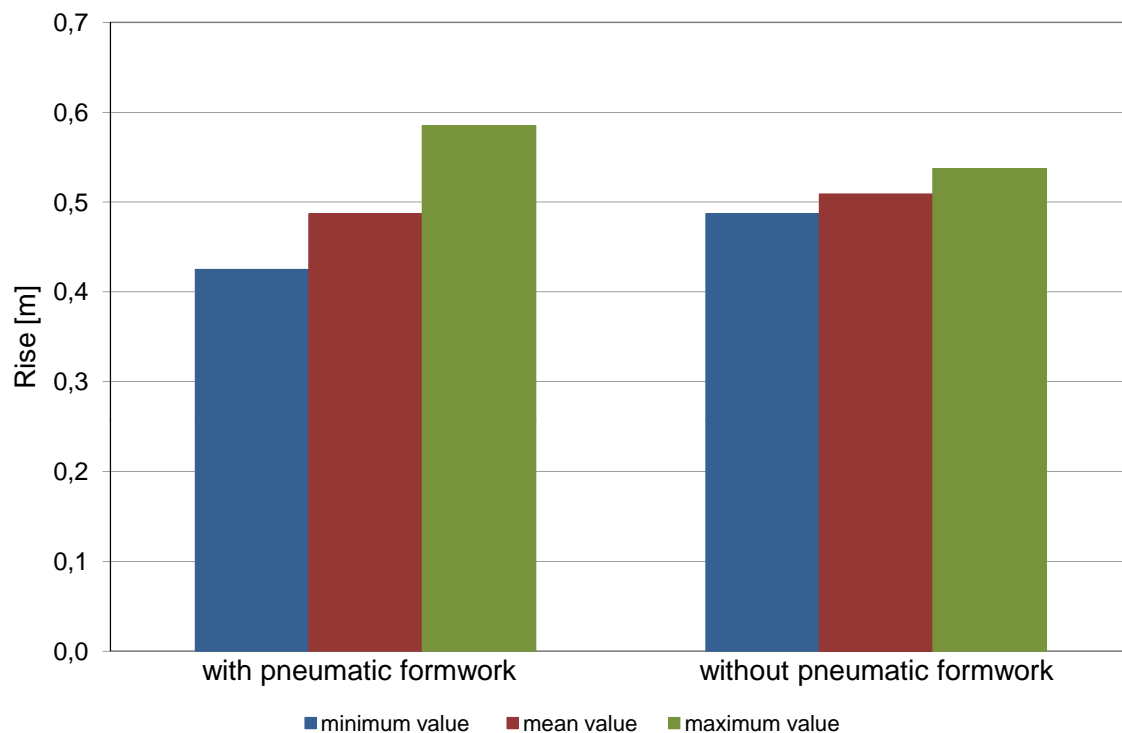


Figure 11.2: Size of the rise during the field experiments in winter 2009/10 and 2010/11

In order to compare these different methods of lifting the ice segments from the ground and thus enabling the creeping process, the size of the rise of the segments in the winter seasons of 2009/10 and 2010/11 are shown in Figure 11.2. The rise is defined in Figure 8.2 in chapter 8.3. The first three bars represent the values measured in the winter of 2009/10 when a pneumatic formwork was used during the creeping process. For purposes of comparison the rises measured in winter 2010/11 are also depicted. The red beams represent the mean values of all sixteen rises and the blue and green columns show the minimum and maximum rise of all segments. It can be observed that the deviation of the size of the rises when the segments are placed on stacks of wood is significantly lower than the deviations appearing with the segments lift method with the pneumatic formwork. This phenomenon can be explained as follows: All segments are placed on stacks of wood of the same height measured from the subsoil. Although the creeping process is different for each segment, as soon as the end parts of the ice touch the ground, the deformation stays constant. Therefore the difference between the maximum and minimum values amounts to less than  $50\text{ mm}$ . When a pneumatic formwork is used the height of the formwork in a specific area is the result of the weight which is placed in this very area. Therefore, inaccuracies in the ice segments could cause problems. If two segments are unequally heavy, the size of the rise can be different even though all the end parts of both segments touch the ground.

In short, the field experiments showed that using a lifting device and placing the segments on stacks of wood, creates more uniform curvatures. Moreover, without the pneumatic formwork the risk of damaging the sensitive membrane is eliminated. The disadvantage of this method, however, is that each segment has to be lifted individually, which takes considerably more time than inflating the pneumatic formwork.

# Chapter 12

## Building larger ice domes

When larger ice domes are to be built, one has to consider the stresses in the finished structure. According to the correlations compiled by Pflüger [65] and cited in equation 2.4 and 2.5 in this thesis, the meridian forces  $N_x$  and the hoop forces  $N_y$  per unit of length in a hemisphere or a spherical cap are proportional to the area load of the self weight  $p_E$  and the radius  $r$  – see equation 12.1.

$$N_x \propto p_E \cdot r \quad N_y \propto p_E \cdot r \quad (12.1)$$

The area load of the self weight  $p_E$  is defined as following:

$$p_E = \gamma \cdot h \quad (12.2)$$

$\gamma$                       specific weight

$h$                       height of the cross section

Therefore the stresses in the membrane are directly proportional to the specific weight  $\gamma$  of the material and the radius  $r$ :

$$\sigma_{xx} \propto \gamma \cdot r \quad \sigma_{yy} \propto \gamma \cdot r \quad (12.3)$$

The height of the cross section  $h$ , however, does not influence the stresses in the dome structure. Thus, by increasing the thickness of the shell, the stresses in the cross section cannot be reduced. The stresses in the ice have to be limited due to the strong creep behavior of the ice. High stresses lead to large deformations of the dome during its lifespan. Therefore, even theoretically, the size of the dome cannot be increased infinitely.

The building of larger ice domes can also be limited by the construction method itself. As already mentioned in chapter 11.1, the maximum size of an ice dome built by the pneumatic formwork method mainly depends on the formwork. If effective solutions are found to decrease the radii in the membrane, larger ice domes than the ones described in this thesis are theoretically possible.

When the segment lift method is used, then the stresses during the creeping process and during the final lifting process are crucial. When the length of the segments is increased, additional lifting points will have to be installed in order to keep the stresses low. Moreover, in all stages in which bending occurs, increasing the height of the cross section reduces the maximum stresses. When the lifting points are arranged accordingly, then larger ice domes are theoretically possible, also with this construction method.

# Bibliography

- [1] Climate data provided by ZAMG, Central Institute for Meteorology and Geodynamics, Austria's national weather service agency. 78, 79, 112, 125, 139, 140, 164, 181
- [2] Environment Canada. URL: <http://ice-glaces.ec.gc.ca/WsvPageDsp.cfm?ID=10167>, May 2011. 22
- [3] The Hotel de Glace, Canada. URL: <http://www.icehotel-canada.com/>, May 2011. 22
- [4] Ice Hotel in Jukkasjärvi, Sweden. URL: <http://www.icehotel.se>, May 2011. 22
- [5] LumiLinna, SnowCastle, Finland. URL: <http://www.snowcastle.net/en/>, May 2011. 22
- [6] Snow Village, Finland. <http://www.snowvillage.fi/>, May 2011. 22
- [7] Alta Igloo Hotel, Norway. URL: <http://www.sorrisniva.no/>, May 2011. 22
- [8] Aurora Ice Museum, USA. URL: <http://www.chenahotsprings.com/>, May 2011. 22
- [9] Iglu Dorf, Switzerland, Germany, Andorra. URL: <http://www.iglu-dorf.com/>, May 2011. 22
- [10] ÖNORM EN 1992 1-1. Bemessung und Konstruktion von Stahlbeton- und Spannbetontragwerken - Teil 1-1: Grundlagen und Anwendungsregeln für Hochbau. *Austrian Standards Institut*, 2009. 61, 63, 68, 186
- [11] DIN 13-1. Metrisches Iso-Gewinde Allgemeiner Anwendung - Nennmasse für Regelgewinde; Gewinde-Nenn Durchmesser von 1 mm bis 68 mm. *German Institute for Standardisation*, 1999. 127, 157
- [12] ÖNORM EN 1993-1-1. Bemessung und Konstruktion von Stahlbauten - Teil 1-1: Allgemeine Bemessungsregeln. *Austrian Standards Institut*, 2007. 127
- [13] RFEM 4 3D. Dlubal software. URL: <http://www.dlubal.de/RFEM-4xx.aspx>, May 2011. 35, 92, 156, 158
- [14] Abaqus-CAE 6.10. Simulia. URL: <http://www.simulia.com/products/abaqus-cae.html>, May 2011. 120, 121, 134, 135



- [15] RSTAB 7. Dlubal software. URL: <http://www.dlubal.de/RSTAB-7xx.aspx>, May 2011. 91, 152
- [16] A. Traetteberg, L.W. Gold and R. Frederking. The strain rate and temperature dependence of Young's modulus of Ice. *Proceedings, IAHR Third International Symposium on Ice Problems*, pages 479–486, 1975. 26
- [17] Sattler AG. Data sheet of 641 polyplan complan. 42, 186
- [18] Sattler AG. URL: <http://www.sattler-ag.com/sattler-web/de/>, May 2011. 42
- [19] All World Wars. Ice railway bridge over the Dnieper by Hauptmann Ludwic Schmeller. URL: <http://www.allworldwars.com/Ice-Railway-Bridge-Over-The-Dnieper-by-Ludwig-Schmeller.html>, May 2011. 22
- [20] Association of Finnish Civil Engineers RIL. Snow constructions - General rules for design and construction. *RIL 218-2002*, 2002. 25, 26
- [21] David P. Billington. *Thin shell concrete structures*. McGraw-Hill Book Company, United States of America, 1965. 16, 92, 179
- [22] Bruce Campbell, editor. *Heinz Isler as Structural Artist - An exhibition organized by the Art Museum and the School of Engineering and Applied Science, Princeton University*. The Art Museum, Princeton University, Princeton, New Jersey, 1980. 21
- [23] Central Institute for Meteorology and Geodynamics, Austria's national weather service agency. URL: <http://zamg.at/>, May 2011. 29, 164
- [24] Clemens Preisinger, Johannes Harrer, Camillo Ressler and Johann Kollegger. Stahlbetonschalen ohne Schalung - ein neuer Weg im Schalenbau. *Beton- und Stahlbetonbau*, 1:31–38, 2005. 24
- [25] D.M. Cole. Strain-rate and grain-size effects in ice. *J.Glaciol.* 33, 115, pages 274–280, 1987. 25
- [26] Enerpac. URL: <http://www.enerpac.com/>, May 2011. 126
- [27] F. Donald Haynes. Temperature effect on the uniaxial strength of ice. *5. international conference on port and ocean engineering under Arctic conditions*, pages 667–681, 1980. 25
- [28] Karl Girkmann. *Flächentragwerke: Einführung in die Elastostatik der Scheiben, Platten, Schalen und Faltwerke*. Springer-Verlag, 1978. 17, 18, 137, 179
- [29] Erwin Heinle and Jörg Schlaich. *Kuppeln aller Zeiten - aller Kulturen*. Deutsche Verlags-Anstalt, Stuttgart, 1996. 14, 15, 179
- [30] Helmut Pottman, Andreas Asperl, Michael Hofer and Axel Kilian. *Architectural Geometry*. Bentley Insitut Press, 2007. 15

- [31] I. Hawkes and M. Mellor. Deformation and fracture of ice under uniaxial stress. *Journal of Glaciology* 11,61, pages 103–131, 1972. 25
- [32] Heinz Isler. New shapes for shells. In *Vorbericht C-3; International Colloquium on Construction Processes of Shell Structures*, Madrid, 1959. 21
- [33] Jürgen Joedicke, editor. *Dokumente der modernen Architektur – Schalenbau: Konstruktion und Gestaltung*. Karl Krämer Verlag, Stuttgart, 1962. 15
- [34] Johann Kollegger. Method for the production of double-bent shells. *European Patent No. 1706553*, 2008. 24
- [35] Johann Kollegger and Clemens Preisinger. Verfahren zur Herstellung von zweifach gekrümmten Schalen. *Austrian Patent Application*, 2004. 24
- [36] Johann Kollegger, Clemens Preisinger and Michael Kaulfus. Ice shells for temporary event architecture. *Structural Engineering International*, 14:274–276, 2004. 24
- [37] Johann Kollegger, Sonja Dallinger and Herbert Pardatscher. Schale aus ebenen Flächentragwerkelementen. *European Patent Application No. EP 09450102*, 2009. 29
- [38] Johann Kollegger, Sonja Dallinger and Herbert Pardatscher. Verfahren zur Herstellung einer Schale. *Austrian Patent No. AT 506.902*, 2011. 29
- [39] Johann Kollegger, Sonja Dallinger, Herbert Pardatscher and Anton Schweighofer. Verfahren zur Herstellung einer Schale aus zumindest zwei dünnwandigen, flächigen Tragelementen. *Austrian Patent Application: No. A2014/2009*, 2009. 29
- [40] John D. Fox Jr. and Robert Ott. Ice thickness and ice bridges: An Annotated Bibliography. Welborn, M. (ed.) *Region III Forest Resources & Practices Riparian Management Annotated Bibliography. Compiled by Region III Science/Technical Committee. Report to the Alaska Board of Forestry. AK DNR Division of Forestry, and AK Dept. of Fish & Game*, pages 103–126, 2000. 22
- [41] Michael Kaulfus. Verfahren zur Herstellung von zweifach gekrümmten Schalen aus Eis. Master’s thesis, Vienna University of Technology, 2004. 24
- [42] Kenji Ishizawa, Tsutomu Kokawa and Toshio Hannuki. Construction of Ice Domes at Asuka Station in Antarctica. *Antarctic Record*, 37:115–127, 1993. 23
- [43] Tsutomu Kokawa. A Field Study on a 10m-span Ice Shell. *Bull. Hokkaido Tokai Univ. Dept. of Art and Technology*, 7:29–40, 1987. 23
- [44] Tsutomu Kokawa. An Experimental study on Creep Collapse of Ice Dome. *Bull. Hokkaido Tokai Univ. Dept. Art and Technology*, 7:19–28, 1987. 26
- [45] Tsutomu Kokawa. Construction and Creep Test of 15-m Span Ice Dome. *Proceedings of the 9th International Symposium on Ice, Sapporo*, 2:390–399, 1988. 23

- [46] Tsutomu Kokawa. Field Study of a 30-m Span Ice Dome. *Journal of IASS*, 43: 93–100, 2002. 23
- [47] Tsutomu Kokawa. Field Experiment of Ice Dome Spanning 20-30 Meters. *International Journal of Offshore and Polar Engineering*, 12:264–270, 2002. 23
- [48] Tsutomu Kokawa. Ice shell construction for winter activity. *IASS-APCS 2003, Taipei, Taiwan, CD-ROM of International Symposium on New Perspective for Shell and Spatial Structure*, 2003. 23
- [49] Tsutomu Kokawa. State of the Art Developments in Ice Shell Construction. *CD-ROM: Proceedings of 17th Canadian Hydrotechnical Conference*, pages 973–982, 2005. 23
- [50] Tsutomu Kokawa and Kenji Murakami. Challenge to 20-m Span Ice Dome. *Proceedings of the IASS Symposium on Membran Structures and Space Frames, Osaka*, 1:297–304, 1986. 23
- [51] Johann Kollegger. Construction method for free-formed reinforced concrete shells. In F. del Pozo und A. de las Casas, editor, *10 years of progress in shell and spatial structures - 30 anniversary of IASS*. Madrid, 1989. 21
- [52] Johann Kollegger. Untersuchungen an einem Kunststoffhüllrohr für Spannglieder mit nachträglichem Verbund. *Bauingenieur*, 1994. 69
- [53] Johann Kollegger. Verfahren zur Herstellung von Schalen aus Beton und Eis. *Beton - Zement*, 1:18–22, 2005. 24
- [54] Stefan Krispel and Johann Kollegger. Bau einer Stahlbetonschale ohne Schalung. *Beton - Zement*, 2:24–29, 2006. 14, 24
- [55] M. Johnston, R. Frederking and G.W. Timco. Properties of decaying first-year sea ice at five sites in parry channel. *Proceedings of the 17th International Conference on Port and Ocean Engineering under Arctic Conditions*, 1:131–140, 2003. 26
- [56] Malcom Mellor, James H. Smith. Creep of Snow and Ice. *Physics of Snow and Ice: proceedings*, pages 843–855, 1967. 26
- [57] Herbert Mang. Flächentragwerke. In Gerhard Mehlhorn, editor, *Der Ingenieurbau - Rechenorientierte Baumechanik*. Verlag Ernst & Sohn, Berlin, 1996. 15
- [58] Melcom Mellor and David M.Cole. Stress/Strain/Time Relations for Ice under uniaxial Compression. *Cold Regions Science and Technology*, 6:207–230, 1983. 26
- [59] Nirmal K. Sinha. Rate sensitivity of compressive strength of columnar-grained ice. *Experimental Mechanics*, 21:209–218, 1981. 26
- [60] ÖNORM EN 1995-1-1. Allgemeine Regeln für den Holzbau. *Austrian Standards Institute*, 2009. 85
- [61] Oberndorfer. URL: <http://www.oberndorfer.at/>, May 2011. 61

- [62] Frei Otto. *Form-Kraft-Masse: Experimente*. Institut für leichte Flächentragwerke, 1990. 15, 20
- [63] Frei Otto. *Pneu und Knochen*. in IL35, Mitteilung des Instituts für leichte Flächentragwerke (IL), Universität Stuttgart, 1995. 20, 179
- [64] Paul Barrette and Chris Brassard. Flexural Strength of ice from the Rideau Canal: a laboratory Investigation. *Technical Report - CHC-TR-068*, 2009. 25, 26
- [65] Alf Pflüger. *Elementare Schalenstatik*. Springer-Verlag, 1981. 17, 18, 41, 52, 94, 171, 179, 180
- [66] Clemens Preisinger. *Numerical and experimental investigations regarding the transformation of flat slabs to double curved shells*. PhD thesis, Vienna University of Technology, 2006. 24
- [67] Ekkehard Ramm and Eberhard Schunk, editors. *Heinz Isler, Schalen*. vdf Hochschulverlag AG, ETH Zürich, 3. Auflage 2002. 15, 20, 21
- [68] W. Rautner and J. Ramsberger. Kuppelbau - ein Benchmark für Fertigteile. *Beton-Zement*, 1:36–38, 2006. 20
- [69] R.O. Ramseier. Growth and mechanical properties of river and lake ice. *Manuscript Report Series, No.40, Department of the Enviroment, Ottawa, Canada*, 1974. 25
- [70] Bernd Schneider. Ermittlung der Biegesteifigkeit und der Verformbarkeit von gerissenen Stahlbetonquerschnitten. Master's thesis, Vienna University of Technology, 2008. 42, 44
- [71] Florian Schrems. Experimentelle Untersuchung des viskoelastischen Verhaltens von Eis. Master's thesis, Vienna University of Technology, Institute for Mechanics of Materials and Structures, 2010. 26
- [72] S.J. Jones. The confined compressive strength of polycrystalline ice. *J. Glaciol.* 28, pages 171–177, 1982. 25
- [73] S.J. Jones. High strain-rate compression tests on ice. *J.Phys. B,1001*, 32:6099–6101, 1997. 25
- [74] Stephen J. Jones. Comparison of the strength of iceberg and other freshwater ice and the effect of temperature. *Technical Report TR-200607: NRC Institute for Ocean Technology; National Research Council Canada*, 2006. 25
- [75] Hans Straub. *Die Geschichte der Bauingenieurkunst: Ein Überblick von der Antike bis in die Neuzeit*. Birkhäuser Verlag, 1992. 14
- [76] ECONIC system. URL: [www.econicsystems.com](http://www.econicsystems.com), October 2009. 63

- [77] Takaya Suzuki, Tsutomu Kokawa, Koji Watanabe. Ice Pantheon Project 2010. In *Proceedings of the International Association for Shell and Spatial Structures (IASS) Symposium 2010, Shanghai*, 2010. 21, 23, 179
- [78] Teufelberger. URL: <http://www.teufelberger.com>, May 2011. 63
- [79] Teufelberger. Informationen und Produkte - Stahl- und Faserseile. URL: [http://www.teufelberger.com/uploads/tx\\_txconceptdownloads/10-05-19\\_stahl-faserseilkatalog.pdf](http://www.teufelberger.com/uploads/tx_txconceptdownloads/10-05-19_stahl-faserseilkatalog.pdf), May 2011. 63, 64, 186
- [80] Tsutomu Kokawa. Simplified formula for stationary creep deflection for ice dome. *20th International Conference on Port and Ocean Engineering under Arctic Conditions*, pages 177–186, 2009. 26
- [81] Tsutomu Kokawa, Osamu Itoh, Koji Watanabe. Ice-Shells-Review and Recent Application. *Jour*, 41:23–29, 2000. 23
- [82] Ventur. URL: <http://www.ventur.eu/>, May 2011. 50

# List of Figures

1.1	Ice Dome built during this thesis (pictures: Günter R. Wett) . . . . .	13
2.1	a) Examples of shells in nature b) Pantheon in Rome [29] . . . . .	14
2.2	Load transfer of a beam, an arch and a dome [21] . . . . .	16
2.3	a) Definition of the parameters in equation 2.2 and 2.3 by [28] b) Definition of the parameters in equation 2.4 and 2.5 by [65] . . . . .	18
2.4	Stresses in the slab and the hemispherical dome . . . . .	19
2.5	Definition of the sectional forces and moments . . . . .	19
2.6	Construction methods of shells by Otto [63] . . . . .	20
2.7	LumiLinna - Snow Castle in Kemi, Finland . . . . .	22
2.8	Construction sequence of Kokawa's ice dome construction method [77] .	23
2.9	Transforming a concrete plate into a shell . . . . .	24
2.10	Laboratory experiment . . . . .	24
2.11	Ice dome 2005 . . . . .	25
2.12	Stages of creep . . . . .	27
3.1	Basic principle of the new construction methods . . . . .	28
3.2	Map of Austria - Obergurgl . . . . .	29
3.3	Air temperature in Obergurgl . . . . .	30
4.1	Pneumatic formwork method - from the starting position to the finished shell . . . . .	32
4.2	Pneumatic formwork method - plan view . . . . .	33
4.3	Pneumatic formwork method - sectional view . . . . .	34
4.4	Correlation between $D_P$ and $D_S$ . . . . .	35
4.5	Meridian section forces $N_x$ [ $kN/m$ ] . . . . .	36
4.6	Hoop section forces $N_y$ [ $kN/m$ ] . . . . .	36
4.7	Section moments $M_x$ [ $kNm/m$ ] . . . . .	36

4.8	Section moments $M_y$ [kNm/m]	37
4.9	Spherical cap with the central angle $\theta$	38
4.10	Correlation between $M/A$ and the central angle $\theta$ and $Z$ and $\theta$	39
4.11	Schematic drawing of the force distribution of a hemispherical dome under self weight	40
4.12	Meridian and hoop forces in the finished shell structure	40
5.1	Glued seams - specimen 1 to 7	43
5.2	Sewed seams - specimen 9 to 11	44
5.3	Welded seams - specimen 12 to 14	45
5.4	Load-displacement diagram of the 1 <sup>st</sup> series of experiments	45
5.5	Load-displacement diagram of the 2 <sup>nd</sup> series of experiments	46
5.6	Experiment setup of the 3 <sup>rd</sup> series of experiments	47
5.7	Stress-strain diagram of the 3 <sup>rd</sup> series of experiments	48
5.8	Change of the Young's modulus the 3 <sup>rd</sup> series of experiments	49
5.9	Change of the Young's modulus the 3 <sup>rd</sup> series of experiments	49
5.10	Change of the Poisson ratio the 3 <sup>rd</sup> series of experiments	50
5.11	Pneumatic formwork a) schematic drawing of the main parts of the pneumatic formwork b) Picture of the inflated pneumatic fomwork	51
5.12	Production of the pneumatic formwork	52
5.13	Static systems: circular cylinder and spherical shell [65]	52
5.14	Different shapes of the pneumatic formwork	53
5.15	Pneumatic formwork reinforced with ropes and chains	54
6.1	Small wooden model	55
6.2	Large wooden model	56
6.3	Small timber model - erection process	57
6.4	Large timber model - erection process	57
6.5	Pneumatic formwork: a) two concentric circles glued together on the their edges for the small wooden model b) hemispherical shaped membrane for the large wooden model	58
6.6	Tendons in circumference direction: a) in the small wooden model b) in the large wooden model	58
6.7	Sketch of the joint in the cirumference direction	59
6.8	Cylindrical element a) wooden rod in the radial interfaces b) aluminum tube in the circumference direction	60



6.9	Trapezoid . . . . .	62
6.10	Sketch of a precast element . . . . .	62
6.11	Precast concrete element - mold, reinforcement and ducts a) prior to and b) during casting . . . . .	62
6.12	Load-displacement-diagram of a tested steel rope with a diameter of 5 mm . . . . .	65
6.13	Details of the anchorage system in the concrete shell a) 2 part clamp ring on a radial tendon b) compression spring to regulate the tension in the tendons in circumference direction . . . . .	66
6.14	Pictures of the assembly on site . . . . .	67
6.15	Arrangement of the 96 precast elements . . . . .	68
6.16	Details of the concrete shell a) steel ring to anchor the tendons in radial direction b) winch . . . . .	69
6.17	Erection processs of the concrete shell . . . . .	70
6.18	The finished concrete shell . . . . .	71
6.19	Hose water level . . . . .	72
6.20	Erection process of the concrete shell . . . . .	73
6.21	Correlation between the lifted weight and the air pressure during the erection process of the concrete shell . . . . .	74
6.22	Measured and theoretically calculated air pressure during the erection process of the concrete shell . . . . .	74
7.1	Pneumatic formwork of the large ice shell a) inflated with air b) pro- tected with a layer of styrofoam plates . . . . .	77
7.2	Schematic sketch of the ice plate and the ice elements . . . . .	77
7.3	Formwork of the large ice shell a) assembly of the inner formwork b) positioned formwork . . . . .	78
7.4	Climate data from 14 <sup>th</sup> to 28 <sup>th</sup> December 2008[1] . . . . .	78
7.5	Sectional views for the basic sketch in Figure 7.2 . . . . .	79
7.6	Picture of a) the ice plate and b) the individual ice elements . . . . .	80
7.7	Spring - anchorages of the tendons in radial direction a) sketch of the large ice shell b) picture of the small ice shell . . . . .	81
7.8	Drawing of the cross section before and after the erection process . . .	82
7.9	Winches a) built-in steel parts to anchore the winches b) winch . . . .	82
7.10	Erection of the small ice shell . . . . .	83
7.11	Finished small ice shell . . . . .	84

7.12	Lifting process of the large ice shell . . . . .	85
7.13	Sketches of the wooden inner formwork . . . . .	85
7.14	Stresses in the wooden board . . . . .	86
8.1	Key elements of the segment lift method . . . . .	88
8.2	Static system during the lifting process . . . . .	90
8.3	Correlation between the stresses and the size of the rise . . . . .	91
8.4	Variation of the rises taken into account in Figure 8.7 . . . . .	92
8.5	Distribution of the hoop forces . . . . .	93
8.6	Distribution of the meridian forces . . . . .	93
8.7	Section forces of the finished dome considering different sizes of the rise	94
8.8	Distribution of the hoop forces . . . . .	95
8.9	Distribution of the meridian forces . . . . .	96
9.1	Specimen number 4 a) mold b) reinforcement . . . . .	98
9.2	Lifting devices for the ice beams a) U-shaped line supports b) lifting device with hydraulic jack . . . . .	99
9.3	Setup of the specimens 1 to 4 . . . . .	99
9.4	Specimens during the creep process a) specimen no. 1 b) specimen no. 2 c) specimen no. 4 d) specimen no. 4 . . . . .	100
9.5	Deformations of specimen 1 . . . . .	101
9.6	Deformations of specimen 2 . . . . .	102
9.7	Deformations of specimen 3 . . . . .	102
9.8	Deformations of specimen 4 . . . . .	104
9.9	Percentage of the measured deformation of the calculated deformation in the final cracking state for specimen 1 to 4 . . . . .	104
9.10	Height difference between the ends of the beams and their supports over the time . . . . .	105
9.11	Rise of the specimen 1 to 4 before and after the creeping process . . .	106
9.12	Reinforcement ratio of the specimens 1 to 4 and the segments of the ice shell . . . . .	106
10.1	Plan view of the ice segments . . . . .	109
10.2	Preparations for making the ice plate a) leveling the working surface, winter 2010/11 b) mold for the ice plate, winter 2009/10 c) pneumatic formwork folded and positioned under the future ice plate, winter 2009/10 d) U-shaped steel beams with rods in order to lift the future ice segments with the lifting device, winter 2010/11 . . . . .	110

10.3 Producing ice, winter 2010/11 . . . . .	111
10.4 Climate data from 18 <sup>th</sup> to 25 <sup>th</sup> December 2009 . . . . .	112
10.5 Climate data from 7 <sup>th</sup> to 14 <sup>th</sup> December 2010 . . . . .	113
10.6 Arrangement of the reinforcement in an ice segment . . . . .	114
10.7 Reinforcement in the middle of the cross section of the ice segments a) inserting the reinforcement, winter 2010/11 b) arrangement of the reinforcement and the rope clips, winter 2010/11 c) reinforcement and outside formwork, winter 2009/10 d) reinforcement and assembly brack- ets of the inner formwork, winter 2009/10 . . . . .	114
10.8 Cutting the ice segments a) winter 2009/10 b) winter 2009/10 c) winter 2010/11 d) winter 2010/11 . . . . .	115
10.9 Creating the cuts which served as predetermined breaking points, winter 2009/10 . . . . .	116
10.10 Sixteen individual ice segments, winter 2009/10 . . . . .	116
10.11 Position of the pneumatic formwork . . . . .	117
10.12 Production of the pneumatic formwork . . . . .	118
10.13 Bending moments per width in the ice segment for different contact areas of the pneumatic formwork . . . . .	119
10.14 Stresses in the ice segment during lifting and creeping . . . . .	119
10.15 Normal stresses $S_{11}$ in $N/m^2$ . . . . .	120
10.16 Measured and calculated deformations . . . . .	122
10.17 Creeping process of the ice segments, winter 2009/10 . . . . .	123
10.18 Creeping process of the ice segments, showing their respective number, winter 2009/10 . . . . .	123
10.19 Deflection of the ice segment 1 due to creeping in a certain period of time	124
10.20 Deflection of the ice segment 16 due to creeping in a certain period of time . . . . .	124
10.21 Change of the rise of all 16 segments and the air pressure in the first 100h after inflating the formwork . . . . .	125
10.22 Climate data from 12 <sup>th</sup> to 17 <sup>th</sup> January 2010 . . . . .	126
10.23 Lifting device . . . . .	127
10.24 Description of a stroke with the lifting device . . . . .	128
10.25 U-shaped steel beams and threaded rods situated in the ice segment . .	128
10.26 Position of the U-shaped steel beams and the line supports from the stacks of wood . . . . .	129
10.27 Lifting the ice segments by means of the lifting devices . . . . .	129

10.28	Exaggerated sketch of the cracking pliers . . . . .	130
10.29	Usage of the <i>cracking pliers</i> . . . . .	131
10.30	Placing the ice segments on stacks of wood . . . . .	131
10.31	Ice segments after lifting a) positioned on the stacks of wood b) ends of the ice segments without support . . . . .	132
10.32	Measured and calculated deformations . . . . .	133
10.33	Initial deformation of the ice segment [m] . . . . .	134
10.34	Moments per width in the ice segment . . . . .	135
10.35	Normal stresses S11 in $N/m^2$ . . . . .	136
10.36	Normal stresses S11 in $N/m^2$ . . . . .	136
10.37	Creeping process of the ice segments . . . . .	137
10.38	Development of the rise with age of all sixteen segments . . . . .	138
10.39	Creeping process of the ice segments . . . . .	138
10.40	Mean value of the rise . . . . .	139
10.41	Climate data from 15 <sup>th</sup> to 23 <sup>rd</sup> December 2010 . . . . .	140
10.42	Deformation measured on the 22 <sup>nd</sup> of December 2010 . . . . .	141
10.43	Deformation measured on the 11 <sup>th</sup> of January 2011 . . . . .	141
10.44	Climate data from 20 <sup>th</sup> December 2010 to 17 <sup>th</sup> January 2011 . . . . .	142
10.45	Schematic drawing of the mounting tower . . . . .	143
10.46	Building the wooden mounting tower . . . . .	144
10.47	Compression arch with tension chain . . . . .	144
10.48	Connection between the tension chain and the ice segment . . . . .	145
10.49	Tension chains . . . . .	145
10.50	Force - strain diagram of the chain . . . . .	146
10.51	Position of the chain . . . . .	147
10.52	Impact on the ice segments due to an imposed horizontal support dis- placement . . . . .	148
10.53	Simplified static system of chain subjected to line load . . . . .	149
10.54	Assumed shape of the membrane in the area of the chains . . . . .	149
10.55	Lifting ice segments, winter 2009/10 . . . . .	150
10.56	Lifting the ice segments, winter 2010/11 . . . . .	151
10.57	Lifting process of an ice segment . . . . .	152
10.58	Statical systems of the different positions . . . . .	153

10.59	Stresses in the ice segment during the lifting process with the crane . .	154
10.60	Forces in the chains and the cranes during the lifting process . . . . .	154
10.61	Ice segments fixed to the mounting tower a) immediately after lifting b) with gaps already partly filled . . . . .	155
10.62	Last working stage a) filling the gaps b) detaching the ice shell form the mounting tower . . . . .	156
10.63	Last working stage a) dismantling the mounting tower b) removing the temporary tension chains . . . . .	157
10.64	Finished ice shell a) and b) picture: Günter R. Wett . . . . .	158
10.65	Meridional forces in the actual shell structure . . . . .	159
10.66	Hoop forces in the actual shell structure . . . . .	159
10.67	Moments $M_y$ in the actual shell structure . . . . .	160
10.68	Moments $M_x$ in the actual shell structure . . . . .	160
10.69	Opening in the ice dome on the side facing the sun . . . . .	161
10.70	Monitoring the base diameter and the height of the ice dome . . . . .	162
10.71	Monitoring the thickness of the ice dome . . . . .	163
10.72	Temperature in February 2011 . . . . .	164
10.73	Sunshine duration from December 2010 to March 2011 . . . . .	165
11.1	Ice Dome built within this thesis (pictures: Günter R. Wett) . . . . .	169
11.2	Size of the rise during the field experiments in winter 2009/10 and 2010/11	169

# List of Tables

2.1	Material properties of ice . . . . .	26
4.1	Overview of the experiments . . . . .	34
4.2	Overview of required air pressure . . . . .	37
5.1	Data sheet of 641 Polyplan Complan® [17] . . . . .	42
5.2	1 <sup>st</sup> series of experiments . . . . .	44
5.3	2 <sup>nd</sup> series of experiments . . . . .	46
5.4	3 <sup>rd</sup> series of experiment . . . . .	47
6.1	Precast concrete parts - material properties [10] . . . . .	61
6.2	Dimensions of the precast elements . . . . .	63
6.3	Properties of the steel ropes produced by the company Teufelberger [79] . . . . .	64
6.4	Young's modulus of a tested steel rope with a diameter of 5 mm during 5 load cycles . . . . .	64
6.5	Results of the load tests carried out on different anchorage systems for ropes . . . . .	66
6.6	Length of the tendons in circumference direction . . . . .	69
6.7	Necessary tensile force at the active end during tensioning . . . . .	70
9.1	Dimensions of the four specimens . . . . .	97
9.2	Moments and stresses in the specimen 1-4 . . . . .	100
10.1	Percentage of the changes . . . . .	163

# Appendix A

## Pneumatic Formwork Method

This appendix includes drawings and sketches of the experiments carried out with the Pneumatic Formwork Method.

All drawings are to scale and the scale is mostly given on the drawing header. Unless it is noted otherwise on the drawing, the dimensions are given in centimeters.

This appendix is structured as following:

### **A.1 Concrete shell (3)**

### **A.2 Ice shells (10)**

### **A.3 Pneumatic formwork (2)**

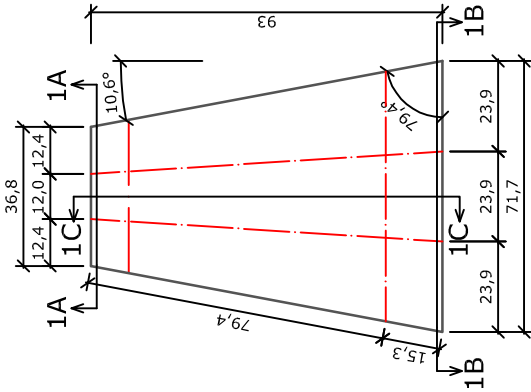
(The number in the brackets represents the number of drawings on this topic)



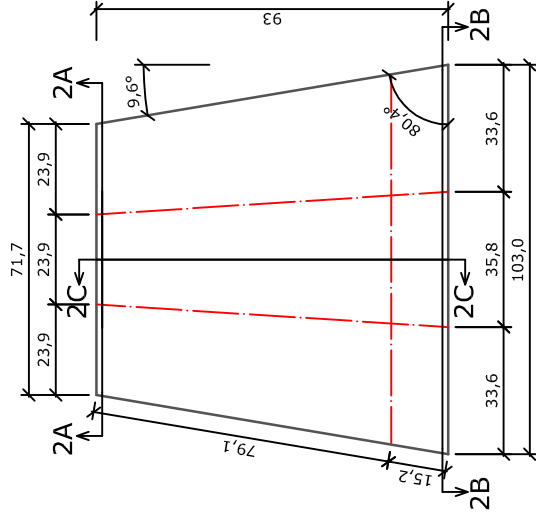
## A.1 Concrete shell

- Betonkuppel - Betonfertigteile - Typ 1 bis 6 (1)
- Betonkuppel - Betonfertigteile - Sonderelemente 1S bis 6S (1)
- Betonkuppel - Grundriss-Seilnummern (1)

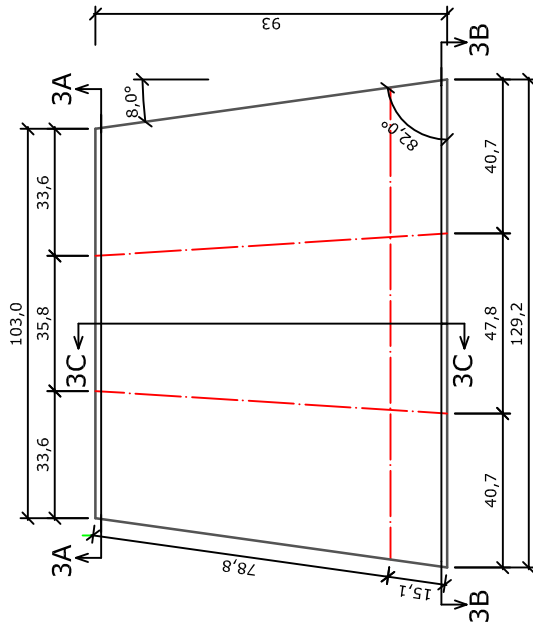
## Elementtyp 1



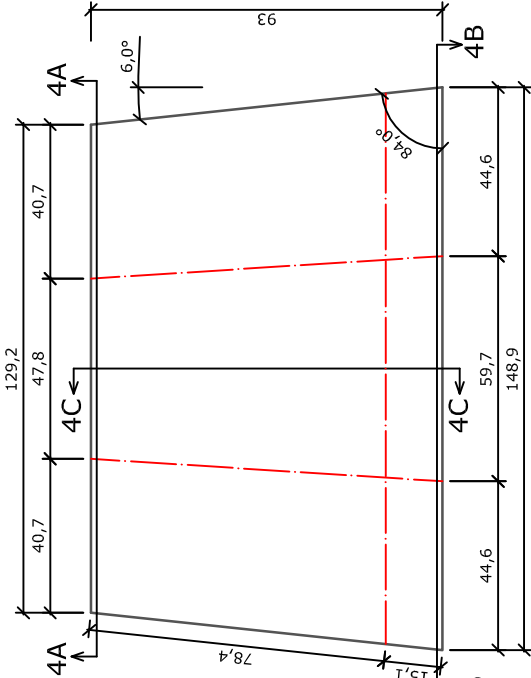
Elementtyp 2



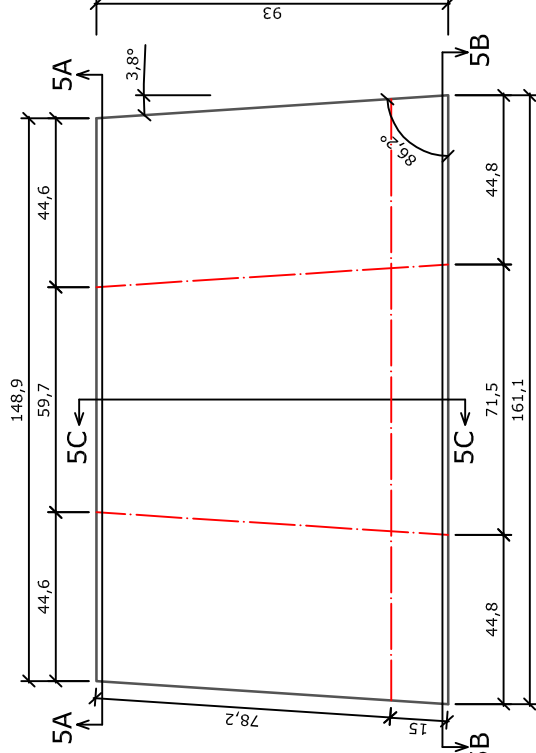
Elementtyp 3



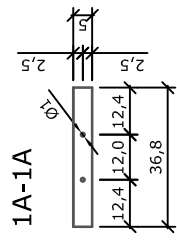
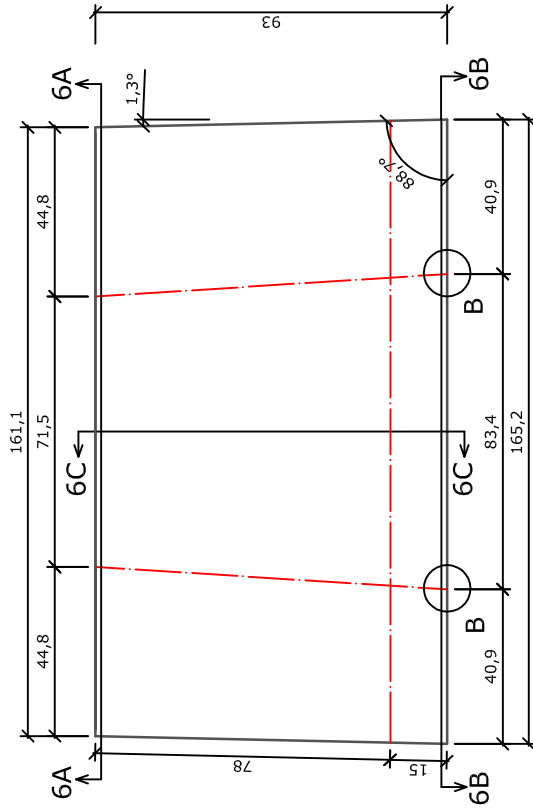
Elementtyp 4



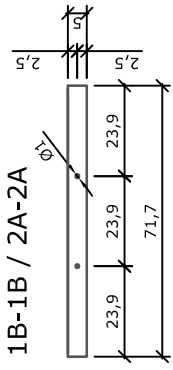
Elementtyp 5



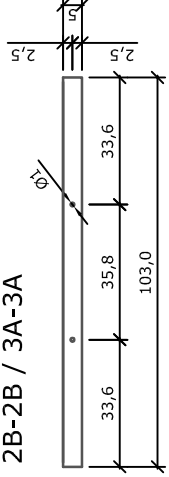
Elementtyp 6



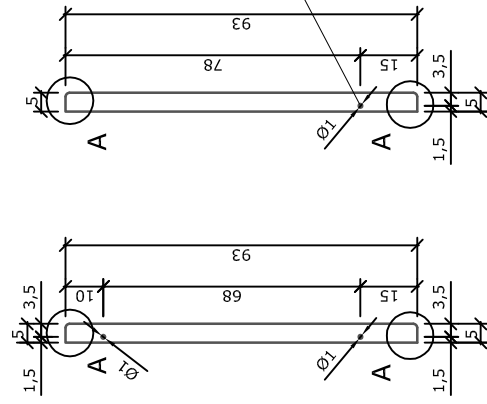
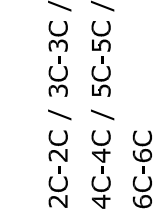
1A-1A



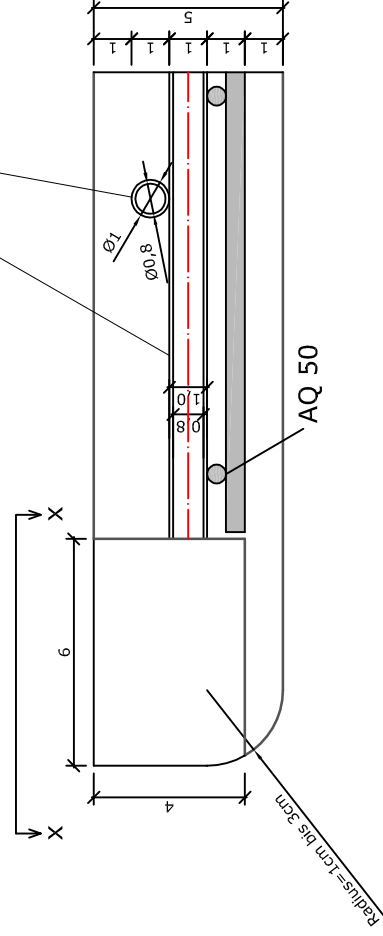
1B-1B / 2A-2A



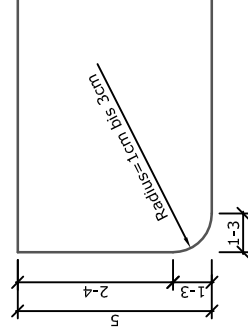
2B-2B / 3A-3A



Detail B 1:2 Randausführung für Elementtyp 6



Detail A 1:2

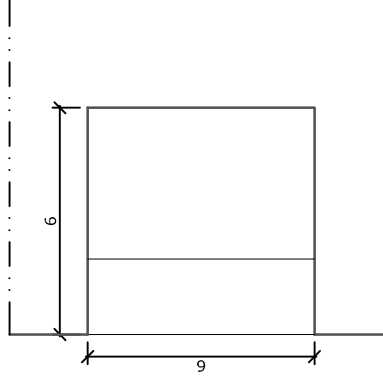



Bewehrung der Fertigteile  
mit AQ 50 an der Unterseite  
gemäß Detail B

Spanngliedachse

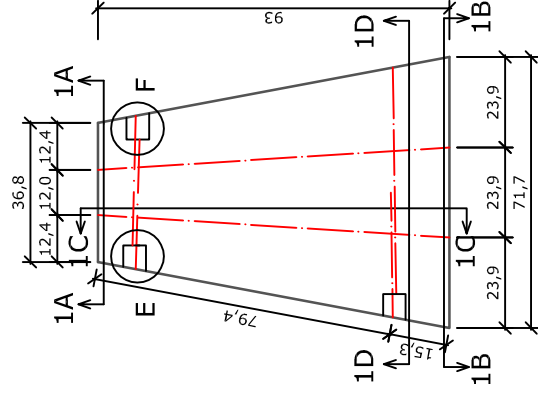
Maße in cm

Draufsicht X-X 1:1

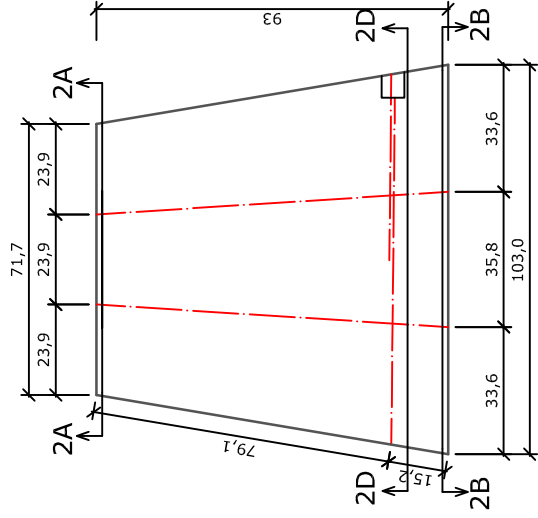


AENDREZ-INDEX-C AENDREZ-INDEX-B AENDREZ-INDEX-A AENDREZ-INDEX-E		AENDRESI AENDRESI AENDRESI AENDRESI	AENDDAAT AENDDAAT AENDDAAT AENDDAAT
Aenderung:      Bezeichnung:		erstl.: Datum:	
Abgabedatum: 1:20/7:2		Plannr.: 20.10.08	Planart: DETAILPLAN
<b>INSTITUT FÜR TRAKONSTRUKTIONEN   BETONBAU</b> Technische Universität Wien, Karlsplatz 13/712, 1040 Wien Tel. 0659/3772469      email: stollinger@tuwien.ac.at			
<div style="text-align: right;">  </div>			
Bauvorhaben: <b>BETONKUPPEL</b>		pos. Phase:  GZ:	KONT. BEF. SWERB. Form-Nr.: U 0 0 1
Planinhalt: <b>BETONFERTIGTEILELEMENTE</b> TYP 1 BIS 6			

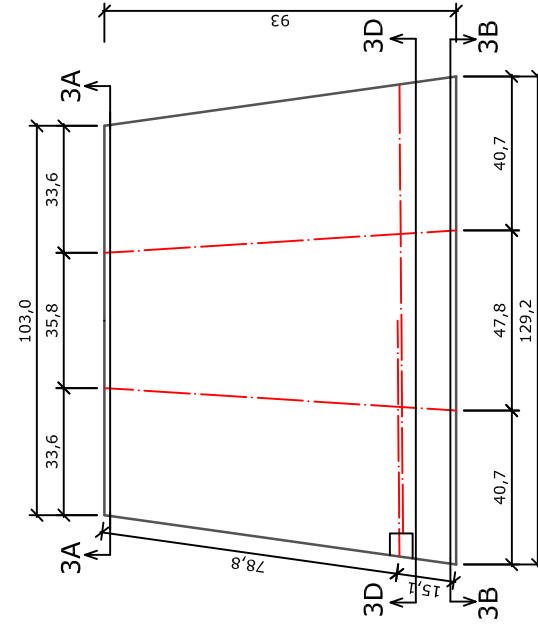
## Elementtyp (1S)



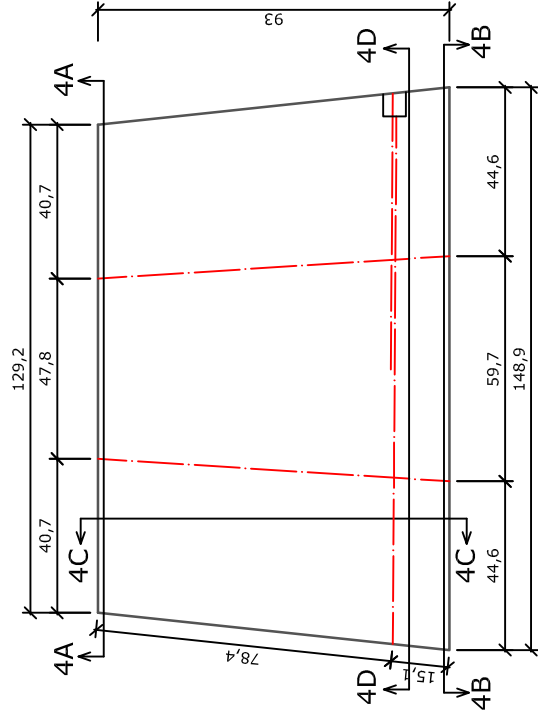
## Elementtyp (2S)



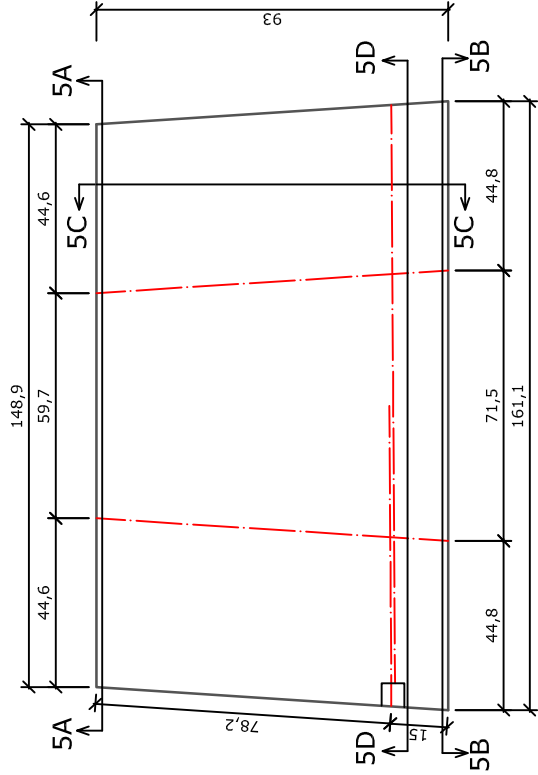
## Elementtyp (3S)



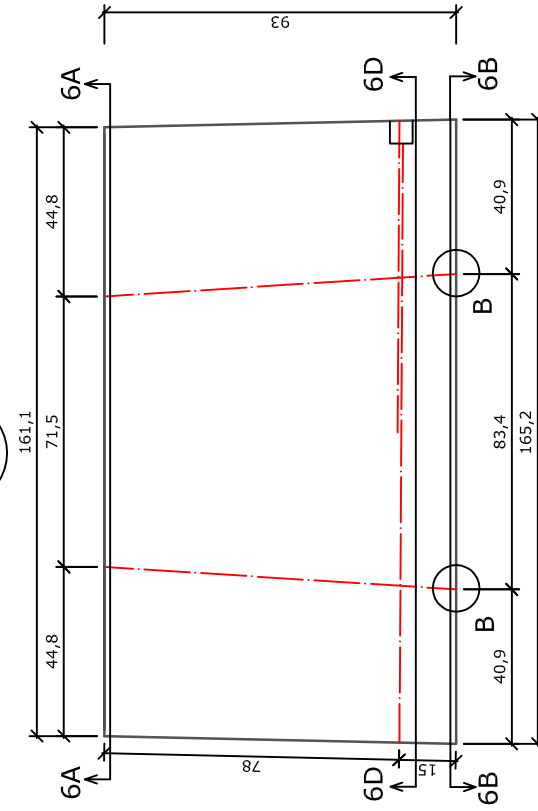
## Elementtyp (4S)



## Elementtyp (5S)



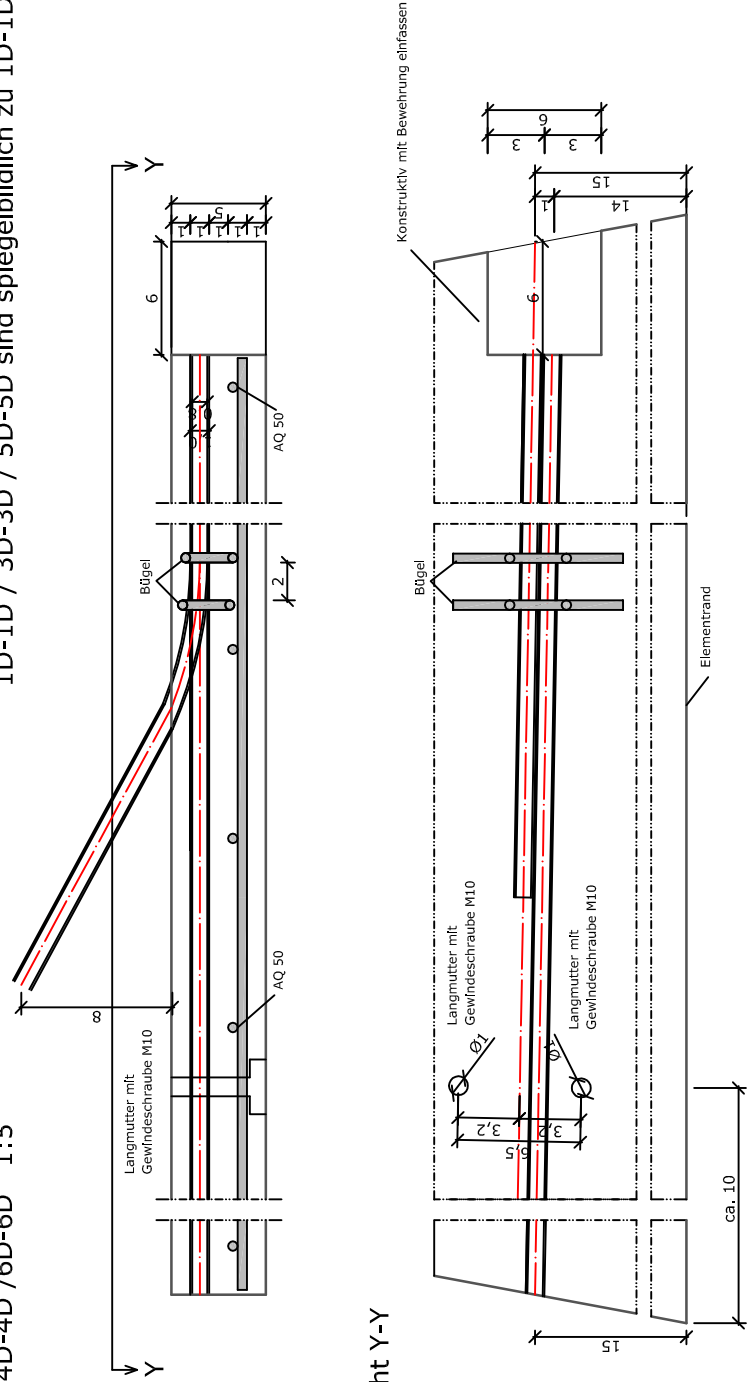
## Elementtyp 65



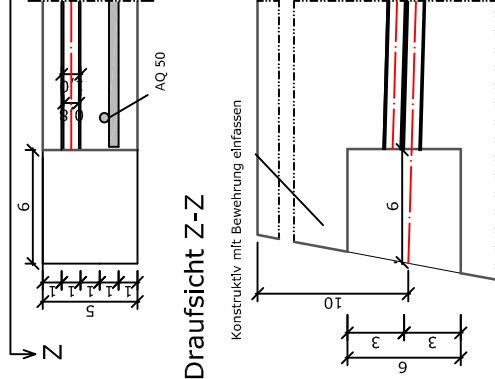
2D-2D / 4D-4D / 6D-6D 1:5

1D-1D / 3D-3D / 5D-5D sind spiegelbildlich zu 1D-1D

## Draufsicht Y-Y

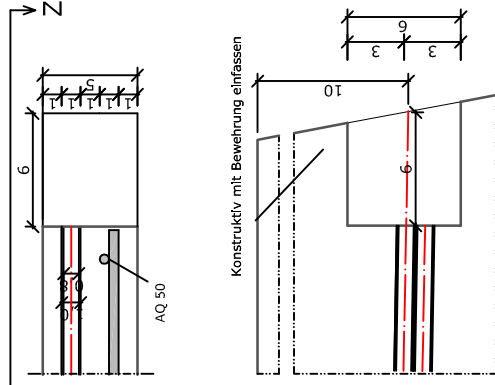


Detail E 1:5

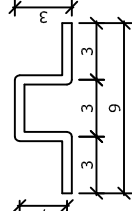


## Draufsicht Z-Z

Detail F 1:5

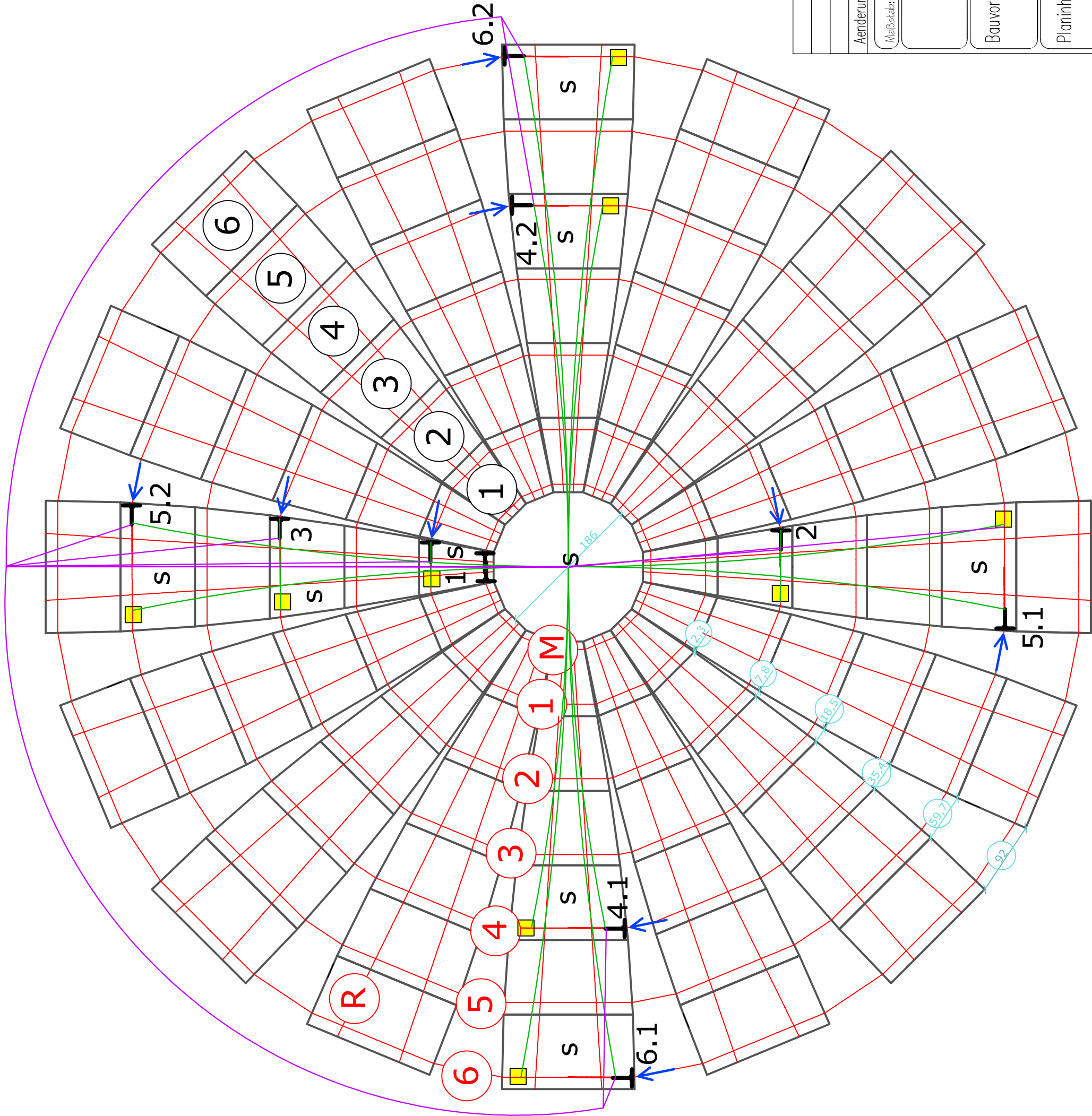


Bügel 1:5



Standardelemente		Sonderelemente	
Elementtyp	Anzahl	Elementtyp	Anzahl
①	15 Stück	①S	1 Stück
②	15 Stück	②S	1 Stück
③	15 Stück	③S	1 Stück
④	14 Stück	④S	2 Stück
⑤	14 Stück	⑤S	2 Stück
⑥	14 Stück	⑥S	2 Stück

[illegible]



Spanngliedachse

Seilwinde

Feder mit Schalter

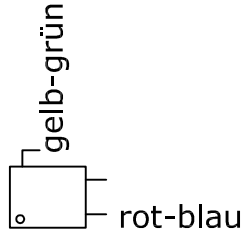
S Sonderelement

Einzugsrichtung der Seile

2 poliges Kabel

3 poliges Kabel

Schalter



C	AENDBEZ-INDEX-C	AENDERST	AENDDAT
B	AENDBEZ-INDEX-B	AENDERST	AENDDAT
A	AENDBEZ-INDEX-A	AENDERST	AENDDAT
Aenderung: Bezeichnung:		erst.:	Datum:
Maßstab: 1:50	Datum: 20.11.08	Planart: ÜBERSICHTSPALN	erst.: DALLINGER
INSTITUT FÜR TRAGKONSTRUKTIONEN I BETONBAU Technische Universität Wien, Karlsplatz 13/212, 1040 Wien Tel. 0650/3172489 email: sdalling@mail.tuwien.ac.at			
Bauvorhaben: BETONKUPPEL		zug. Pläne:	
		GZ:	
Planinhalt: GRUNDRISS-SEILNUMMER		Plan-Nr.:	BÜTEIL
		Ü	0 0 1

## A.2 Ice shells

- Große Eiskuppel - Grundriss (1)
- Große Eiskuppel - Schnitt A-A, Detail D (1)
- Große Eiskuppel - Detail B (1)
- Große Eiskuppel - Detail C (1)
- Kleine Eiskuppel - Grundriss (1)
- Kleine Eiskuppel - Schnitt A-A, Detail B,C,D (1)
- Eiskuppeln - Holzabschalung (1)
- Große Eiskuppel - Kopplungsstelle (1)
- Kleine Eiskuppel - Kopplungsstelle (1)
- Eiskuppel - Seilwindenaufstandsfläche (1)

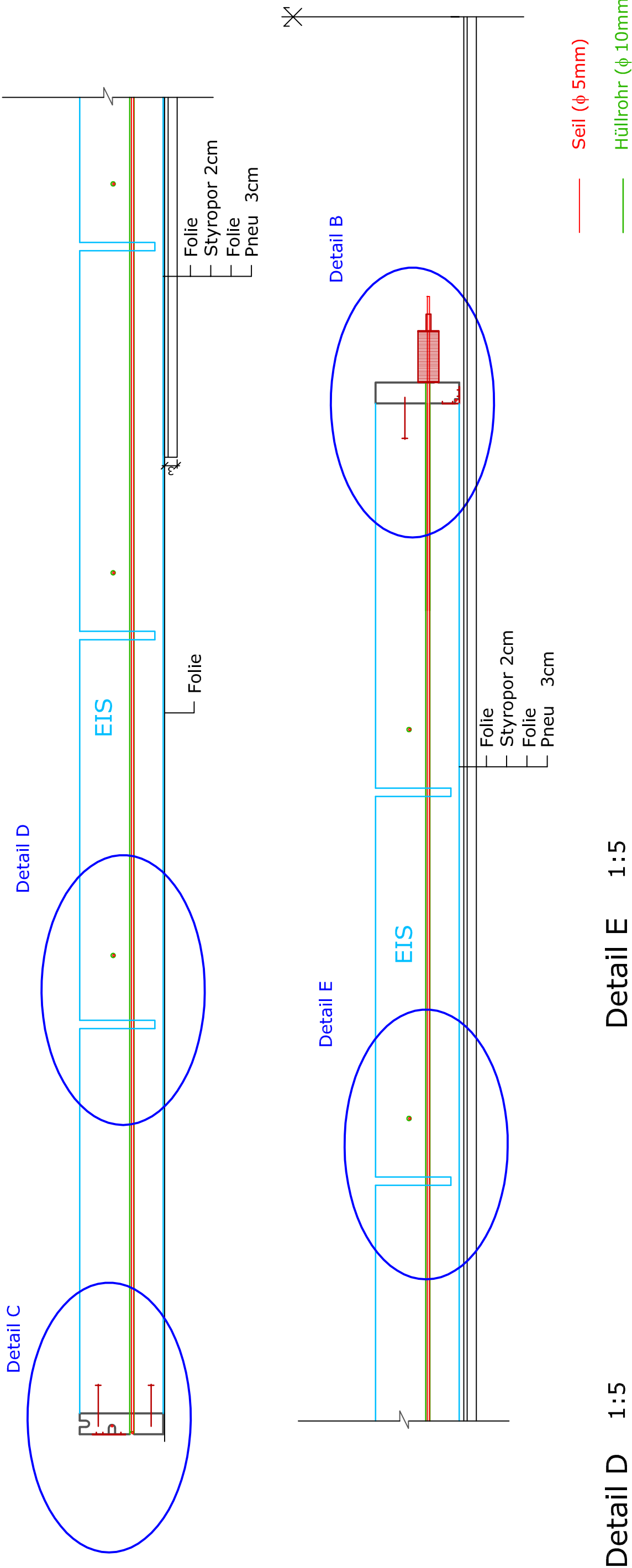


# Große Eiskuppel

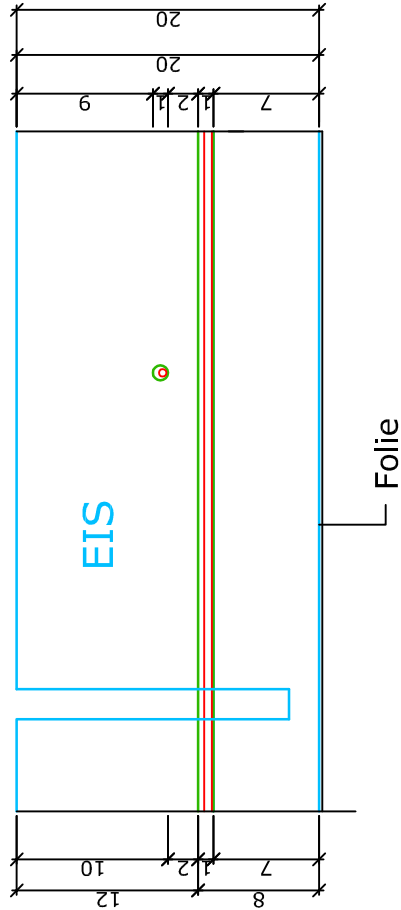
# GRUNDRISS



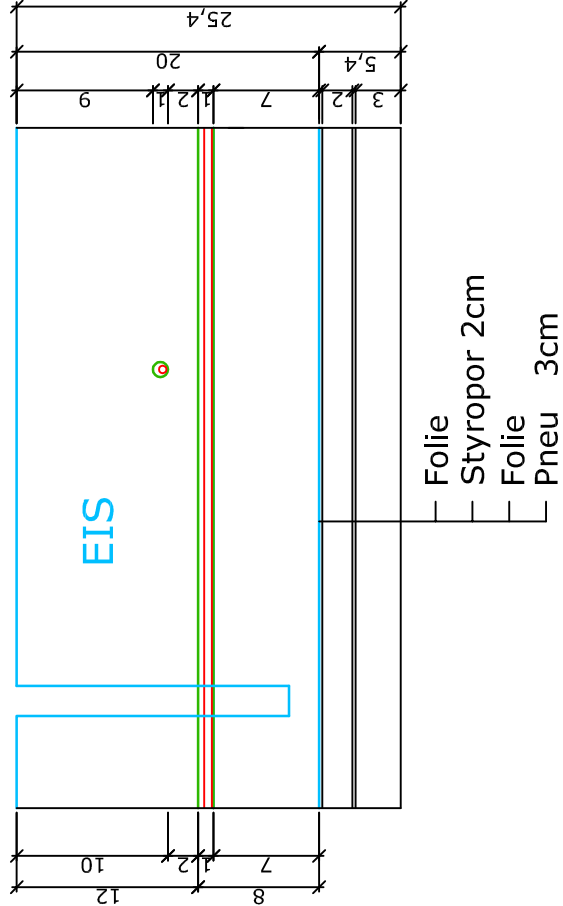
Schnitt A-A 1:10



Detail D 1:5



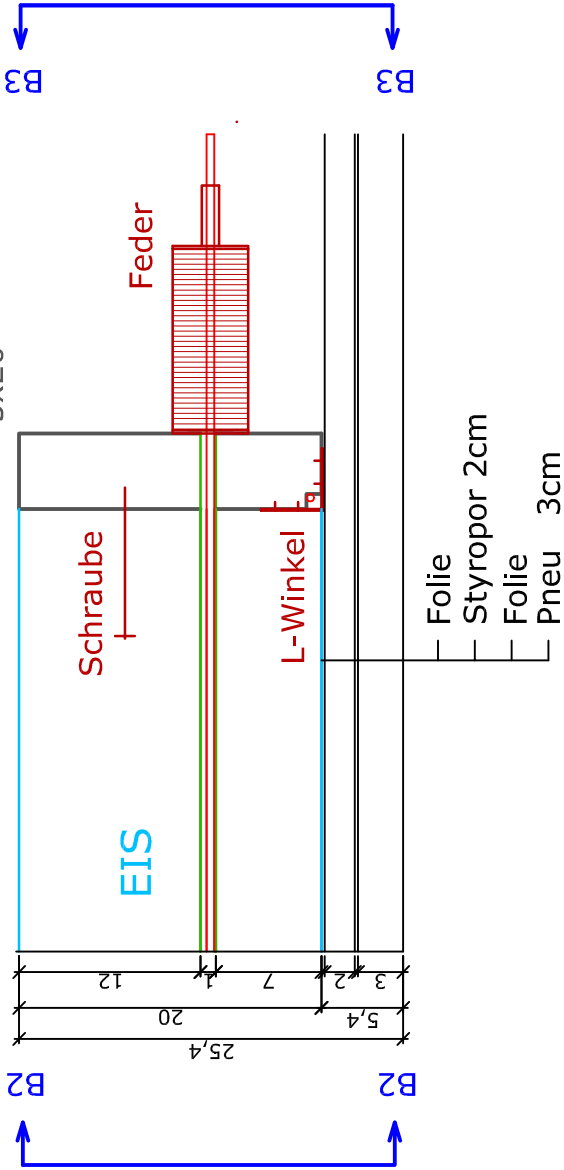
Detail E 1:5



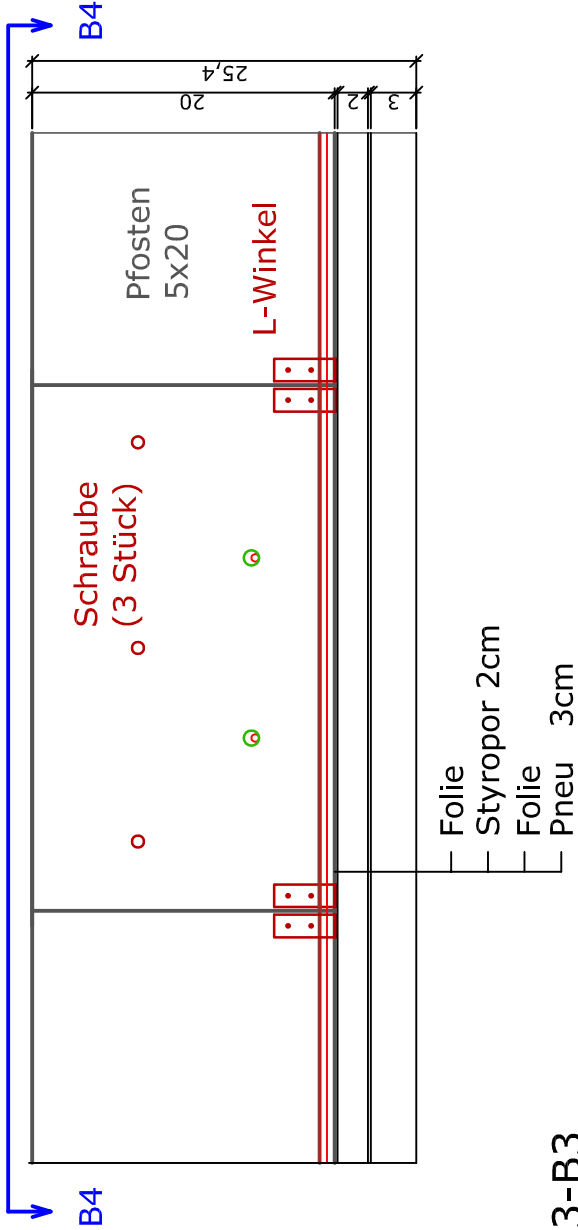
		AENDBEZ-INDEX-C	AENDERST	AENDDAT
		AENDBEZ-INDEX-B	AENDERST	AENDDAT
		AENDBEZ-INDEX-A	AENDERST	AENDDAT
Aenderung:	Bezeichnung:		erst.:	Datum:
Maßstab:	1:10/1:5	Datum:	20.11.08	Planart: DETAILPLAN
erst.: DALLINGER				
INSTITUT FÜR TRAKONSTRUKTIONEN I BETONBAU				
Technische Universität Wien, Karlsplatz 13/212, 1040 Wien				
Tel. 0650/3172489 email: sdalling@mail.tuwien.ac.at				
Bauvorhaben: Große Eiskuppel		zug. Pläne:		
		GZ:		
Planinhalt:		Plan-Nr.:	BÜTEL	INDEX
Schnitt A-A		Ü	0	0
Detail D		Ü	0	1

Detail B 1:5

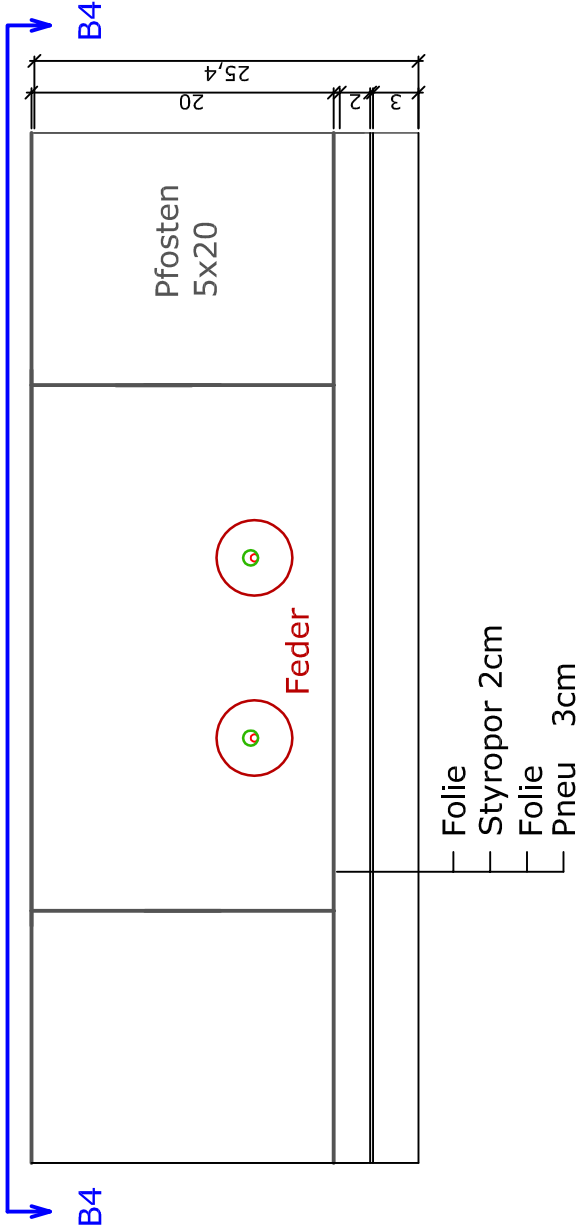
B1-B1



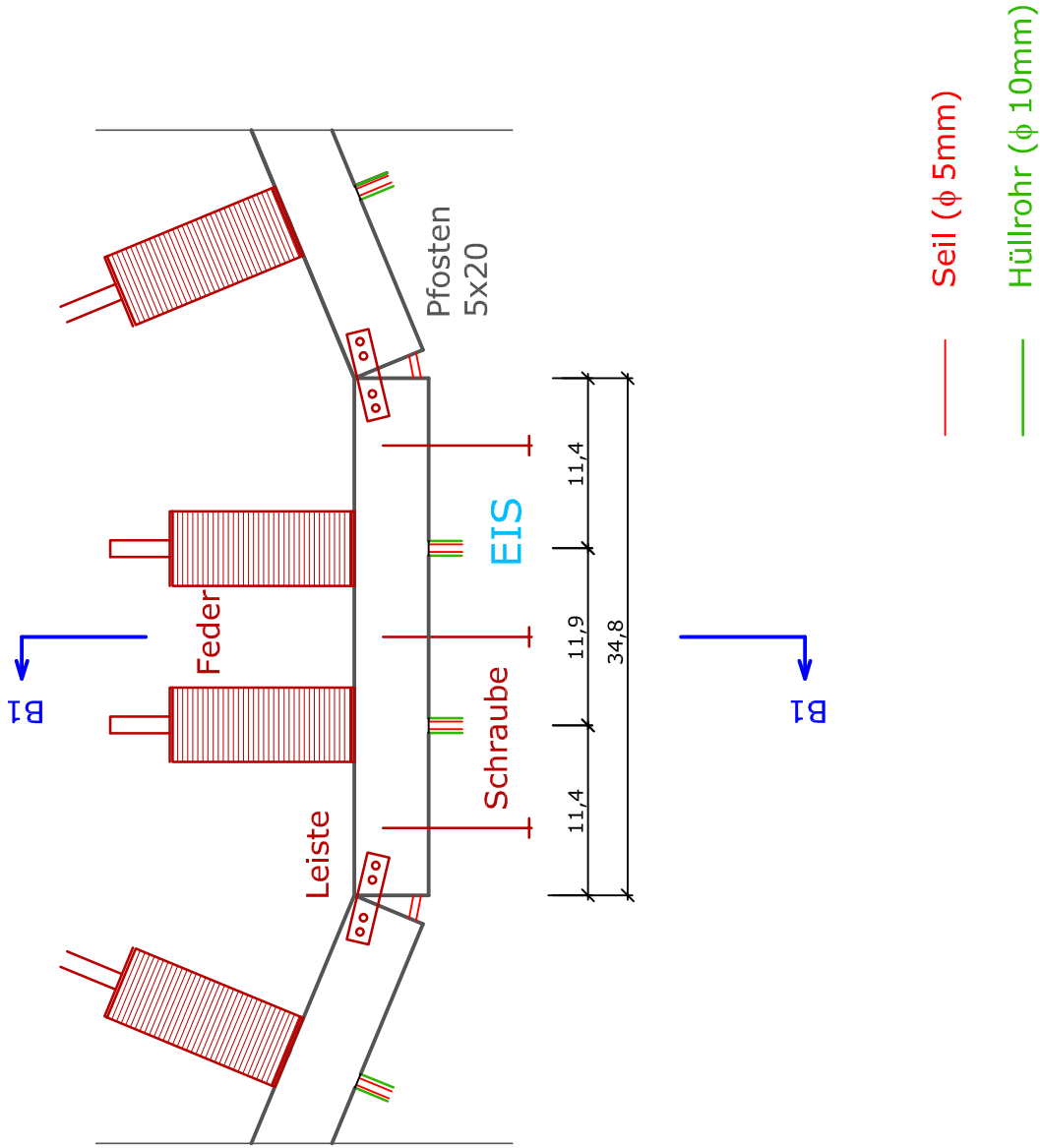
B2-B2







B3-B3



B4-B4

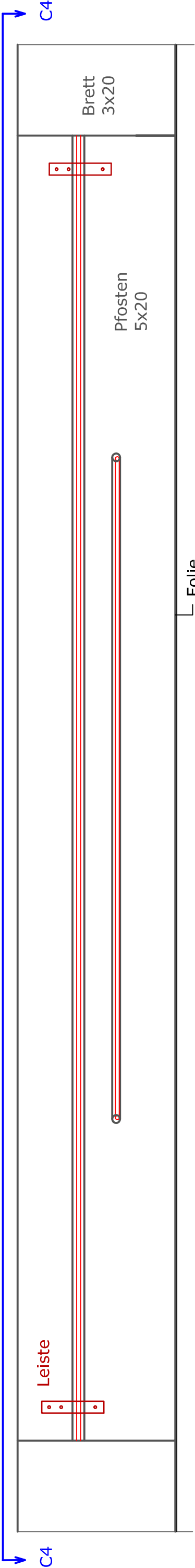


	AENDBEZ-INDEX-C	AENDERST	AENDDAT
	AENDBEZ-INDEX-B	AENDERST	AENDDAT
	AENDBEZ-INDEX-A	AENDERST	AENDDAT
Aenderung:	Bezeichnung:	erst.:	Datum:
Maßstab: 1:5	Datum: 20.11.08	Planart: DETAILPLAN	erst.: DALLINGER
INSTITUT FÜR TRAGKONSTRUKTIONEN I BETONBAU Technische Universität Wien, Karlsplatz 13/212, 1040 Wien Tel. 0650/3172489 email: sdalling@mail.tuwien.ac.at			
			
Bauvorhaben: Große Eiskuppel		zug. Pläne:	
		GZ:	
Planinhalt: Detail B		Plan-Nr.:	BÜTEIL
		Ü	0 0 1
			INDEX

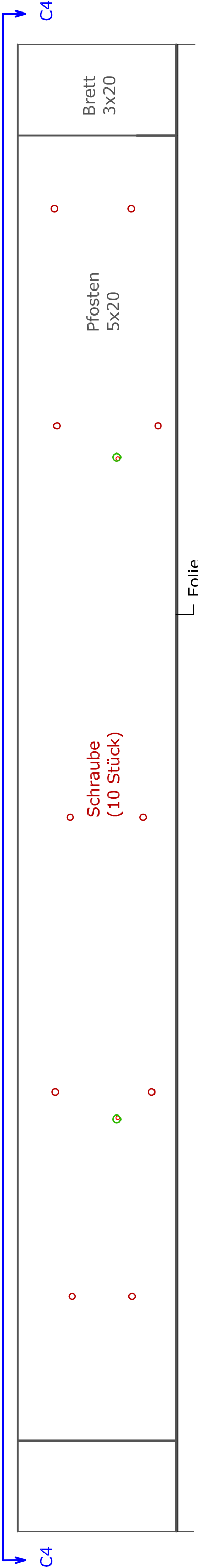


Detail C 1:5

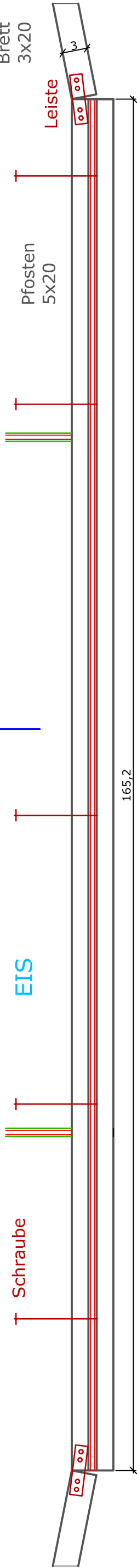
C2-C2



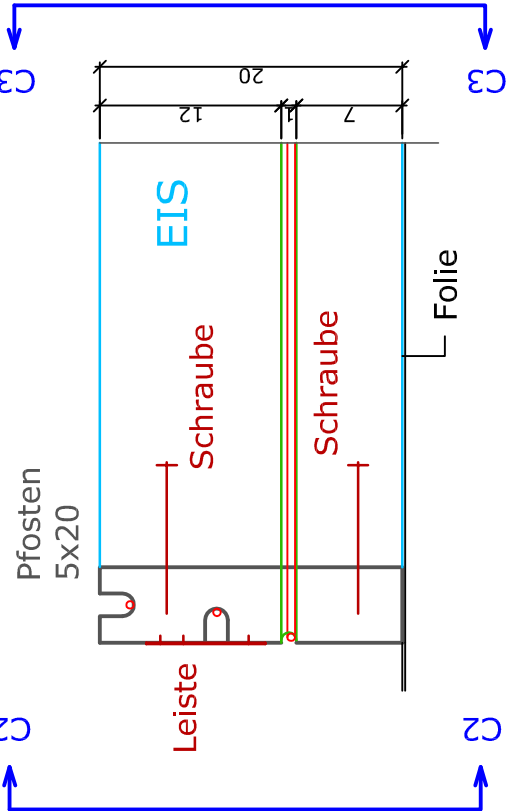
C3-C3



C4-C4



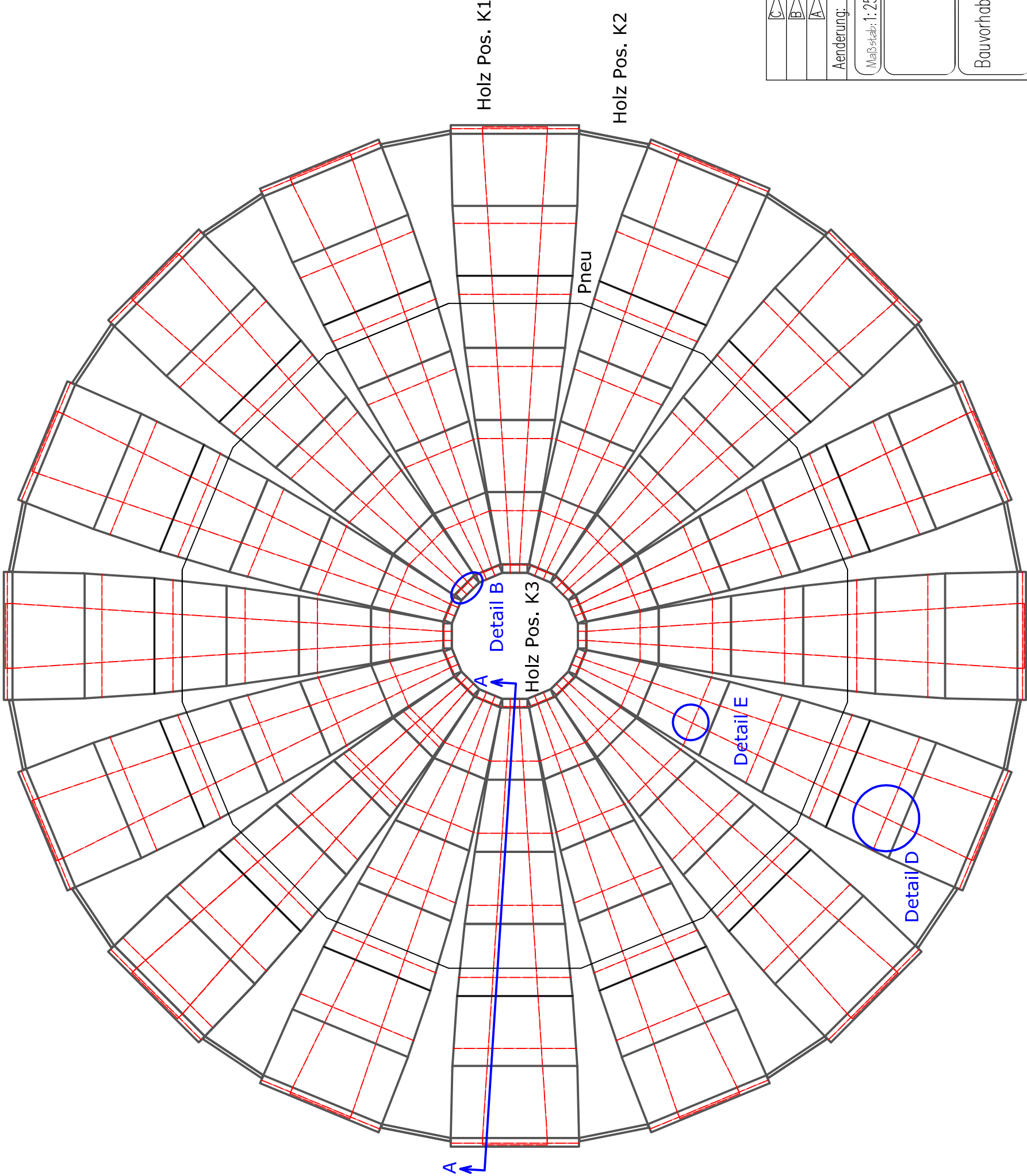
C1-C1



- Seil ( $\phi$  5mm)
- Hüllrohr ( $\phi$  10mm)

	AENDBEZ-INDEX-C	AENDERST	AENDDAT
	AENDBEZ-INDEX-B	AENDERST	AENDDAT
	AENDBEZ-INDEX-A	AENDERST	AENDDAT
Aenderung:	Bezeichnung:	erst.:	Datum:
Maßstab: 1:5	Datum: 20.11.08	Planart: DETAILPLAN	erst.: DALLINGER
INSTITUT FÜR TRAGKONSTRUKTIONEN I BETONBAU Technische Universität Wien, Karlsplatz 13/212, 1040 Wien Tel. 0650/3172489 email: sdalling@mail.tuwien.ac.at			
TU WIEN			
Bauvorhaben: Große Eiskuppel		zug. Pläne:	
Planinhalt: Detail C		GZ:	
Plan-Nr.:		BÜTEIL	INDEX
Ü		0	1

Spanngliedachse



Holz Pos. K1

Holz Pos. K2

Pneu

Detail B

Holz Pos. K3

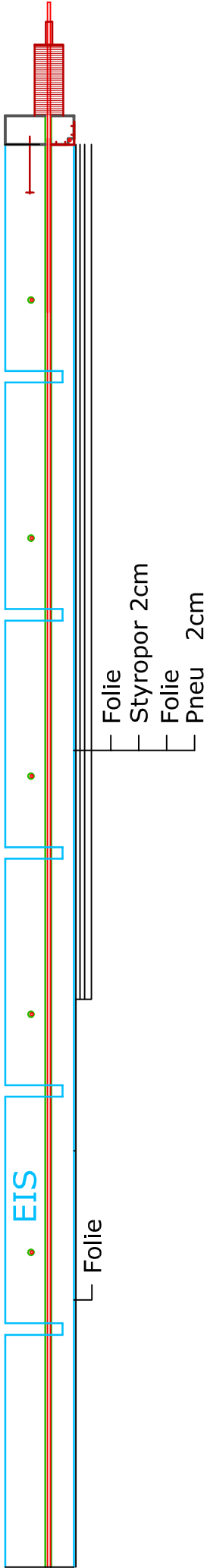
A

Detail E

Detail D

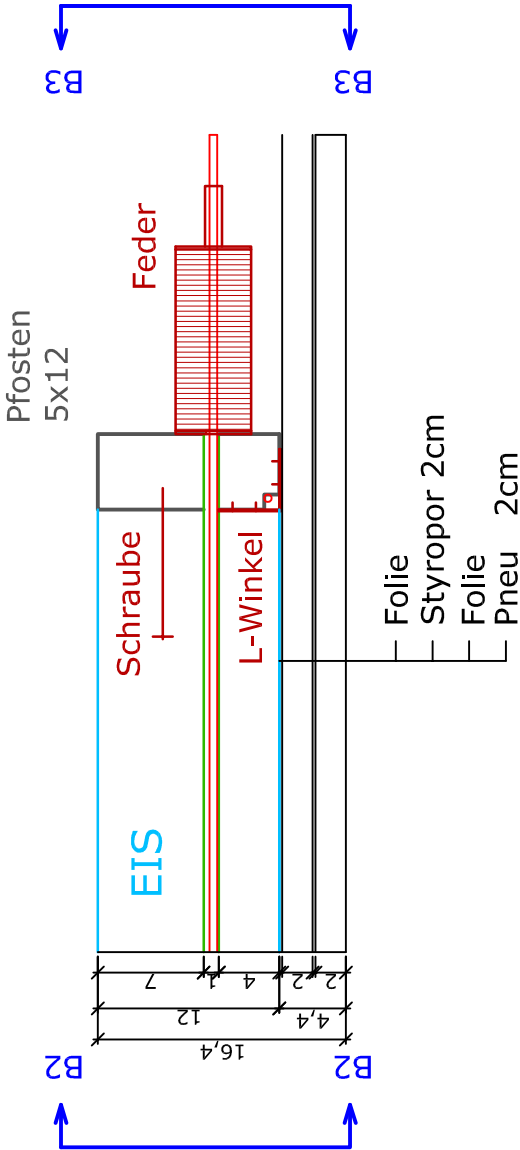
	AENDBEZ-INDEX-C	AENDERST	AENDDAT
	AENDBEZ-INDEX-B	AENDERST	AENDDAT
	AENDBEZ-INDEX-A	AENDERST	AENDDAT
Aenderung:	Bezeichnung:	erst.:	Datum:
Maßstab: 1: 25	Datum: 20.11.08	Planart: ÜBERSICHTSPLAN	erst.: DALLINGER
INSTITUT FÜR TRAGKONSTRUKTIONEN I BETONBAU Technische Universität Wien, Karlsplatz 13/212, 1040 Wien Tel. 0650/3172489 email: sdalling@mail.tuwien.ac.at			
Bauvorhaben: Kleine Eiskuppel		zug. Pläne:	
		GZ:	
Planinhalt: GRUNDRISS		Plan-Nr.:	BÜTEIL
		Ü	0 0 1

Schnitt A-A

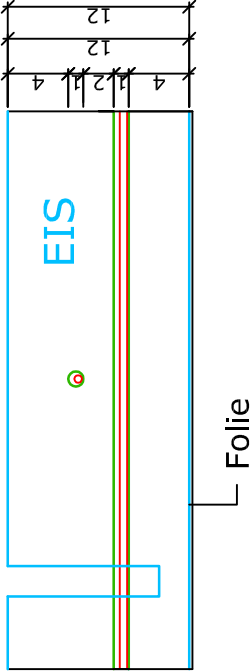


Detail B

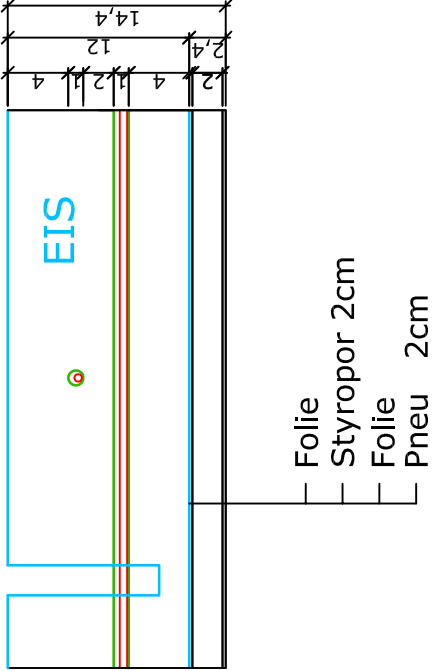
B1-B1



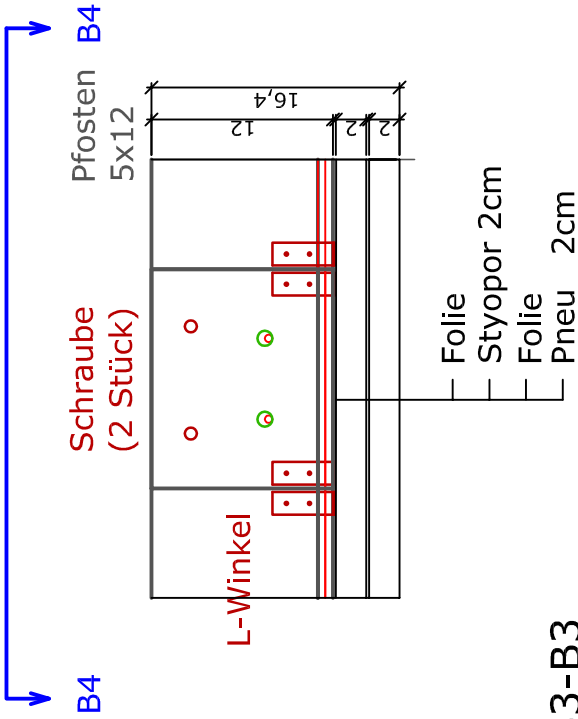
Detail D



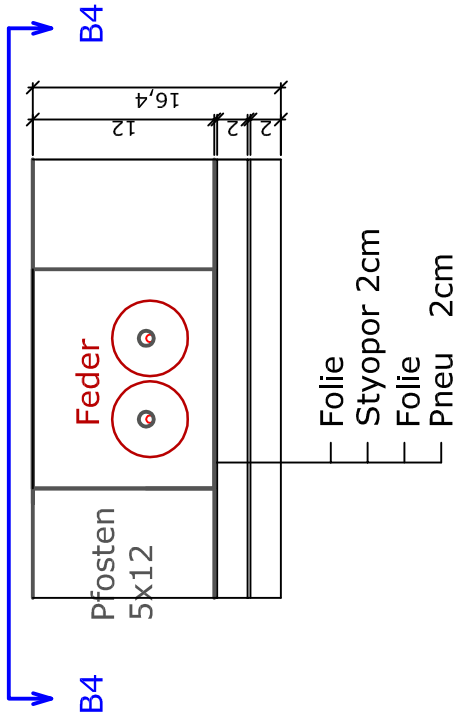
Detail E



B2-B2



B3-B3

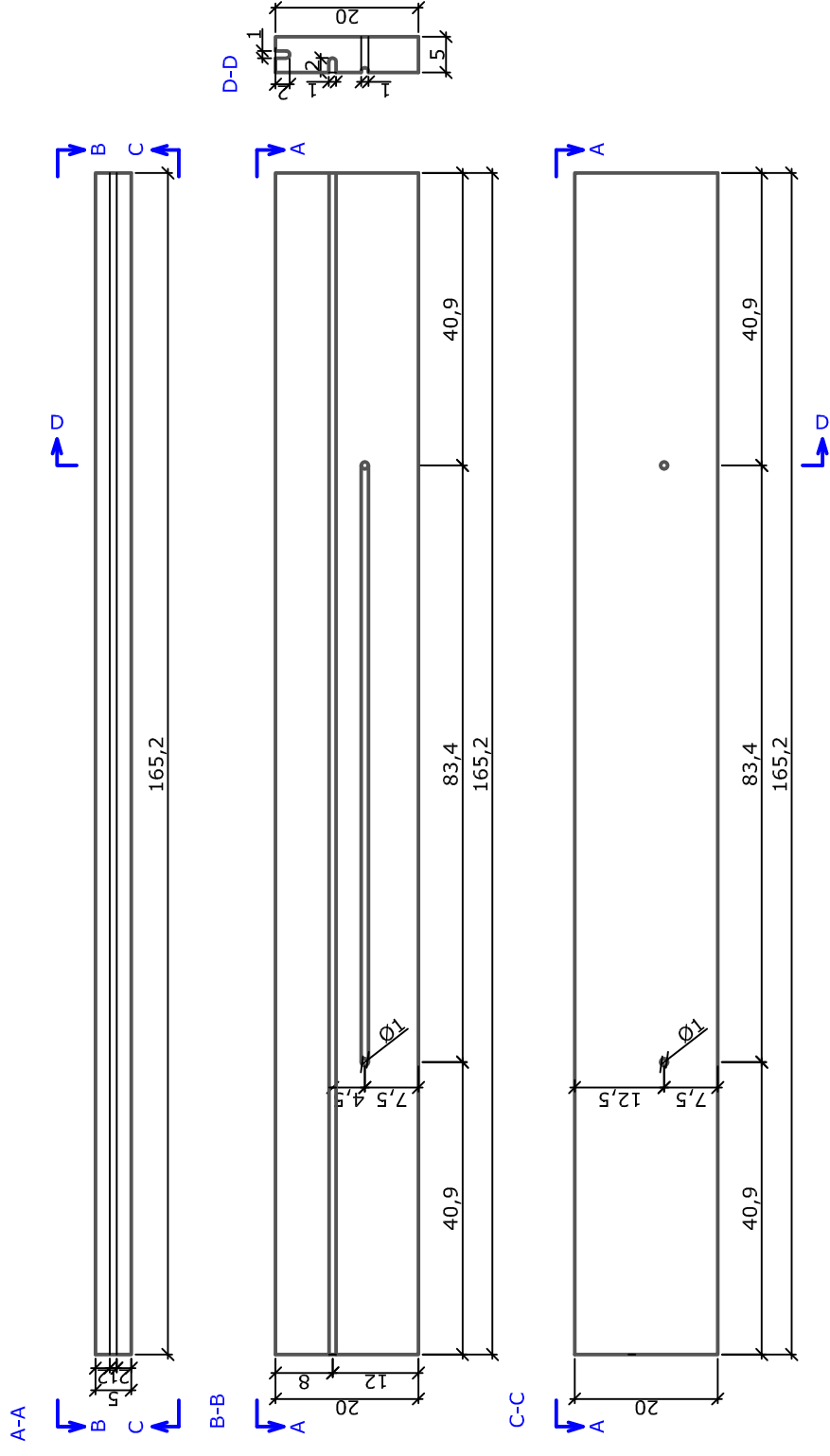


Seil (φ 5mm)

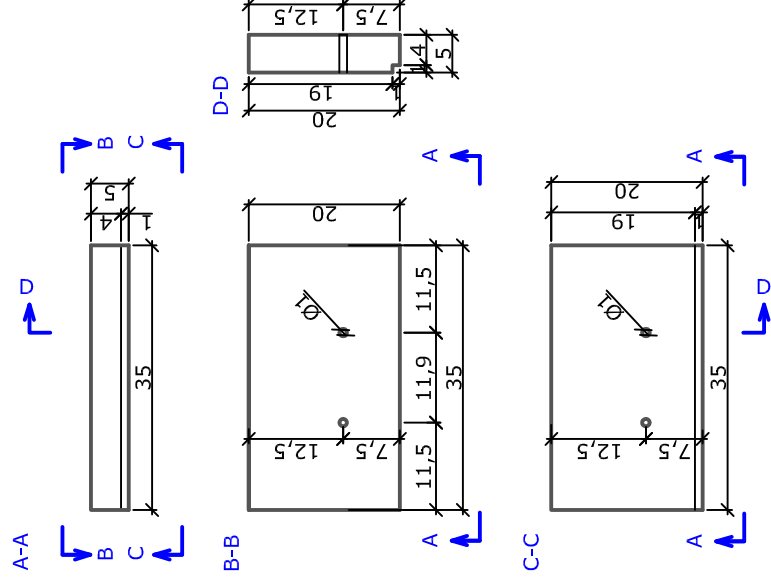
Hüllrohr (φ 10mm)

	AENDERST	AENDERST	AENDERST	AENDERST	AENDERST
	AENDERST	AENDERST	AENDERST	AENDERST	AENDERST
	AENDERST	AENDERST	AENDERST	AENDERST	AENDERST
Aenderung:	Bezeichnung:	erst.:	Datum:		
Maßstab: 1:10/1:5	Datum: 20.11.08	Planart: DETAILPLAN	erst.: DALLINGER		
INSTITUT FÜR TRAGKONSTRUKTIONEN I BETONBAU Technische Universität Wien, Karlsplatz 13/212, 1040 Wien Tel. 0650/3172489 email: sdalling@mail.tuwien.ac.at					
TU WIEN					
Bauvorhaben: Kleine Eiskuppel			zug. Pläne:		
			GZ:		
Planinhalt: Schnitt A-A Detail B, D, E			Plan-Nr.:	BÄUTEIL	INDEX
			Ü	0	1

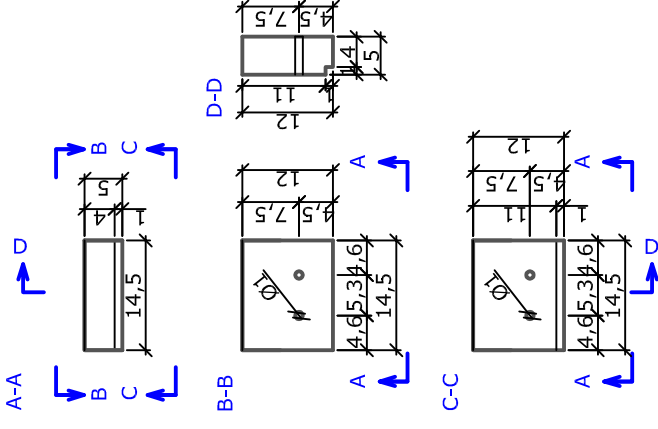
# Position G1



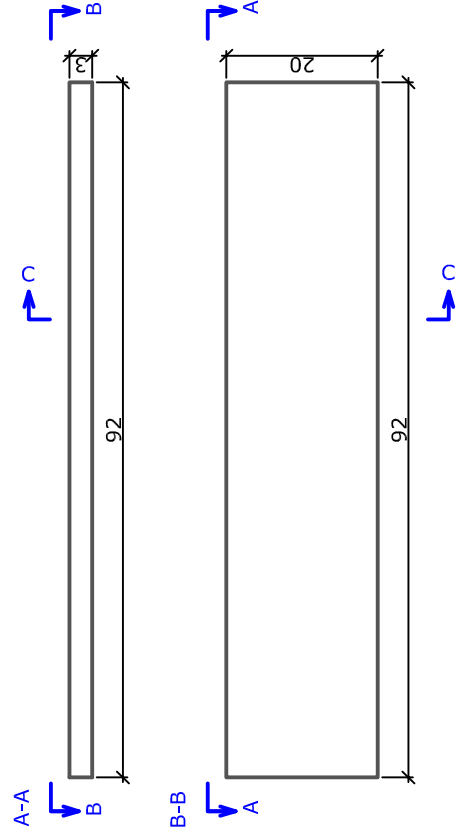
## Position G3



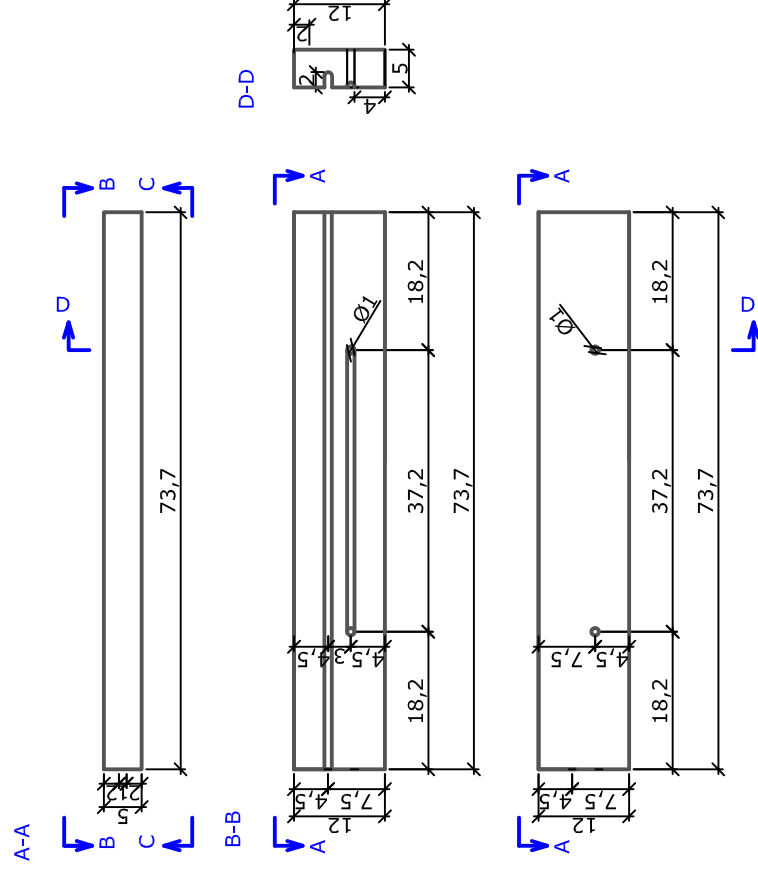
### Position K3



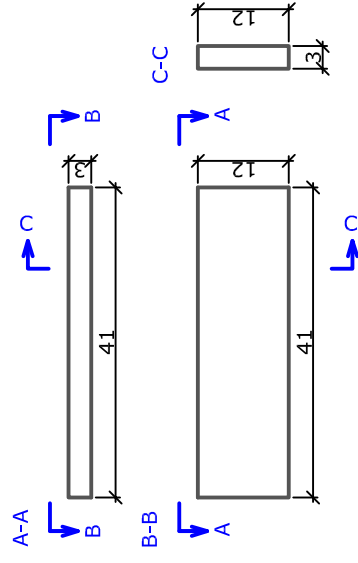
## Position G2



# Position K1

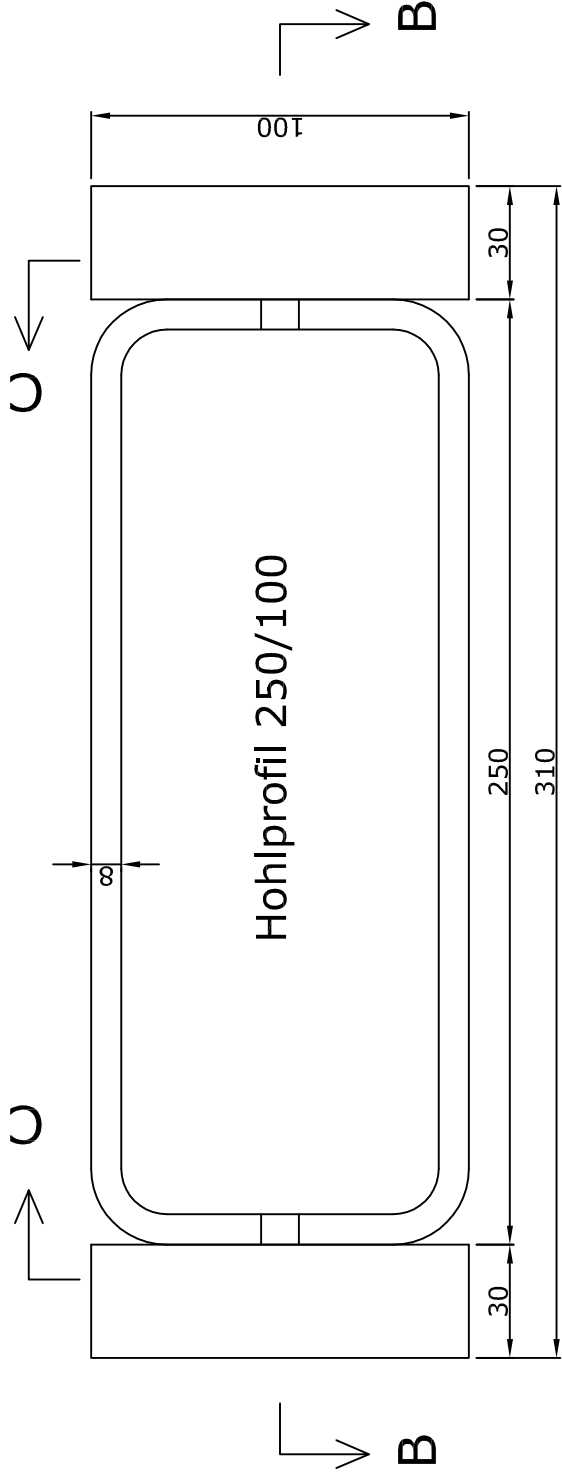


## Position K2

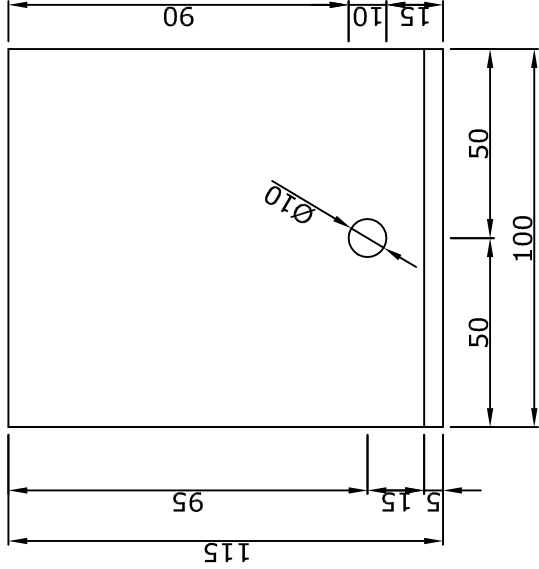


<input checked="" type="checkbox"/> C	AENDBEZ-INDEX-C	AENDERST	AENDDAT
<input checked="" type="checkbox"/> B	AENDBEZ-INDEX-B	AENDERST	AENDDAT
<input checked="" type="checkbox"/> A	AENDBEZ-INDEX-A	AENDERST	AENDDAT
Aenderung:	Bezeichnung:	erst.:	Datum:
Maßstab: 1:10	Datum: 20.11.08	Planart: ÜBERSICHTSPLAN	erst.: DALLINGER
INSTITUT FÜR TRAGKONSTRUKTIONEN I BETONBAU Technische Universität Wien, Karlsplatz 13/212, 1040 Wien Tel. 0650/3172489      email: sdalling@mail.tuwien.ac.at			
Bauvorhaben: Eiskuppeln		zug. Pläne:	
		GZ:	
Planinhalt: HOLZABSCHALUNG		Plan-Nr.:	BAUTEIL
		Ü	0 0 1

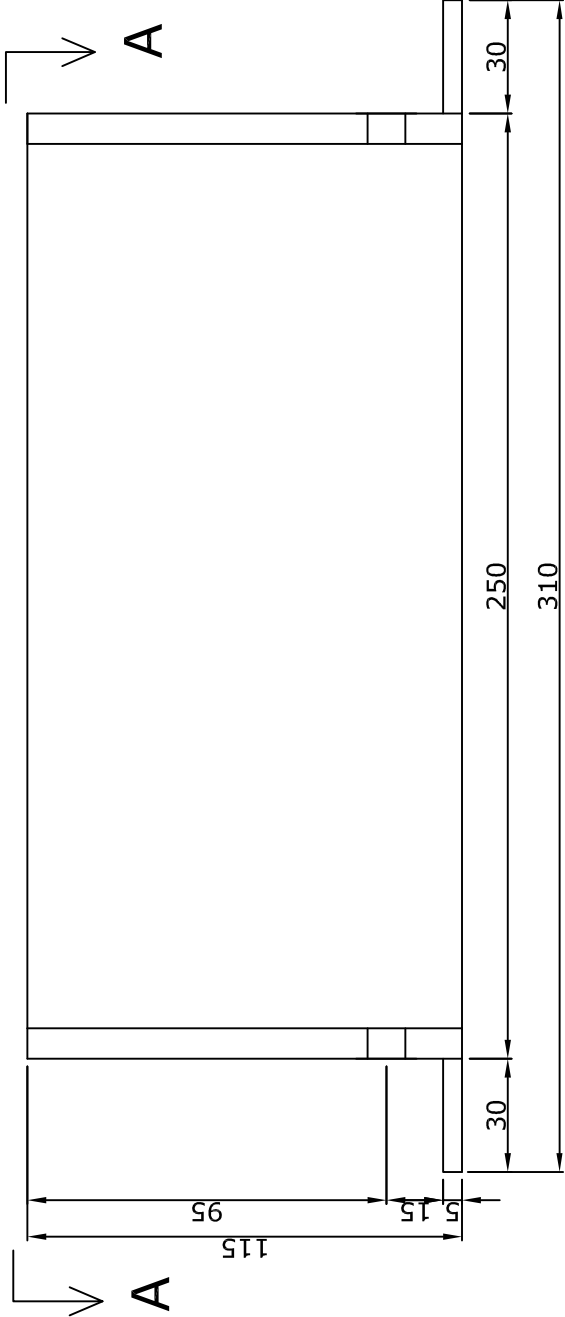
Grundriss A-A



Schnitt C-C



Schnitt B-B

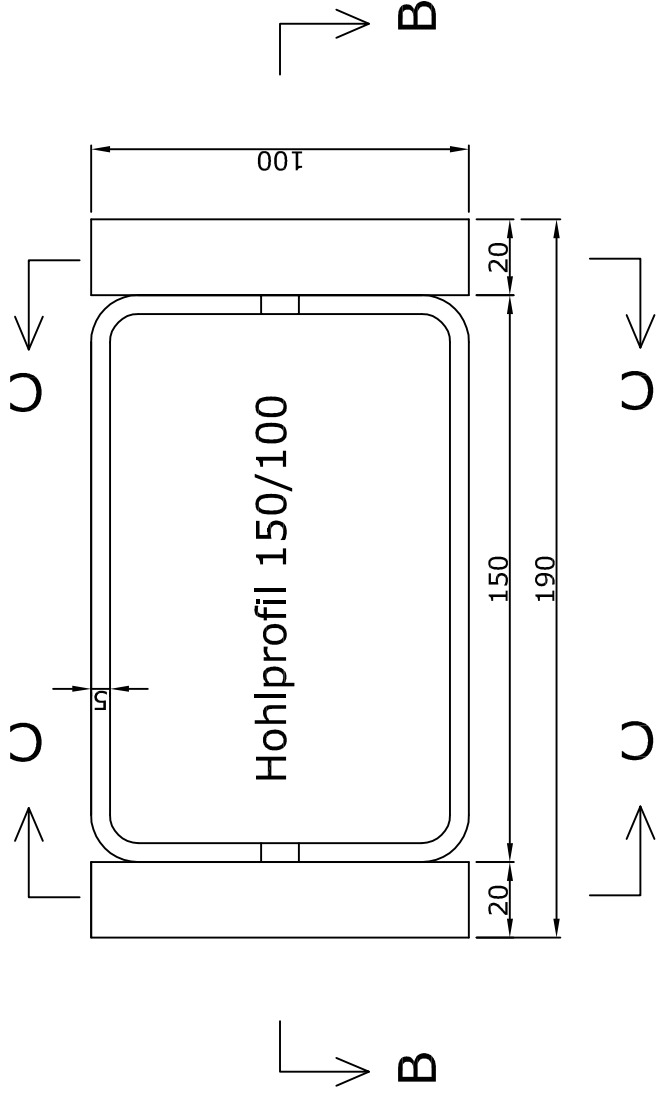


7 Stück

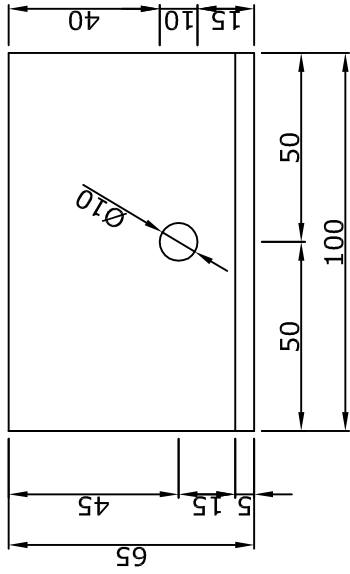
Maße in mm

C	AENDBEZ-INDEX-C	AENDERST	AENDDAT
B	AENDBEZ-INDEX-B	AENDERST	AENDDAT
A	AENDBEZ-INDEX-A	AENDERST	AENDDAT
Aenderung: Bezeichnung:		erst.:	Datum:
Maßstab: 1:2	Datum: 21.11.08	Planart: DETAILPLAN	ersch.: DALINGER
INSTITUT FÜR TRAGKONSTRUKTIONEN I BETONBAU Technische Universität Wien, Karlsplatz 13/212, 1040 Wien Tel. 0650/3172489 email: sfdilling@mail.tuwien.ac.at			
Bauvorhaben: große Eiskuppel		zug. Pläne:	
GZ:		GZ:	
Planinhalt: Kopplungsstelle		Plan-Nr.: Ü 0 0 1	
INDEX		INDEX	

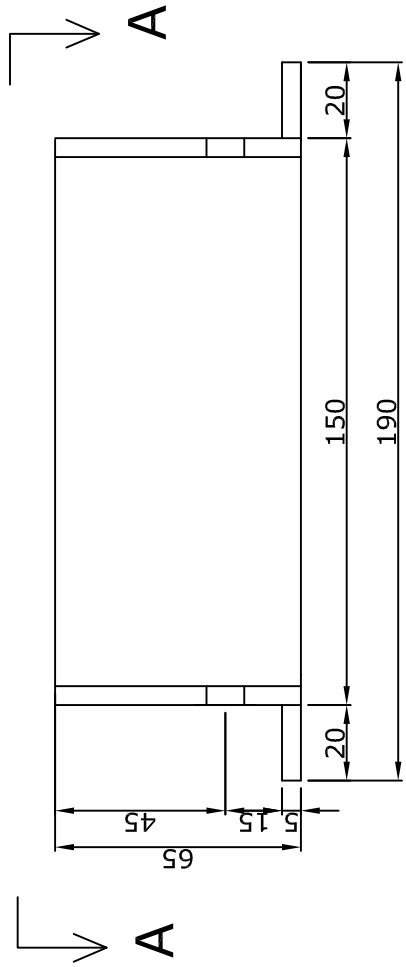
Grundriss A-A



Schnitt C-C



Schnitt B-B

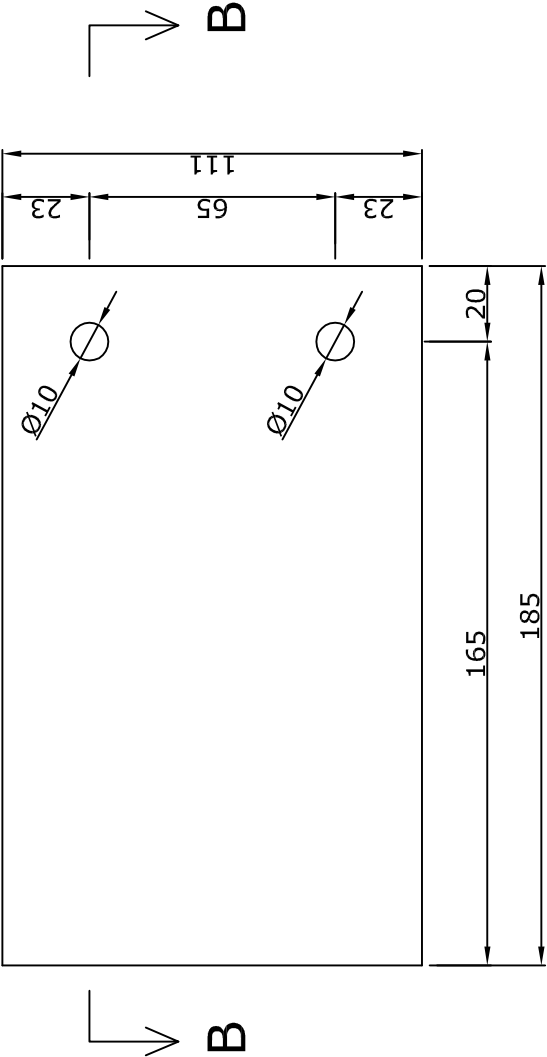


7 Stück

Maße in mm

	AENDBEZ-INDEX-C	AENDERST	AENDDAT
	AENDBEZ-INDEX-B	AENDERST	AENDDAT
	AENDBEZ-INDEX-A	AENDERST	AENDDAT
Aenderung: Bezeichnung:		erst.:	Datum:
Maßstab: 1:2	Datum: 21.11.08	Planart: DETAILPLAN	ersch.: DALINGER
INSTITUT FÜR TRAGKONSTRUKTIONEN I BETONBAU Technische Universität Wien, Karlsplatz 13/212, 1040 Wien Tel. 0650/3172489 email: sdalling@mail.tuwien.ac.at			
Bauvorhaben: <b>kleine Eiskuppel</b>		zug. Pläne:	
GZ:			
Planinhalt: <b>Kopplungsstelle</b>		Plan-Nr.:	BAUTEIL
		Ü	0 0 2
		INDEX	

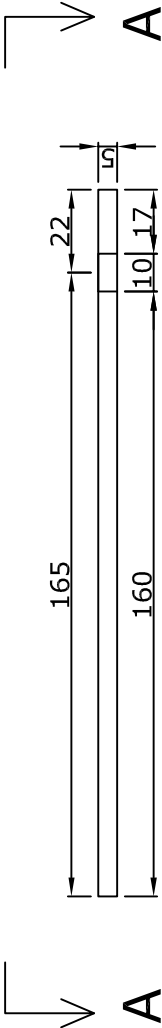
Grundriss A-A



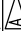


14 Stück

Maße in mm

Schnitt B-B



	AENDBEZ-INDEX-C	AENDERST	AENDDAT
	AENDBEZ-INDEX-B	AENDERST	AENDDAT
	AENDBEZ-INDEX-A	AENDERST	AENDDAT
Aenderung: Bezeichnung:		erst.:	Datum:
Maßstab: 1:2	Datum: 21.11.08	Planart: DETAILPLAN	ersch.: DALINGER
INSTITUT FÜR TRAGKONSTRUKTIONEN I BETONBAU Technische Universität Wien, Karlsplatz 13/212, 1040 Wien Tel. 0650/3172489 email: sfdalling@mail.tuwien.ac.at			
Bauvorhaben: Eiskuppel		zug. Pläne:	
		GZ:	
Planinhalt: Seilwindenaufstands- fläche		Plan-Nr.:	INDEX
		Ü 0 0 3	

### A.3 Pneumatic formwork

- Endgültige Pneuforn für eine Halbkugel mit einem Durchmesser  $8,4\,m$  (1)
- Pneu - Kleine Eiskuppel (1)







# Appendix B

## Segment Lift Method

This appendix includes drawings and sketches of the experiments carried out with the Segment Lift Method.

All drawings are to scale and the scale is mostly given on the drawing header. Unless it is noted otherwise on the drawing, the dimensions are given in centimeters.

This appendix is structured as following:

**B.1 Creating the ice segments (11)**

**B.2 Deforming the ice segments (18)**

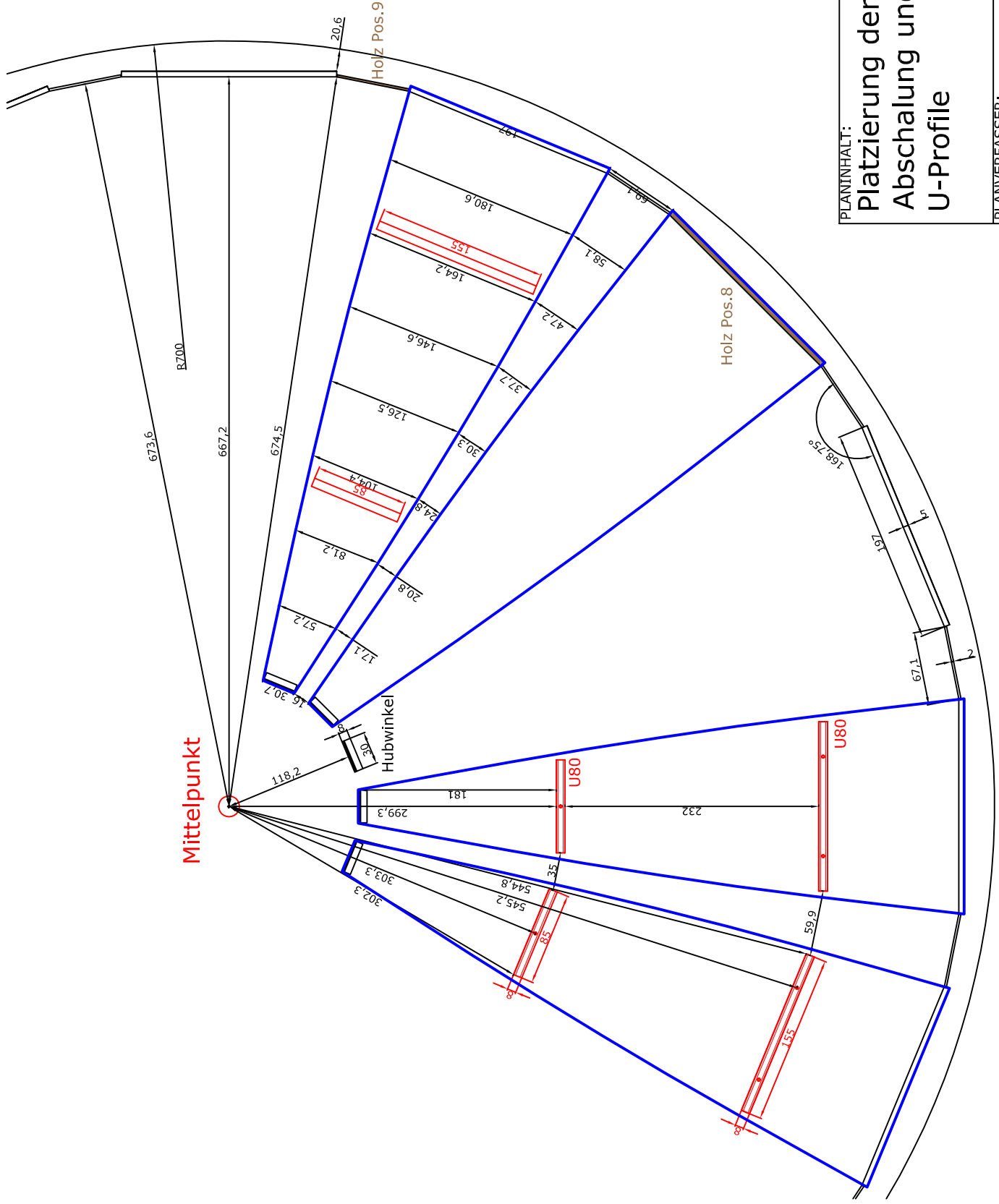
**B.3 Mounting tower (11)**

**B.4 Finished Position (4)**

(The number in the brackets represents the number of drawings on this topic)

## B.1 Creating the ice segments

- Platzierung der Abschalung und U-Profile (1)
- Platzierung des Pneu (1)
- Bestimmung der 16tel Punkte (1)
- Abschalung und Stahleinbauteile eines Segments (1)
- U-Profile 1,2 (1)
- Holzpostionen (1)
- Stahlflasche (1)
- Hubwinkel (1)
- Bewehrung (1)
- Markierungsfolie (1)
- Einschnitte (1)



PLANINHALT:

Platzierung der  
Abschalung und  
U-Profile

MASSSTAB:

1:50 A4

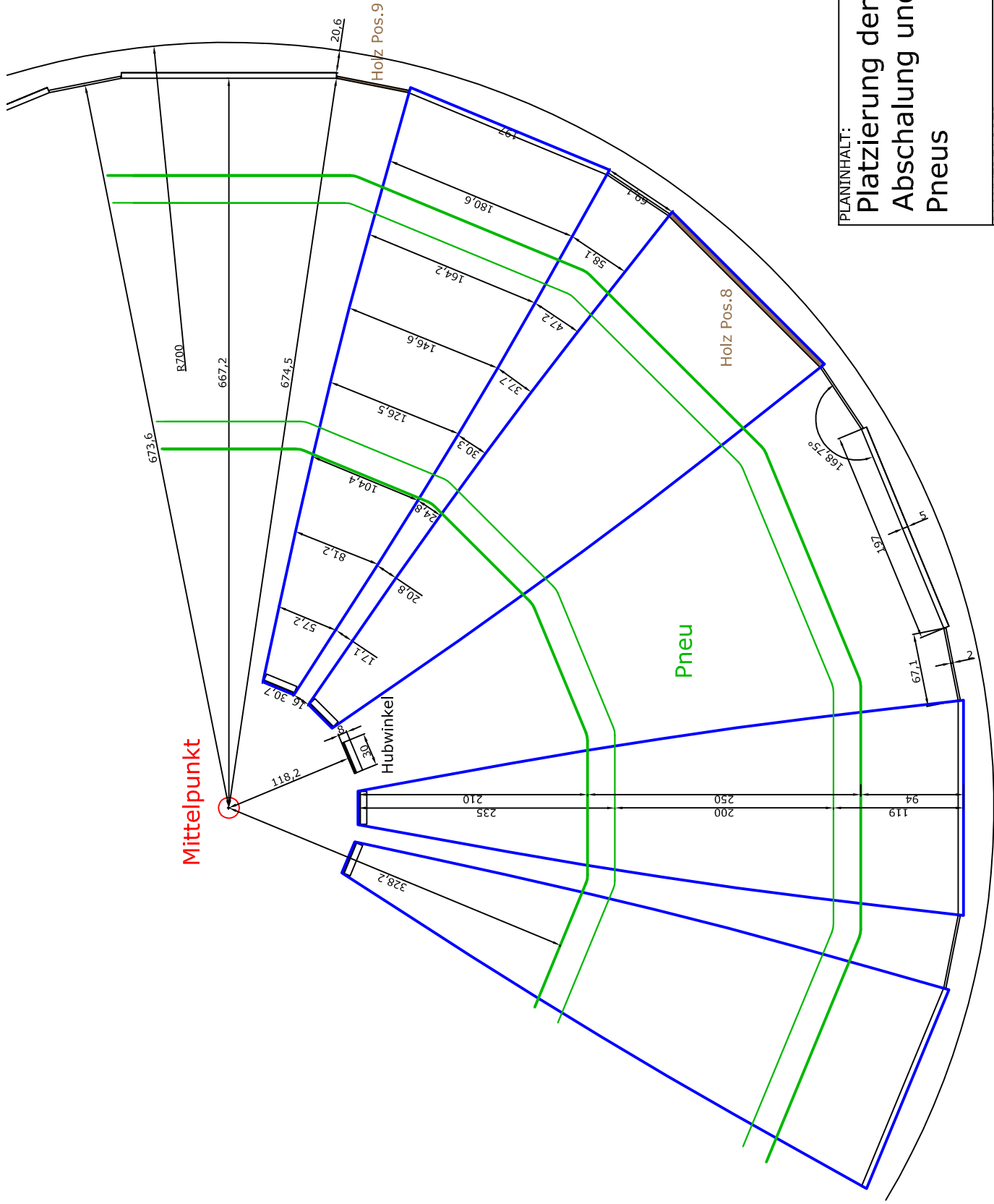
1:40 A3

PLANVERFASSTER:

Sonja Dallinger

DATUM:

12.11.10



PLANINHALT:

Platzierung der  
Abschalung und des  
Pneus

MASSSTAB:

1:50 A4

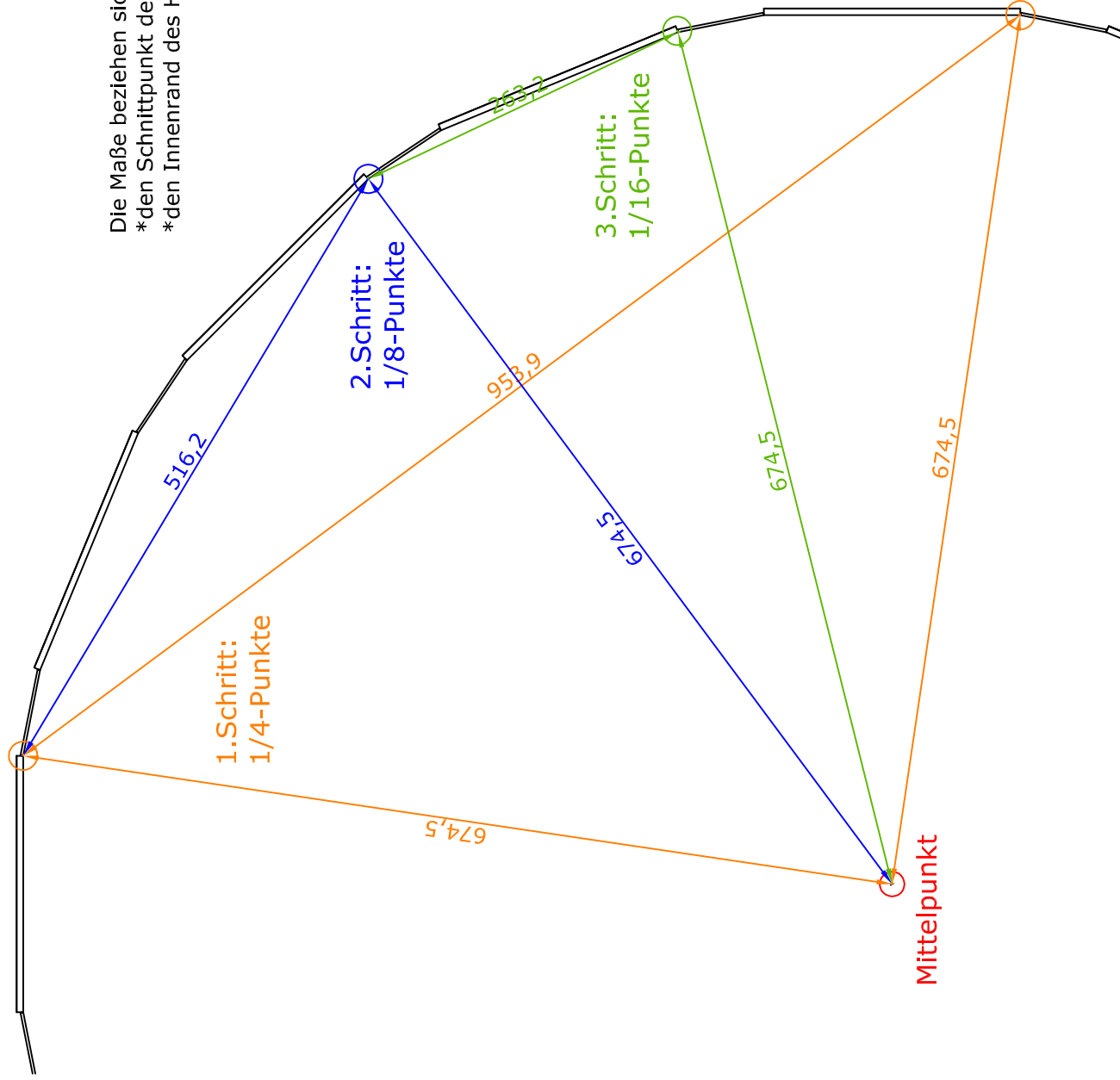
1:40 A3

PLANVERFASSTER:

Sonja Dallinger

DATUM:

15.11.09

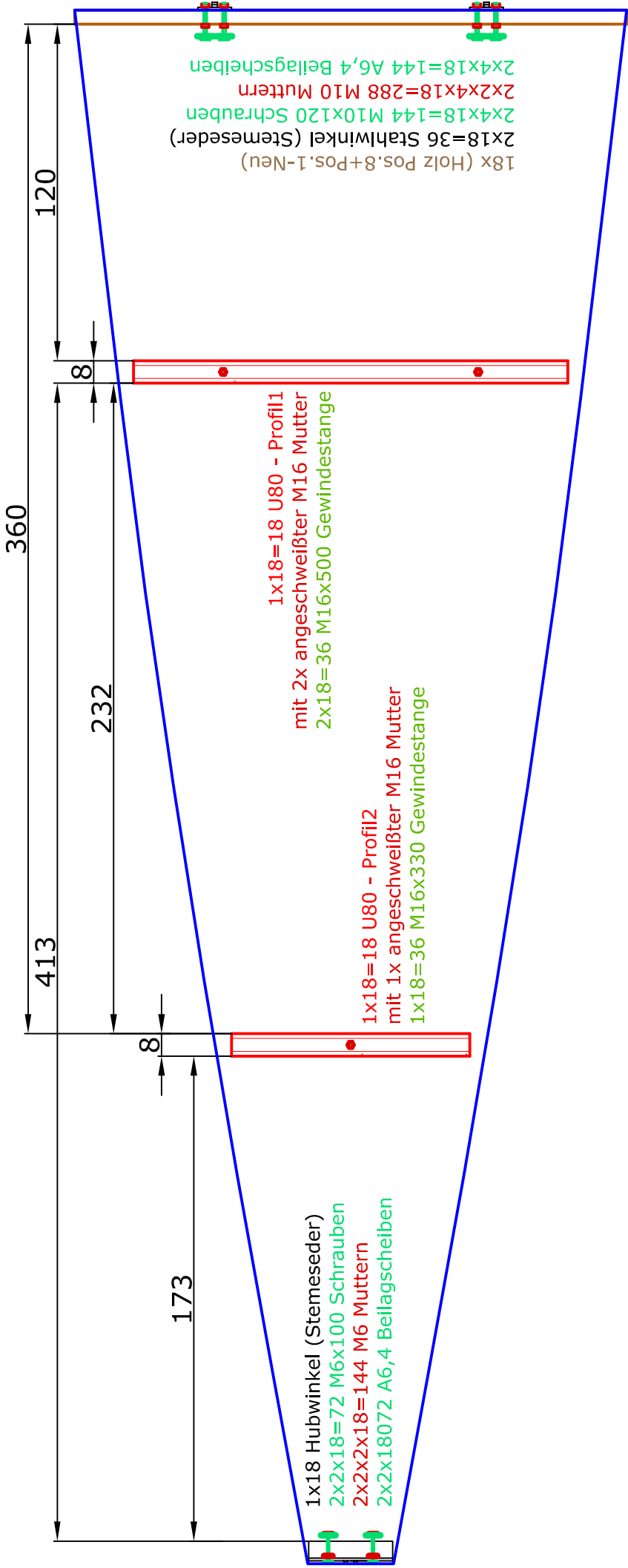


Die Maße beziehen sich auf  
 \*den Schnittpunkt der beiden Abschalungen  
 \*den Innenrand des Holzes

PLANINHALT: Bestimmung der 16tel Punkte	MASSTAB: 1:50 A4
	1:40 A3
PLANVERFASSTER: Sonja Dallinger	DATUM: 12.11.10

PLANINHALT: Abschalung und Stahleinbauten eines Segments	MASSTAB: 1:20 A4 1:15 A3
	DATUM: 17.11.10
PLANVERFASSER: Sonja Dallinger	

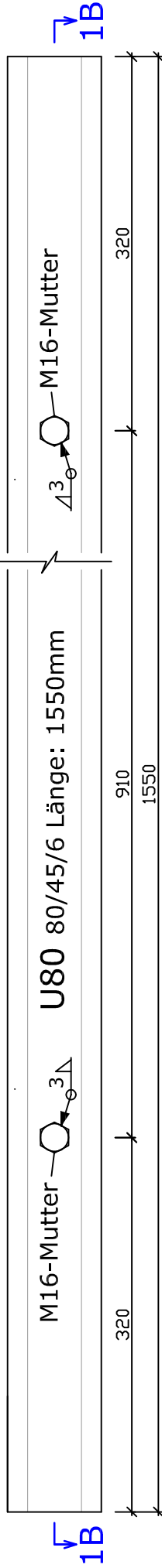
zur Montage:  
mind.66x Stahlflaschen  
mind.260x 4x60TX Holzschrauben



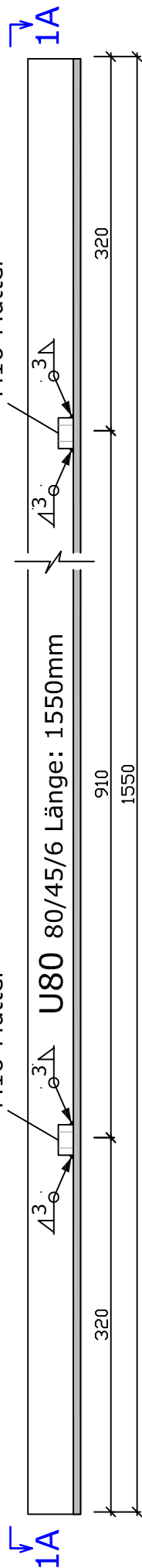


# U-Profil 1

Draufsicht 1A-1A

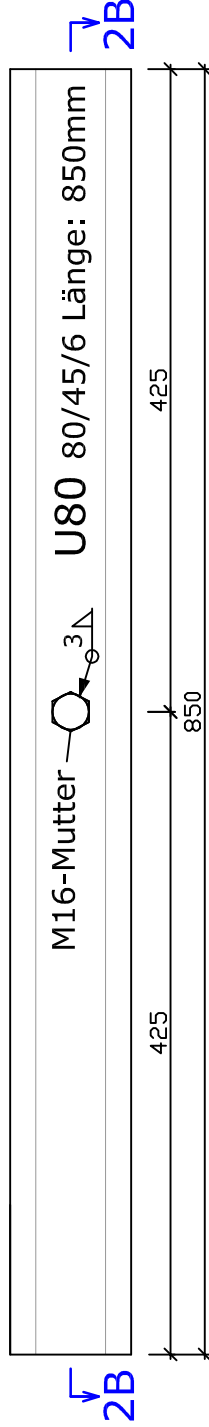


Schnitt 1B-1B

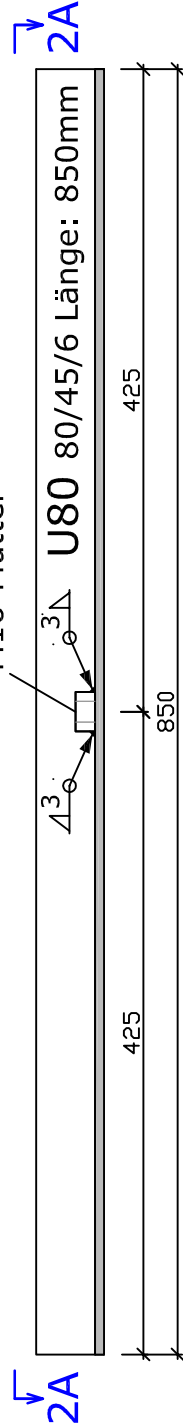


# U-Profil 2

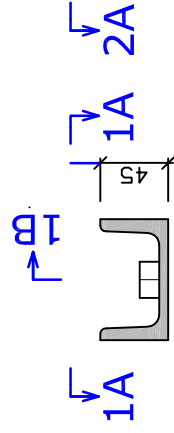
Draufsicht 2A-2A



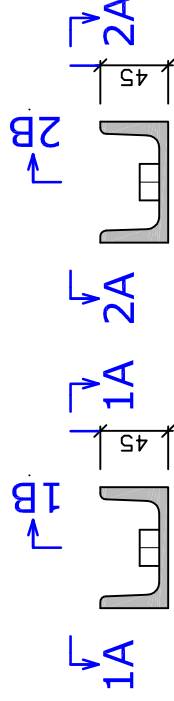
Schnitt 2B-2B



Schnitt 1C-1C



Schnitt 2C-2C

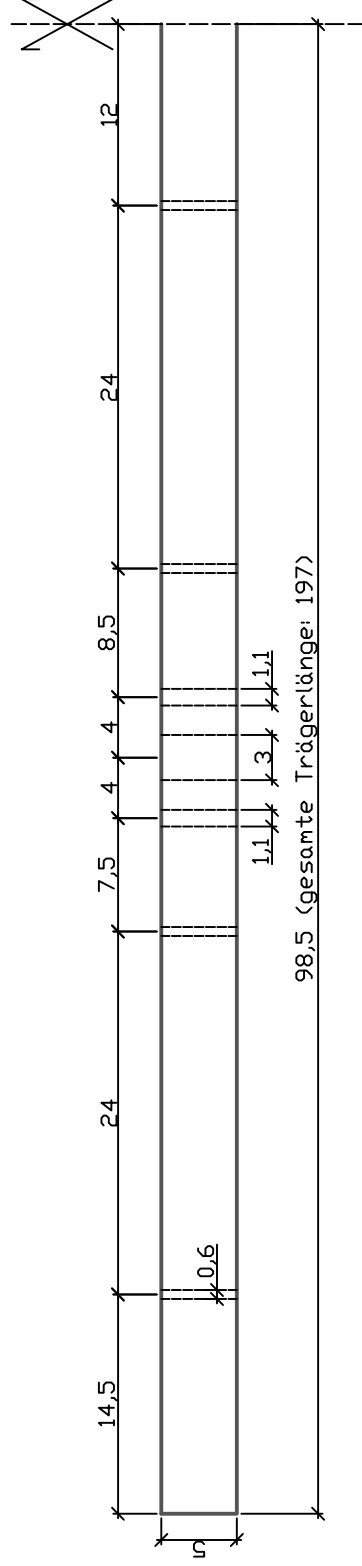
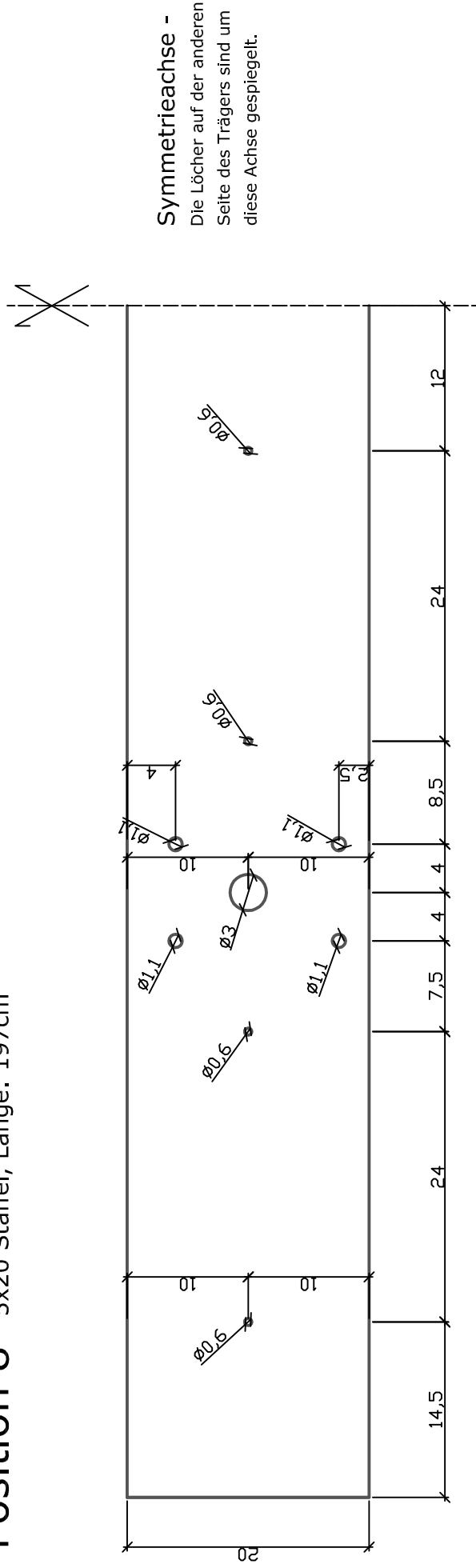


Maße in mm

STAHLTEILE	
PLANINHALT:	MASSSTAB:
U-Profil 1,2	1:5
PLANVERFASSTER:	DATUM:
Sonja Dallinger	20.10.10
sdalling@mail.tuwien.ac.at	
Tel. +43-1-58801-21262	

Stahlgüte: S235

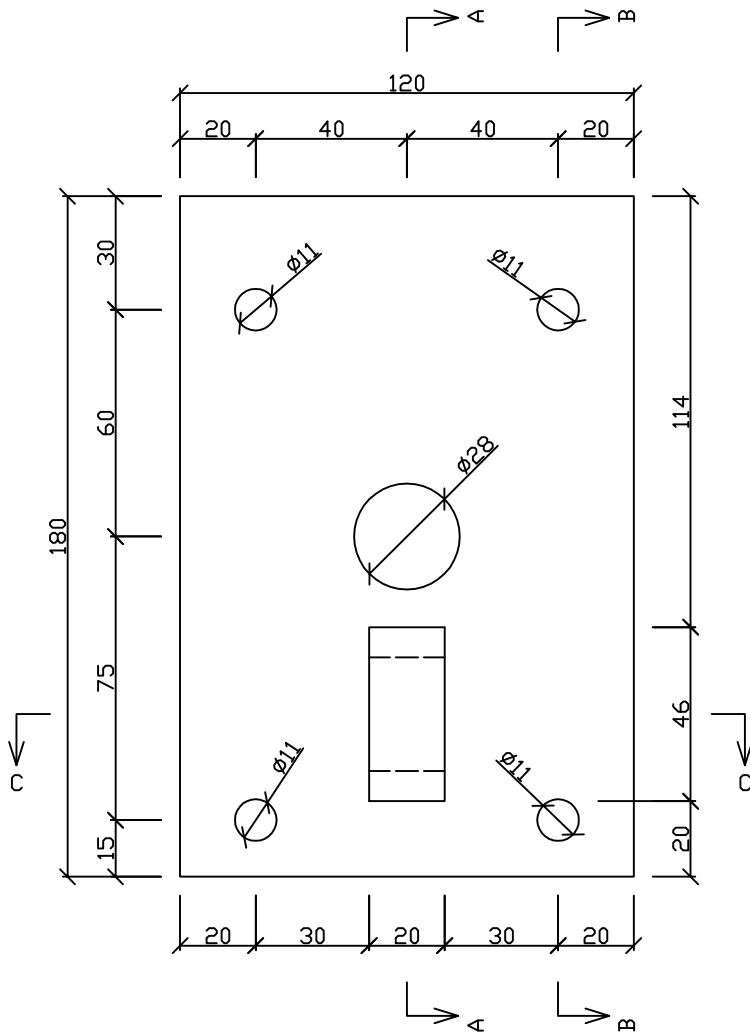
## Position 8 5x20 Staffel, Länge: 197cm



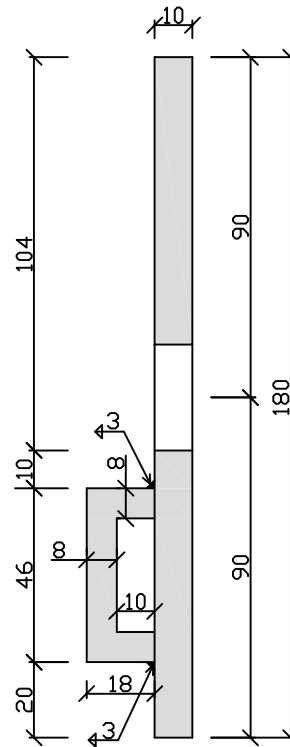
Maße in cm

Eiskuppel		
PLANINHALT:	MASSSTAB:	DATUM:
Pos. 8,9	1:5	22.10.10
PLANVERFASSTER:		
Sonja Dallinger		
sdalling@mail.tuwien.ac.at		
Tel. +43-1-58801-21262		

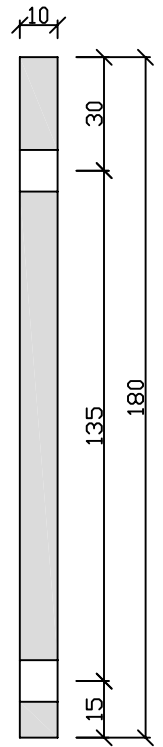
## Position 9 2x20 Latte, Länge: 67,1cm



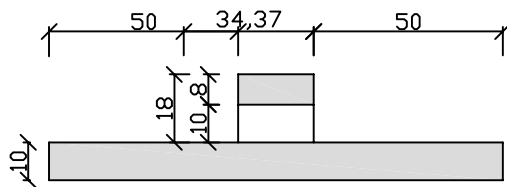
Schnitt A-A



Schnitt B-B



Schnitt C-C



36 Stück

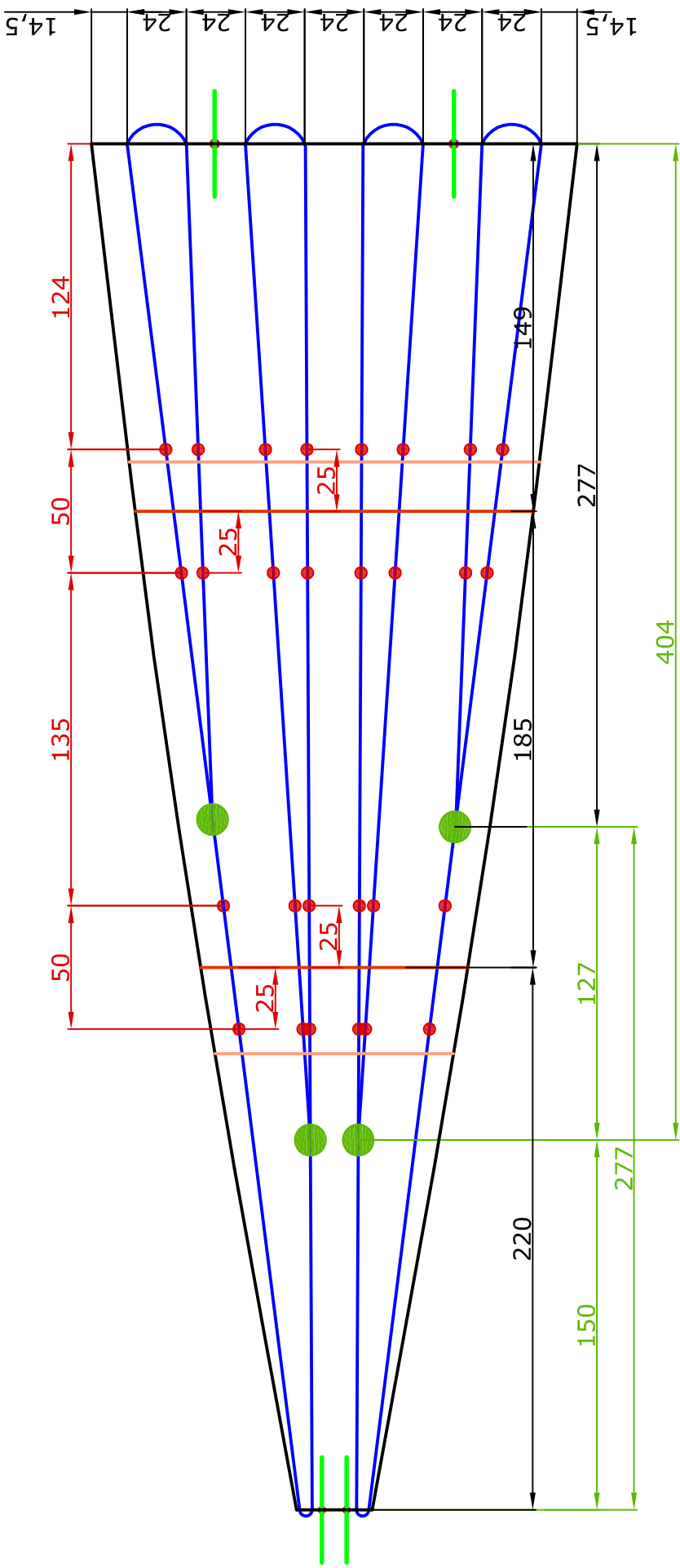
Maße in mm

PLANINHALT: <b>Stahllasche</b>	MASSSTAB: <b>1:2</b>
PLANVERFASSER: <b>Sonja Dallinger</b> sdalling@mail.tuwien.ac.at Tel. +43-1-58801-21262	DATUM: <b>18.10.10</b>



PLANINHALT: <b>Bewehrung</b>	MASSSTAB: <b>1:25 A4</b> <b>1:20 A3</b>
	DATUM: <b>12.11.10</b>
PLANVERFASSTER: <b>Sonja Dallinger</b>	

Segmentform Obergurgl 2010/11-V2  
 -1cm pro Seite



• Seilklemme klein

● Seilklemme groß

— Bewehrung: 2 Seile je 19m

— Loch durch das später die Kette geführt wird

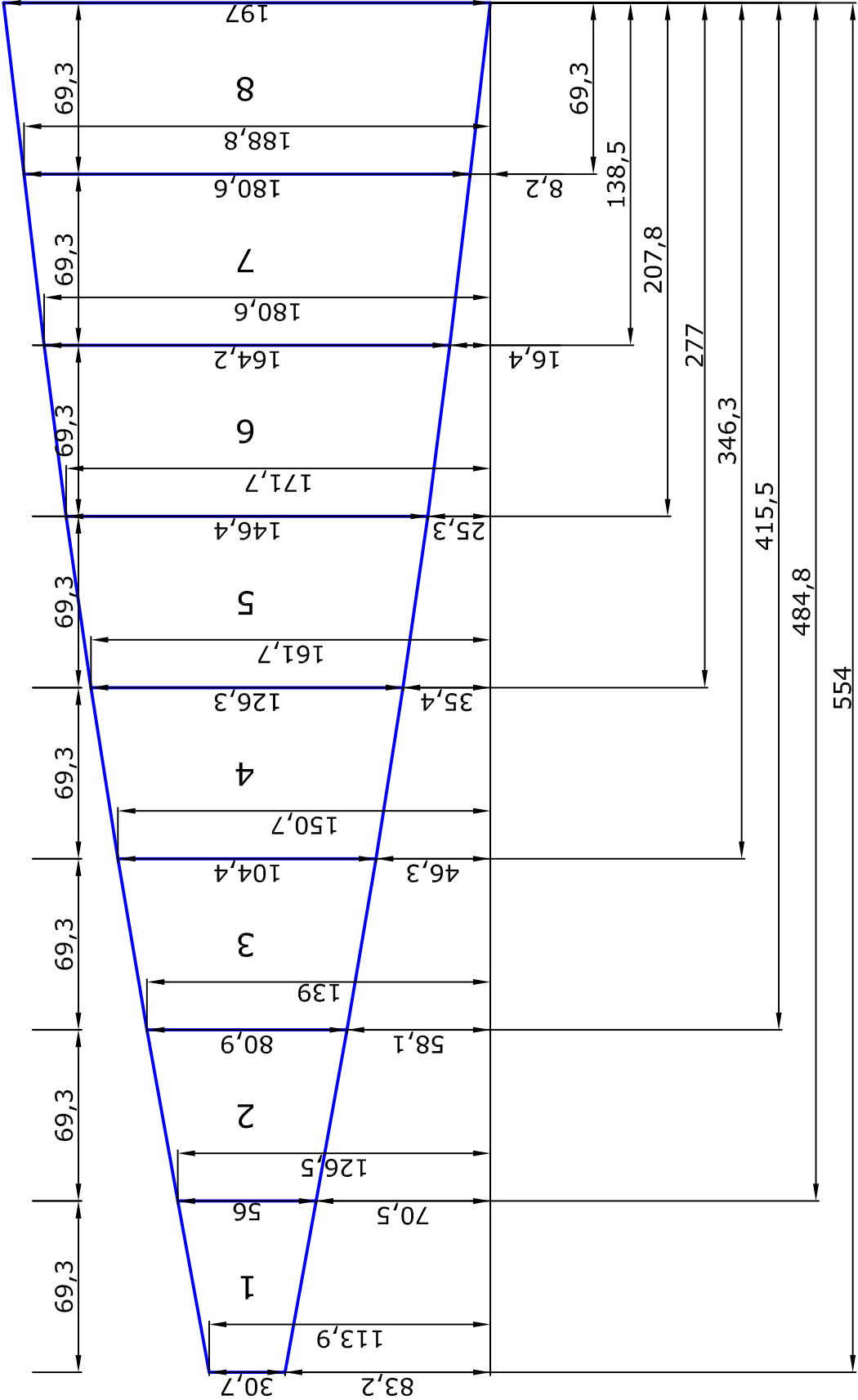
— Anhebepunkte mit der Hebevorrichtung

— Auflagerpunkte Kriechen

PLANINHALT: Markierungsfolie	MASSSTAB: 1:25 A4 1:20 A3
	DATUM: 12.11.10
PLANVERFASSTER: Sonja Dallinger	

Segmentform Obergurgl 2010/11-V2

-1cm pro Seite





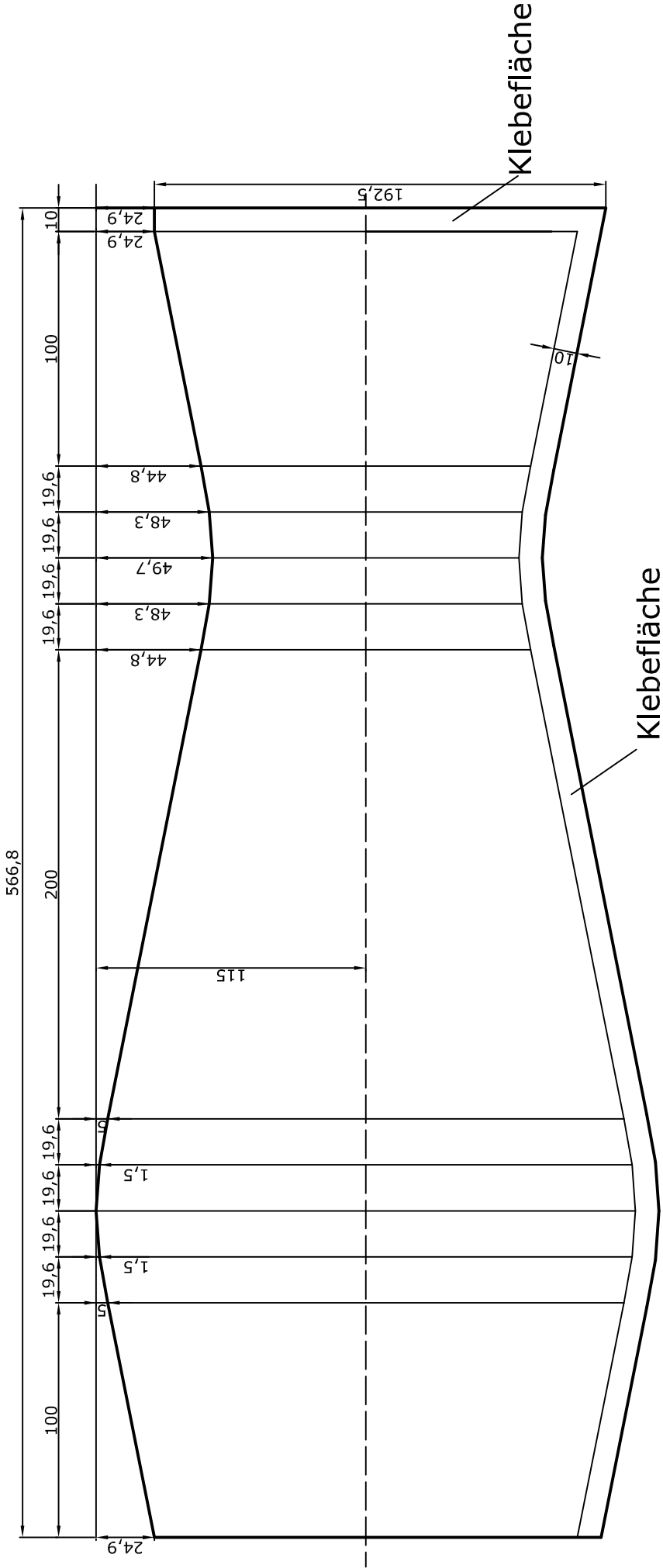
## B.2 Deforming the ice segments

- Zuschnitt - Pneu (1)
- Hebevorrichtung (1)
- Hebevorrichtung groß (2)
- Hebevorrichtung klein (2)
- Hebevorrichtung, Holzstapel (3)
- Hebevorrichtung groß - Draufsicht 1-1, Schnitte 2-2, 3-3, 4-4 (1)
- Hebevorrichtung groß - Detail A (1)
- Hebevorrichtung groß - Details B,C (1)
- Hebevorrichtung klein - Draufsicht 1-1, Schnitte 2-2, 3-3 (1)
- Hebevorrichtung klein - Detail A, B, C (1)
- Stahlteile, Platten 1,2,3,4; Ring 1,2 (1)
- Stahlzange (2)
- Pewag Teile (1)



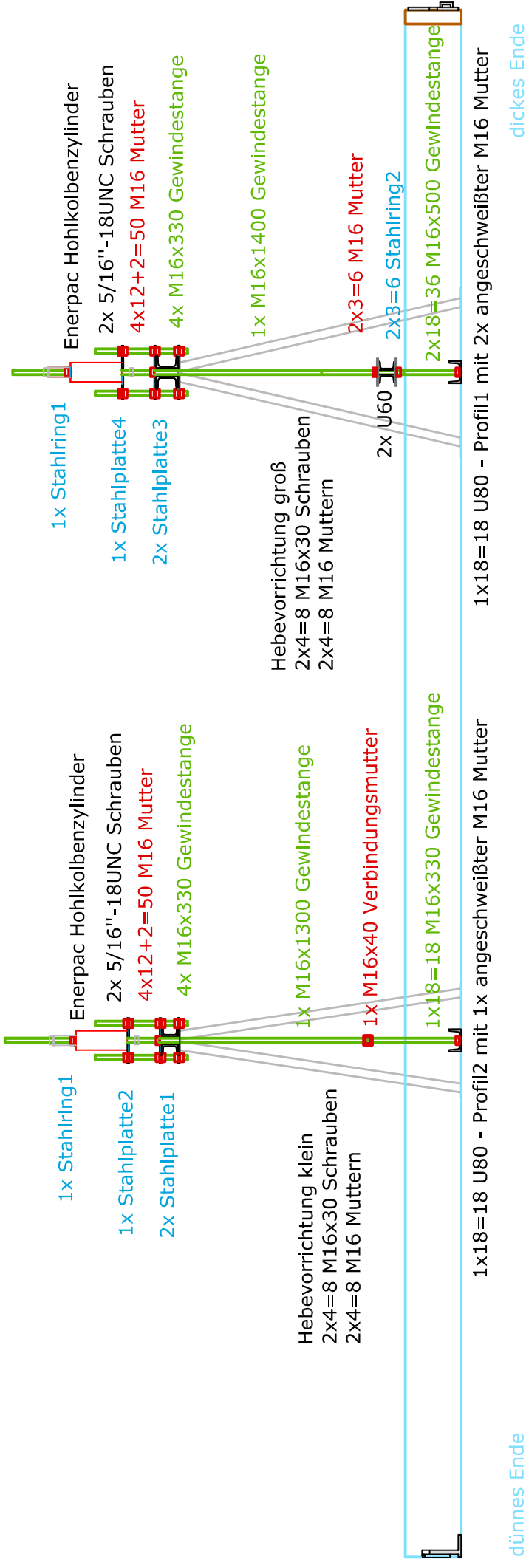
PLANINHALT:	MASSTAB:
	1:25 A4 1:20 A3
PLANVERFASSER:	DATUM:
	05.10.09
Sonja Dallinger	

16 Stück



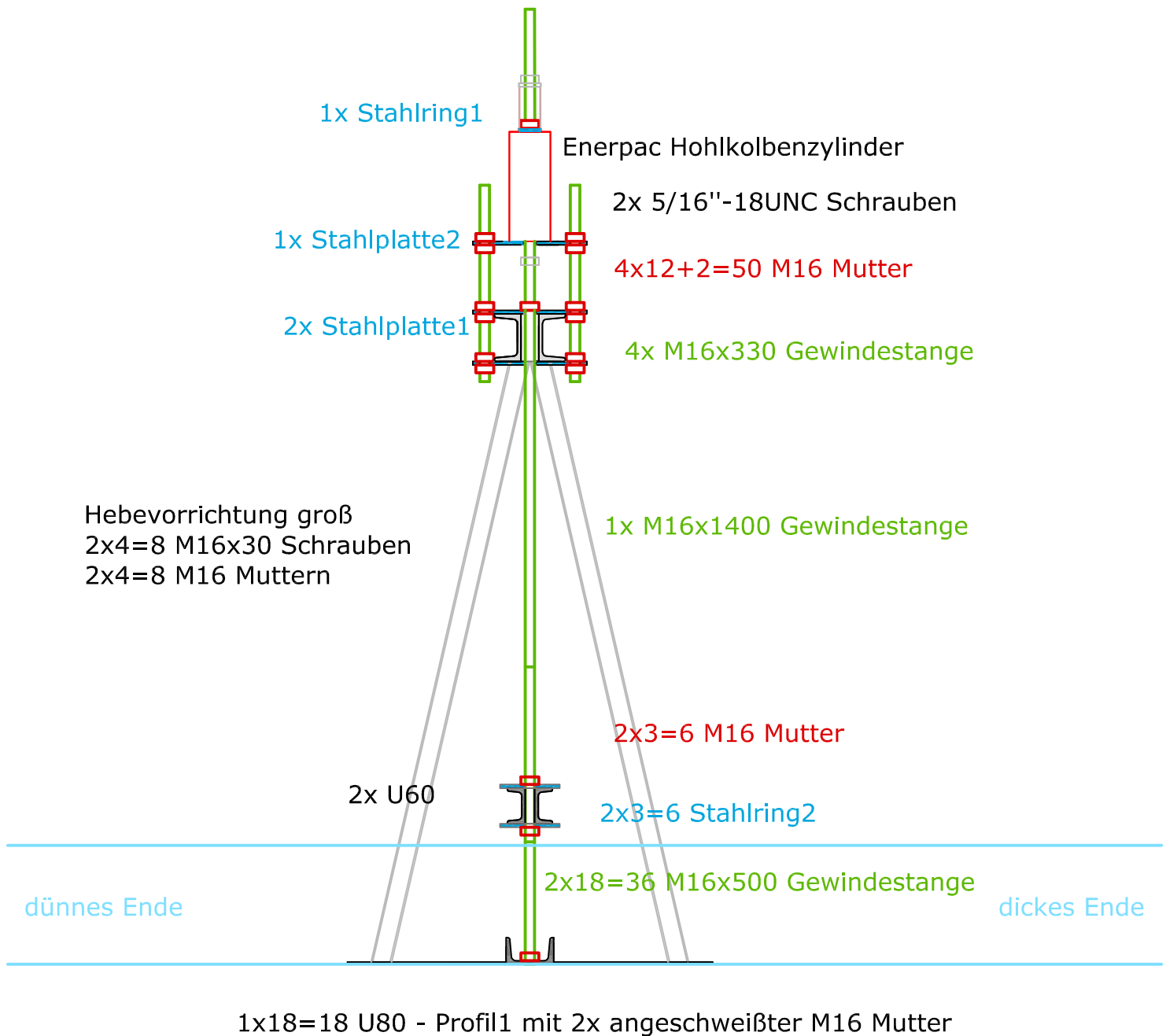
PLANINHALT: <b>Hebevorrichtung</b>	MASSSTAB: <b>1:20 A4</b> <b>1:15 A3</b>
PLANVERFASSER: <b>Sonja Dallinger</b>	DATUM: <b>17.11.10</b>

- 1x Hebevorrichtung klein
- 1x Hebevorrichtung groß
- 2x Stahlplatte1
- 1x Stahlplatte2
- 2x Stahlplatte3
- 1x Stahlplatte4
- 2x Stahlring1
- 6x Stahlring2
- 2x U60-Profil Länge 1100
- 2x Enerpac Hohlkolbenzylinder
- 2x 5/16"-18UNC Schrauben
- 122x M16 Muttern
- 1x M16 Verbindungsmutter
- 16x M16x30 Schrauben
- 1x M16x1300 Gewindestange
- 1x M16x1400 Gewindestange
- 26x M16x330 Gewindestange
- 36x M16x500 Gewindestange

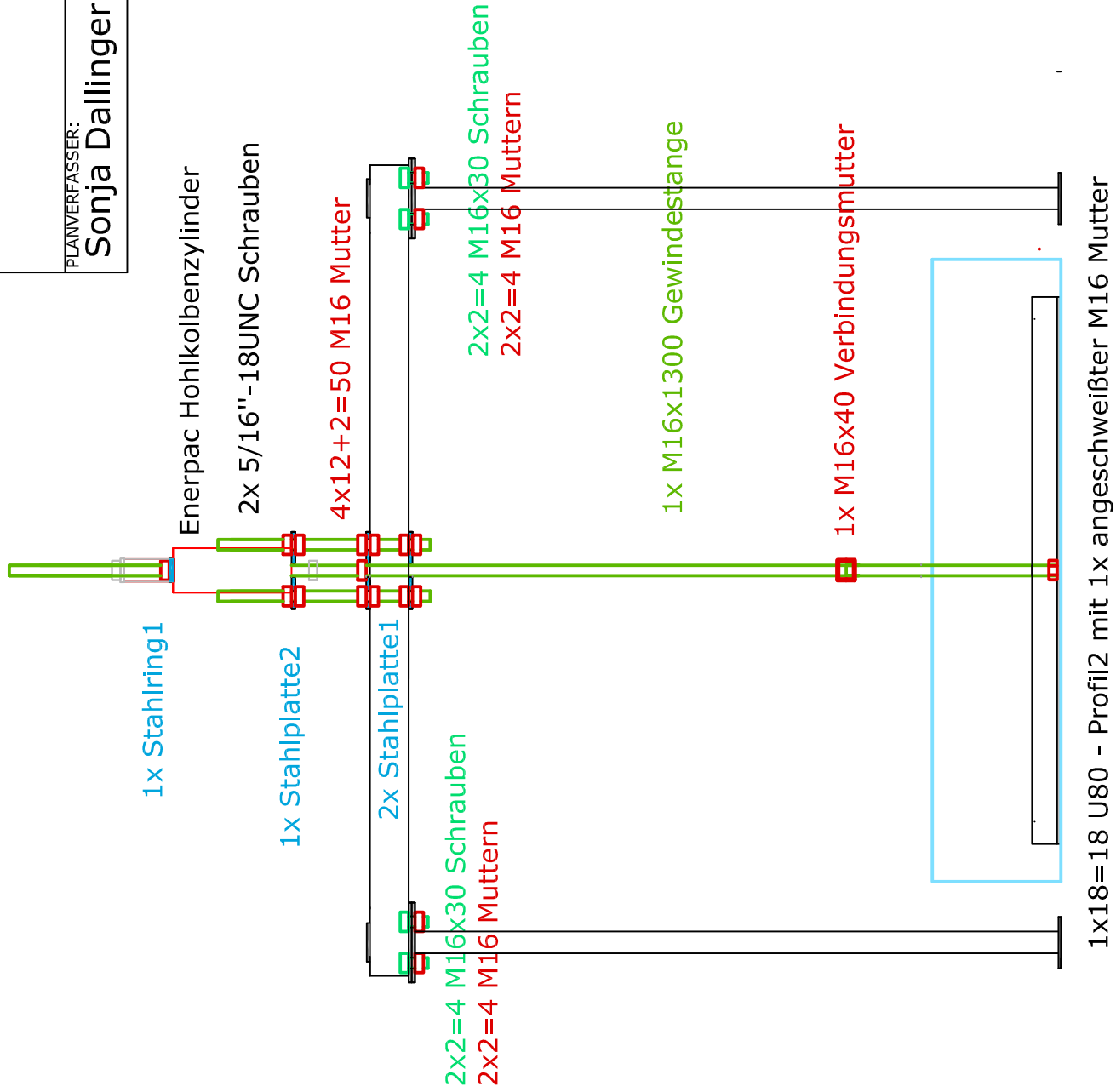




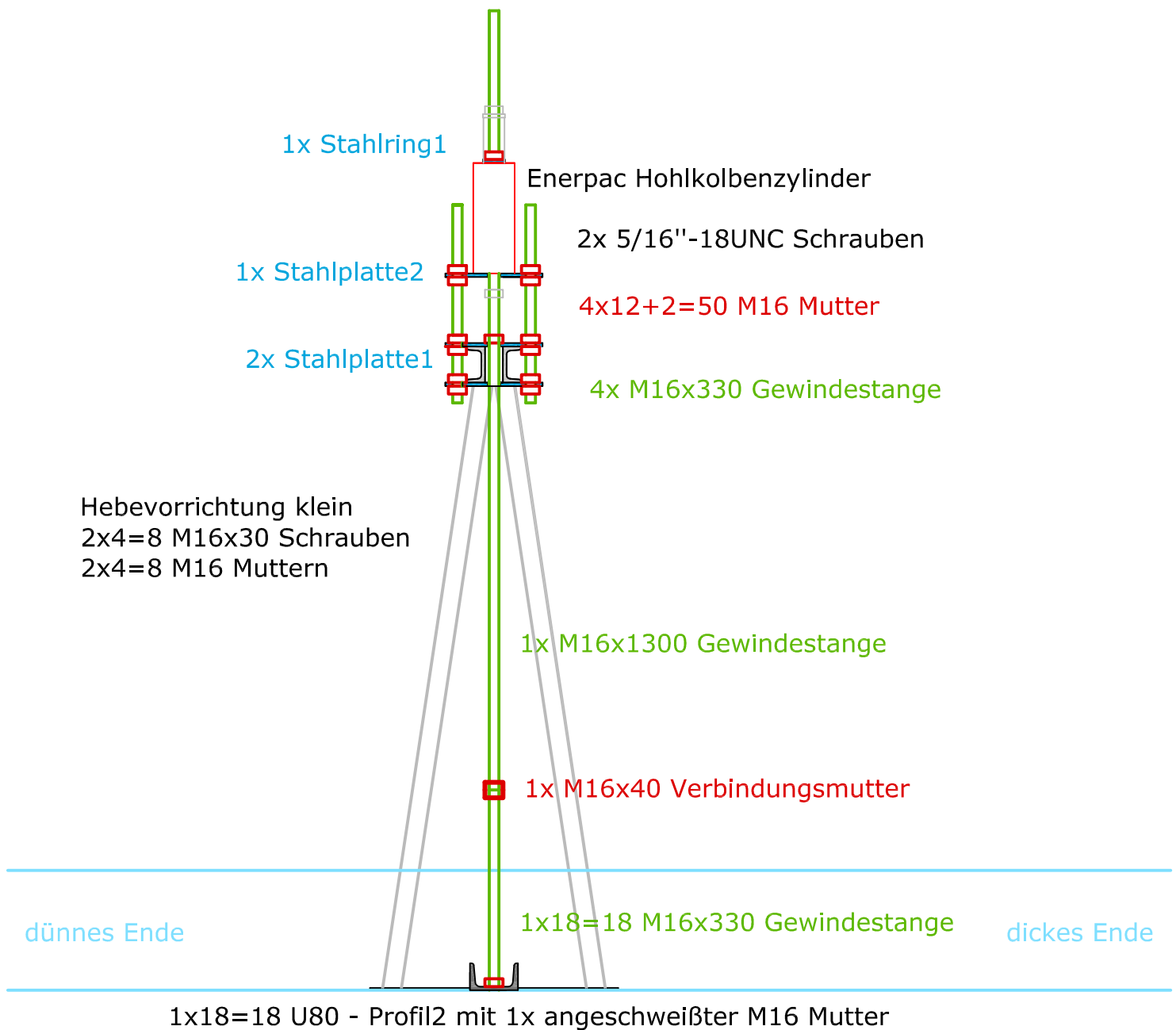
PLANINHALT: <b>Hebevorrichtung groß</b>	MASSSTAB: <b>1:10 A4</b>
PLANVERFASSER: <b>Sonja Dallinger</b>	DATUM: <b>17.11.10</b>



PLANINHALT:	MASSTAB:
Hebevorrichtung klein	1:10 A4
PLANVERFASSTER:	DATUM:
Sonja Dallinger	17.11.10



PLANINHALT: <b>Hebevorrichtung klein</b>	MASSSTAB: <b>1:10 A4</b>
PLANVERFASSER: <b>Sonja Dallinger</b>	DATUM: <b>17.11.10</b>

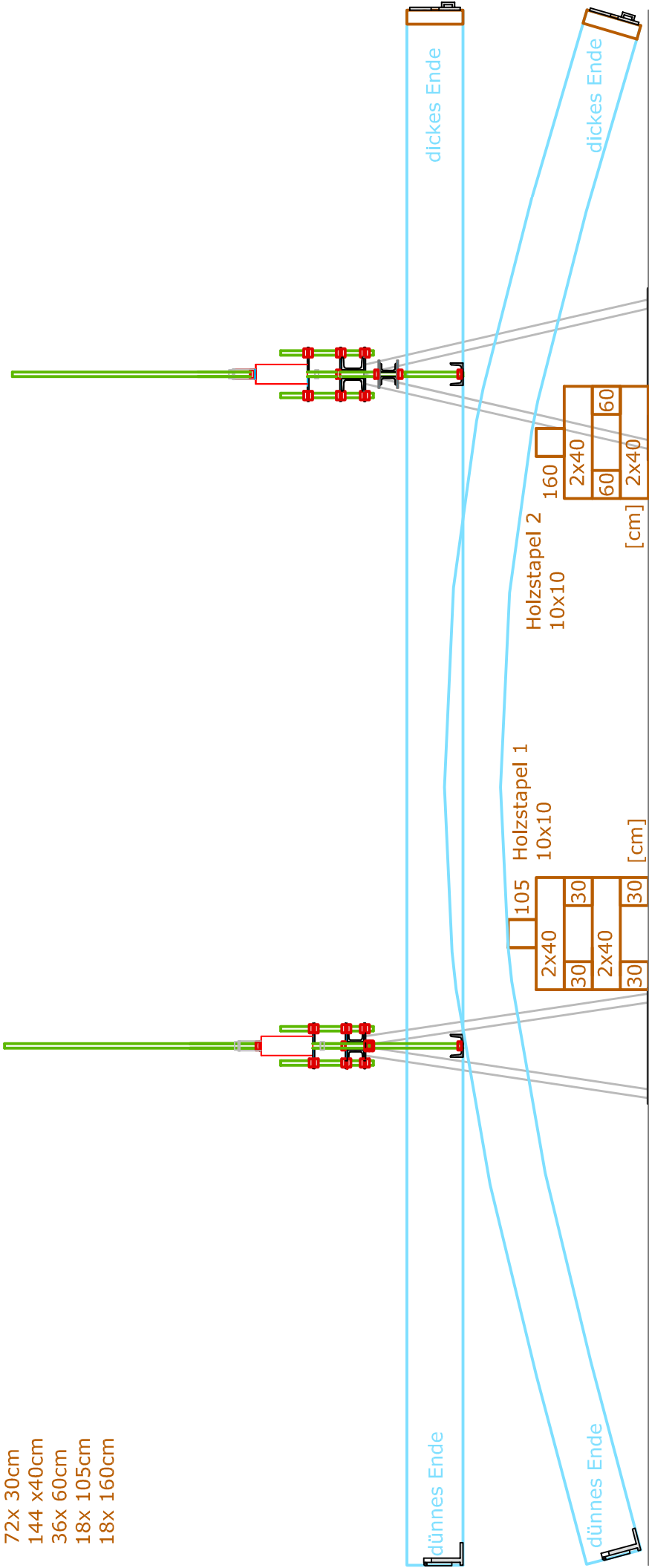


PLANINHALT: Hebevorrichtung, Holzstapel	MASSSTAB: 1:20 A4 1:15 A3
PLANVERFASSER: Sonja Dallinger	DATUM: 17.11.10

PLANINHALT: Hebevorrichtung, Holzstapel	MASSSTAB: 1:20 A4 1:15 A3
	PLANVERFASSER: Sonja Dallinger
	DATUM: 17.11.10

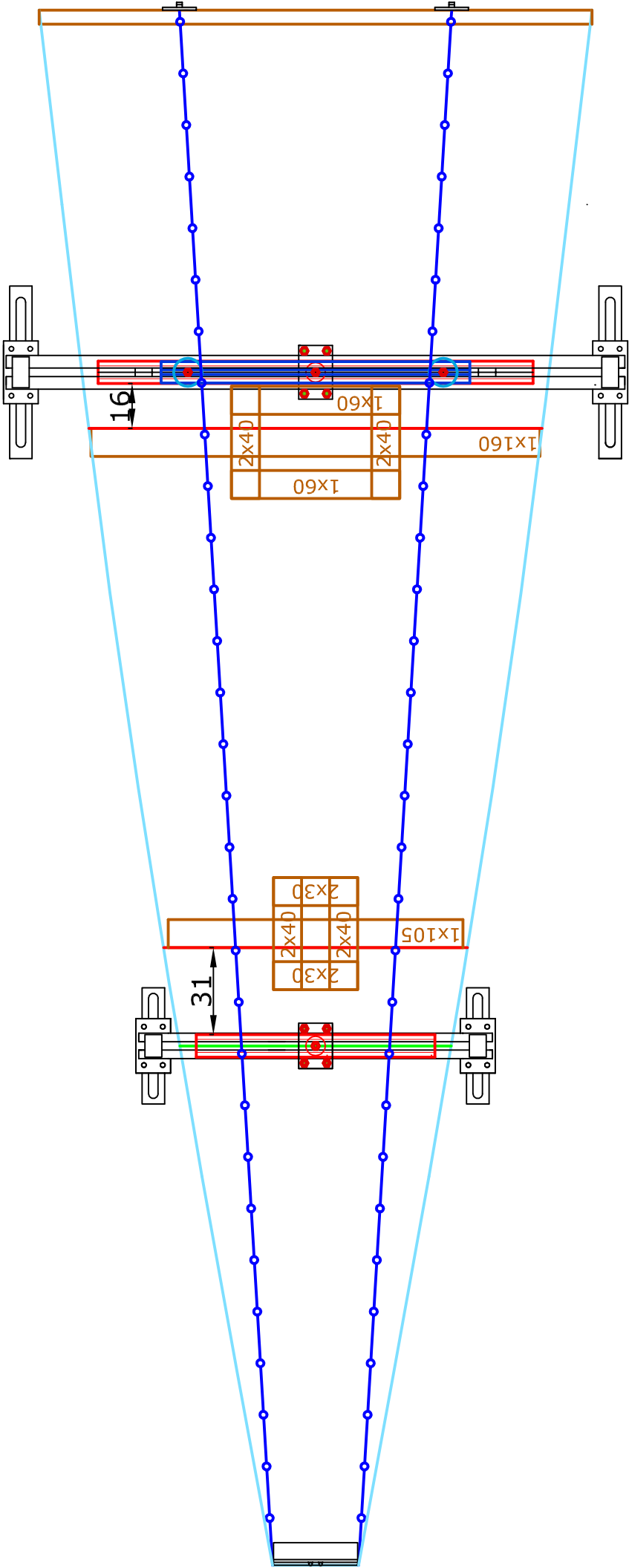
- Holzstapel 1  
 10x10cm Staffeln  
 1x 105cm  
 4x 40cm  
 4x 30cm
- Holzstapel 2  
 10x10cm Staffeln  
 1x 160cm  
 4x 40cm  
 2x 60cm
- \*18 = 18x 105cm  
 \*18 = 72x 40cm  
 \*18 = 72x 30cm
- \*18 = 18x 160cm  
 \*18 = 72x 40cm  
 \*18 = 60x 60cm

- Holzstapel 1+2  
 10x10cm Staffeln  
 72x 30cm  
 144 x40cm  
 36x 60cm  
 18x 105cm  
 18x 160cm

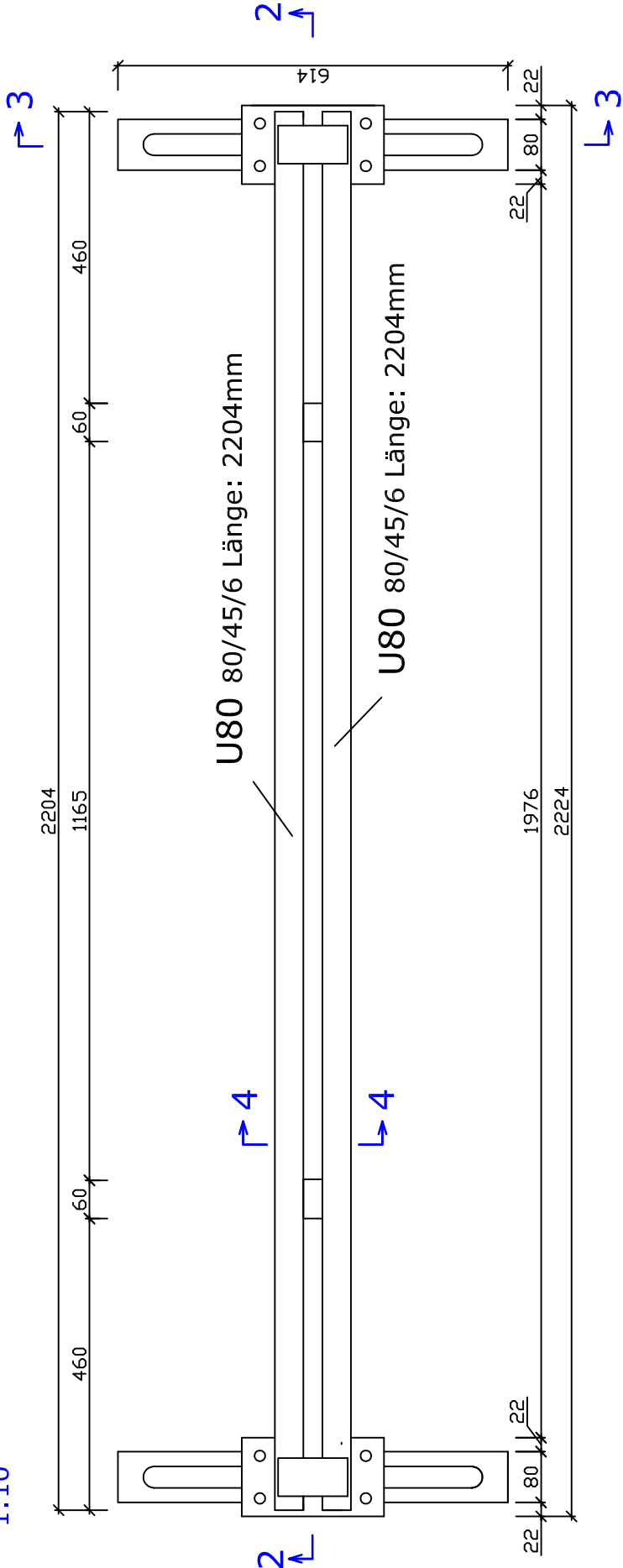




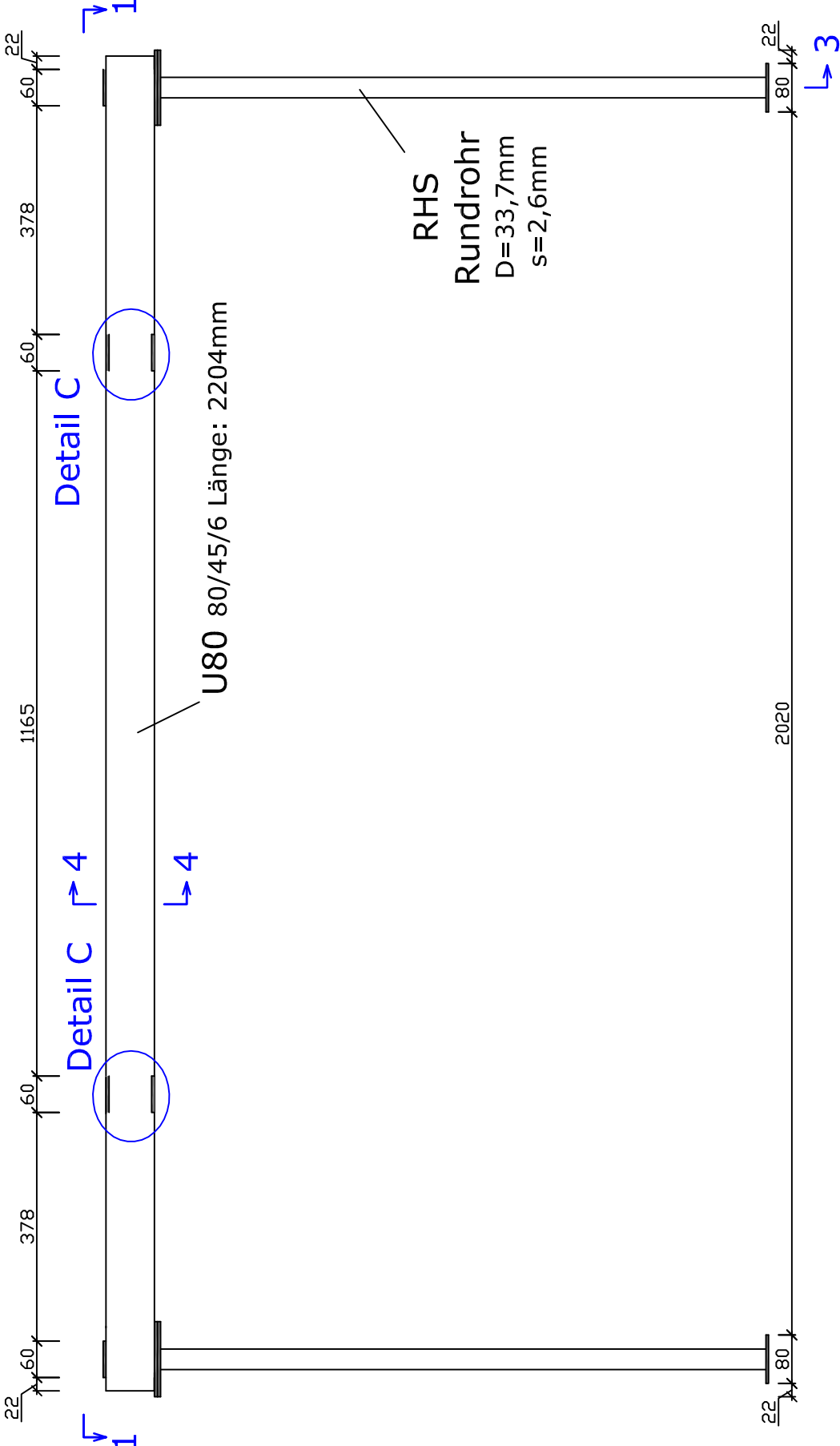
PLANINHALT: Hebevorrichtung, Holzstapel	MASSSTAB: 1:20 A4 1:15 A3
	PLANVERFASSTER: Sonja Dallinger
DATUM: 17.11.10	



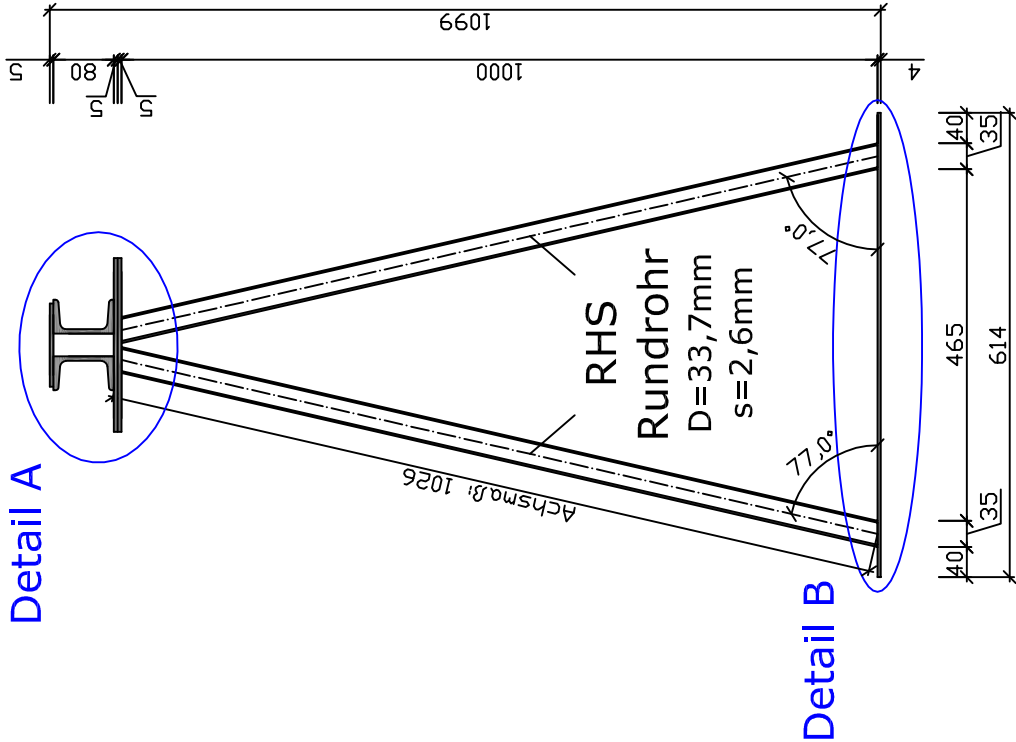
Draufsicht 1-1  
1:10



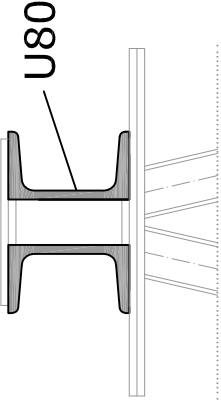
Schnitt 2-2  
1:10



Schnitt 3-3  
1:10



Schnitt 4-4  
1:5



Stahlgüte: S235

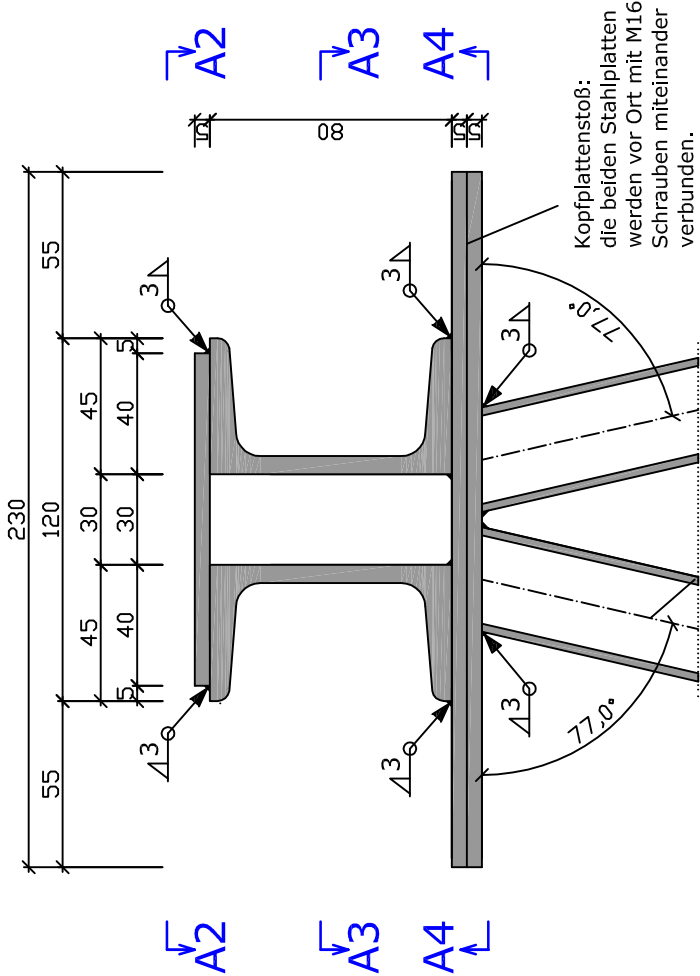
Maße in mm

HEBEVORRICHTUNG GROSS		
PLANINHALT:	MASSTAB:	
Draufsicht 1-1	1:10	
Schnitte 2-2, 3-3, 4-4	1:5	
PLANVERFASSTER:	DATUM:	
Sonja Dalling	20.10.10	
sdalling@mail.tuwien.ac.at		
Tel. +43-1-58801-21262		

Detail A

Schnitt A1-A1

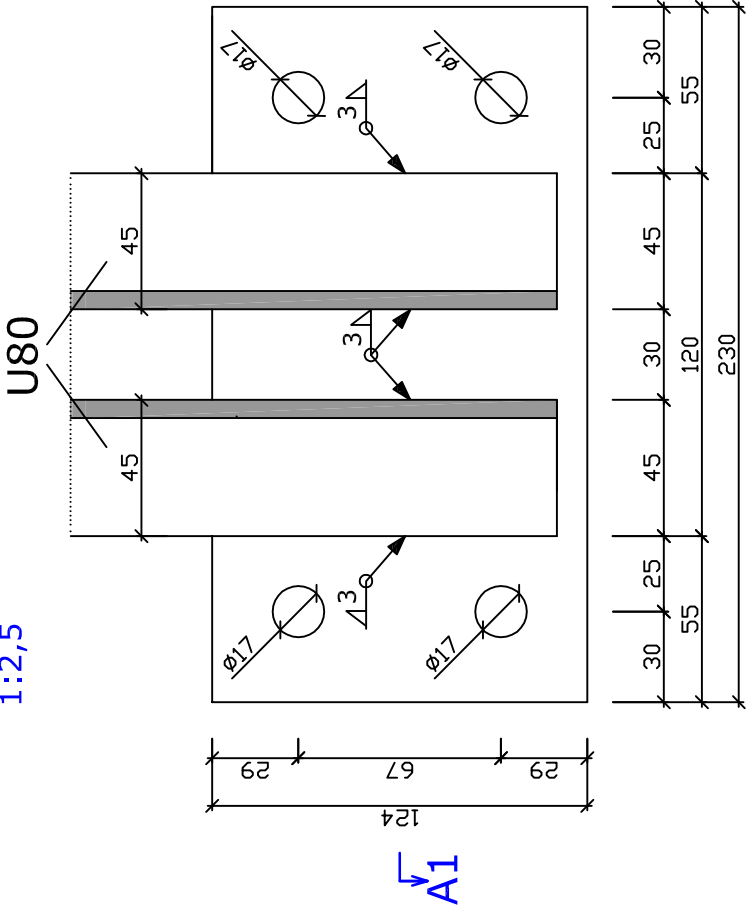
1:2,5



RHS Rundrohr  
D=33,7mm s=2,6mm

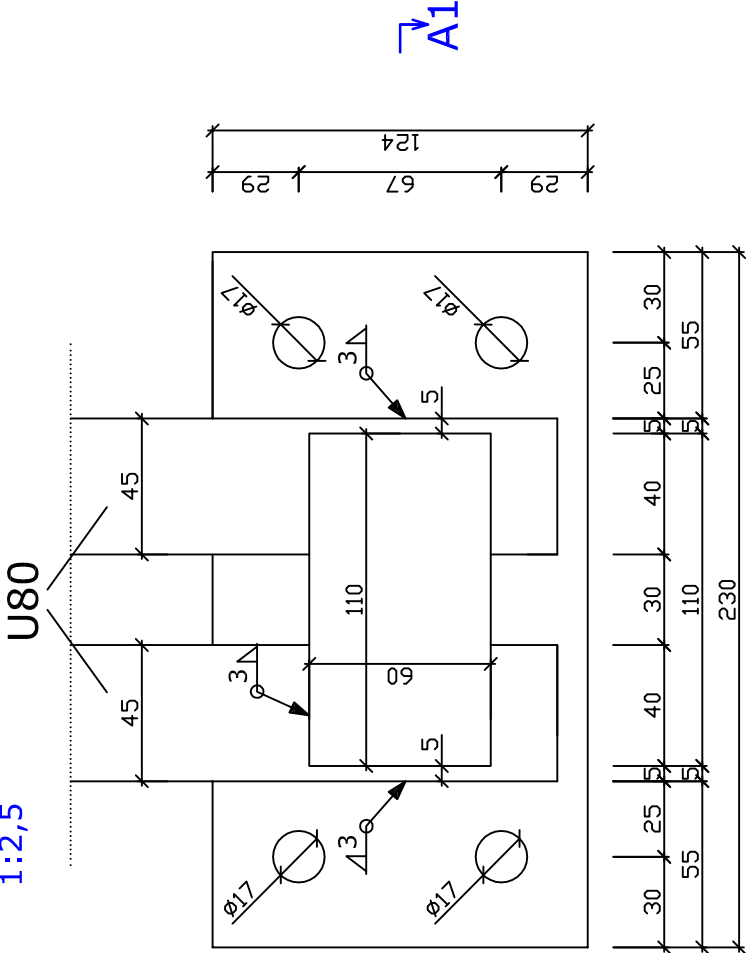
Schnitt A3-A3

1:2,5



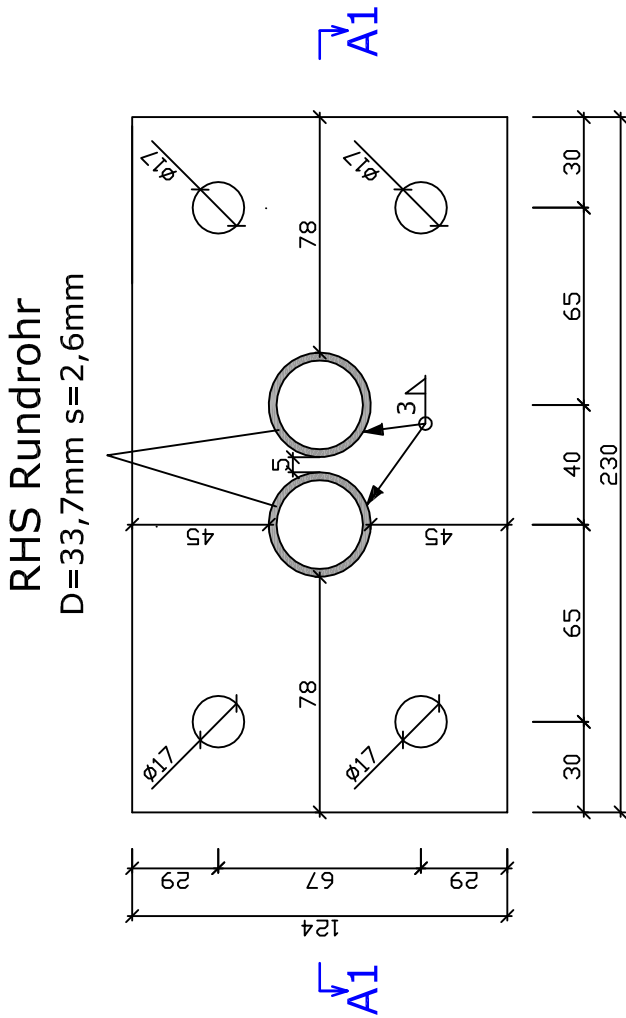
Schnitt A2-A2

1:2,5



Schnitt A4-A4

1:2,5

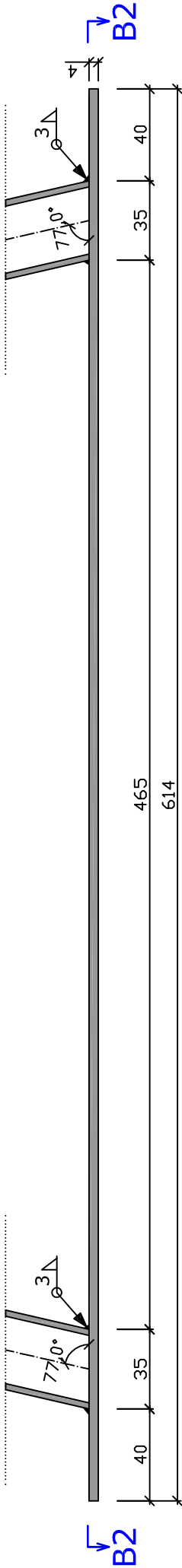


Stahlgüte: S235

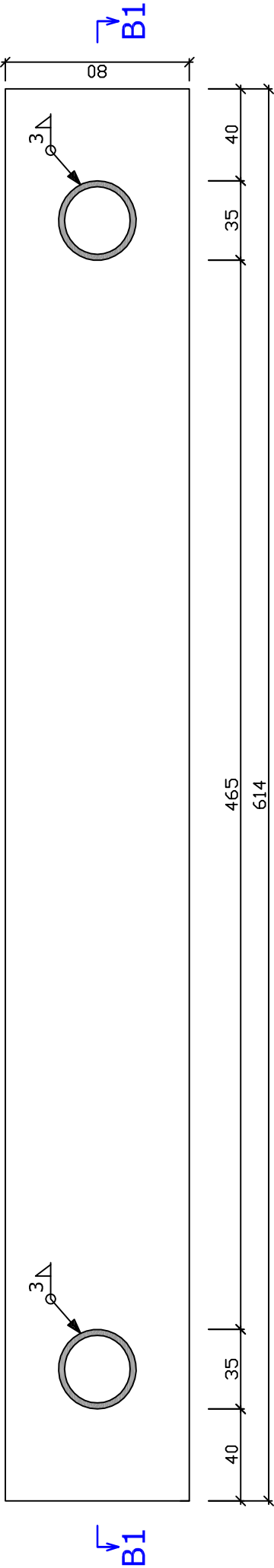
Maße in mm

HEBEVORRICHTUNG GROSS		
PLANINHALT:	MASSTAB:	1:2,5
PLANVERFASSTER:	DATUM:	20.10.10
Sonja Dalling sdalling@mail.tuwien.ac.at Tel. +43-1-58801-21262		

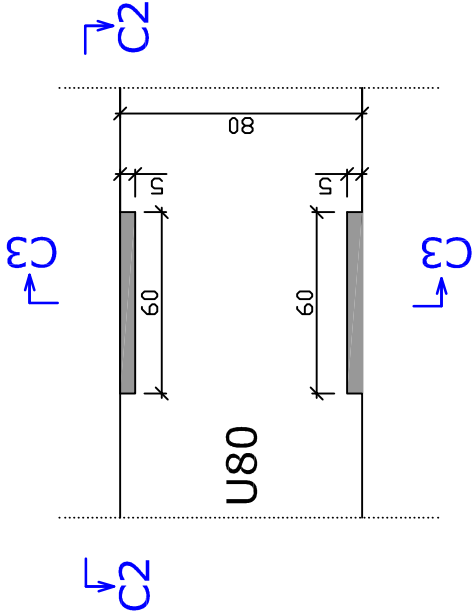
Detail B  
Schnitt B1-B1  
1:2,5



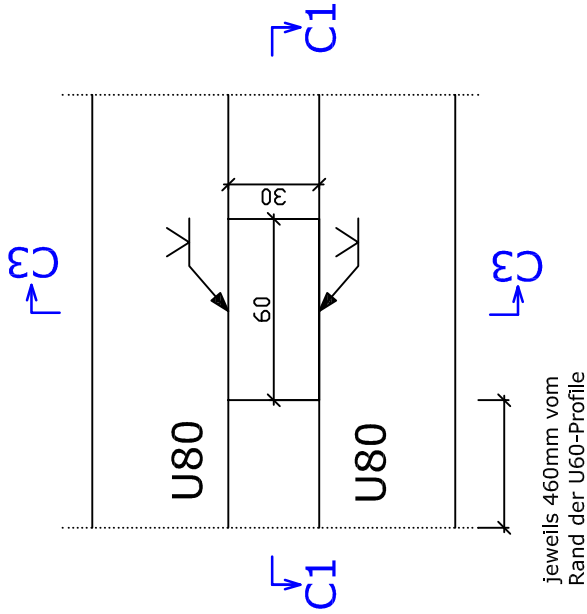
Schnitt B2-B2  
1:2,5



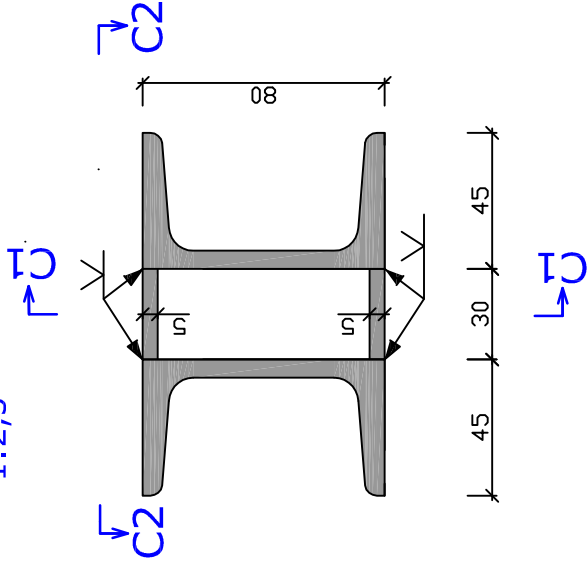
Detail C  
Schnitt C1-C1  
1:2,5



Schnitt C2-C2  
1:2,5



Schnitt C3-C3  
1:2,5

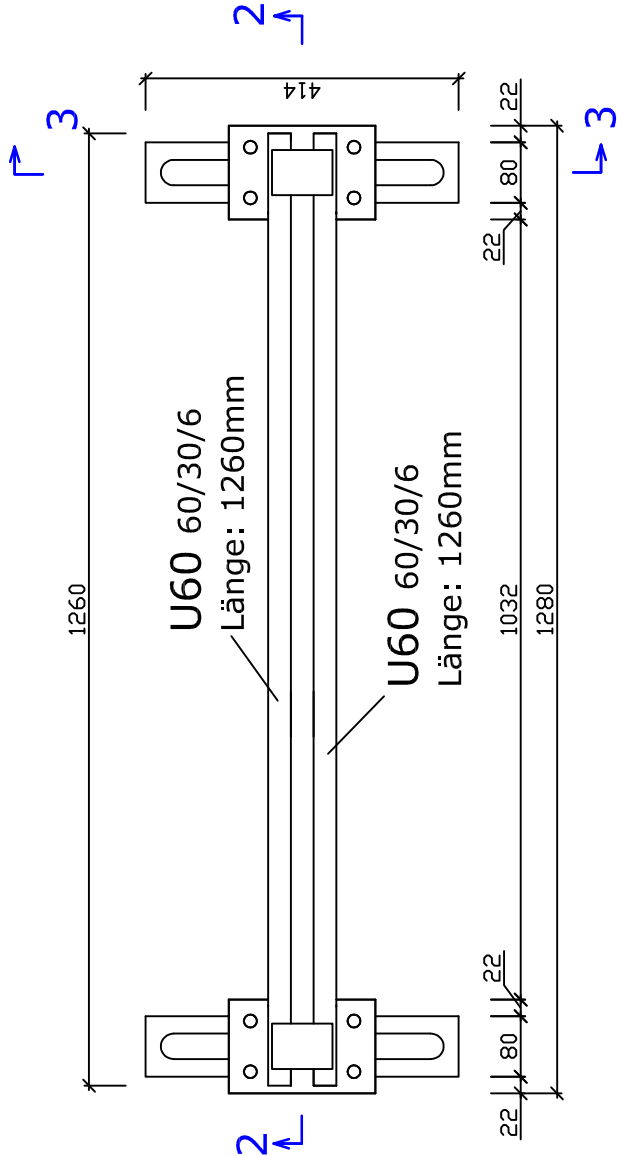


Stahlgüte: S235

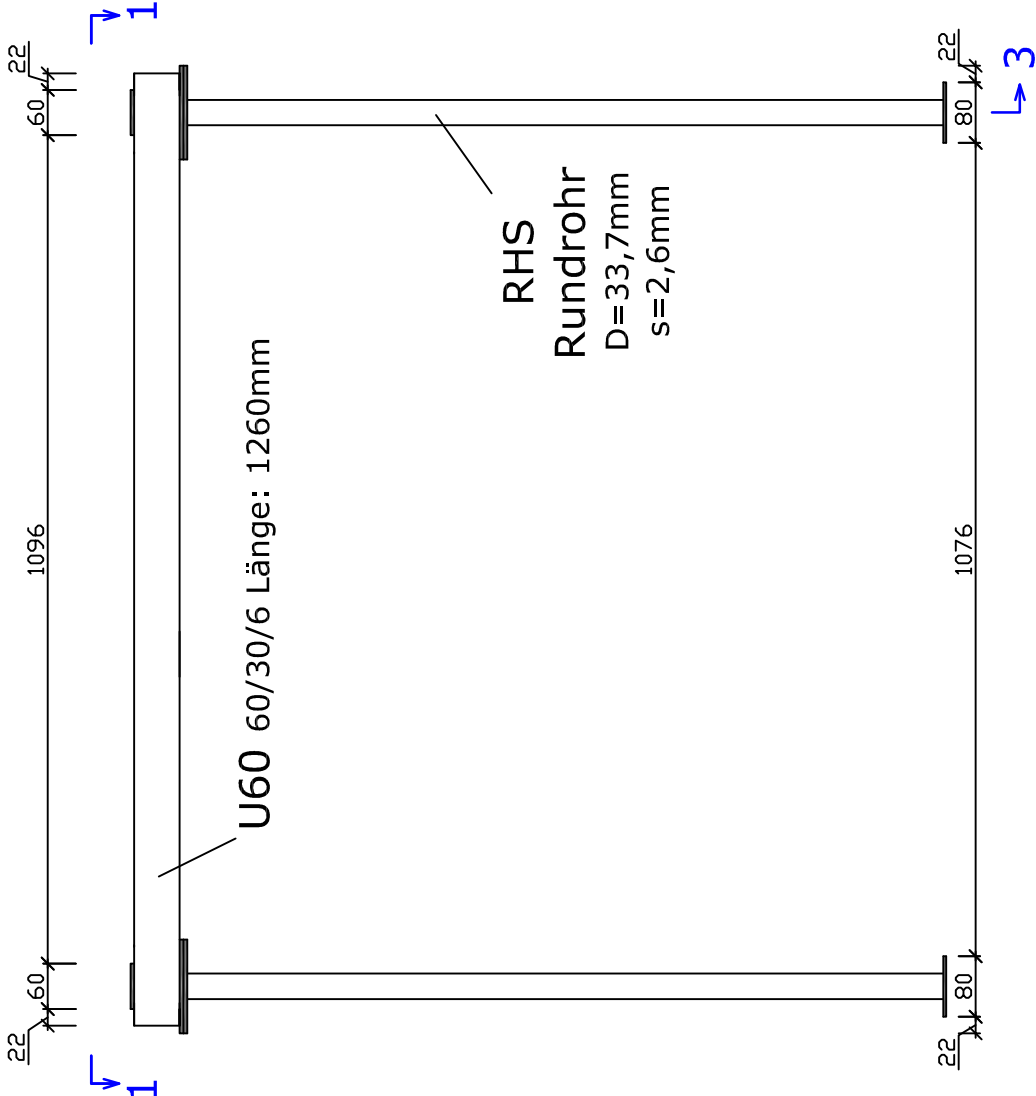
Maße in mm

HEBEVORRICHTUNG GROSS		
PLANINHALT:	MASSTAB:	1:2,5
DETAILS B, C		
PLANVERFASSTER:	DATUM:	20.10.10
Sonja Dalling		
sdalling@mail.tuwien.ac.at		
Tel. +43-1-58801-21262		

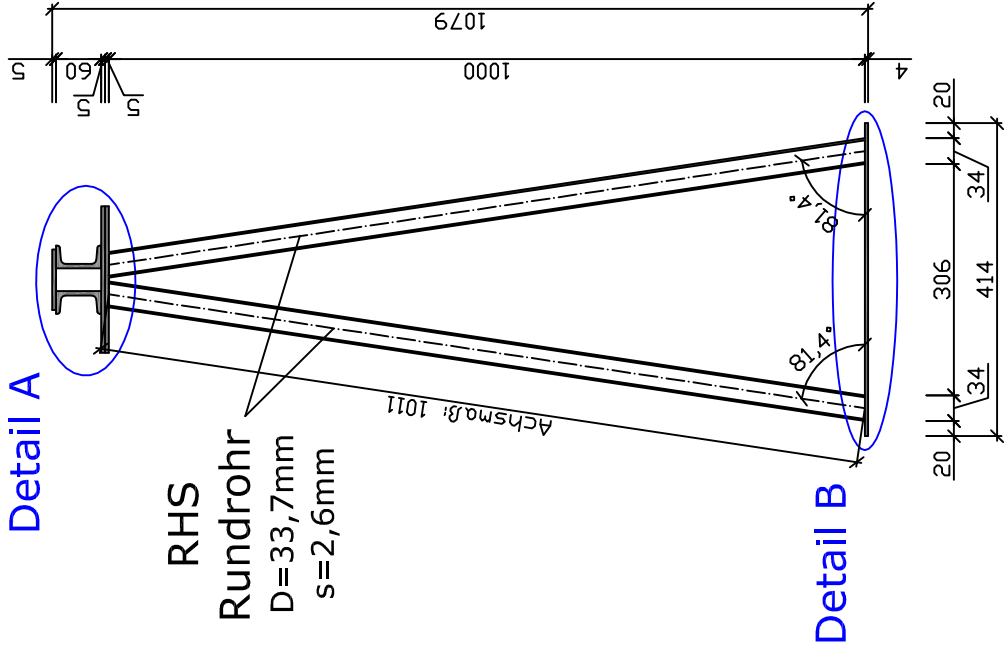
Draufsicht 1-1  
1:10



Schnitt 2-2  
1:10



Schnitt 3-3  
1:10

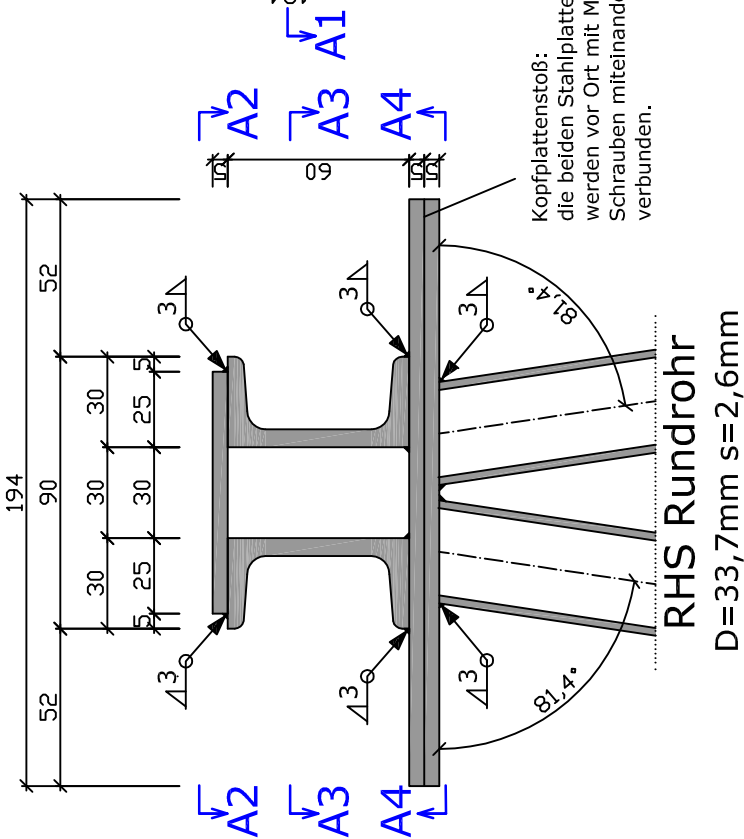


Stahlgüte: S235

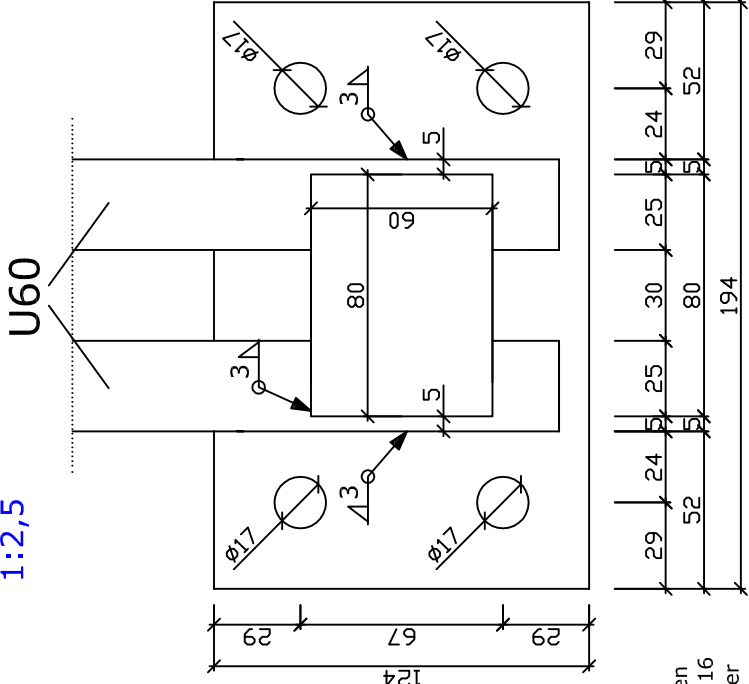
Maße in mm

HEBEVORRICHTUNG KLEIN		
PLANINHALT:	MASSTAB:	
Draufsicht 1-1	1:10	
Schnitte 2-2, 3-3	1:5	
PLANVERFASSTER:	DATUM:	
Sonja Dalling	20.10.10	
sdalling@mail.tuwien.ac.at		
Tel. +43-1-58801-21262		

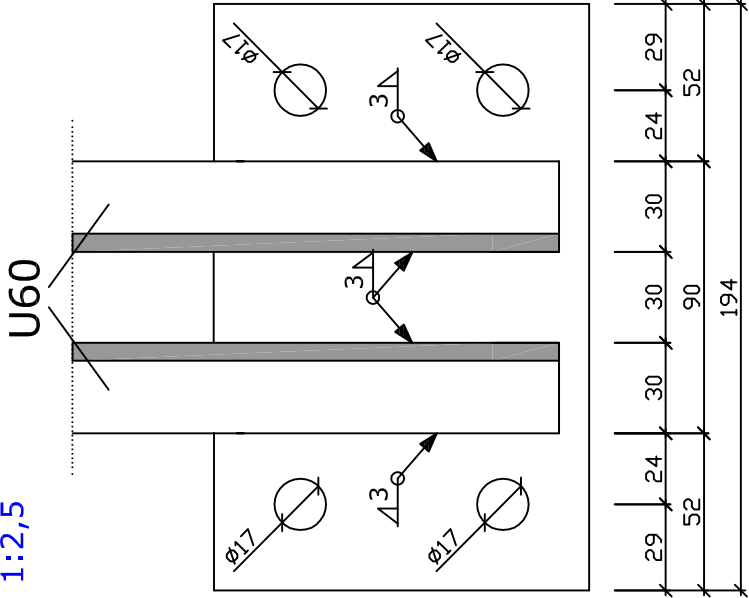
Detail A  
Schnitt A1-A1  
1:2,5



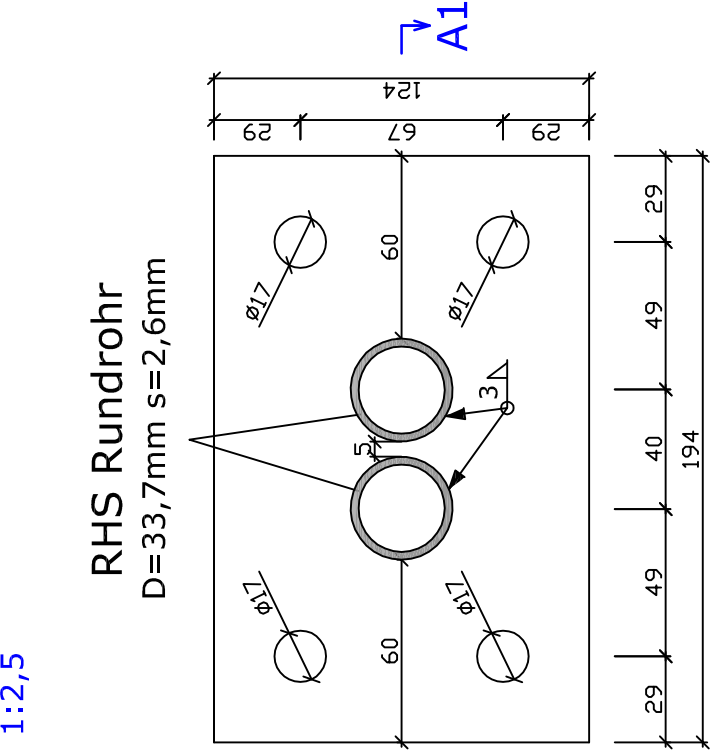
Schnitt A2-A2  
1:2,5



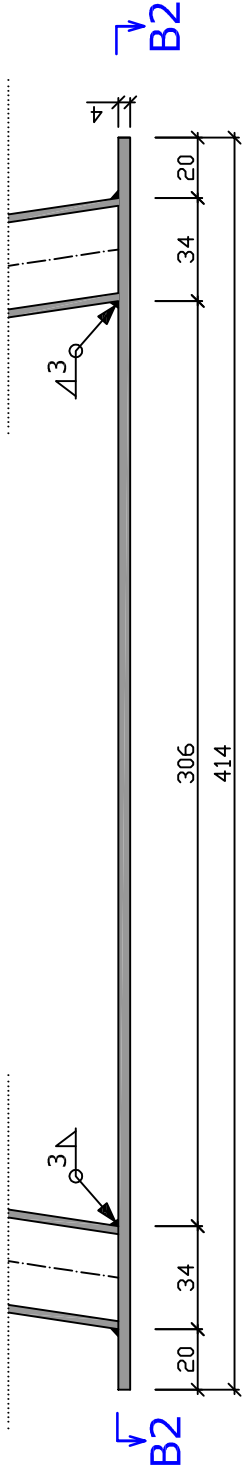
Schnitt A3-A3  
1:2,5



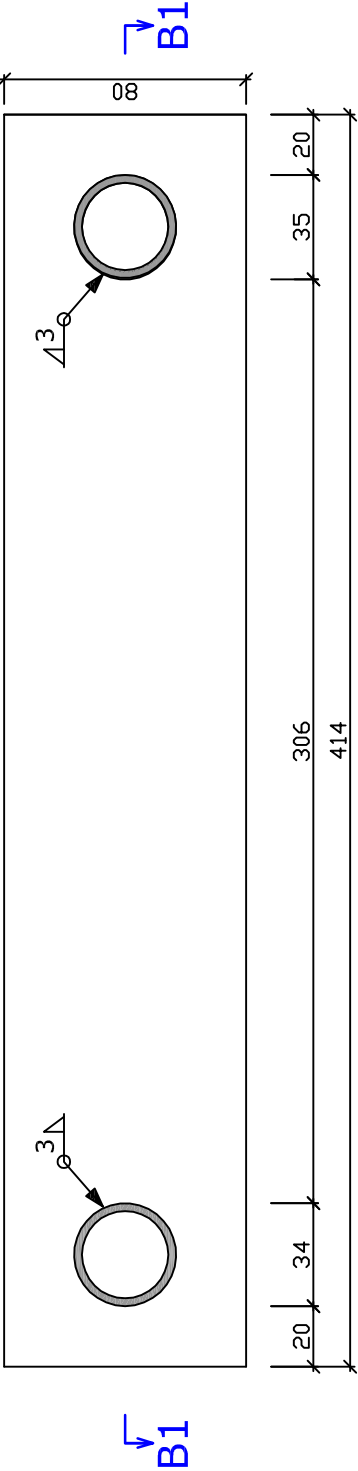
Schnitt A4-A4  
1:2,5



Detail B  
Schnitt B1-B1  
1:2,5



Schnitt B2-B2  
1:2,5



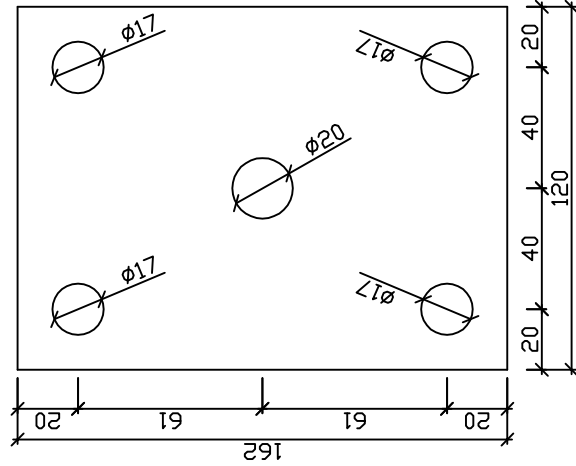
Stahlgüte: S235

Maße in mm

HEBEVORRICHTUNG KLEIN		
PLANINHALT:	MASSTAB:	1:2,5
PLANVERFASSER:	DATUM:	20.10.10
Sonja Dalling sdalling@mail.tuwien.ac.at Tel. +43-1-58801-21262		

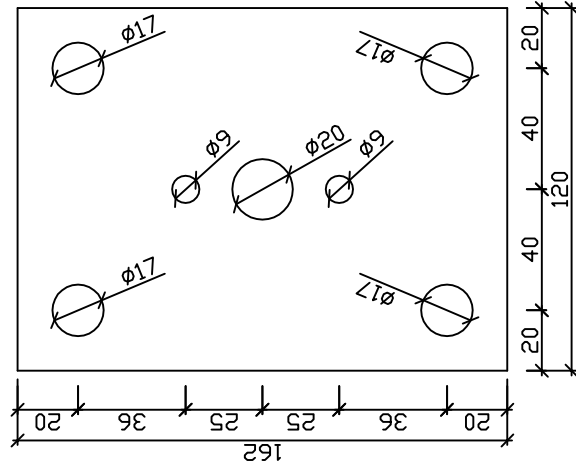
## Stahlplatte 1

2 Stück Dicke: 6mm



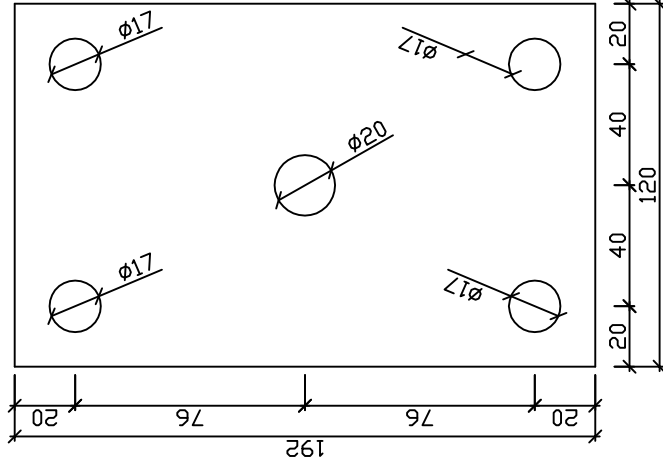
## Stahlplatte 2

1 Stück Dicke: 6mm



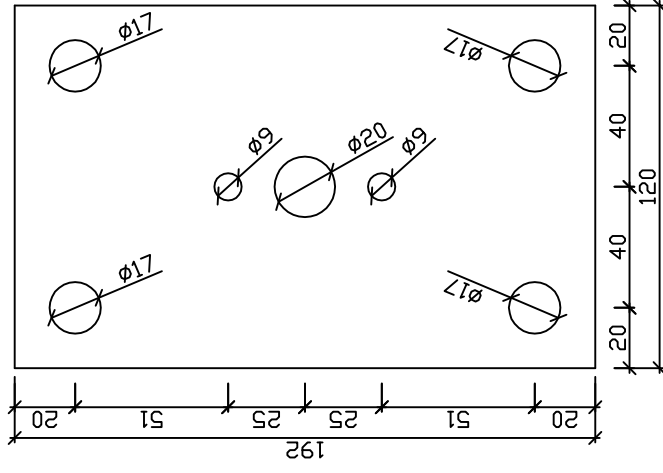
## Stahlplatte 3

2 Stück Dicke: 6mm



## Stahlplatte 4

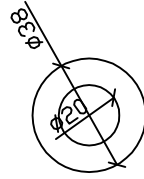
1 Stück Dicke: 6mm



## Stahlring 1

2 Stück

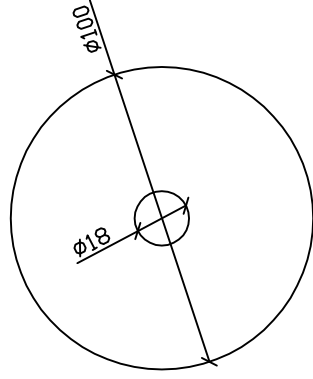
Dicke: 6mm



## Stahlring 2

6 Stück

Dicke: 6mm



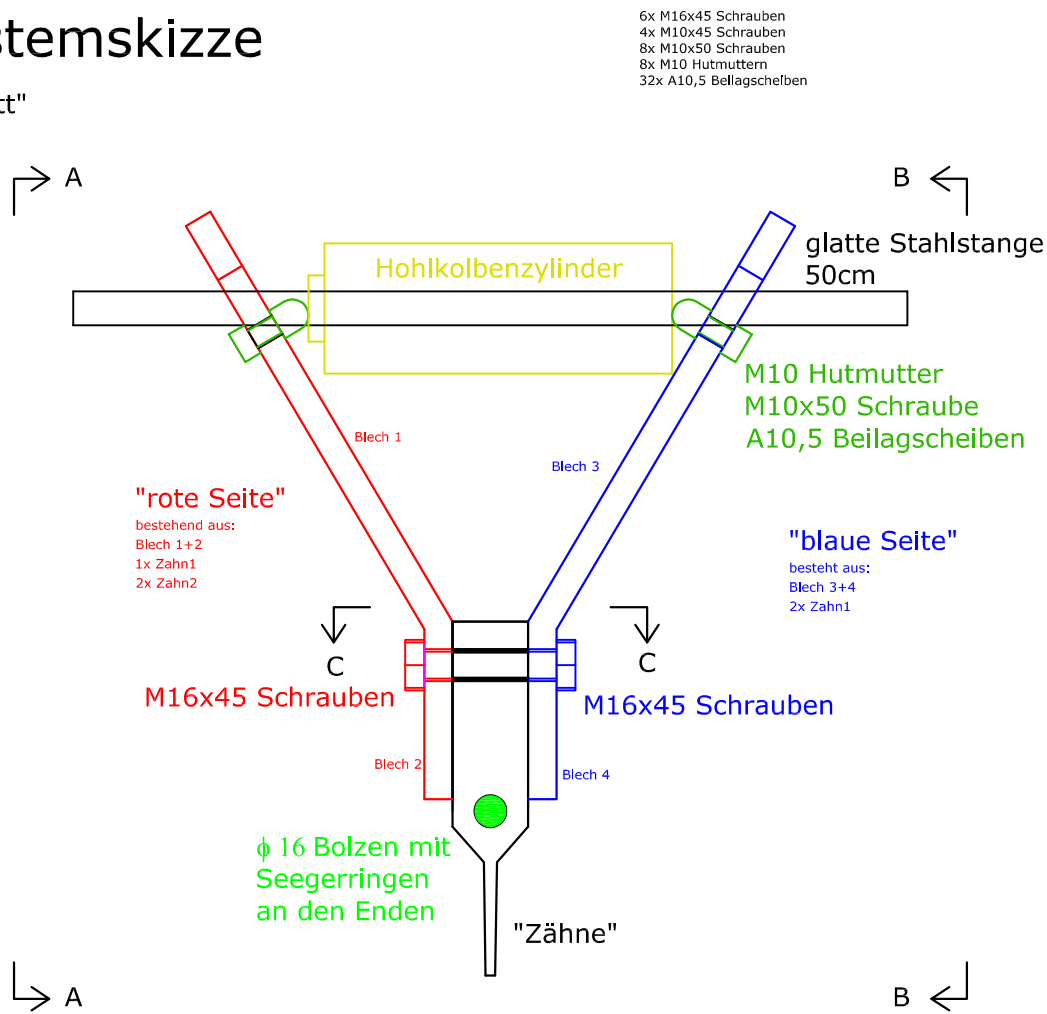
Stahlgüte: S235

Maße in mm

STAHLTEILE	
PLANINHALT:	MASSSTAB:
Platten 1,2,3,4; Stahlring 1,2	1:2,5
PLANVERFASSTER:	DATUM:
Sonja Dallinger sdalling@mail.tuwien.ac.at Tel. +43-1-58801-21262	20.10.10

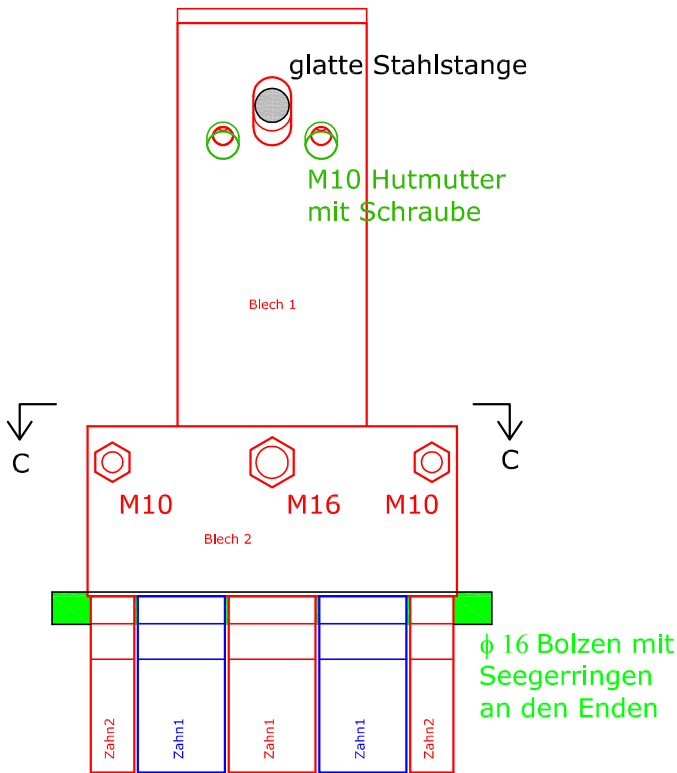
Systemskizze

"Schnitt"



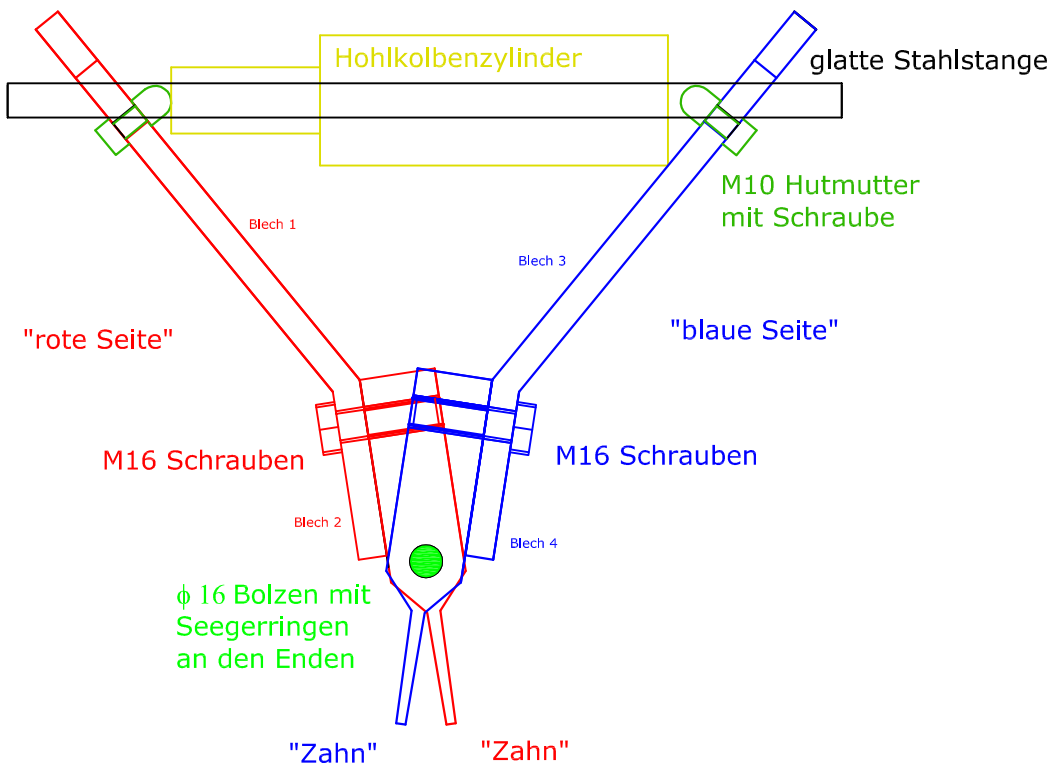
Systemskizze

Ansicht - rote Seite A-A



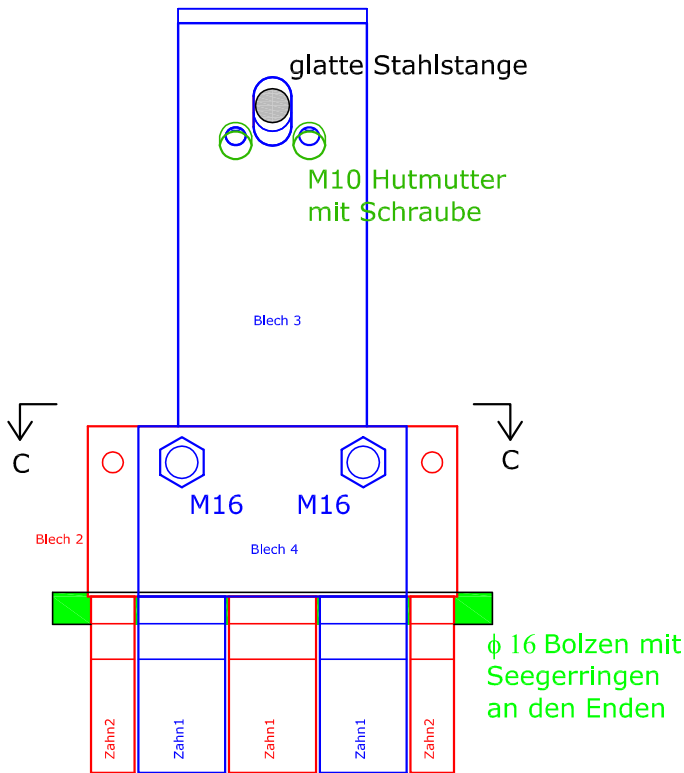
Systemskizze

geöffneter Zustand - "Schnitt"



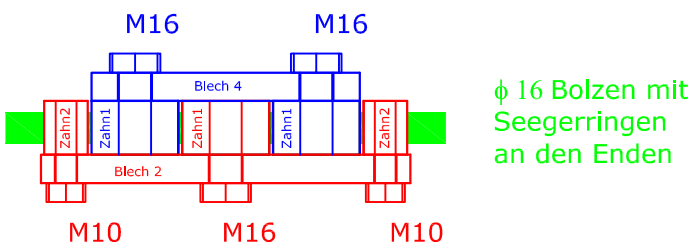
Systemskizze

Ansicht -blaue Seite B-B



Systemskizze

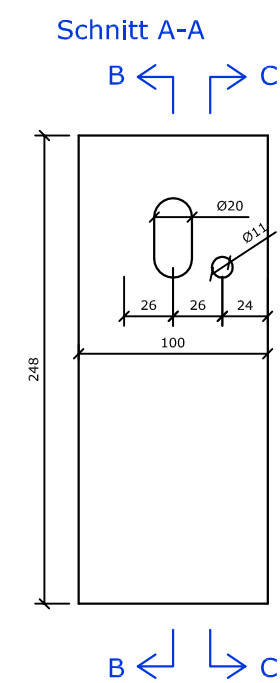
Schnitt C-C



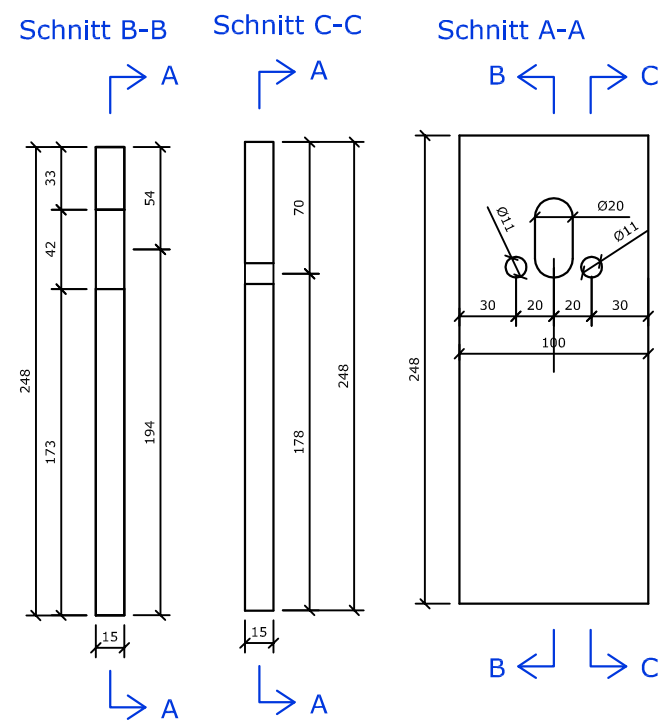
PLANINHALT: Stahlzange zum Brechen der Einschnitte	MASSTAB: 1:5
PLANVERFASSER: Sonja Dallinger	DATUM: 12.11.10



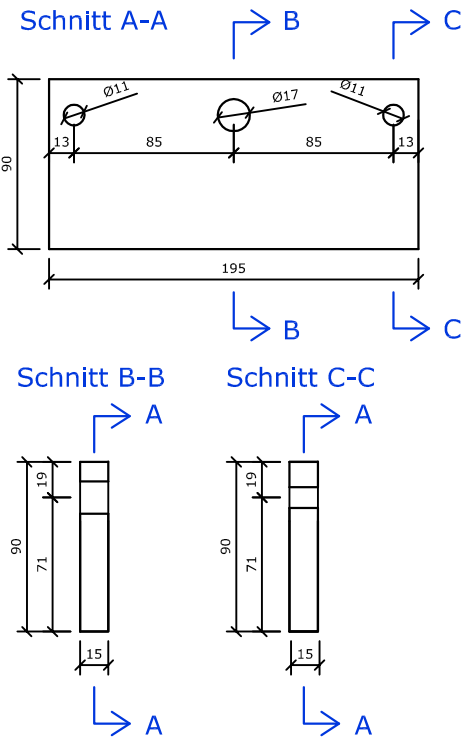
Blech 1 2 Stück



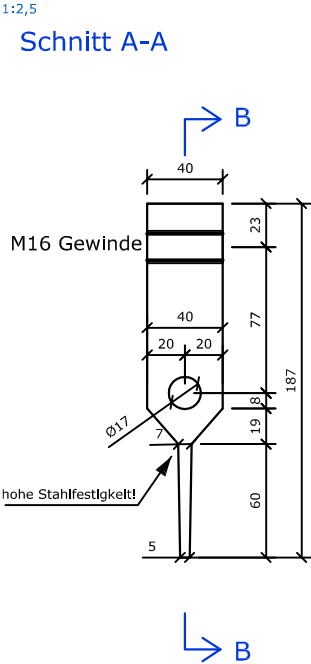
Blech 3 2 Stück



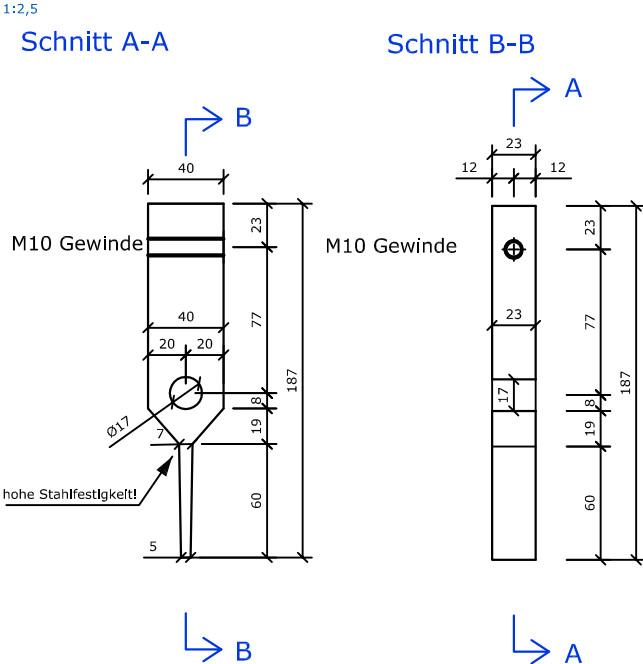
Blech 2 2 Stück



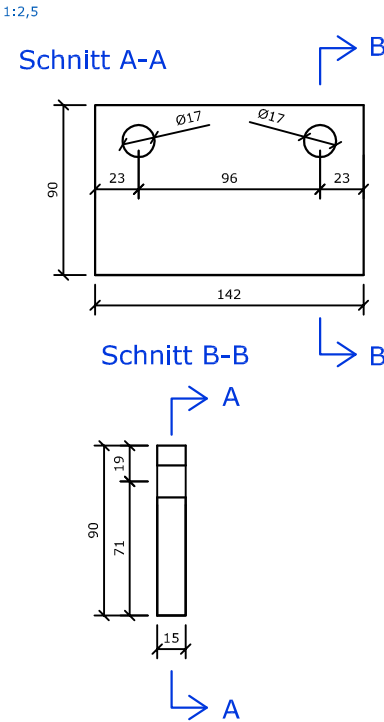
Zahn 1 6 Stück



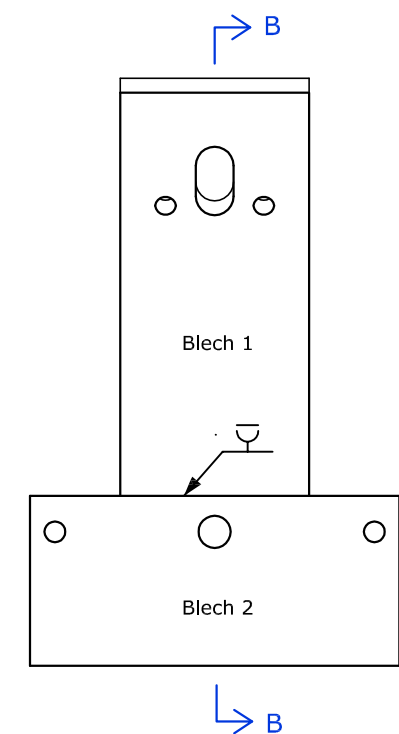
Zahn 2 4 Stück



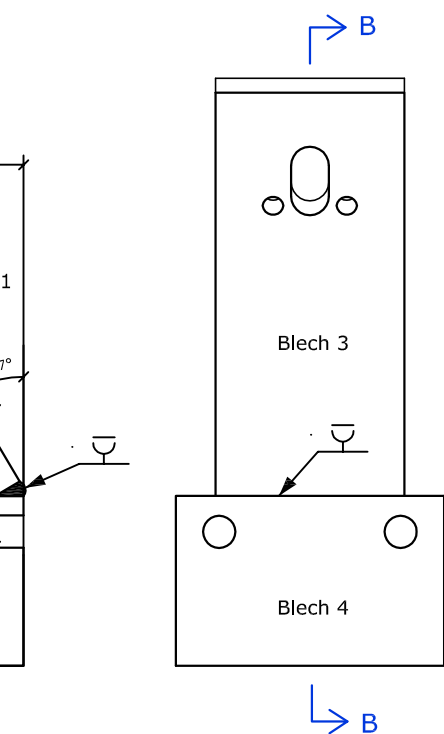
Blech 4 2 Stück



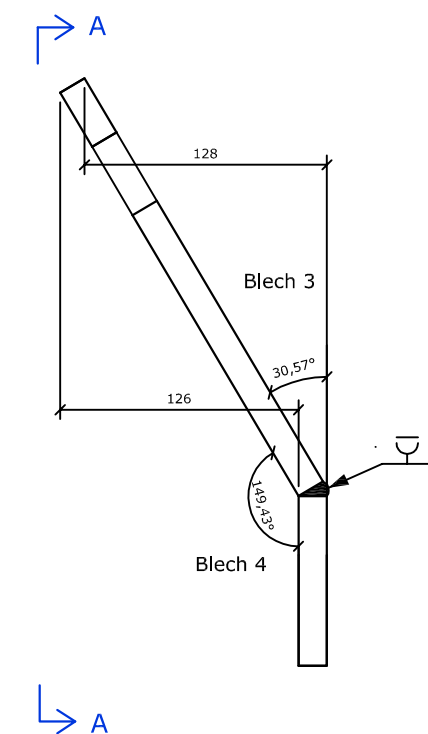
Blech 1+2 2 Stück  
Ansicht A-A



Blech 3+4 2 Stück  
Ansicht A-A

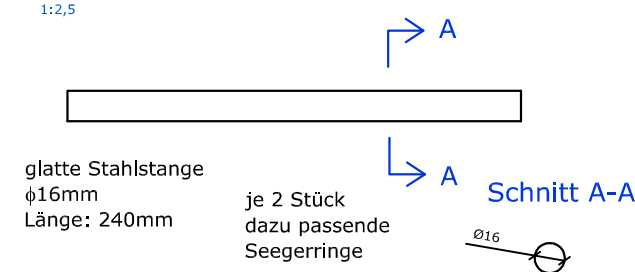


Schnitt B-B



Stahlgüte: S 235  
Korrosionsschutz

Bolzen 2 Stück



**Zähne und Bolzen:**  
Stahlgüte:  
mindestens: Streckgrenze=69kN/cm<sup>2</sup>  
zulässige  
Normalspannung=41kN/cm<sup>2</sup>  
Korrosionsschutz

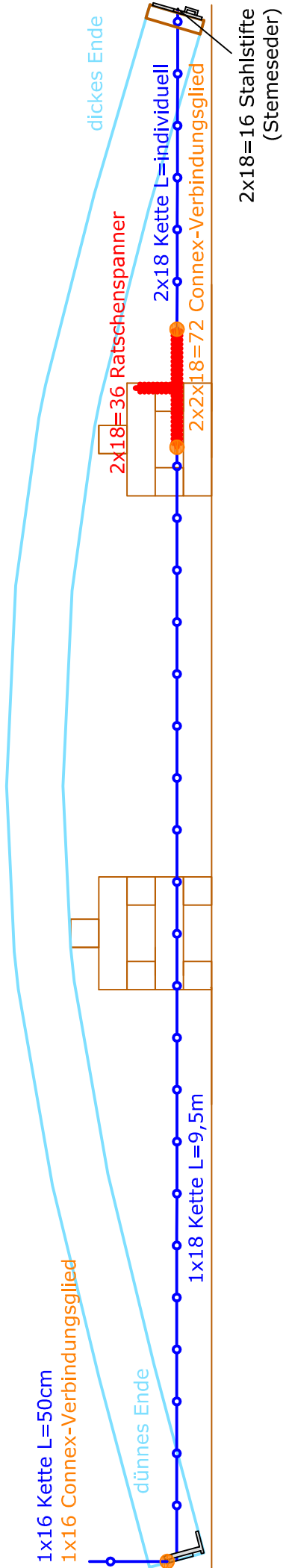
**Bleche:**  
Stahlgüte: S 235  
Korrosionsschutz

PLANINHALT: <b>Stahlzange zum Brechen der Einschnitte</b>	MASSTAB: <b>1:4</b>
PLANVERFASSER: <b>Sonja Dallinger</b>	DATUM: <b>12.11.10</b>

"Aufhängung" 16x

- 1x16 M16x250 Gewindestange
- 1x16 M16 Mutter
- 1x16 M16 Ringmutter
- 2x16=32 Connex-Verbindungsglied
- 1x16 Kette
- 1x16 Parallelhaken PSW

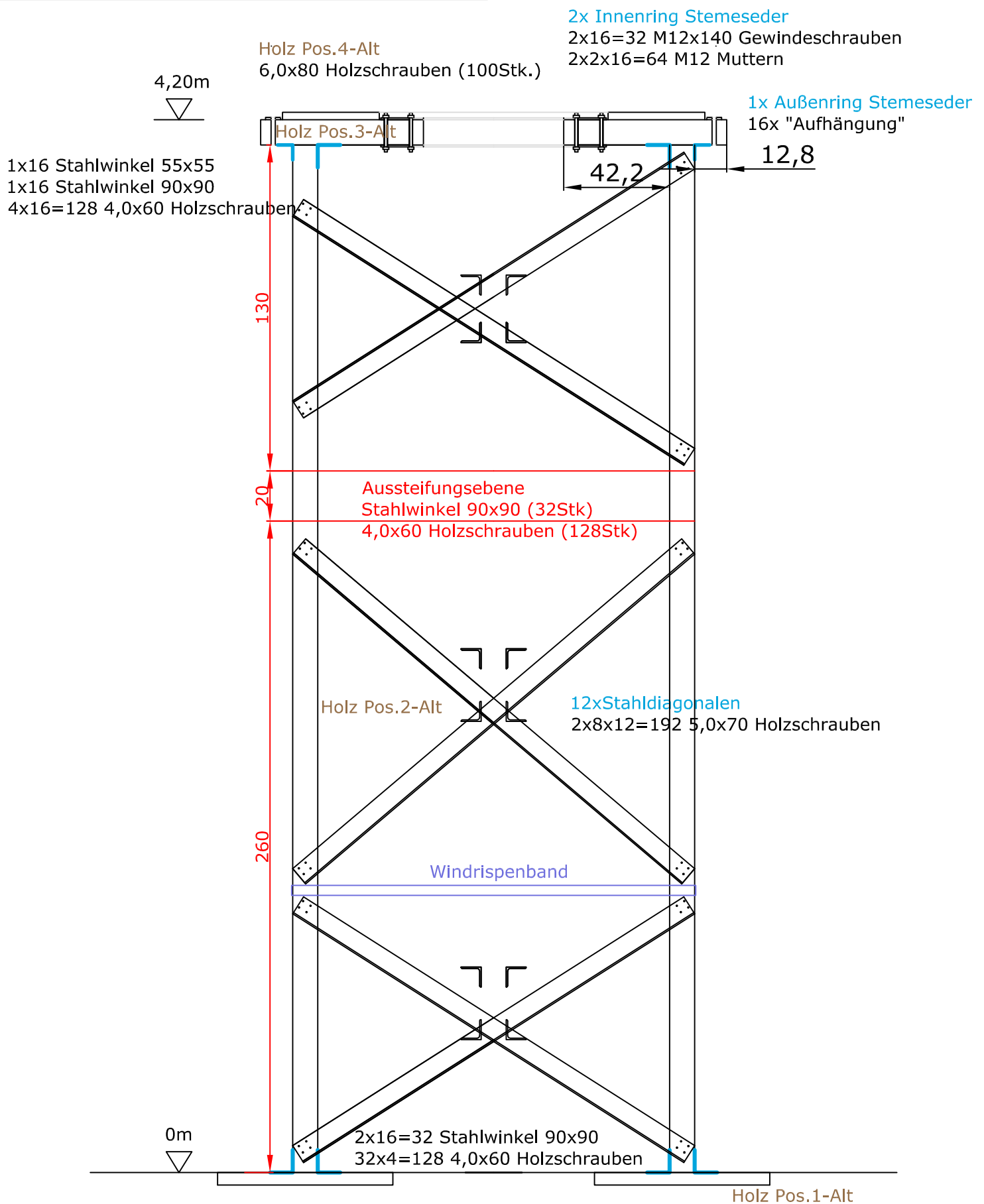
PLANINHALT: Pewag Teile	MASSTAB: 1:20 A4 1:15 A3
PLANVERFASSTER: Sonja Dallinger	DATUM: 17.11.10



### B.3 Mounting tower

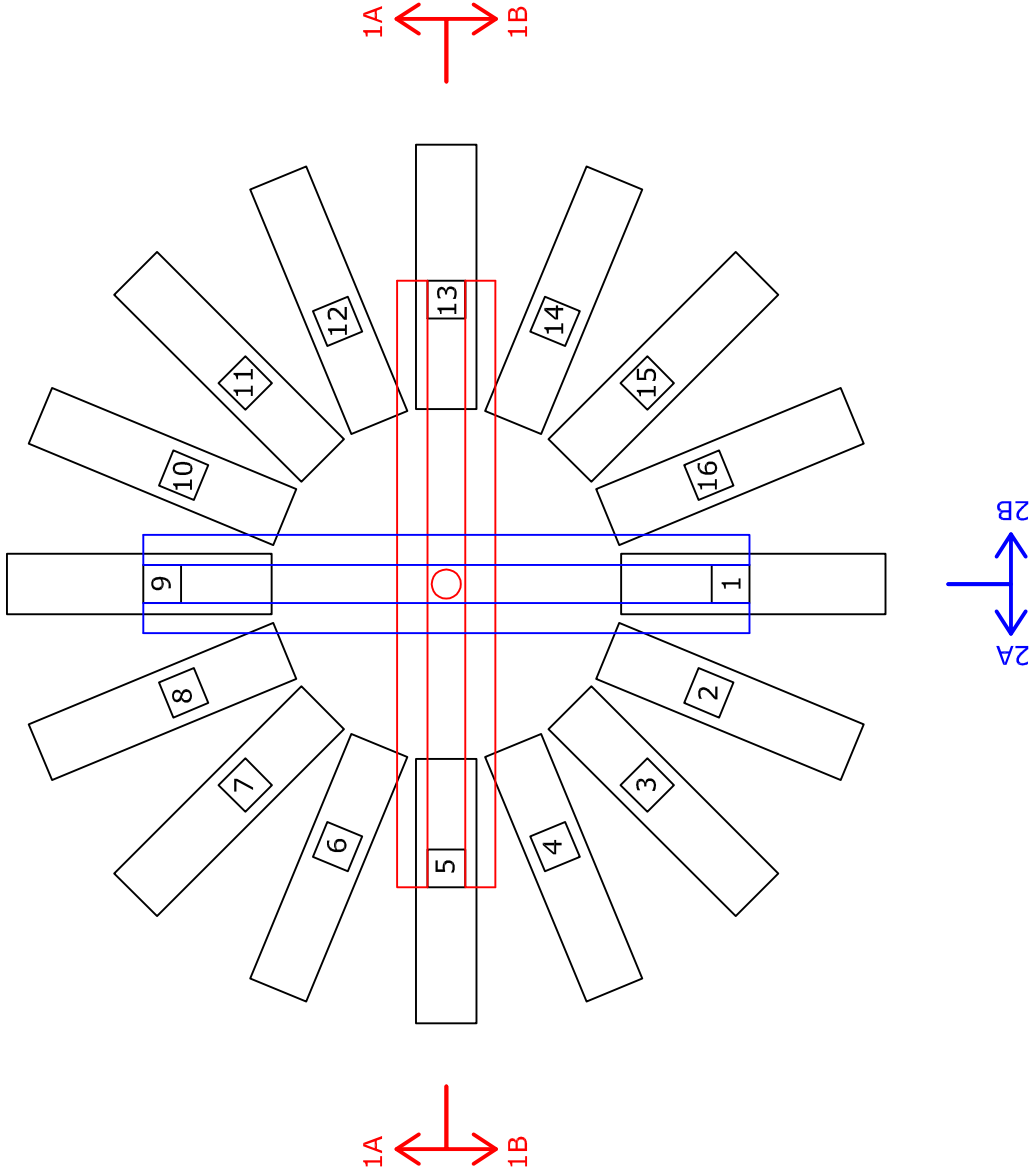
- Montageturm - schematische Darstellung (1)
- Montageturm - Fundament (1)
- Montageturm - Grundriss Diagonalen (1)
- L-Profil 1,2,3,4 (1)
- Montageturm - Diagonalen - Schnitt 1A-1A (1)
- Montageturm - Diagonalen - Schnitt 2A-2A (1)
- Montageturm - Diagonalen - Schnitt 1B-1B (1)
- Montageturm - Diagonalen - Schnitt 2B-2B (1)
- Innenring 1 (1)
- Außenring 1 (1)
- Montageturm - Holzpositionen (1)

PLANINHALT: <b>Montageturm - schematische Darstellung</b>	MASSSTAB: <b>1:20 A4 1:15 A3</b>
PLANVERFASSER: <b>Sonja Dallinger</b>	DATUM: <b>17.11.10</b>





PLANINHALT: Montageturm - Grundriss Diagonalen	MASSTAB: 1:20 A4 1:15 A3
	DATUM: 17.11.10
PLANVERFASSTER: Sonja Dallinger	

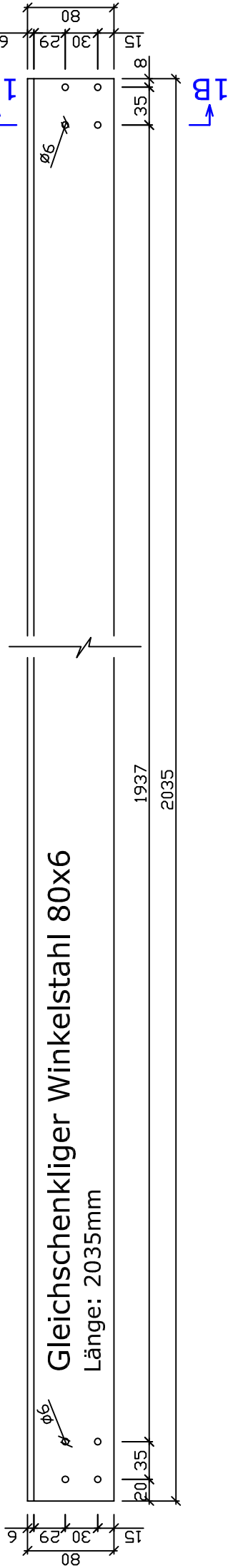


L-Profil 1

1:5

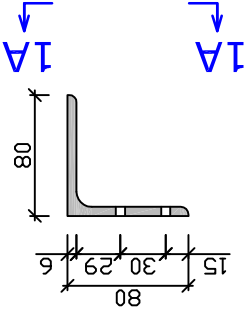
Ansicht 1A-1A

2 Stück



Schnitt 1B-1B

1:5

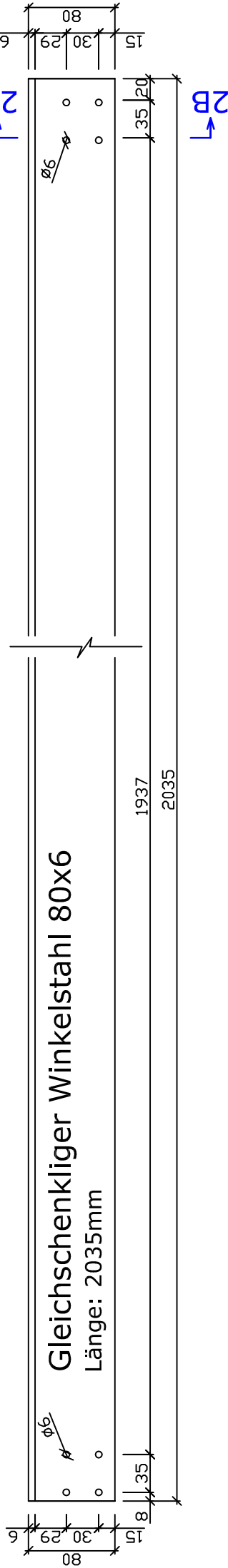


L-Profil 2

1:5

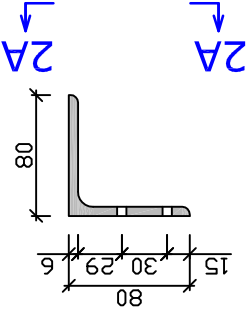
Ansicht 2A-2A

2 Stück



Schnitt 2B-2B

1:5

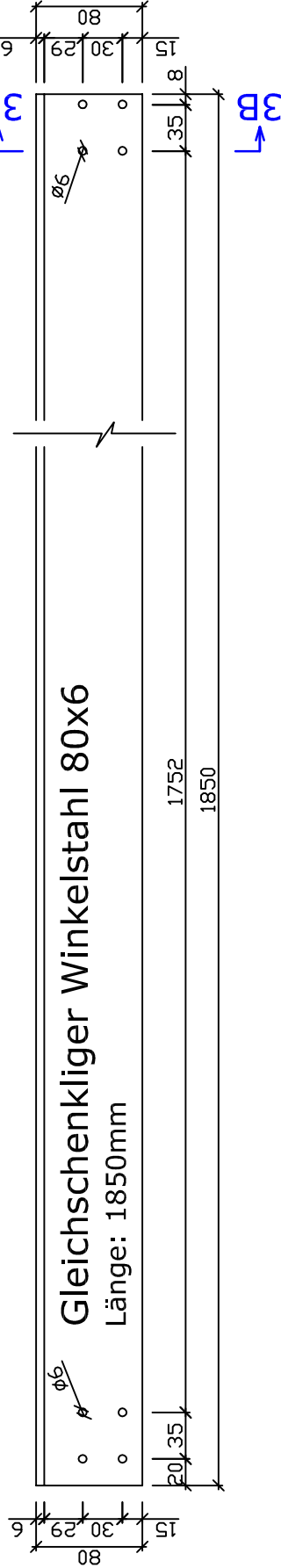


L-Profil 3

1:5

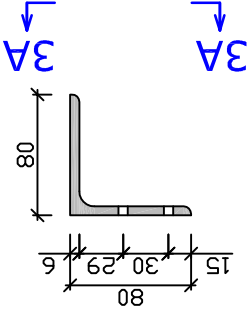
Ansicht 3A-3A

4 Stück



Schnitt 3B-3B

1:5

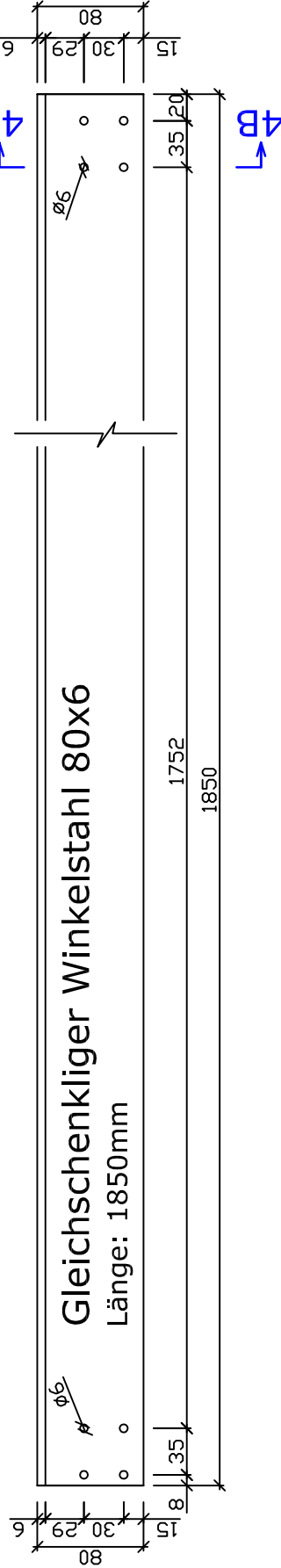


L-Profil 4

1:5

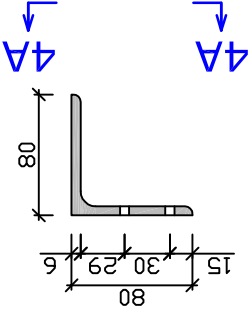
Ansicht 4A-4A

4 Stück



Schnitt 4B-4B

1:5

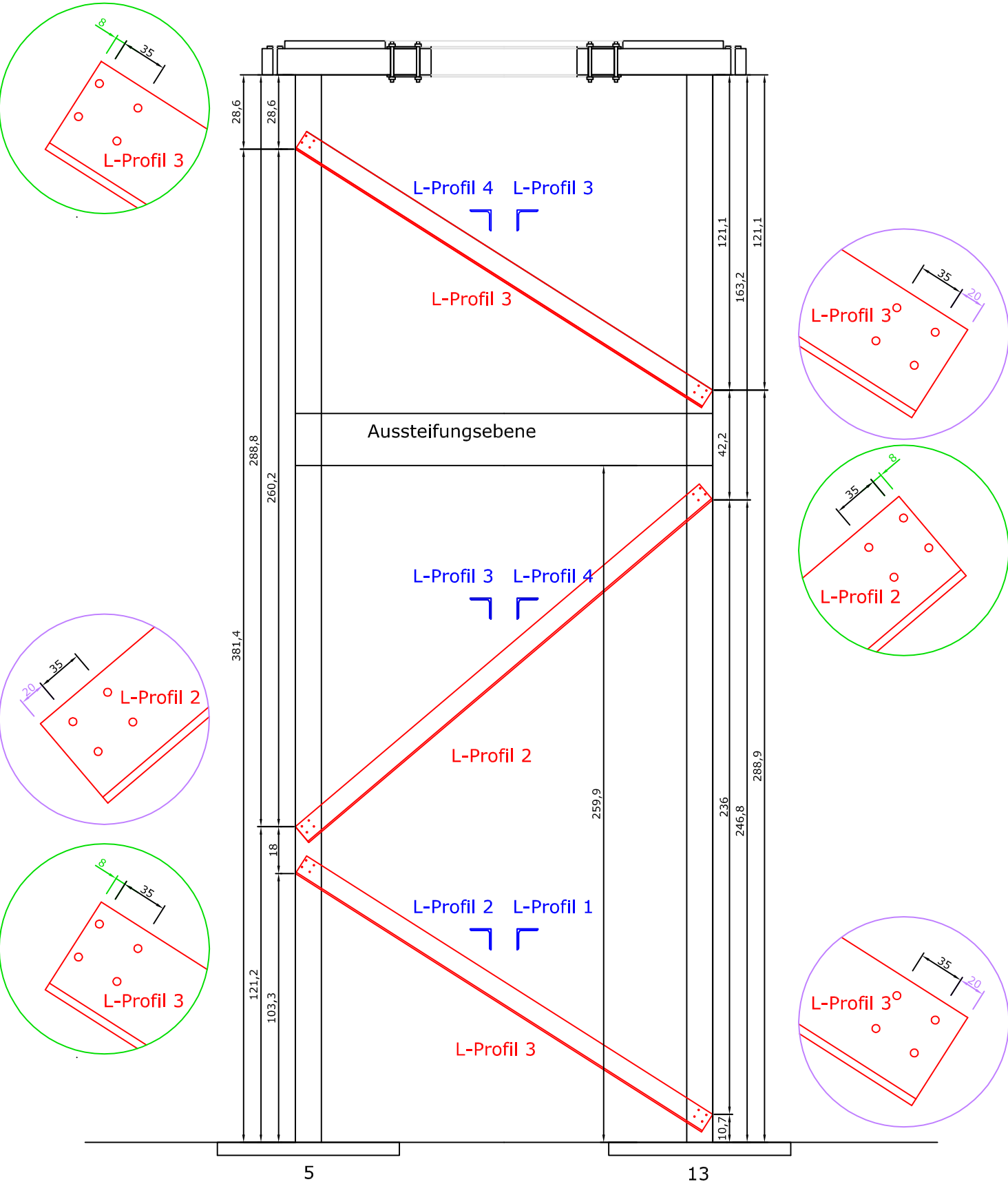


Stahlgüte: S235

Maße in mm

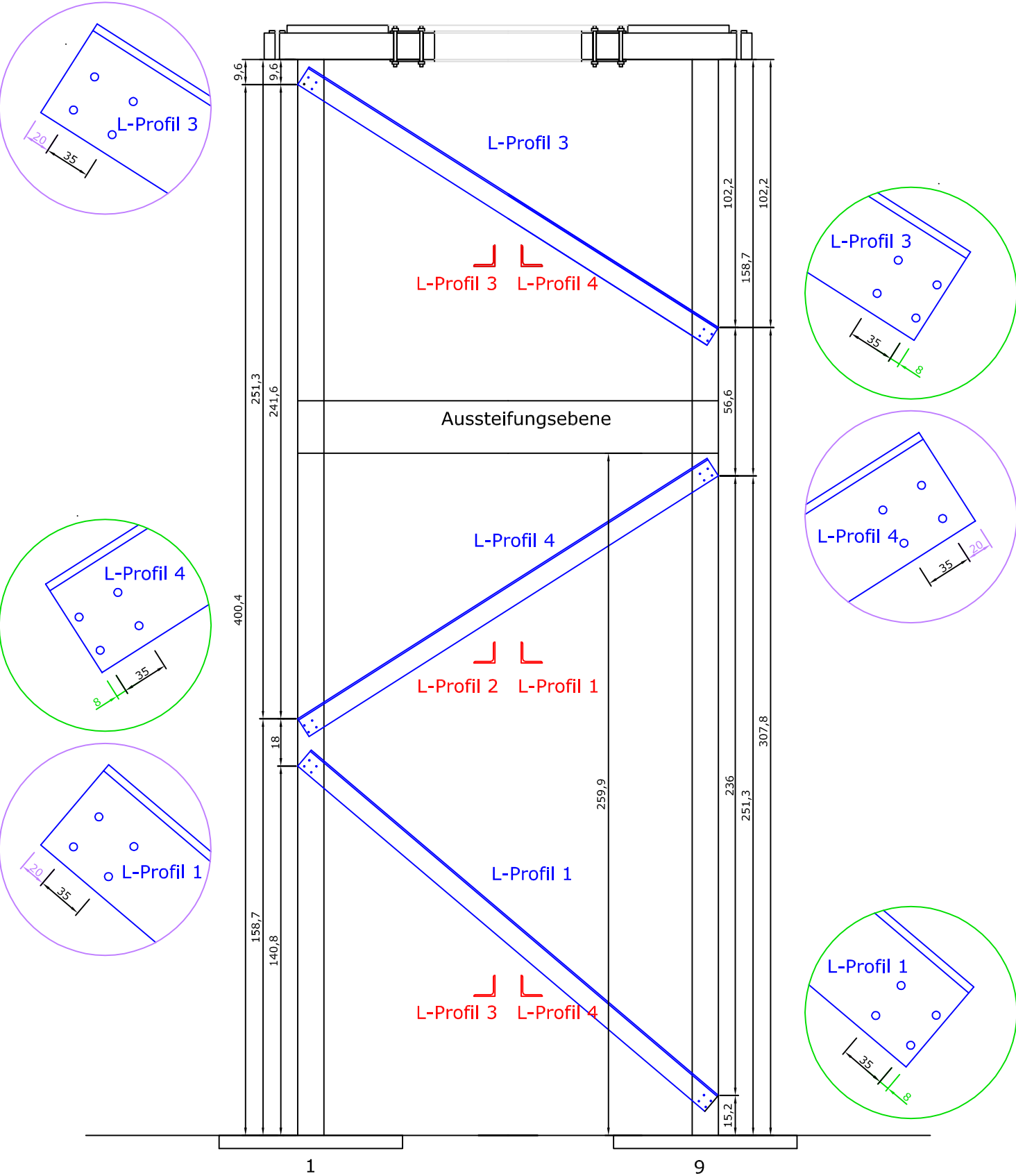
STAHLTEILE		
PLANINHALT:	MASSTAB:	
L-Profil 1,2,3,4	1:5	
PLANVERFASSTER:	DATUM:	
Sonja Dalling	20.10.10	
sdalling@mail.tuwien.ac.at		
Tel. +43-1-58801-21262		

PLANINHALT: <b>Montageturm -          Diagonalen -          Schnitt 1A-1A</b>	MASSSTAB: <b>1:20 A4          1:15 A3</b>
PLANVERFASSER: <b>Sonja Dallinger</b>	DATUM: <b>17.11.10</b>

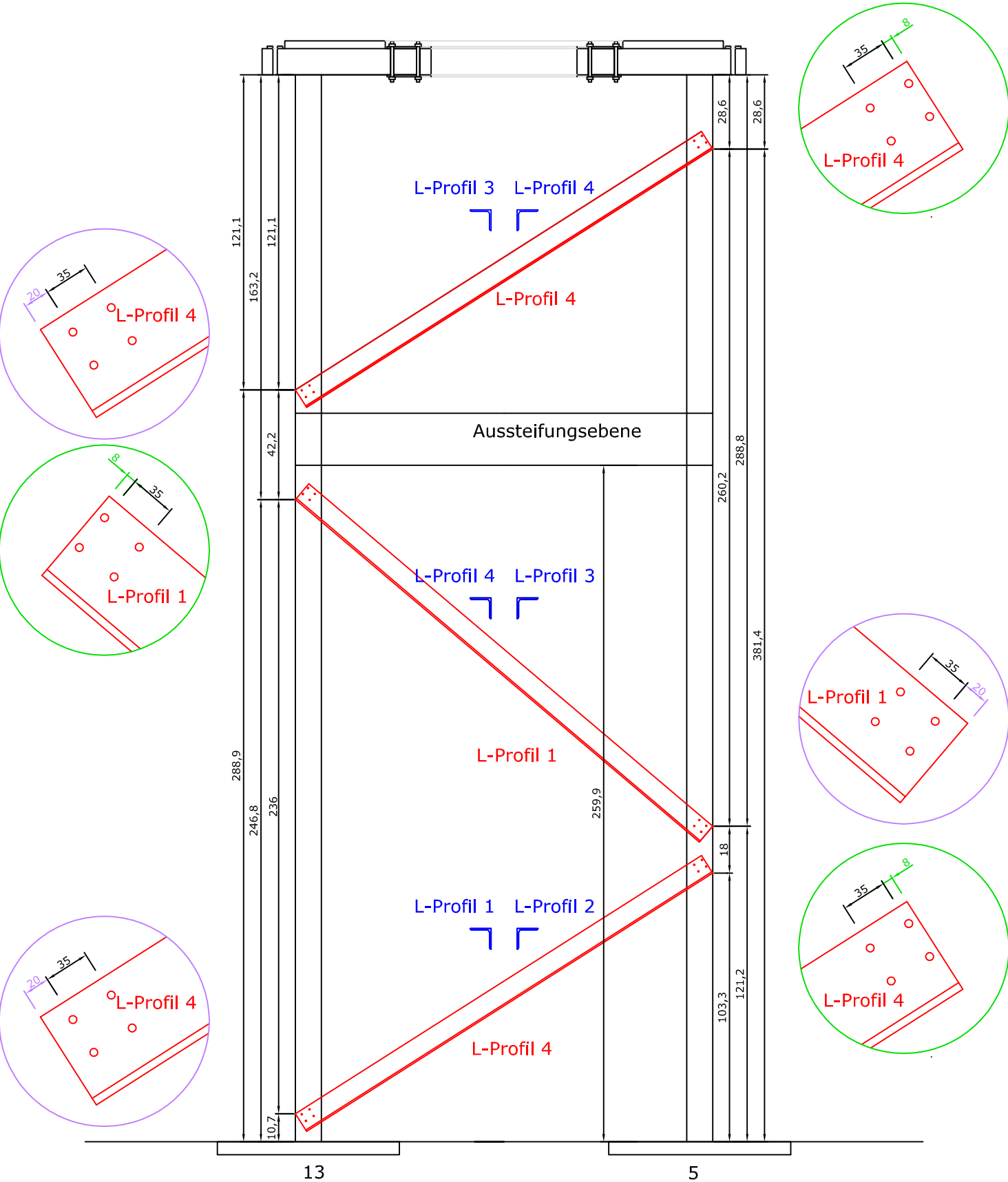




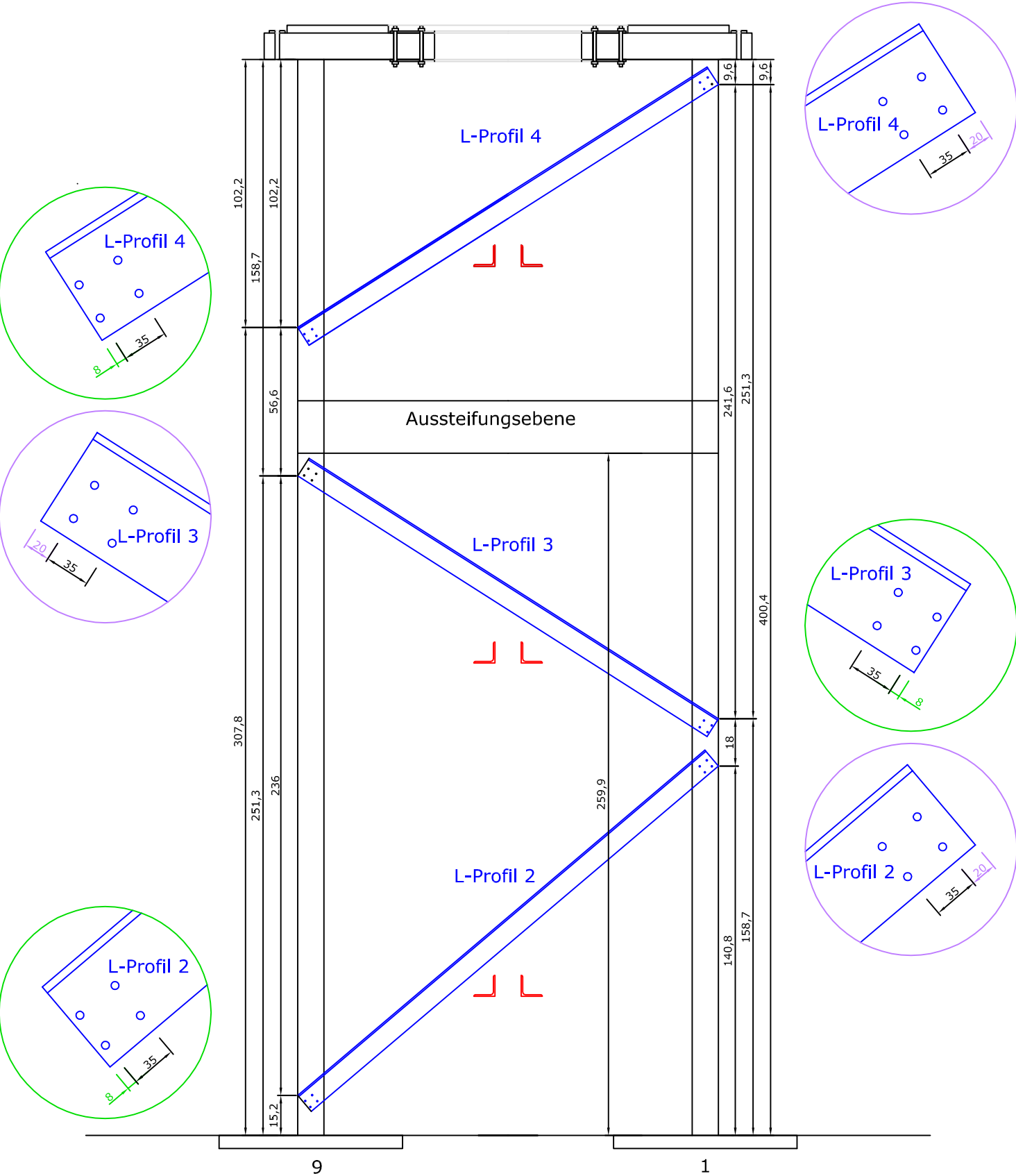
PLANINHALT: <b>Montageturm -          Diagonalen -          Schnitt 2A-2A</b>	MASSSTAB: <b>1:20 A4          1:15 A3</b>
PLANVERFASSER: <b>Sonja Dallinger</b>	DATUM: <b>17.11.10</b>



PLANINHALT: <b>Montageturm -</b> <b>Diagonalen -</b> <b>Schnitt 1B-1B</b>	MASSSTAB: <b>1:20 A4</b> <b>1:15 A3</b>
PLANVERFASSER: <b>Sonja Dallinger</b>	DATUM: <b>17.11.10</b>

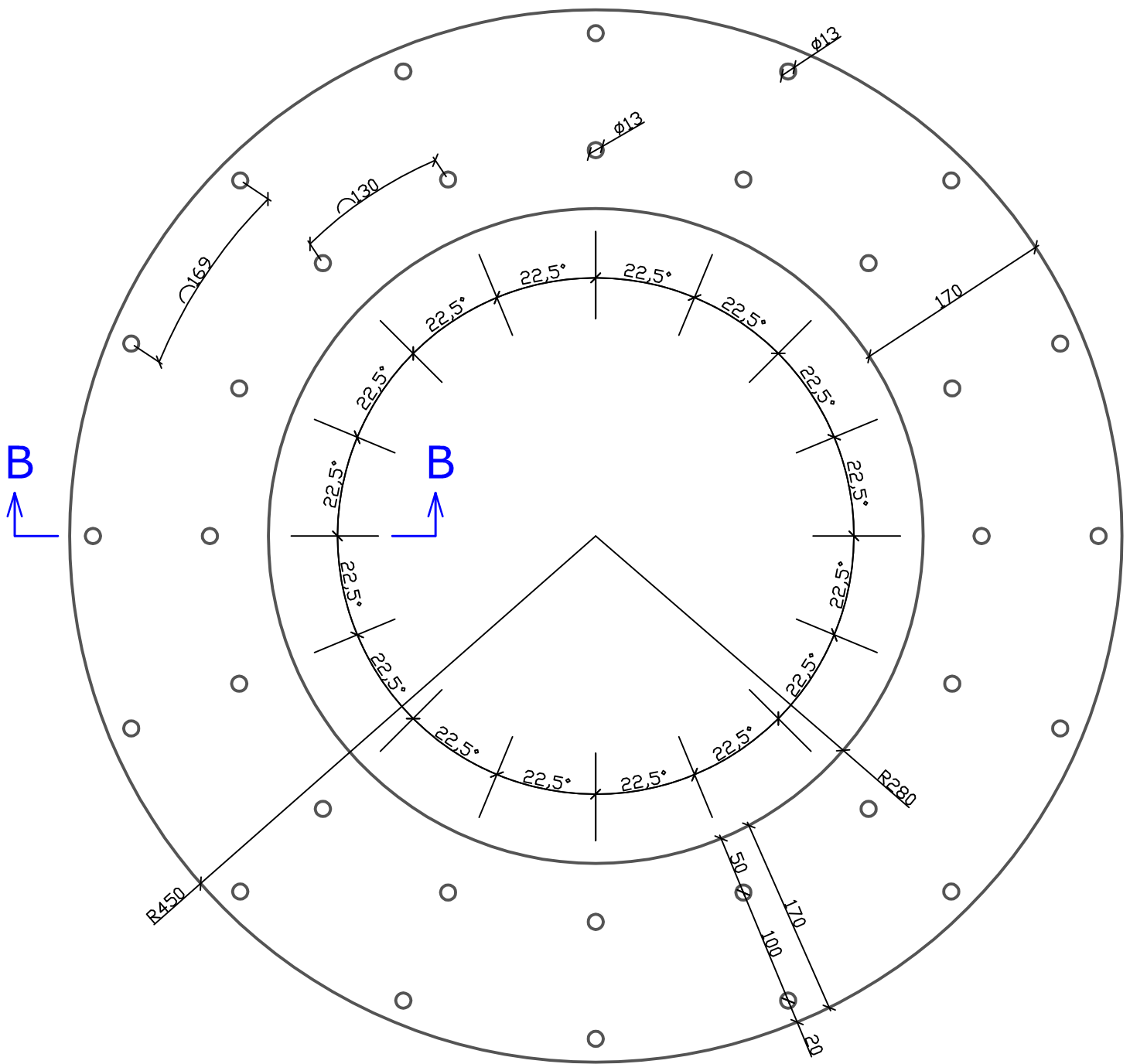


PLANINHALT: <b>Montageturm -</b> <b>Diagonalen -</b> <b>Schnitt 2B-2B</b>	MASSSTAB: <b>1:20 A4</b> <b>1:15 A3</b>
PLANVERFASSER: <b>Sonja Dallinger</b>	DATUM: <b>17.11.10</b>



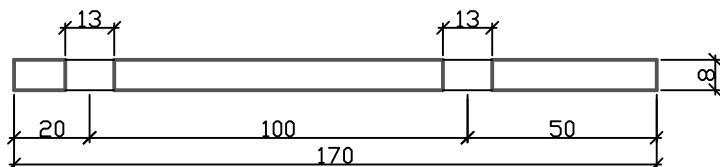
# Draufsicht

1:5



## Schnitt B-B

1:2

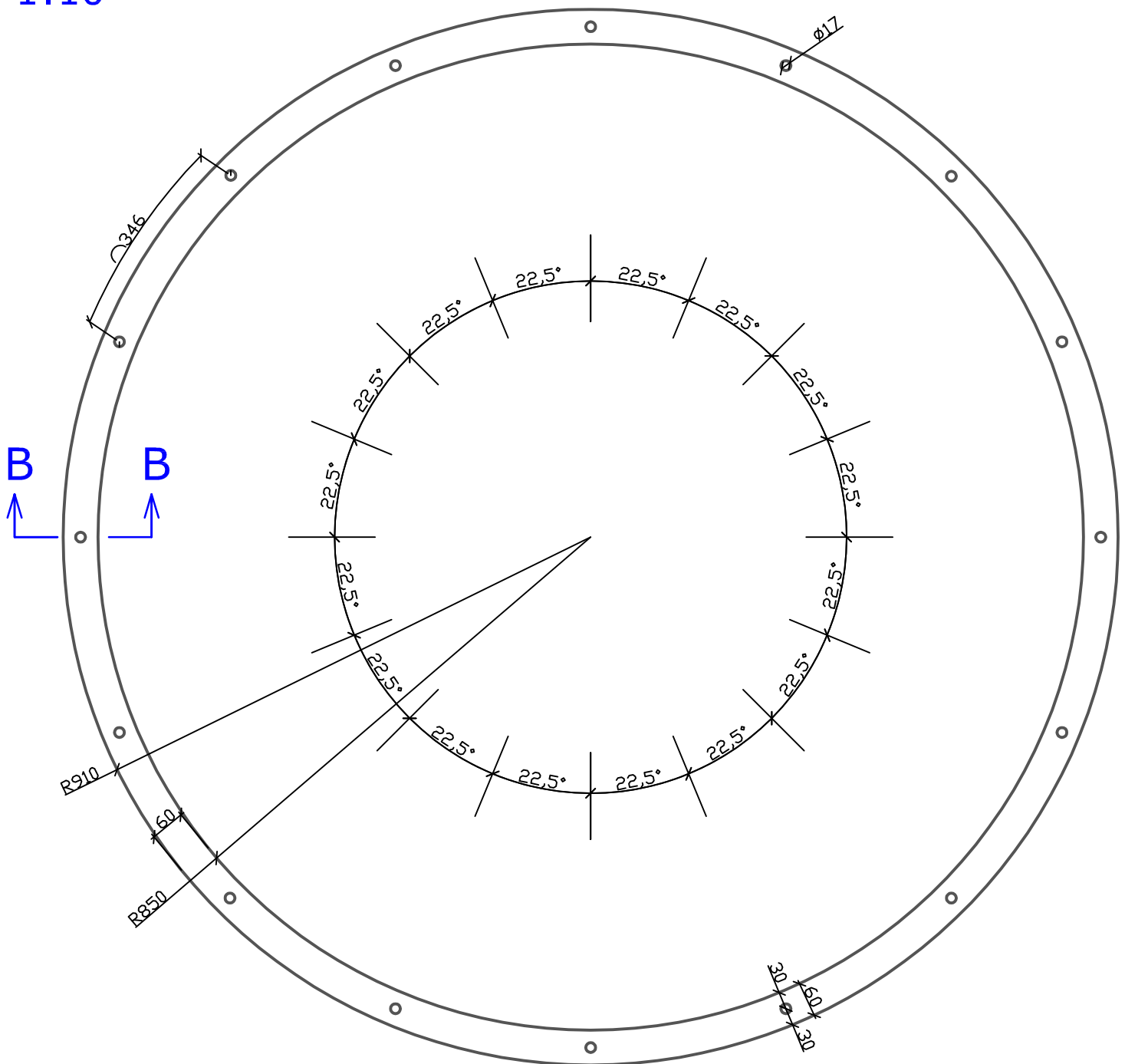


Maße in mm

PLANINHALT:	MASSSTAB:
Innenring	1:5
	1:2
PLANVERFASSER:	DATUM:
Sonja Dallinger	12.11.09
sdalling@mail.tuwien.ac.at	
Tel. +43-1-58801-21262	

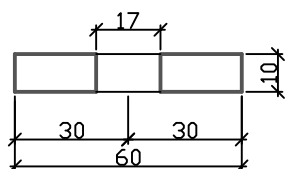
# Draufsicht

1:10



## Schnitt B-B

1:2



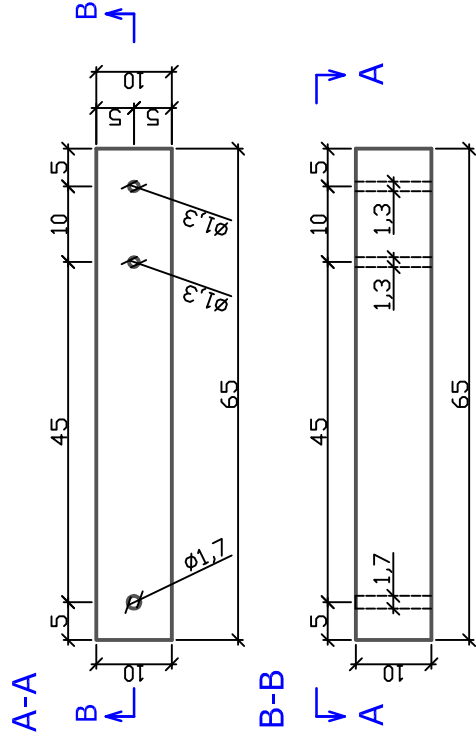
Maße in mm

PLANINHALT:	MASSTAB:
Außenring	1:10
	1:2
PLANVERFASSTER:	DATUM:
Sonja Dallinger	12.11.09
sdalling@mail.tuwien.ac.at	
Tel. +43-1-58801-21262	

Pos.	Anzahl	Breite x Höhe [cm]	Länge [cm]	Holzart	Löcher
1-Alt	16	5 x 16	70	Vollholz	-
2-Alt	16	10 x 10	410	BSH	-
3-Alt	16	10 x 10	65	BSH	Plan
4-Alt	16	Plan		Schalttafel	-

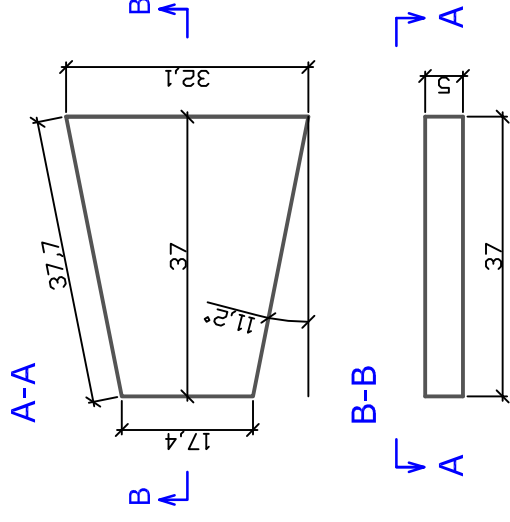
## Position 3-Alt

10x10 Staffeln, Länge: 65cm



## Position 4-Alt

Dicke: 2-3cm



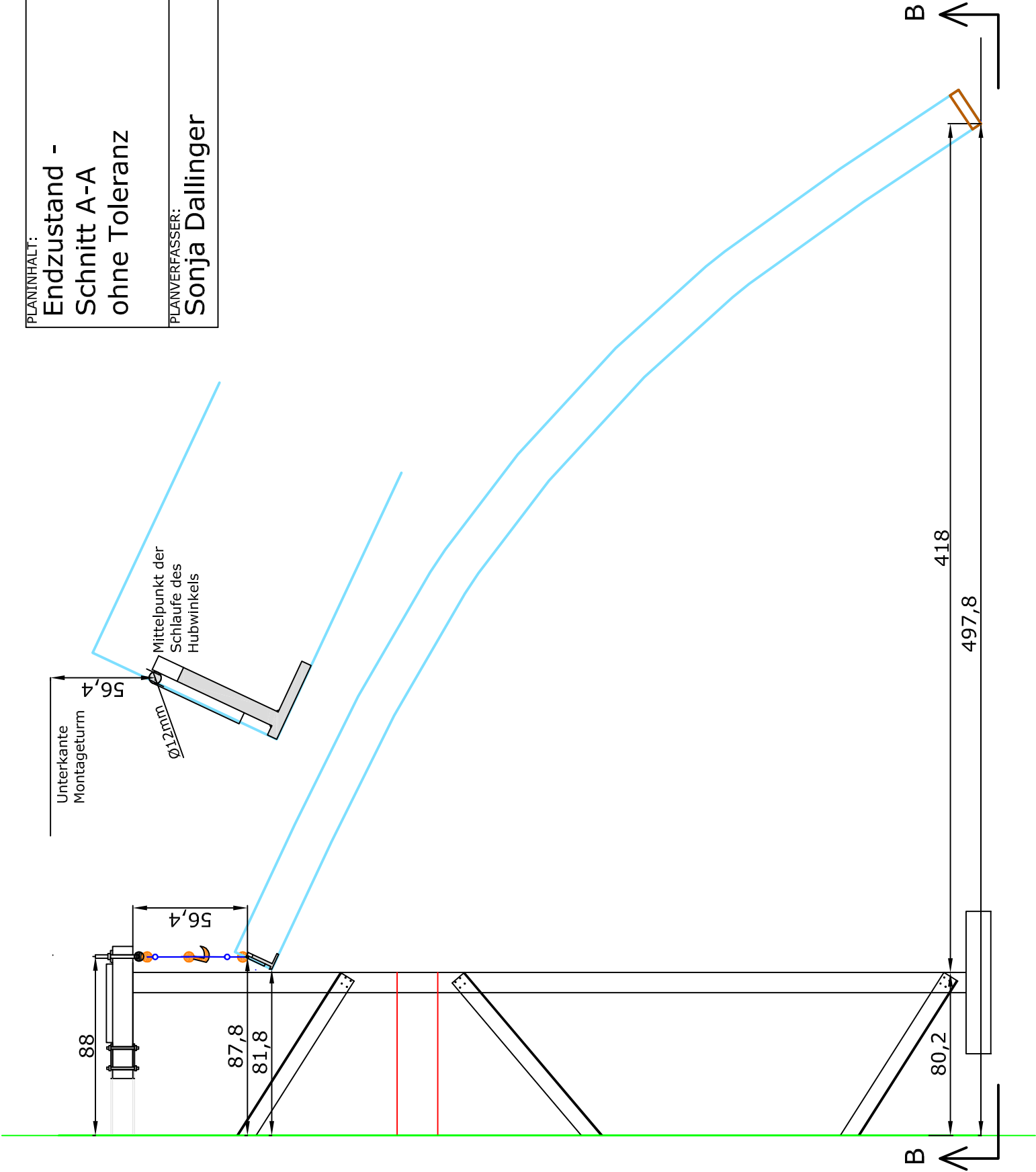
Maße in cm

Eiskuppel		
PLANINHALT:	MASSTAB:	1:10
Montageturm		
Holzpositionen		
PLANVERFASSTER:	DATUM:	12.11.09
Sonja Dallinger		
sdalling@mail.tuwien.ac.at		
Tel. +43-1-58801-21262		

## B.4 Final Position

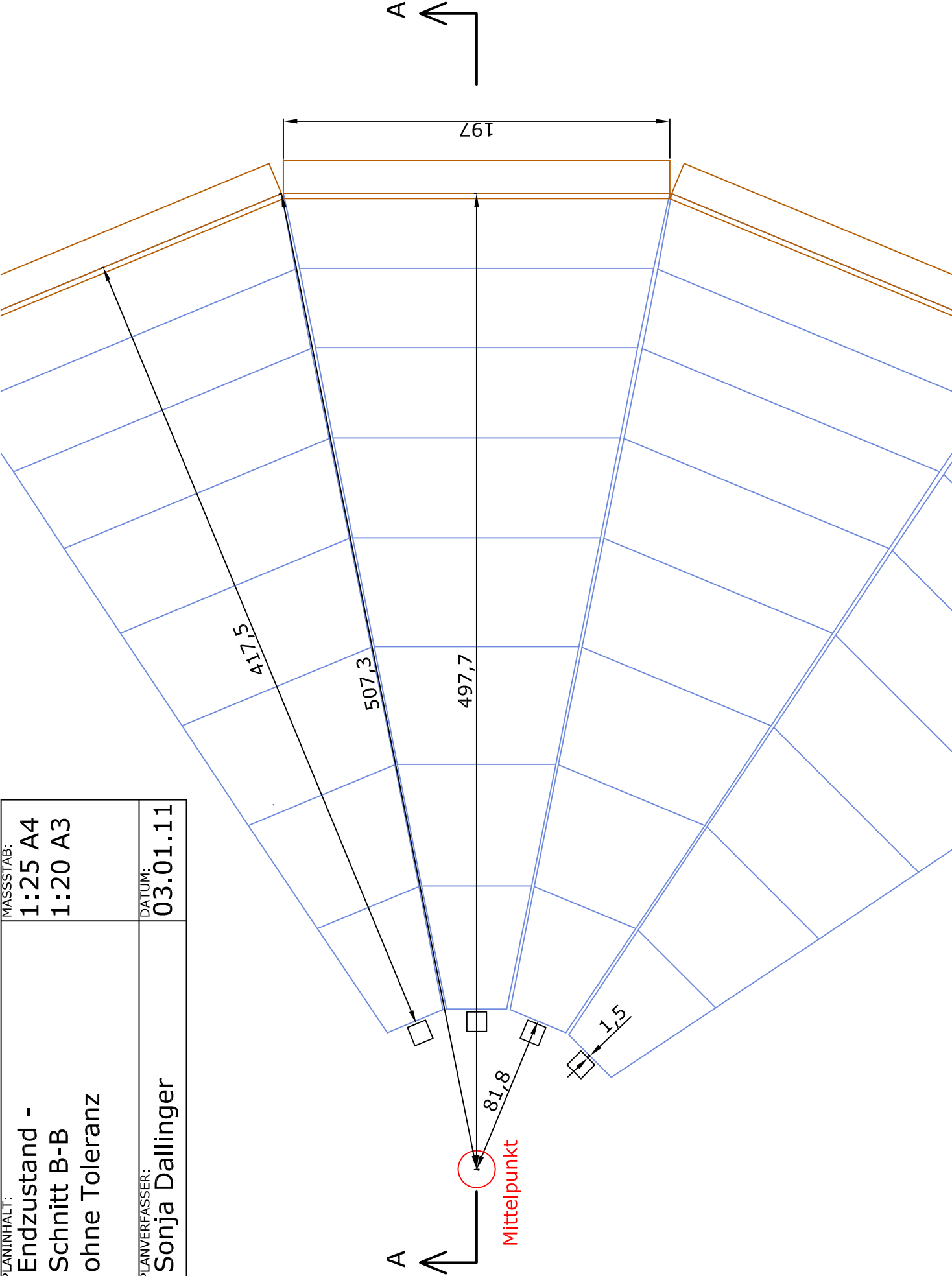
- Endzustand - Schnitt A-A ohne Toleranz (1)
- Endzustand - Schnitt B-B ohne Toleranz (1)
- Bestimmung der 16tel Punkte - Endlage (1)
- Aufhängung (1)

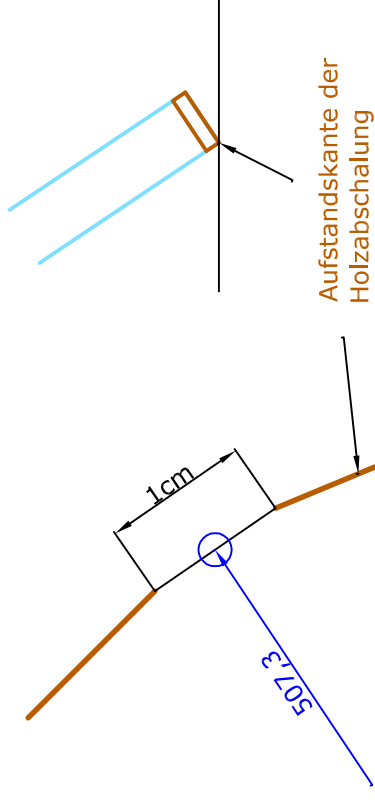
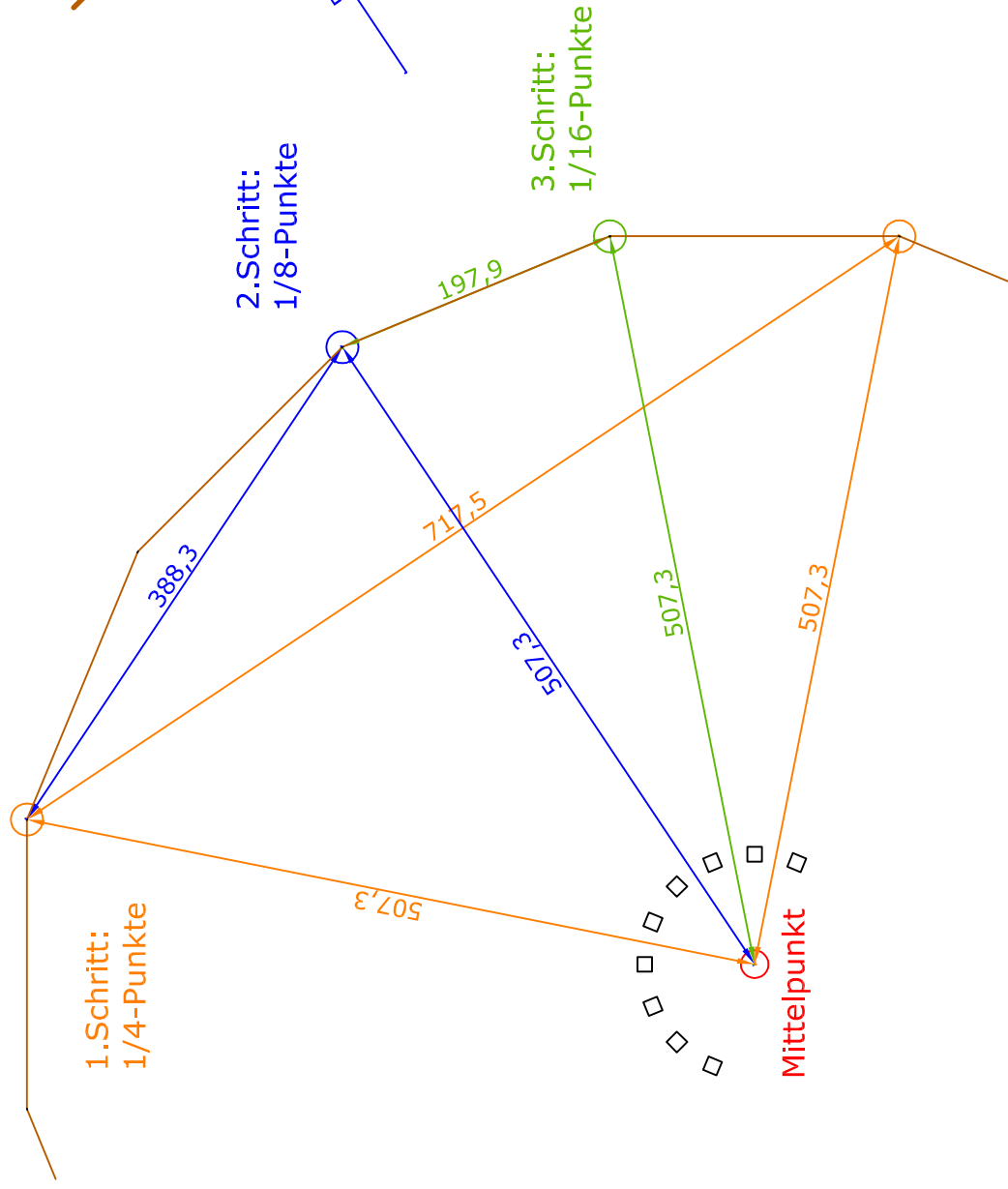
PLANINHALT: Endzustand - Schnitt A-A ohne Toleranz	MASSTAB: 1:25 A4 1:20 A3
	DATUM: 03.01.11
PLANVERFASSTER: Sonja Dallinger	





<b>PLANINHALT:</b> Endzustand - Schnitt B-B ohne Toleranz	<b>MASSSTAB:</b> 1:25 A4 1:20 A3
<b>PLANVERFASSTER:</b> Sonja Dallinger	<b>DATUM:</b> 03.01.11





PLANINHALT:	Bestimmung der 16tel Punkte Endlage	
	MASSSTAB:	1:50 A4 1:40 A3
PLANVERFASSTER:	Sonja Dallinger	
DATUM:	03.01.11	

M16x500 Gewindestange

M16 Mutter

10x10 Querhaupt - Holz

M16 Ringmutter

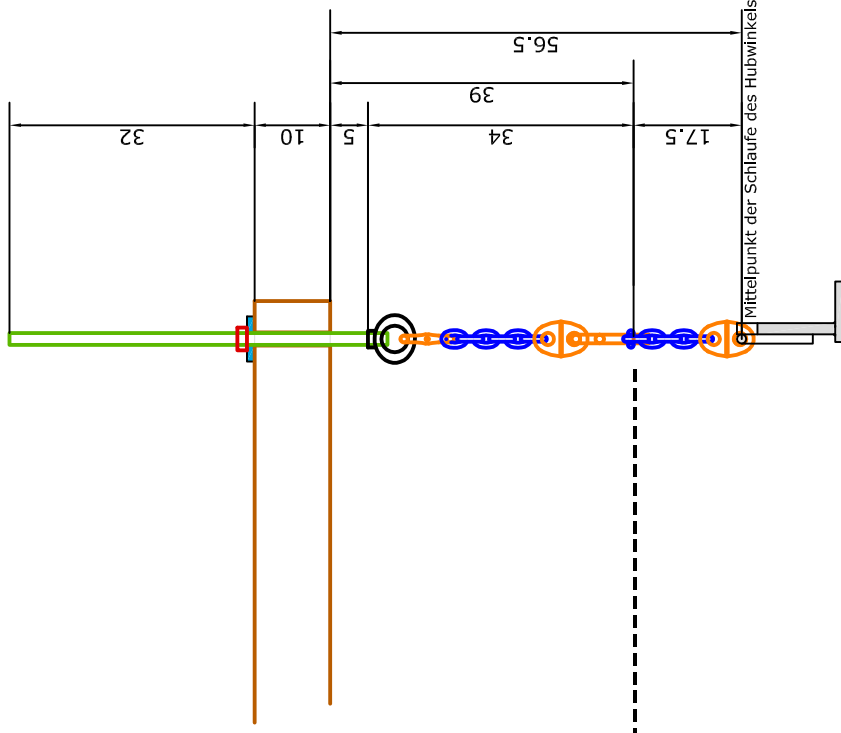
Connex-Verbindungsglied

Kette - 6 Glieder

Connex-Verbindungsglied

Parallelhaken PSW

Kette - im 6. Glied einhacken  
Hubwinkel



PLANINHALT:

Aufhängung

MASSSTAB:

1:10 A4

PLANVERFASSTER:

Sonja Dallinger

DATUM:

17.01.11